

# TECHNISCHE UNIVERSITÄT MÜNCHEN

Lehrstuhl für Analytische Lebensmittelchemie

Metabolomics in host-pathogen interactions  
- An investigation of Chlamydia infected human cells -

Constanze Müller

Vollständiger Ausdruck der von der Fakultät für Wissenschaftszentrum Weihenstephan für Ernährung, Landnutzung und Umwelt der Technischen Universität München zur Erlangung des akademischen Grades eines

Doktors der Naturwissenschaften

genehmigten Dissertation.

Vorsitzender: Univ.-Prof. Dr. E. Grill

Prüfer der Dissertation:

1. Priv.-Doz. Dr. Ph. Schmitt-Kopplin
2. Univ.-Prof. Dr. M. Rychlik
3. Univ.-Prof. Dr. J. Rupp, Universität zu Lübeck

Die Dissertation wurde am 10.07.2012 bei der Technischen Universität München eingereicht und durch die Fakultät für Wissenschaftszentrum Weihenstephan für Ernährung, Landnutzung und Umwelt am 19.11.2012 angenommen.

---

## Table of content

Acknowledgement .....	I
List of tables .....	II
List of figures .....	III
List of abbreviations .....	VII
<b>1 Introduction .....</b>	<b>1</b>
1.1 Motivation and overview of thesis .....	1
1.2 Metabolites .....	5
1.3 Metabolomics .....	7
1.3.1 Definition .....	7
1.3.2 General workflow in metabolomics .....	9
1.3.3 Applications and benefit of metabolomics .....	10
1.3.4 Metabolomics of host-pathogen interactions .....	11
1.4 Technologies in metabolomics .....	12
1.4.1 Liquid chromatography .....	12
1.4.2 Mass spectrometry .....	15
1.4.2.1 Electrospray ionization .....	16
1.4.2.2 Ion cyclotron resonance Fourier transform mass spectrometry .....	17
1.4.2.3 Time of flight mass spectrometry .....	20
1.4.3 Data analysis .....	22
1.4.3.1 Unsupervised methods .....	22
1.4.3.2 Supervised method .....	23
1.4.3.3 Network visualization and elemental formula calculation .....	24
1.4.3.4 Van Krevelen diagram and Kendrick plot .....	25
1.5 Chlamydia .....	26
1.5.1 Chlamydia-associated diseases .....	28
1.5.1.1 Chlamydia trachomatis .....	28
1.5.1.2 Chlamydia pneumoniae .....	29
1.5.2 Previously described metabolic host-pathogen interactions between Chlamydia and the human host cell .....	30
1.5.3 Hypoxia and the impact of oxygen environment on Chlamydia infection .....	33
1.5.4 The role of IFN- $\gamma$ in the human immune response to Chlamydia infection .....	36
<b>2 Molecular cartography in acute and persistent <i>C. pneumoniae</i> infections – a non-targeted metabolomic approach .....</b>	<b>38</b>
2.1 Introduction .....	38
2.2 Objectives .....	40
2.3 Materials and method development .....	41
2.3.1 Materials .....	41
2.3.2 Methods and method development .....	42
2.3.2.1 General considerations .....	42
2.3.2.2 Sample preparation procedures .....	43
2.3.2.2.1 Cell cultivation, infection and metabolite extraction .....	43
2.3.2.2.2 Determination of optimal infection time .....	45
2.3.2.2.3 Investigation and selection of cell disruption procedure .....	47
2.3.2.3 Analytical methods .....	50
2.3.2.3.1 ICR/FT-MS analysis .....	50
2.3.2.3.2 RP separation .....	51
2.3.2.3.3 HILIC separation .....	55
2.3.2.3.4 UPLC <sup>®</sup> -ToF-MS analyses .....	58

---

2.3.2.4 Data analysis .....	58
2.3.2.4.1 Cleaning of ICR/FT-MS data .....	59
2.3.2.4.2 Treatment of UPLC <sup>®</sup> -ToF-MS data and MZmine elaboration .....	60
2.3.2.4.3 HCA.....	60
2.3.2.4.4 PCA.....	60
2.3.2.4.5 PLS-DA .....	61
2.3.2.4.6 Wilcoxon-Mann-Whitney test .....	61
2.3.2.4.7 Correlation analysis .....	61
2.3.2.4.8 Annotation and pathway mapping .....	62
2.3.2.4.9 MetaboAnalyst .....	62
2.3.2.4.10 Venn diagram .....	63
2.3.2.4.11 Network visualization and elemental formula calculation.....	63
2.3.2.4.12 Filtering of UPLC <sup>®</sup> -ToF-MS annotations based on retention time-logD regression.....	64
2.3.2.4.13 Data alignment .....	65
2.4 Results and discussion .....	66
2.4.1 Data overview.....	67
2.4.1.1 Reproducibility .....	67
2.4.1.2 Mass detection, metabolite recovery and convergence between different instrumentations .....	69
2.4.2 Metabolic permutations after an active, normoxic infection .....	72
2.4.2.1 Important modifications in amino acid metabolism.....	77
2.4.2.2 Important modifications in the lipid metabolism.....	79
2.4.2.3 Important modifications in the carbohydrate metabolism and nucleosides..	82
2.4.2.4 Summary of important permutations in the central metabolism.....	83
2.4.2.5 Key „unknown“ metabolites affected by infection .....	84
2.4.3 Metabolic permutations after an active and persistent infection .....	90
2.4.3.1 Better growth, higher infectivity and persistence of Chlamydia as an environmental effect – investigation of metabolic adaption in non-infected cells to different cultivation conditions .....	92
2.4.3.2 Chlamydia-specific metabolite alterations in active and persistent infection	96
2.5 Summary.....	102
2.6 Perspectives .....	104
<b>3 Effects of <i>C. trachomatis</i> infection on the lipid homeostasis.....</b>	<b>107</b>
3.1 Introduction .....	107
3.2 Objectives .....	109
3.3 Nomenclature of lipids .....	110
3.4 Materials and method development.....	111
3.4.1 Materials.....	111
3.4.2 Methods and method development.....	111
3.4.2.1 General consideration .....	111
3.4.2.2 Protocols for cell cultivation, -disruption and lipid extraction .....	112
3.4.2.3 Overview of UPLC <sup>®</sup> -ToF-MS based targeted analyses of plasmalogens ..	114
3.4.2.4 Overview of ICR/FT-MS based shotgun lipidomics.....	115
3.4.2.5 Development of 2D UPLC <sup>®</sup> -TOF-MS .....	116
3.4.2.6 Hydrolysis .....	119
3.4.2.7 ICR/FT-MS and MS <sup>2</sup> analyses.....	120
3.4.2.8 Lipid annotation .....	121
3.4.2.9 Data analysis for identification of plasmalogens increased in infection .....	121
3.4.2.10 Data analysis for identification of main lipids affected by infection .....	122
3.4.3 Validation of methodology.....	123
3.4.3.1 Validation with standard glycerophospholipids.....	123

3.4.3.2 Detection of odd-chain fatty acid containing glycerophospholipids in infected samples .....	124
3.4.3.3 Detection of eukaryotic plasmalogens.....	124
3.5 Results and discussion .....	125
3.5.1 Identification of plasmalogens increased in infection.....	125
3.5.2 Identification of main lipids affected by infection.....	130
3.5.2.1 Diacyl-glycerophosphocholines and -ethanolamines affected by infection	133
3.5.2.2 Etherlipids affected by infection.....	136
3.6 Summary.....	140
3.7 Perspectives .....	142
4 Summary and concluding remarks.....	144
5 Annex - Investigation of the ionization and fragmentation mechanism of diacylglycerols.....	146
5.1 Introduction .....	146
5.2 Materials and Methods.....	148
5.2.1 Materials.....	148
5.2.2 Methods.....	148
5.3 Results and discussion .....	149
5.4 Summary.....	153
6 Supplementary data .....	154
7 Bibliography .....	166
List of scientific communication.....	i
Curriculum vitae .....	iii

## Acknowledgment

This PhD thesis would not have been possible without the help and support of many wonderful people.

First of all, I would like to thank my supervisor Priv.-Doz. Dr. Philippe Schmitt-Kopplin for the great opportunity to be trained and educated in his lab, for his continuous encouragement and support. His ideas and the helpful discussions broadened my view for many fascinating topics.

Furthermore, I thank all my colleagues who supported me in many ways: scientific know-how, experimental help, proof-reading of this thesis and their friendship, as well as the very warm welcoming in their group.

I am additionally very grateful to our collaborators Inga Dietz and Jan Rupp, as well as Agathe Subtil and Paul Lazarow for their generous help in scientific discussions, sample providing and their trust.

Finally, I would like to express my gratitude to my parents, Marion and Manfred Herrmann, my husband Manuel, my sister Sandra and my brother Lutz, as well as to my grandparents. Their encouragement and endless love have always given me strength to go my way and to write this thesis.

The dissertation has been prepared at the research unit Analytical BioGeoChemistry at the Helmholtz Zentrum München – German Research Center for Environmental Health in the frame of the ERA-NET Pathomics project.

---

## List of tables

Table 1: Terms in metabolomics.....	8
Table 2: Comparison of main advantages of ICR/FT-MS and UPLC <sup>®</sup> -ToF-MS.....	42
Table 3: Cell numbers and infection rates.....	45
Table 4: Numbers of detected and annotated metabolites after first step of disruption experiments.....	48
Table 5: Summary of observations after second step of disruption experiments.....	50
Table 6: Summary of RP column parameters and numbers of detected features.....	52
Table 7: Numbers of detected features for different additives in RP separation.....	53
Table 8: Numbers of detected features for different pre-concentration factors.....	53
Table 9: Numbers of detected features for evaluation of column/buffer system in HILIC separation.....	55
Table 10: Numbers of detected features for evaluation of optimal additive concentration and choice of organic solvent in HILIC separation.....	56
Table 11: Numbers of discriminative m/z detected with different techniques.....	73
Table 12: Statistically significantly increased metabolites with a very high connectivity....	89
Table 13: Numbers of statistically significant affected metabolites in infections under different cultivation conditions.....	97
Table 14: Pathways contribution of metabolites differently regulated in infected cells cultivated under different conditions.....	99
Table 15: Groups of metabolites altered in infected cells with IFN- $\gamma$ under different oxygen atmosphere.....	101
Table 16: Overview and comparison of applied workflows.....	112
Table 17: Evaluation of HILIC columns for glycerophospholipid separation.....	117
Table 18: Identified plasmalogens increased in infection.....	127
Table 19: Identified glycerophosphoethanolamine markers of Chlamydia infection.....	136
Table 20: PUFA containing plasmanyl-glycerophosphoethanolamines.....	138
Table 21: Diacylglycerols species important for Chlamydia infection.....	145
Table 22: Determined DG (18:0/16:0)-dimer fragment ions.....	149

---

## List of figures

Figure 1: Overview of applied metabolomics-strategies and tissue tropism of studies Chlamydia strains.....	2
Figure 2: Illustration of a human cell infected with the intracellular pathogen Chlamydia...	3
Figure 3: Structure of presented thesis.....	5
Figure 4: Assembly of metabolites into pathways and highly connected networks.....	6
Figure 5: Typical workflow of non-targeted metabolomics.....	9
Figure 6: OMICS cascade and central dogma of molecular biology.....	11
Figure 7: Illustration of retention time mechanism of glycerophospholipids in (A) HILIC and (B) RP separation.....	14
Figure 8: Electrospray ionization.....	16
Figure 9: Illustration of ICR/FT-MS.....	18
Figure 10: Illustration of (A) excitation and (B) image current detection inside an ICR cell.....	19
Figure 11: Illustration of maXis™ UHR-ToF-MS.....	21
Figure 12: Illustration of PCA and HCA learning principles.....	23
Figure 13: Van Krevelen diagram for (+)ICR/FT-MS data of Chlamydia infected human cells.....	25
Figure 14: Developmental cycle of Chlamydiales.....	27
Figure 15: Summary and illustration of described metabolic processes in infected human cells as well as important medium components.....	33
Figure 16: Summary and illustration of described metabolic processes under hypoxia....	36
Figure 17: Illustration of experimental design.....	38
Figure 18: Effect of the investigated conditions on the chlamydial development.....	39
Figure 19: Illustration of objectives.....	41
Figure 20: Overview of applied analytical concept and necessary steps during the study....	43
Figure 21: Workflow in cell culturing, quenching and metabolite extraction.....	44
Figure 22: Logarithmic ratio of detected signal intensities for all commonly detected metabolites in infected and non-infected samples 24h p.i. and 48h p.i.....	46
Figure 23: Comparison of annotated metabolites in infected and non-infected cells for 24h p.i. and 48h p.i.....	47
Figure 24: Experimental set-up to define the best suitable cell disruption method.....	48

---

Figure 25: Comparison of detected features after first step of disruption experiments.....	48
Figure 26: Section of (+)ICR/FT-MS mass spectra for disruption experiments.....	49
Figure 27: Illustration of (A) BPC; (B) density map; (C) applied gradient and (D) obtained pressure profile for RP UPLC <sup>®</sup> -ToF-MS analyses .....	54
Figure 28: Retention time window of standard compounds for evaluation of additive concentration in HILIC separation.....	56
Figure 29: Illustration of (A) BPC; (B) density map; (C) applied gradient and (D) obtained pressure profile for HILIC UPLC <sup>®</sup> -ToF-MS analyses .....	57
Figure 30: Overview of data analysis.....	59
Figure 31: Exemplary illustration of resulting metabolome overview after pathway analysis with MetaboAnalyst.....	63
Figure 32: Plot of RP retention times of standards against their predicted logD .....	65
Figure 33: Summary and decision tree of data cleaning and –elaboration.....	66
Figure 34: Structure of results and discussion section.....	67
Figure 35: Illustration of spectra of three randomly chosen biological repetitions of non-infected and infected samples cultivated under 20% oxygen atmosphere.....	68
Figure 36: Van Krevelen diagrams of (+)/(-)ICR/FT-MS detected masses .....	70
Figure 37: (A) Metabolite recovery in (+)/(-)ICR/FT-MS; (B) Venn diagram illustrating the convergence between data of different applied instrumentations; (C) glycolysis illustrating the enhanced metabolite recovery in multi-parallel analysis.....	71
Figure 38: Illustration of study design and data analysis .....	72
Figure 39: PLS-DA models separating infected and non-infected cells.....	73
Figure 40: Distribution of statistically significant metabolites over the KEGG metabolite classes.....	74
Figure 41: Distribution of statistically significant metabolites over the KEGG pathways....	75
Figure 42: Pathway analysis of discriminative metabolites with a signal intensity fold-change $\geq 100\%$ in infected and non-infected cells.....	76
Figure 43: Mainly affected of amino acids and -derivates.....	77
Figure 44: Detected metabolite abundance in Chlamydia infection in the proposed phenylalanine catabolism and connection to the TCA cycle in gram-negative bacteria.....	79
Figure 45: Eicosanoid metabolism affected by infection .....	80
Figure 46: Cholesterol biosynthesis.....	81
Figure 47: RP UPLC-ToF-MS EIC of putative sphinganine [302.305 $\pm$ 0.02] for one technical of each biological repetition.....	82



---

Figure 48: ICR/FT-MS NDP signal intensities in infected and non-infected cells.....	83
Figure 49: Summary of main metabolites affected by <i>C. pneumoniae</i> infection.....	84
Figure 50: Logarithmic ratio of detected signal intensities for statistically significant affected metabolites.....	85
Figure 51: Kendrick-analogous mass difference network based on (+)ICR/FT-MS data..._	86
Figure 52: Kendrick-analogous mass difference network based on (+)ICR/FT-MS data only including statistically significant increased metabolites after infection.....	87
Figure 53: Kendrick plot of statistically significant increased metabolites after infection..._	87
Figure 54: Zoom in the center of Kendrick-analogous mass difference network only including statistically significant increased metabolites after infection.....	88
Figure 55: PCA for cells cultivated and infected under 20% and 2% oxygen atmosphere_	90
Figure 56: Investigation of non-infected cells: (A) PCA score plot; (B) PCA loading plot; (C) Heat map of statistically significant altered metabolites.....	93
Figure 57: (A) Elemental composition with one annotation of metabolites increased in cells cultivated under hypoxia and decreased in IFN- $\gamma$ treated normoxic cells; (B) IFN- $\gamma$ mediated signaling pathway; (C) IDO mRNA expression levels; (D) western blot of IDO protein expression.....	94
Figure 58: Elemental composition with one annotation of metabolites increased in IFN- $\gamma$ treated normoxic cells and decreased in cells cultivated under hypoxia.....	95
Figure 59: Overview of sample set and structure of data analysis.....	98
Figure 60: Principle of data analysis.....	98
Figure 61: Pathway analysis of metabolites statistically significant altered in infected cells cultivated without IFN- $\gamma$ under different oxygen atmosphere.....	100
Figure 62: ICR/FT-MS signal intensities of metabolites statistically significant altered in infected cells cultivated with IFN- $\gamma$ under different oxygen atmosphere.....	101
Figure 63: Structure of glycerophosphocholines and -ethanolamines.....	108
Figure 64: Illustration of sample set-up and objectives.....	109
Figure 65: Workflow to determine Chlamydia-derived plasmalogens.....	115
Figure 66: Workflow of combined shotgun ICR/FT-MS and UPLC <sup>®</sup> -ToF-MS approach to determine lipidome alterations after infection.....	116
Figure 67: Evaluation of HILIC additives for glycerophospholipid separation.....	118
Figure 68: Evaluation of RP columns for glycerophospholipid separation.....	119
Figure 69: Mechanism of acidic hydrolysis of vinyl-ether bond in plasmalogens via hemiacetal formation.....	120
Figure 70: Overview of sample analysis to determine importantly affected lipids.....	122

---

Figure 71: EIC( $[M+H]^+ \pm 0.02$ ) of standard glycerophospholipids in the first and second dimension.....	123
Figure 72: Odd-chain fatty acid containing glycerophospholipids.....	124
Figure 73: Plasmalogens in control and pex19 cells.....	125
Figure 74: RP EIC( $[M+H]^+ \pm 0.02$ ) for Chlamydia-derived plasmalogens in fibroblast sample set.....	126
Figure 75: RP EIC( $[M+H]^+ \pm 0.02$ ) for Chlamydia-derived plasmalogens in isolated EBs.....	126
Figure 76: (+)ICR/FT-MS <sup>2</sup> fragmentation pattern for PE(P-33:0).....	128
Figure 77: Proposed fragmentation mechanism for Chlamydia-derived plasmalogens.....	129
Figure 78: Lipid composition of cell extracts.....	130
Figure 79: Kendrick plot of effected lipids: (A) increased in infection; (B) decreased in infection.....	131
Figure 80: RP UPLC-ToF-MS peak areas of glycerophosphocholines (A) fibroblasts and (B) isolated EBs.....	133
Figure 81: RP UPLC-ToF-MS peak areas of glycerophosphoethanolamines in (A) fibroblasts and (B) isolated EBs.....	134
Figure 82: RP UPLC-ToF-MS peak areas of plasmanyl-glycerophosphocholines (A) fibroblasts and (B) isolated EBs.....	137
Figure 83: RP UPLC-ToF-MS peak areas of plasmanyl-glycerophosphoethanolamines in (A) fibroblasts and (B) isolated EBs.....	138
Figure 84: RP UPLC-ToF-MS peak areas of (A) plasmenyl-glycerophosphocholines and (B) plasmenyl-glycerophosphoethanolamines in fibroblasts.....	139
Figure 85: RP UPLC-ToF-MS peak areas of (A) plasmenyl-glycerophosphocholines and (B) plasmenyl-glycerophosphoethanolamines in isolated EBs.....	140
Figure 86: Structure of diacylglycerols.....	146
Figure 87: Conformation of diacylglycerol-dimer in the gas phase.....	148
Figure 88: (-)ICR/FT-MS <sup>2</sup> fragmentation pattern for DG (18:0/16:0)-dimer.....	148
Figure 89: Proposed intra- and intermolecular fragmentation mechanism for DG (18:0/16:0)-dimer.....	150
Figure 90: Proposed fragmentation mechanism of keten elimination.....	152

## List of abbreviations

(-)	Negative electrospray mode
(+)	Positive electrospray mode
AA	Arachidonic acid and
ADP	Adenosine diphosphate
APCI	Atmospheric pressure chemical ionization
APPI	Atmospheric pressure photo ionization
ATP	Adenosine triphosphate
BPC	Base peak chromatogram
C.	Chlamydia
CID	Collision induces dissociation
CIS-MS	Coordination-ionspray-MS
COPD	Chronic obstructive pulmonary disease
COX	Cyclooxygenase
CPAF	Chlamydia protease-like activity factor
Cpn	Chlamydia pneumoniae
CTL	Control fibroblasts
CTS	Chemical translation service
CV	Coefficient of variance
DFT	Quantum mechanical calculations
DHA	Docosahexaenoic acid
DMEM	Dulbecco's Modified Eagle Medium
EB	Elementary body
EIC	Extracted ion chromatogram
ESI	Electrospray
FCS	Fecal calf serum
GLUT-1	Glucose transporter 1
GSH	glutathione
GSSG	oxidized glutathione
HIF-1	Hypoxia inducible factor 1
HILIC	Hydrophilic interaction liquid chromatography
ICR/FT-MS	Ion cyclotron resonance Fourier transform mass spectrometry
IDO	Indoleamine 2,3-dioxygenase
IFN- $\gamma$	Interferon gamma
LCR	Ligase chain reactions
LDHA	Lactate dehydrogenase A
LoD	Limit of detection
LOX	Lipoxygenase
m/z	Mass to charge ratio
MHC	Major histocompatibility complex
MS	Mass spectrometry
MSI	Metabolomics standard initiative
MW	Megaword
NDP	Nucleoside diphosphate
NEAA	Non-essential amino acids
NMR	Nuclear magnetic resonance
NSAIDs	Non steroidal anti-inflammatory drugs
NTP	Nucleoside triphosphate
P	Sharp particles
p.i.	Post infection
PAMPs	Pathogen-associated molecular patterns
PBS	Phosphate buffered saline
PCA	Principle component analysis
PCR	Polymerase chain reaction
PDH	Pyruvate dehydrogenase
PKD1	Pyruvate dehydrogenase kinase 1

---

<i>PE</i>	<i>Glycerophosphoethanolamines</i>
<i>PL</i>	<i>Glycerophospholipids</i>
<i>PLA</i>	<i>Phospholipase</i>
<i>PLS-DA</i>	<i>Partial least square discriminative analysis</i>
<i>PPP</i>	<i>Pentose phosphate pathway,</i>
<i>PS</i>	<i>Glycerophosphoserines</i>
<i>PUFA</i>	<i>Polyunsaturated fatty acid</i>
<i>QC</i>	<i>Quality control</i>
<i>RB</i>	<i>Reticulated body</i>
<i>RF</i>	<i>Radio frequency</i>
<i>RP</i>	<i>Reversed phase</i>
<i>RPMI</i>	<i>Eagle's minimum essential medium</i>
<i>S/N</i>	<i>Signal-to-noise ratio</i>
<i>SB</i>	<i>Sonic bath</i>
<i>SF</i>	<i>Sonic finger</i>
<i>SM</i>	<i>Sphingolipids</i>
<i>SORI</i>	<i>Sustained off-resonance irradiation</i>
<i>STD</i>	<i>Standard deviation</i>
<i>T3SS</i>	<i>Type three secretion system</i>
<i>TCA cycle</i>	<i>Tricarboxylic acid cycle</i>
<i>TIC</i>	<i>Total ion chromatogram</i>
<i>ToF</i>	<i>Time of flight</i>
<i>UHR</i>	<i>Ultrahigh resolution</i>
<i>UPLC</i>	<i>Ultra performance liquid chromatography</i>
<i>VIP</i>	<i>Variable importance in projection</i>
<i>VLCFA</i>	<i>Very long chain fatty acids</i>

## 1 Introduction

### 1.1 Motivation and overview of thesis

The scientific discipline of metabolomics offers recently enormous possibilities to study the metabolism of human cells and microorganisms on a systems level. One very fascinating field of application is the investigation of host-pathogen interactions in order to learn more about the underlying biology. How do microorganisms intertwine and manipulate their human host and how does the host respond? Alterations in the metabolome after infection are hereby of special interest, since the metabolome describes the ultimate phenotype deduced by permutations in gene expression, modulation of protein function and environmental factors (Mashego et al., 2007). Therefore, metabolomic investigations, together with the availability of complete genomes as well as proteomic and transcriptomic data, promises a much more comprehensive understanding of host-pathogen interactions (Forst, 2006, Mashego et al., 2007, Kafsack et al., Eisenreich et al.). An improved knowledge of biological processes during an infection is essentially required for new therapeutic intervention opportunities and drug development (Forst, 2006), which are obviously necessary considering the facts that infectious diseases are still one of the world's most leading causes of death (WHO, 2008), that drug resistances against our current antibiotics are an increasing phenomenon (Barie, 2012) and that several chronic diseases are linked to bacterial persistent infections and their long-term complications (Monack et al., 2004).

Within this thesis novel multi-parallel analytical approaches have been developed and applied to investigate metabolic host-pathogen interactions between *Chlamydia* and human host cells. *Chlamydia* are pathogens with prevalence of up to 70% in the western hemisphere. They are currently only diagnosable and treatable during their active infection, but especially persistent and recurring infections are associated with serious health problems, like COPD (chronic obstructive pulmonary disease) or Asthma in case of *Chlamydia pneumoniae* (Branden et al., 2005, Hahn et al., 2012) or like pelvic inflammatory disease and infertility after infection with *Chlamydia trachomatis* (Schachter, 1999, WHO, 2001, WHO, 2012a). Both strains *C. pneumoniae* and *C. trachomatis* have been studied in cell culture within this thesis (Figure 1). Since *Chlamydia* are intracellular replicating pathogens, their metabolism and the interactions with the human host has been hardly investigated to this day. In

consequence, our current knowledge about these fascinating pathogens is quite limited.

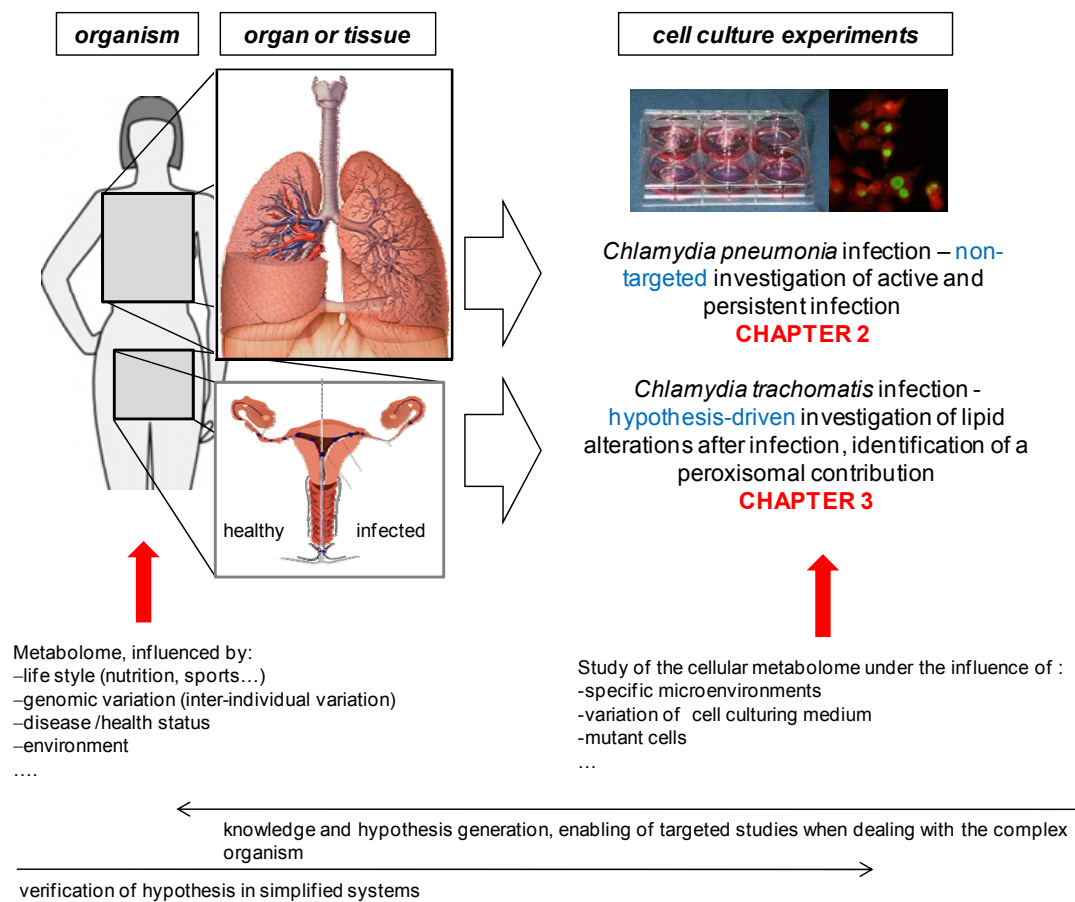
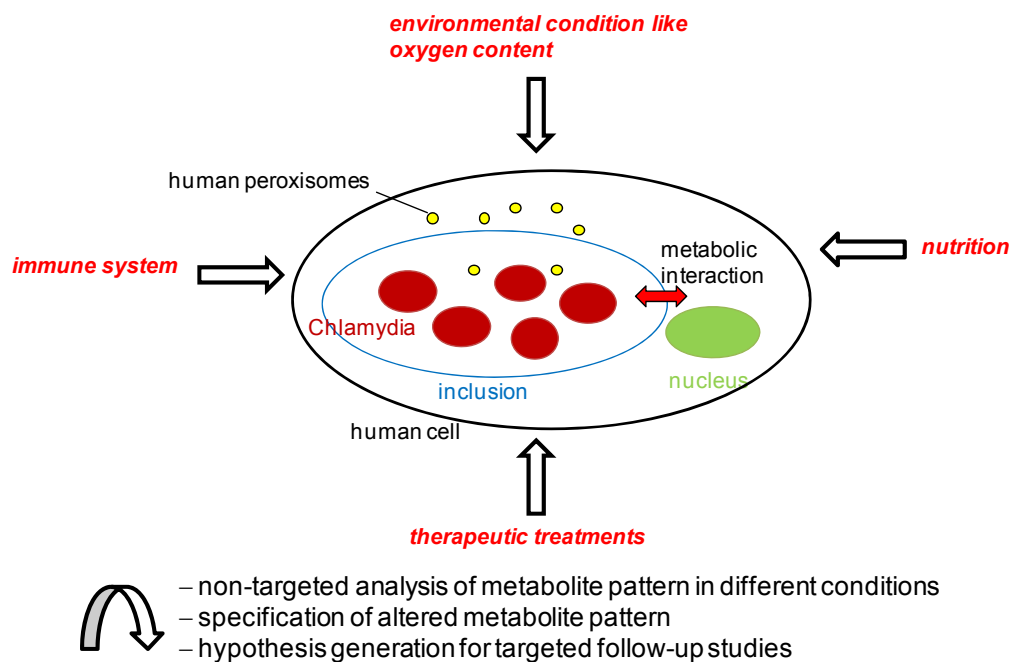


Figure 1: Overview of applied metabolomics-strategies and tissue tropism of studied *Chlamydia* strains

In the first part of the thesis, *C. pneumoniae* infections are studied in a non-targeted manner. Within this first part the strength of non-targeted metabolomics as a powerful screening tool for hypothesis generation based on most important metabolome alterations after infection is illustrated. The non-targeted investigation of the metabolic host-pathogen interactions in active and persistent *C. pneumoniae* infection has been carried out in collaboration with Inga Dietz and Prof. Dr. Jan Rupp (Institute for Medical Microbiology and Hygiene, University of Lübeck, Lübeck, Germany). Thereafter, *C. trachomatis* infections are deeper investigated with a focus on lipid permutations, which has been done in cooperation with Agathe Subtil and Paul Lazarow (Unit of Biology of Cell Interactions, Institute Pasteur, Paris,

France). The second part presents metabolomics as a promising tool for verification of a *priory* hypothesis. In both parts the reader is introduced in the development of the methodology, before the biological results and their interpretation are presented.

Non-targeted metabolomics reaches towards the simultaneous detection of all metabolites in at least two different phenotypes, e.g. infected and non-infected cells. It aims at a “snapshot” of the metabolism in both systems. Metabolites showing the highest variations in these two phenotypes are explored by statistical analysis in order to determine the most relevant cellular modulations. This concept of non-targeted analysis is often helpful when conventional investigations grope in the dark. In addition, it is beneficial in studies combining several phenotypes, like during the investigation of different influencing factors to an infection (Figure 2).



*Figure 2: Illustration of a human cell infected with the intracellular pathogen Chlamydia: Several external stimuli and conditions, like the oxygen concentration in the surrounding atmosphere, nutrition, treatment or activation of the immune system influences the pathogenesis. Consequently, differences in the metabolite pattern can be observed and deeper investigated.*

Such multi-condition experiments are particularly important to simulate and understand processes and interactions occurring in real life. Accordingly, we combined several culturing conditions to investigate an active, a persistent and a

non-persistent *C. pneumoniae* infection. After developing the analytical concept, which integrates several state-of-the-art analytical methods and data elaboration tools, the host–pathogen interactions are explored. This part of the thesis aims at enhanced biological understanding of an active and persistent *Chlamydia* infection, at the definition of starting points for future targeted studies and at the discovery of discriminating markers for new diagnostic and therapeutic concepts. The obtained results give complete new insights into chlamydial infections and validate previous evidence.

The second part of this thesis serves mainly for hypothesis verification, thus it illustrates the power of metabolomics in follow-up investigations. It contracts furthermore to the results of the non-targeted investigation, which shows an impact of *Chlamydia* infection to the cellular lipid homeostasis. Moreover, we have been further motivated to built up a targeted lipidomics investigation since human peroxisomes, which are main compartments essentially required for etherlipid biosynthesis, have been recently found inside the chlamydial inclusion by Agathe Subtil et al. (Unit of Biology of Cell Interactions, Institute Pasteur, Paris, France) (Figure 2). A methodology based on two-dimensional liquid chromatography in combination with ultrahigh resolution mass spectrometry has been developed and the obtained results are illustrated.

Such non-targeted and lipidomics investigations of complex systems like infected cells, which contain a huge number of metabolites characterized by different physicochemical properties and various concentrations, is an analytical challenge only enabled by recent progress in the instrumental development. Nevertheless, no current analytical technique can detect all compounds abundant in a human cell or bacteria (Saito *et al.*, 2009). Thus, new concepts combining several analytical techniques (multi-parallel approaches) and the data integration need to be elaborated. The analytical workflow in the non-targeted as well as in the targeted investigations of this work integrate state-of-the-art direct-injection ultrahigh resolution mass spectrometry and ultrahigh performance liquid chromatography based on two separation principles. For the data elaboration and interpretation sophisticated statistical analysis as well as new visualization tools are implemented. Since the rising and promising, but still quite young, scientific discipline of metabolomics, needs the implementation of guidelines and standards to avoid false positive discoveries, recommendations of consortia like Metabolomics Standard



Initiative (MSI) have been considered during the experimental work and data reporting (Fernie et al., Castle et al., 2006, Fiehn et al., 2006, Dunn et al.). In summary, the thesis is located in the intersection of analytical chemistry, infection biology and fields of data analysis. An overview of the general structure of the presented work is illustrated in Figure 3:

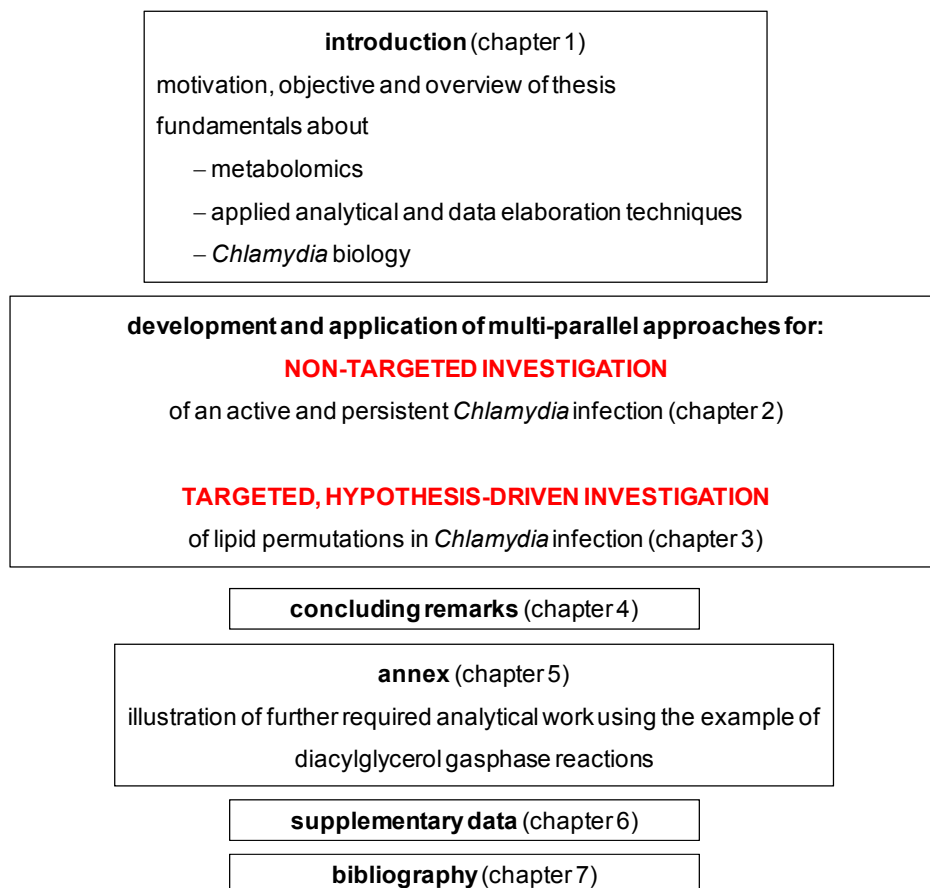


Figure 3: Structure of presented thesis

## 1.2 Metabolites

Metabolites are low molecular weight compounds participating in metabolic reactions. They are attributed with very diverse physicochemical characteristics, ranging from ionic to hydrophobic properties. Furthermore, their concentrations vary in a broad dynamic range (Villas-Boas et al., 2005). The cellular pool of all metabolites, termed as metabolome, results from a permanent chemical transformation, in which metabolites are precursors, intermediates or end products.

Any chemical transformation is hereby subjected to the general mass balance constrain (Bhalla et al., 2005, Soh et al., 2010). The constant input of nutrients from the environment and their assimilation through the metabolism is essential to acquire energy and building blocks for cellular growth, homeostasis and survival (Soh et al., 2010).

The number of existing metabolites in mammals, plants and microbes is still fairly unknown. However, some estimations vary between several hundred thousand and one million (Ott et al., 2006, Dixon et al., 2003). These numbers indicate that our current knowledge may cover only approximately 10% of all existing metabolites.

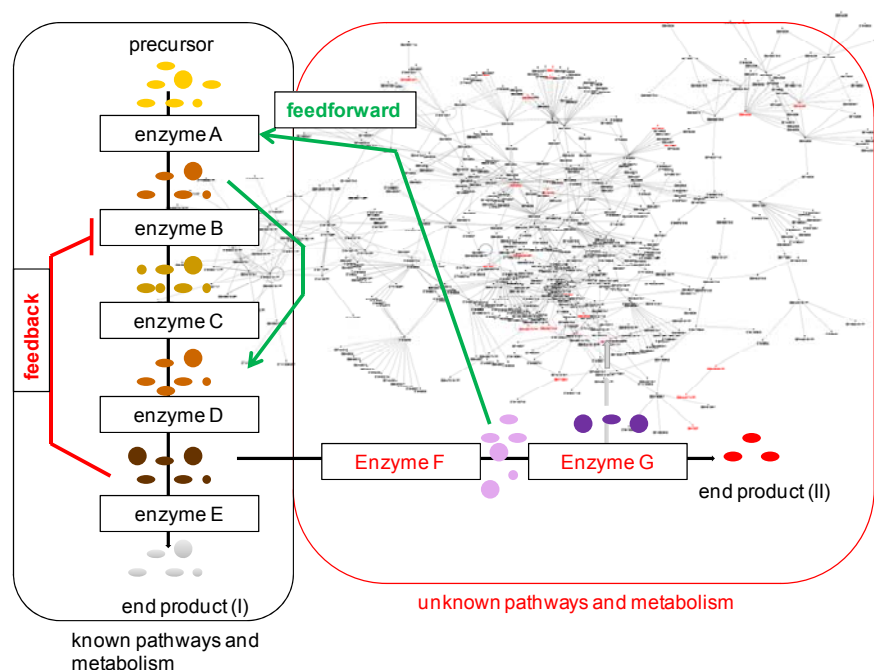


*Figure 4: Assembly of metabolites into pathways and highly connected metabolic network: The metabolism underlies feedback and feedforward regulations. Considering the huge proportion of non-identified metabolites, complete “unknown” pathways are to be expected, which might also influence the “known” metabolism.*

Sets of metabolites are traditionally assembled in pathways, in which the product of one reaction serves as substrate for the next one. The interconnections between such pathways lead to the construction of highly linked metabolic networks (Gruning et al., 2010) (Figure 4). Regulation of this metabolic network occurs at the cellular level of transcription, translation, post-translational modifications or by metabolites. The rate of enzymatic reactions depended on enzyme availability and -properties as

well as substrate and product concentrations. Small important effectors metabolites have been termed “reporter metabolites” (Gruning et al., 2010, Patil et al., 2005). A categorization into two classes is suggested: global and specialized reporters. Whereas global reporter metabolites represent the interconnection between several pathways like ATP or NAD(H), specialized reporters are intermediates in distinct pathways (Fujita, 2009). Changes in global reporter metabolite concentrations or their ratio to each other pinpoints a strong alteration of the metabolism. Instantly, a decreased ratio of ATP:AMP indicates a shortage of cellular energy. Feedback and feedforward control mechanisms are hereby characteristic for metabolic self-regulations, and lead to an adaption of the metabolic processes according to the cellular demand (Gruning et al., 2010).

Taken the above mentioned fact into account, that our current knowledge covers only approximately 10% of existing metabolites, it is very assumable that currently “unknown” compounds might truncate and modulate known pathways. Additionally, this fact shows the existence of completely new metabolic pathways (Breitling et al., 2008). To give just two examples: a novel carbohydrate anabolism and a new pyrimidine catabolism have been discovered in *Escherichia coli* (Fischer et al., 2003, Loh et al., 2006). In consequence, it is absolutely logical that metabolic adaption processes to an external stimulus, like an infection, might affect such „unknown“ metabolites. Another quite reasonable aspect is the influence of intermediates from a novel pathway on the regulation, activation or inhibition of known pathways (Figure 4). The discovery of such „unknown“ intermediates in any infection or disease would offer new therapeutic intervention opportunities.

## 1.3 Metabolomics

### 1.3.1 Definition

As the functional phenotype of a system is characterized by its metabolites, changes in the metabolite pattern reflect environmental and genetic perturbations (Dettmer et al., 2007). The analysis of the entity of metabolites, in general termed as metabolomics, is therefore an important step towards deeper understanding of cellular regulation and adaption processes. This idea was introduced by Oliver and Nicholson in the late 1990ies (Oliver et al., 1998, Nicholson et al., 1999) and the

fascinating scientific discipline of metabolomics has been developing rapidly since that.

Originally, the term metabonomics as “the quantitative measurement of the dynamic multiparametric metabolic response of living systems to pathophysiological stimuli or genetic modification” (Nicholson *et al.*, 1999) has been separated from the terminus of metabolomics, as “a comprehensive analysis, in which all the metabolites of a biological system are identified and quantified” (Fiehn, 2002). Recently, the scientific community mostly uses the phrase metabolomics.

Several termini have been established in the field of metabolomics. Table 1 gives an overview of the used terms and the main applied techniques (Goodacre, 2007):

<b>terminus</b>	<b>aim</b>	<b>preferred analytical technique</b>
targeted metabolite analysis	restricted analysis of several metabolites for verification of <i>a priori</i> hypothesis	HPLC, GS-MS, LC-MS, NMR
metabolite profiling	focus on distinct group of metabolites	LC-MS, CE-MS, LC-NMR, LC-EC
metabolomics	comprehensive analysis of the entire metabolome	LC <sup>n</sup> -MS, GC-MS, ICR/FT-MS, NMR
metabolite flux analysis	analysis of metabolites derived from stable isotope labeled substrates	NMR, MS
metabolic finger-/footprinting	classification of organisms based on their intracellular or extracellular metabolite profile	NMR, MS, MALDI MS, FT IR, RAMAN

Table 1: Terms in metabolomics (Goodarce 2007 modified)

Furthermore, subforms of metabolomics have been developed; according to the analyzed metabolite class several termini are common, like lipidomics for lipid investigations or glycomics for studies of sugar derivates. In particular lipidomics is

growing very fast since lipids are increasingly seen as modulators of cellular functions and second messengers, not to forget their function as structural components.

### 1.3.2 General workflow in metabolomics

The initial step in all metabolomic investigations is the decision of the objective: Shall the study serve the hypothesis generation or shall it verify *a priori* theory? Thus, either a non-targeted or targeted design has to be chosen. Figure 5 illustrates a typical workflow for a non-targeted study.

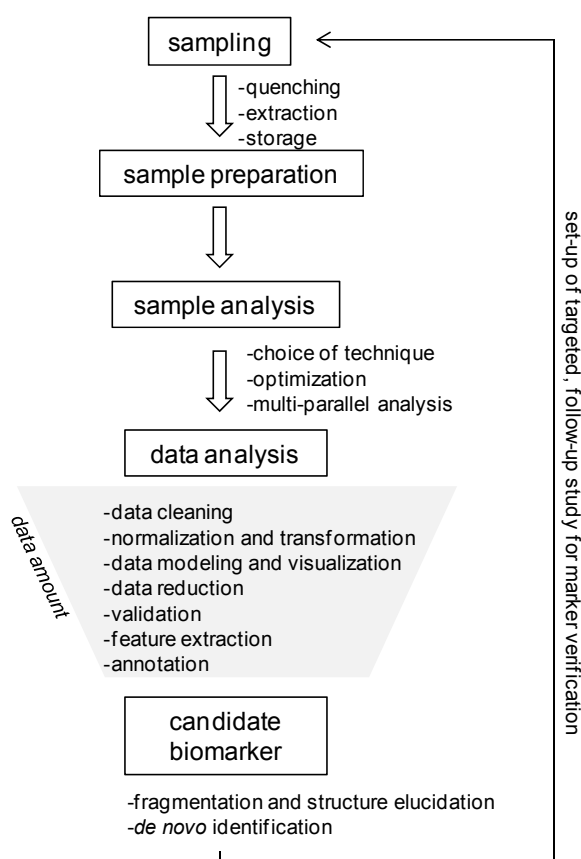


Figure 5: Typical workflow in non-targeted metabolomics: Prior any practical work a sophisticated study design and the number of sufficient biological and technical replicates need to be ensured. Important steps during sampling are quenching, choice of extraction solvents and decision of sample storage. After the sample preparation, which is done according to the needs of the used analytic technique, and sample analysis, a statistical modeling is performed. The data analysis aims at defining of putative biomarkers, which are afterwards identified by MS<sup>2</sup> and/or NMR. Based on the results targeted follow-up studies might be built up.

Moreover, according to the metabolites of interest special requirements need to be considered, for example several lipid species are known to be oxygen and UV radiation sensitive. In consequence, the samples have to be stored in the dark coolness under nitrogen atmosphere or they have to be prepared freshly.

### 1.3.3 Applications and benefit of metabolomics

Nowadays, metabolomics enables to monitor changes in metabolic activity in response to genetic and nutrient perturbations, to decode unknown gene functions (Patil et al., 2005, Saito et al., Ihmels et al., 2004) and investigate processes in disease, infection and during therapeutic treatments (Robertson et al., 2011). Metabolomics will thus improve diagnosis and therapy of divers diseases by e.g.:

- discovery of (pre-) disease markers inferred by metabolite shifting as well as monitoring of health/disease status
- easy and fast differentiation between cancerogenous and healthy tissue
- monitoring and adaption of drug responses, which is required for personalized therapeutic regimes (“personalized medicine”)
- discovery of new lead structures for novel therapeutic agents
- identification of microorganisms via fingerprinting techniques

All these examples might also lead to time-, labor and cost savings and holds therefore economic advantages. Besides its tremendous potential for medicine and biology, also applications in environmental science and bioengineering stand to benefit from metabolomics.

The integration of metabolomics data in the other omics disciplines (proteomics, transcriptomics and genomics), as imposed by systems biology (Figure 6), and thus the combination of all available molecular-biological and phenotypic knowledge will provide by far a more comprehensive understanding of biological processes (Kell, 2006).

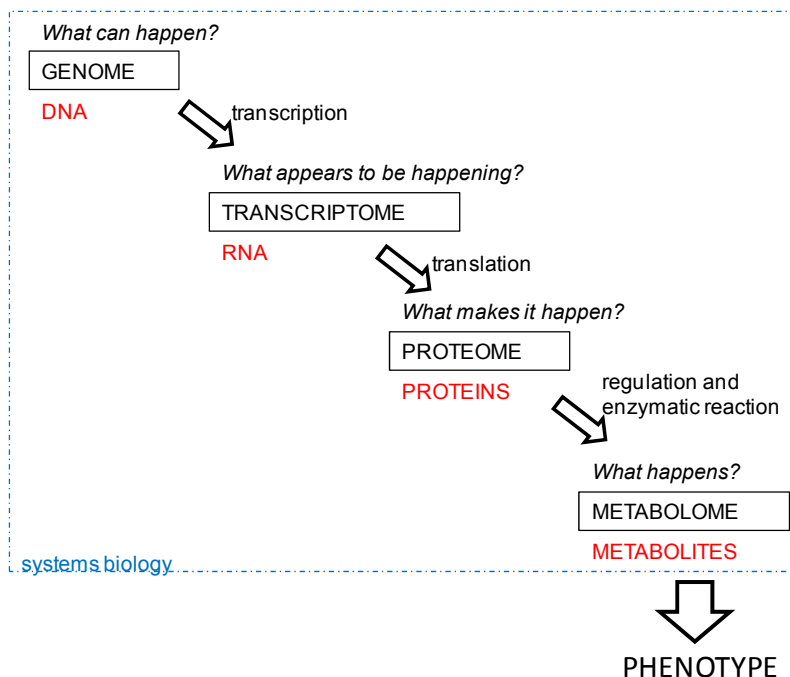


Figure 6: OMICS cascade and central dogma of molecular biology (Dettmer et al. 2007, modified, with permission): The genetic information is transcribed into RNA and thereafter translated into proteins. Proteins may interact with each other, exhibit regulatory functions, serve as structural elements or act as enzymes in chemical transformations of metabolites. The cell's metabolite interior reflects in consequence the final phenotype resulting from regulation and adaptation processes.

#### 1.3.4 Metabolomics of host-pathogen interactions

This thesis is based on medical-biological oriented metabolomics and focuses on host-pathogen interactions. Host-pathogen interactions occur between at least two distinct organisms: between microbes, which can either be pathogens or commensals, and their mammalian host. The ultimate goal of such investigations is the understanding of the underlying biology next to the establishment of a robust framework for therapeutic intervention opportunities and drug development (Forst, 2006). The metabolomic analysis of intracellular pathogens is hereby extremely reasonable, since the host's and pathogen's metabolisms are likely to be strongly intertwined. The parasite needs nutrients derived from the host while the host struggles to maintain its homeostasis (Forst, 2006). Furthermore, the host may have to cope with waste products, toxins and pathogenic factors altering its cell architecture (Forst, 2006). In other words, the infection of a human cell leads probably to a deregulation of its metabolism. Previously, several studies have

focused on the identification of host-pathogen interaction and diagnostic markers for intracellular pathogens like e.g. *Schistosoma* (Wang et al., 2004), *Trichinella* (Martin et al., 2006), *Plasmodium* (Teng et al., 2009b, Olszewski et al., 2009, Li et al., 2008) and *Trypanosoma brucei* (Coustou et al., 2008), but to this day *Chlamydia*-host interactions on a metabolic level have been hardly investigated.

## 1.4 Technologies in metabolomics

Investigations of host-pathogen metabolomics benefit from recent improvements in sampling technologies and analytical developments, like multidimensional chromatography, ultrahigh pressure liquid chromatography and ultrahigh resolution mass spectrometry. Such enhanced analytical possibilities allow the sensitive and simultaneous detection of up to several thousand metabolites (Saito et al., 2009). However, there is no single analytical technique currently capable to detect and quantify all metabolites in one system. This is mainly due to the chemical diversity of metabolites. Nevertheless, technical progress and the development of multi-parallel approaches have made many advances and may lead to the detection of all metabolites in the future. Mass spectrometry (MS), either as standalone instrument or coupled to separation techniques like capillary electrophoresis (CE) or liquid chromatography (LC), and nuclear magnetic resonance spectroscopy (NMR) are the most commonly applied technologies in metabolomic research (Saito et al., 2009).

### 1.4.1 Liquid chromatography

Any chromatography bases on interactions, which do occur between the analytes in the sample and the mobile/stationary phase. These interactions are either of chemical or physical nature. Predominate ones are hydrogen-bridging, dipol-dipol or ion-dipole interactions, van-der-Waals-forces and hydrophobic interactions (reviewed in Buszewski *et al.*, 2011). Based on this multitude of possible interactions and their different strength the partitioning of each analyte in the mobile phase strongly depends on its physicochemical characteristics. Subsequently, the different retention behaviors on the stationary phase can be used for separation of the analytes.



The efficiency of a chromatographic separation can be measured by the number of theoretical plates or (normalized to the length of the column) by the theoretical plate height (HEPT). It is influenced by various factors. This is theoretically explained by the Van Deemter equation. The equation reflects the influences of the lateral or Eddy diffusion (A term), longitudinal diffusion (B term) and mass transfer (C term) on the separation efficiency. Main parameters to be considered are accordingly the particle size ( $d_p$ ) and characteristics of the packing material, the velocity ( $v$ ) and viscosity ( $\gamma$ ) of the mobile phase, as well as the diffusion coefficient ( $D_m$ ) of the analyte in the mobile phase, the retention factor and temperature.

$$\text{HEPT} = A + B/v + Cv$$

$$A = 2\lambda d_p$$

$$B = 2\gamma D_m$$

$$C = \omega d_p^2 / D_m$$

Additionally, aspects like column dimension, column material, mobile phase and gradient set-up need to be considered during the development of LC-MS methods and the ionization process after LC separation should not be forgotten, since a sufficient choice of solvents, additives and pH of the mobile phase can support the ionization (Kostiainen et al., 2009).

In the past years substantial improvements in chromatographic equipment and instrumentation enhanced the separation efficiency and its speed (Guillarme et al., 2009, Lu et al., 2008). The development of UPLC<sup>®</sup> techniques as well as improvements in particle science are to be mentioned at first. They enable high-throughput analysis of very complex samples in short run times. The package of analytical columns with small and homogenous distributed particles results in enhanced efficiency, optimum velocity and mass transfer, but causes also a higher back pressure (Guillarme et al., 2009). UPLC<sup>®</sup> systems usually use sub-2 $\mu\text{m}$  particle sizes and allow a pressure of up to 1000bar. One of the first examples of enhancing the analytical separation and speed by applying of an UPLC<sup>®</sup> instead of a HPLC has been given by Guillarme et al. 2008 (Guillarme et al., 2008).

Matrix effects from which direct injection MS may suffer are decreased by performing LC separation prior to MS injection. Moreover, a differentiation of isobaric compounds can be achieved by chromatographic analysis. The availability of stationary phases with different column chemistries allows the optimal separation



### 1.4.2 Mass spectrometry

Continuous development of mass detectors, improved pumping technologies and stronger magnetic fields enable recently enormous mass resolution and enhanced mass accuracy in mass spectrometry. This is especially the case for ion cyclotron resonance Fourier transform mass spectrometers (ICR/FT-MS), but also other detector types, such as Time of Flight mass spectrometers (ToF), have undergone a large development. During this work the absolutely outstanding ICR/FT-MS (solariX™, Bruker, Bremen, Germany) equipped with a 12 Tesla superconducting magnet has been applied for direct injection experiment and a modern UHR-qTOF mass spectrometer (maXis™, Bruker, Bremen, Germany) served for LC-MS analysis, as it offers the required detection speed.

Mass resolution ( $R$ ) is extremely important when dealing with complex samples, since it describes the ability to differentiate closely located signals from each other ( $m/z$  - mass per charge). It is defined as the smallest difference in  $m/z$  that can be separated (Gross, 2011):

$$R=(m/z)/(\Delta m/z).$$

The resolution power of an instrument is defined as the peak width at a specific percentage of the peak height, usually at 50% (FWHM) (Gross, 2011). Mass accuracy increases with enlarged resolution and determines how precise the measured mass reflects the exact mass. The mass error is commonly calculated as:

$$\text{relative error [ppm]}=(\Delta m/z)/(m/z)\times 10^6.$$

The implemented ICR/FT-MS instrument provides a resolution power of approximately 300,000 (FWHM) at  $m/z$  300 and a mass accuracy <100ppb, and thus allows direct calculation of the elemental composition out of a detected signal. The maXis™ UHR-qTOF instrument on the other hand shows mass accuracies <1ppm and a resolution power of 50,000 FWHM.

### 1.4.2.1 Electrospray ionization

Electrospray ionization (ESI) is an atmospheric pressure soft ionization technique, like also APPI (atmospheric pressure photo ionization) and APCI (atmospheric pressure chemical ionization). It enables almost fragment free ionization of a wide range of polar, hydrophilic compounds, which makes ESI the preferred ionization source in metabolomics (Lu et al., 2008).

The basic working principle of ESI is schematically illustrated in Figure 8. The applied high voltage (3-5kV) at the tip of the ESI needle supplies charge for the analytes. The nebulization of the liquid sample is supported by the nebulizer gas, which is typically nitrogen. Nitrogen is furthermore applied as dry gas, which is heated up to 200°C and supports the solvent evaporation. As a result of gradual solvent evaporation of the nebulized sample the droplet size shrinks and the repulsive coulombic forces between ions in the droplet increase. This leads to a disruption of the charged droplets and production of desolvated ions. A very interesting review about our current knowledge of ESI ionization has been recently given by Kebarle et al. (Kebarle et al., 2009).

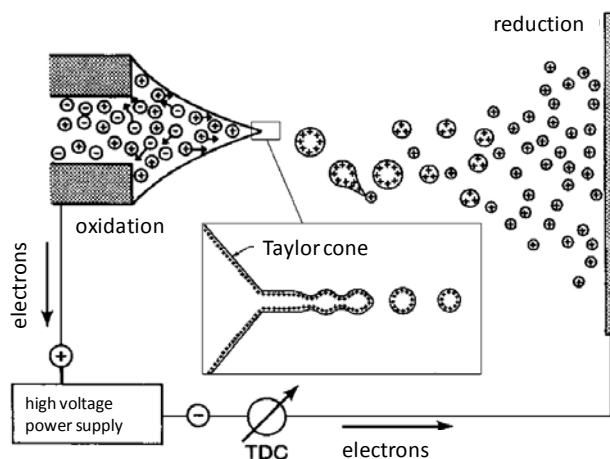


Figure 8: Electrospray ionization (Gross, 2011): The analytes are charged by the applied high voltage at the ESI needle tip. During evaporation of the solvent, which is supported by heated dry gas, the formed ions suffer from increased repulsive coulombic forces. This leads eventually to a disruption of the droplets.

Dependant on the polarity of the applied high voltage analytes of different characteristics can be preferably ionized. If positive ionization is chosen basic compounds, such as amines and amides, are very well ionizable, whereas in

negative mode acidic structures and sugars derivatives are favored to be ionized. The sensitivity is in general better in positive ionization since in this mode ions can be generated by a variety of different mechanisms, like proton or alkali attachments. Further important influencing factors on the ionization process are the ion polarity, pH, presence of salts and concentration of the intrinsic analytes in the sprayed solution (Gross, 2011).

#### 1.4.2.2 *Ion cyclotron resonance Fourier transform mass spectrometry*

Ion cyclotron resonance Fourier transform mass spectrometry combines excellent mass accuracy (<100ppb) and ultrahigh resolution. It enables therefore the distinction of several thousands of ions and the determination of the elemental composition for the detected masses. ICR/FT-MS furthermore offers a high dynamic range, allowing the detection of analytes with very different concentrations. This makes ICR/FT-MS an ideal tool for non-targeted metabolomic analysis. When properly used, similarities and dissimilarities between numerous types of biological samples can be rapidly identified with this outstanding technique (Bhalla et al., 2005). Applications of ICR/FT-MS in the field of metabolomics have been reviewed by Ohta et al. 2010 (Ohta et al., 2010).

A detailed description of ICR/FT-MS fundamentals is beyond this thesis and is given in a number of excellent publications (Marshall et al., 1998, Marshall, 2000, Hendrickson et al., 1999, Heeren et al., 2004, Guan et al., 1995), but a short overview of the instrumentation and principles should be given (Figure 9). An ICR/FT-MS instrument is divided into four main parts, namely the ionization unit, the ion optics, the quadrupole interface and the detector cell. The electrospray generated ions are focused and forwarded through a number of funnel systems and an octapole, where the ions are bunched. A selective ion filtering in the quadrupole is possible. Further accumulation and dissociation of ions can be obtained in the hexapole, before the ionized analytes reach the ICR detection cell.

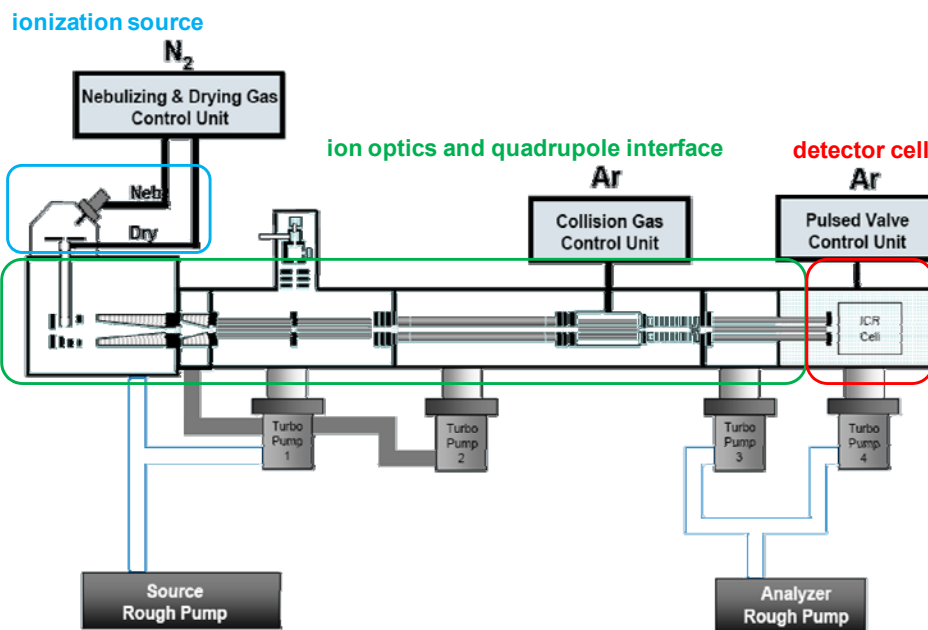


Figure 9: Illustration of ICR/FT-MS (solarix™ Bruker) (Daltonics, 2009): Ions are generated in the ionization source and forwarded through the ion optics unit and the quadrupole interface into the ICR detection cell. The detected signals are frequencies of currents induced by orbiting ions. A Fourier transformation is applied to calculate the corresponding mass spectrum.

The heart of any ICR/FT-MS is the ICR cell, which is embedded in a spatial uniform magnetic field. Within the magnetic field moving charged particles are subjected to the Lorentz Force, which is perpendicular to the magnetic field vector. The magnetic field thus bends the moving ions into orbits (Hendrickson et al., 1999). The Lorentz Force is defined as:

$$F=qvB=ma$$

(F...force; q...charge; v...velocity of the ions;  
B...magnetic field strength; m...mass; a...acceleration)

The second term in the equation gives the general definition of a Newton force. Considering the angular acceleration ( $a=v^2/r$ ) and the angular velocity ( $\omega=v/r$ ) the equation can be transformed into:

$$\omega=qB/m,$$

which defines the cyclotron frequency of an ion within the ICR cell (Hendrickson et al., 1999). Consequently, the cyclotron frequency is only dependent on the magnetic field strength and on the mass to charge ratio.

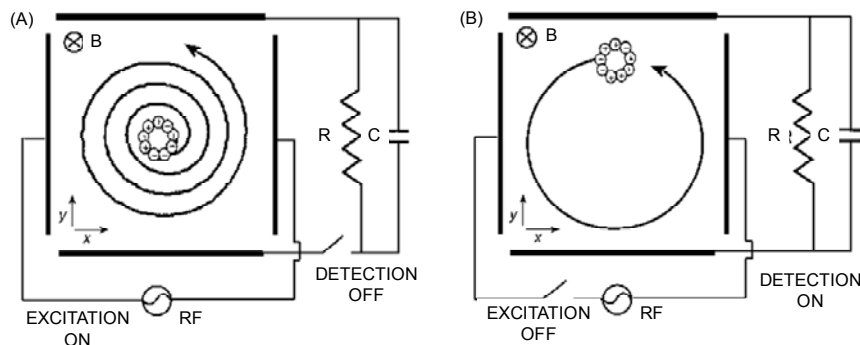


Figure 10: Illustration of (A) excitation and (B) image current detection inside an ICR cell (Gross, 2011). The ion cyclotron motion is indicated by the circular arrow. Two excitation plates are positioned in front of each other and orthogonal to the two detector plates. (A) The implementation of RF electric field results in ion excitation. (B) Ion detection occurs by current induction in the detector plates.

When entering the detection cell each ion moiety is furthermore excited since the initial orbits are too small for detection. Radio frequency (RF) potentials are applied through the excitation plates, which are two outer segments in front of each other and orthogonal positioned to the detector plates (Figure 10). Each  $m/z$  unit will cope with the excitation frequency reaching the resonance. Thus the ions are brought in phase and the orbiting radius of the cycling ions becomes larger and detectable (Barrow et al., 2005).

The detection happens through the induction of current in the detector plates, which is caused by the ion movements. The frequency of the induced current reflects the cyclotron frequency and its intensity corresponds to the number of ions. The frequencies are then converted into a mass spectrum using a mathematical procedure known as Fourier transformation (Barrow et al., 2005).

Another outstanding characteristic of ICR/FT-MS is the MS/MS opportunity. Besides the possibility to perform CID fragmentations (collision induces dissociation) in the hexapole, ICR/FT-MS enables SORI (sustained off-resonance irradiation) experiments inside the ICR cell. The advantage of SORI is the precise isolation of

m/z units. Furthermore, multi-fragmentations ( $MS^n$ ) are possible. The precision in isolation and fragmentation is of high value when dealing with complex samples.

#### 1.4.2.3 Time of flight mass spectrometry

The first Time of flight mass spectrometer (ToF) was constructed and presented by Stephens in 1946 (Gross, 2011). ToF instruments provide several advantages, like e.g.: (i) their speed of detection, (ii) scan free detection of all m/z, (iii) comparable simple construction, design and inexpensiveness relative to ICR/FT-MS and (iv) detection of very small masses (>80 Da) (Gross, 2011). These advantages have presented ToF instruments as one of the most widely used techniques in metabolomics research especially when coupled with LC systems.

The basic principle of ToF-MS is to measure the difference in the required flying times of ions with different mass to charge ratios. Hereby the ions fly along a field free drift path of defined length. Lighter particles will be faster than equally charged heavier ones. The time of flight is proportional to the square root of m/z:

$$t = \frac{s}{\sqrt{2eU}} \sqrt{\frac{m}{z}}$$

(t...time; s...distance; U...voltage; e...electron charge;  
m...mass; z...integer number of charge)

A general overview of the used maXis™ UHR-ToF (UHR - ultrahigh resolution) is given in Figure 11. It is a hybrid QqToF, dual stage reflector instrument, which uses orthogonal ion acceleration. “Q” (capital letter) refers to a mass selective mass resolving quadrupole, whereas “q” indicates a quadrupole collision cell. In this work the hybrid instrument will be generally named ToF.



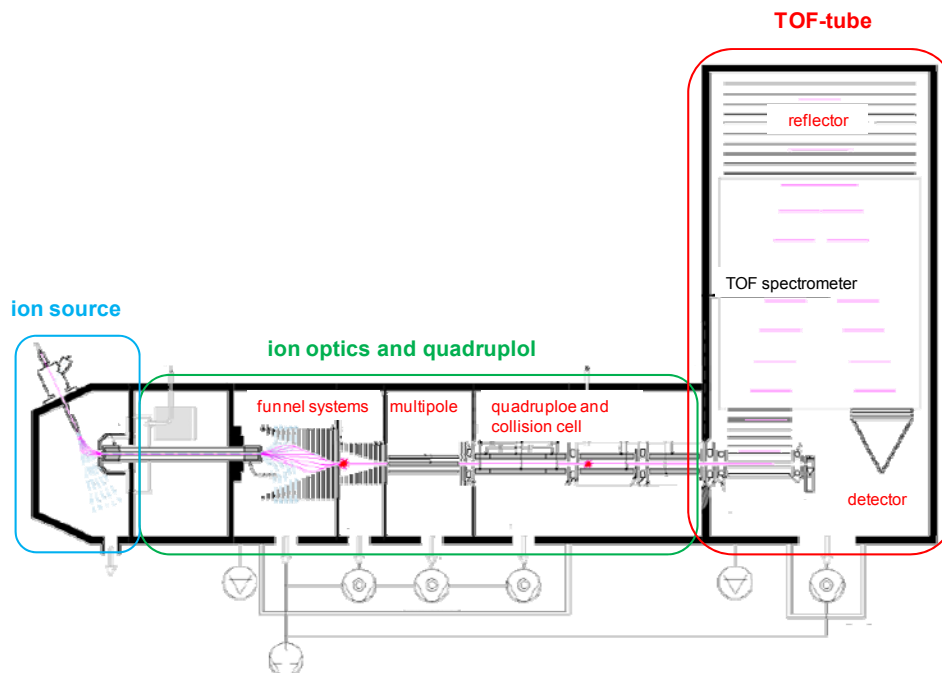


Figure 11: Illustration of maXis™ UHR-ToF (Daltonics, 2008)

Once formed, the ions are forwarded through the funnel system and the multipole. Thereafter a mass-selective quadrupole allows focusing on single  $m/z$  ranges, which can subsequently be fragmented inside the collision cell as a result of linear ion acceleration and collision with argon atoms (CID). The cooling cell is a multipole ion guide, which reduces pressure in the orthogonal acceleration stage (Daltonics, 2008). The ToF tube includes an orthogonal acceleration, reflector and detector unit (Daltonics, 2008). The orthogonal acceleration is used to accelerate ions towards the reflector and ensure hereby that all ions start the journey almost simultaneously (Chernushevich et al., 2001). But even though, they have different linear velocities and positions, which cause slight differences in final kinetic energy. To normalize these energy differences, the implementation of a reflector is crucial (Chernushevich et al., 2001). The reflector, which acts as an ion mirror, improves therefore the mass resolution.  $M/z$  of the same mass having different kinetic energies will penetrate the reflector to different depths, which compensates for their varying starting energies (Daltonics, 2008).

### 1.4.3 Data analysis

Non-targeted analysis generates a tremendous amount of data and requires therefore the application of statistical tools, firstly to discover occurring patterns in the data set and secondly to compress the very large amount of data into smaller, more discernable, informative datasets (Boccard *et al.*, 2010, Lucio, 2008). Two general concepts are here to be distinguished: unsupervised and supervised methods. Unsupervised techniques are usually applied in the first step of data analysis to explore the data set in terms of pattern recognition, as well as to identify outliers and reduce the dimensionality of the data. Supervised techniques are applied to find features that fit a predetermined grouping (Butte, 2002, Boccard *et al.*, 2010). Both techniques allow a visualization of the data.

Prior to modeling a data pre-treatment is usually necessary. This is important when the detected features vary in their intensities in several orders of magnitudes: By performing centering, scaling or/and transformation the features of the data are transformed into the same scale and thus it can be avoided that the resulting model is mainly influenced by high abundant species (Boccard *et al.*, 2010).

#### 1.4.3.1 Unsupervised methods

Principal Component Analysis (PCA) is a strong and frequently used multivariate statistical model. The dimensionality of the data is reduced by transforming the original data into a few linear principle components that account for the maximal variation in a dataset (Lucio, 2008, Boccard *et al.*, 2010). The main information in the data set is hereby conserved (Figure 12). Another advantage of PCA is the fast and powerful visualization of the data, in which samples with comparable metabolite profiles are grouped closely together, whereas those with different metabolite profiles separate from each other. Consequently, PCA also allows the rapid exploration of outliers (Brereton, 2009). It is a key technology in metabolomics.

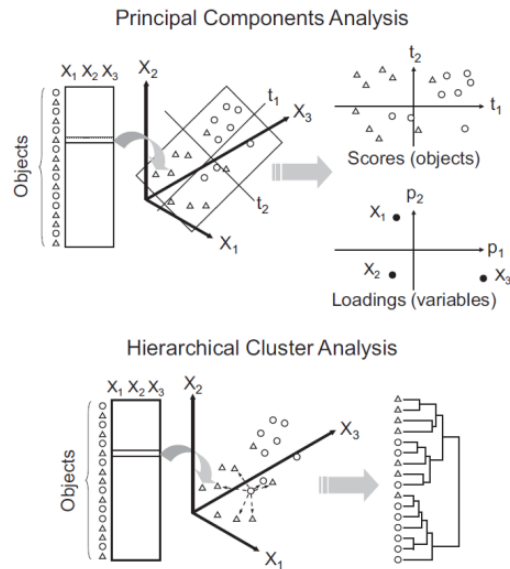


Figure 12: Illustration of PCA and HCA learning principles (Boccard et al. 2010, with permission): PCA projects the multivariate data into a few principal components which account for the maximal variance. HCA clusters the objects by similarity measures. The similarity is calculated by distance and linkage functions.

One further method to reduce the complexity of datasets is Hierarchical Cluster Analyses (HCA). The data is organized into clusters based on similarity and distance measures (Figure 12). The outcome is a dendrogram and a heat map, which illustrates the clusters and the corresponding expression profiles (Butte, 2002).

#### 1.4.3.2 Supervised method

A Partial Least Square-Discriminative Analysis (PLS-DA) can be understood as the regression extension of the PCA (Wold, 1978). In this supervised method the latent variables ( $X$ ) are calculated in purpose to gain a good correlation with the  $Y$  block; the covariance between  $X$  and  $Y$  is maximized. The  $X$  block contains the observations and variables. The  $Y$  block includes the class information. In other words: with the supervised PLS-DA it is possible to extract observations, which are discriminative for one class or the other (Lucio, 2008). Unfortunately, PLS-DA models tend to overfitting, therefore cross-validation and permutation test are essential. For cross-validation parts of the data are kept out during model

development and the model is built up using the remaining data. The kept out data is afterwards predicted based on the generated model, and the predicted and actual values for this data are compared with each other. The difference between the predicted and actual values are squared, summed and expressed as  $Q^2$  (goodness of prediction), which is therefore an index of the validity of the model. The value varies between 0 (no fit) and 1 (perfect fit), values higher than 0.5 are in principle understood as good; if  $Q^2 > 0.9$  the model is excellent (Eriksson, 2006). Furthermore, a permutation test should be performed to verify the model's validity. In this test information from the Y block is randomly permuted. A model is valid, if the values of permuted Y vectors are lower than the original value and the regression of  $Q^2$  intersects below 0.05 (Eriksson, 2006).

#### 1.4.3.3 *Network visualization and elemental formula calculation*

Network calculation has been enabled by an in-house written Matlab program based on an undirected graph (Tziotis et al., 2011), in which the vertices represent the exact masses and the edges are predefined by differences according to common biochemical reactions. A polynomial-time algorithm compares all mass differences in the provided mass list with defined mass differences corresponding to biochemical modulations. A highly connected network and/or several sub-networks are resulting. By knowing the modulation of the elementary composition of each biochemical transformation, it is feasible to calculate the elemental compositions of connected masses as long as at least one single elemental formula is known for the sub-graph. During visualization highly connected nodes are centered and less connected ones are assembled in the periphery. The number of neighbors for one node is referred to as the degree of connectivity. The development and further application of the network calculations is an ongoing work within the dissertation of Dimitrios Tziotis (Research unit Analytical BioGeoChemistry, Helmholtz Zentrum München, Munich, Germany).

The investigation of metabolic networks enables next to visualization the identification of highly connected metabolites. These are probably due to their central position important precursors, intermediates or end products in several pathways. Additionally, novel pathways may be discovered by following along the mass transformation routes.

#### 1.4.3.4 Van Krevelen diagram and Kendrick plot

Due to the expected high complexity of the metabolome data, visualization strategies from scientific disciplines dealing with very complex data matrices have been adapted (Hertkorn et al., 2008, Hughey et al., 2001, Kim et al., 2003). The Van Krevelen diagram displays the hydrogen/carbon (H/C) ratio of molecules against their oxygen/carbon (O/C) ratio. This plot has been initially developed to describe the composition of coal and is currently widely used in the fields of petroleomics and NOM research (Kim et al., 2003, Hertkorn et al., 2008). Applications in metabolomic research have been reviewed by Ohta et al. (Ohta et al., 2010).

In a Van Krevelen diagram it is possible to localize areas of metabolite classes. Since classes of metabolites are specified by different molecular compositions, a first impression of the sample's composition can be obtained. However, even though classes of compounds tend to appear in specific areas, a molecule with a corresponding H/C and O/C ratio does not necessarily belong to this class.

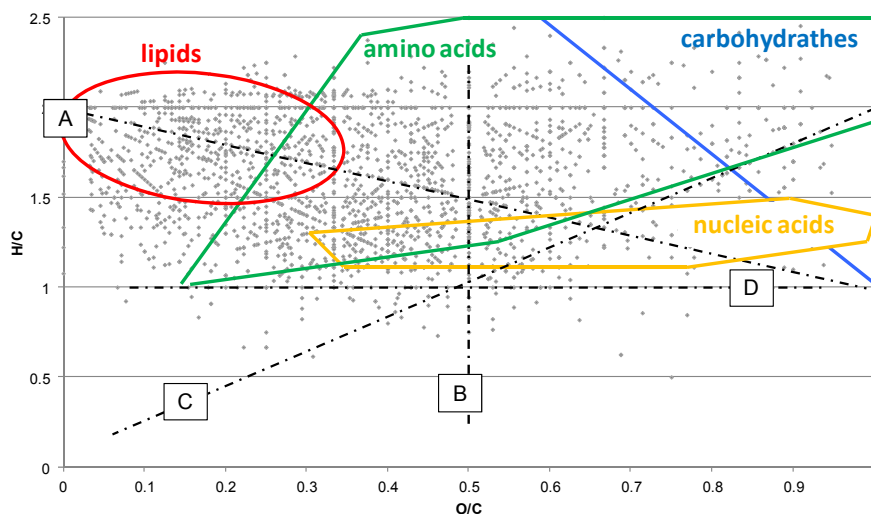


Figure 13: Van Krevelen diagram for (+)ICR/FT-MS data of *Chlamydia* infected human cells. Distinctive areas and lines represent regions of predominant appearance of metabolite classes and formal chemical alterations: (A) methylation/demethylation ( $\pm\text{CH}_2$ ); (B) hydrogenation/dehydrogenation ( $\pm\text{H}_2$ ); (C) hydration/condensation ( $\pm\text{H}_2\text{O}$ ); (D) oxidation/reduction ( $\pm\text{O}$ ) (adapted from Kim et al., 2003, Hertkorn et al., 2008, Schmitt-Kopplin et al. 2010)

A second common plot for visualization and interpretation of complex, ultrahigh resolution mass spectrometry data is the Kendrick plot (Hughey et al., 2001,

Hertkorn *et al.*, 2008). It bases on the fact that each nuclide has a distinct mass defect, depending on its relative binding energy to carbon 12. Thus, molecules of different elemental composition differ in their mass defect and it becomes possible to distinguish series of compounds from each other. In the classical Kendrick plot homologous series differing in their number of CH<sub>2</sub> units, but having the same number of heteroatoms and double bonds are visualized. The mass of CH<sub>2</sub> is therefor converted from 14.01565 to exactly 14.0000. In other words the molecule's mass is normalized to the mass of CH<sub>2</sub> units. Thereafter, the mass defect to the closest integer nominal mass is calculated:

$$KM = \text{IUPAC mass} \times (14/14.01565)$$

$$KMD = NM - KM$$

(KM...Kendrick mass, KMD...Kendrick mass defect; NM... Nominal mass)

This conversion is also possible for any characteristic mass difference, e.g. H<sub>2</sub>, COO or H<sub>2</sub>O (Kim *et al.*, 2003).

## 1.5 Chlamydia

The order *Chlamydiales* is composed of gram negative, obligate intracellular bacteria that infect a wide range of species. Besides the human pathogens *Chlamydia trachomatis*, *Chlamydia psittaci* and *Chlamydia pneumoniae*, symbiotic living and putative pathogenic environmental bacteria exist, such as *Parachlamydiaceae*, *Waddliaceae* or *Simkaniaceae* (Everett *et al.*, 1999, Hackstadt, 1999, Ossewaarde *et al.*, 1999). All in common is a unique biphasic developmental cycle (Figure 14), which is next to rRNA data the fundament for the categorization into this order (Amann *et al.*, 1997, Hackstadt, 1999).

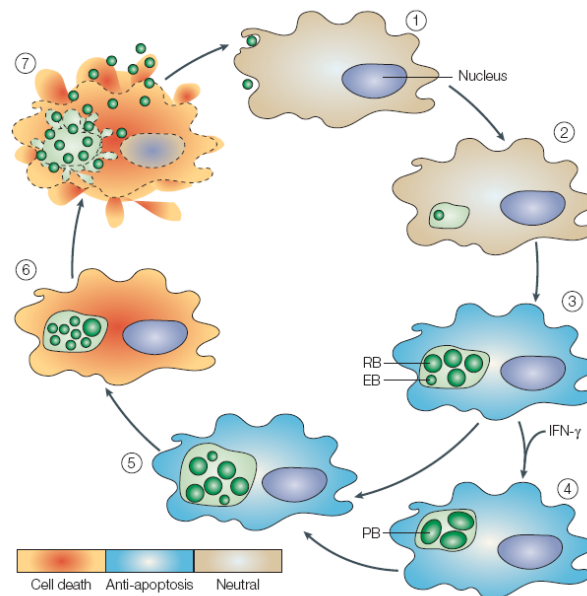


*Figure 14: Developmental cycle of Chlamydiales: (1/2) invasion of infectious EBs into the host cell; (3) intracellular growth and replication of RBs (0-24h p.i.); (4) persistent state (PB); (5) differentiation of RBs to EBs; (6/7) lyses of the host cell (48-72h p.i.). The ability of Chlamydia to interfere with the host cells programmed cell death (apoptosis) is further illustrated (Byrne et al., 2004, with permission).*

The metabolic-inactive but infectious elementary bodies (EB;  $\sim 0.25\text{-}0.3\mu\text{m}$ ) invade the host cell by endocytosis. For this invasion two mechanisms are discussed: either a zipper-like microfilament-dependent phagocytosis (Finlay et al., 1997) or an uptake by receptor mediated endocytosis (Hodinka et al., 1988). However, after the entry *Chlamydia* are surrounded by a host derived vacuole, which is referred to as inclusion, and in which *Chlamydia* stay during the complete developmental cycle. After internalization EBs transform into the bigger, metabolic-active but non-infectious reticulate bodies (RB,  $\sim 0.8\text{-}1.0\mu\text{m}$ ), which proliferate by cell divisions. In the following, RBs transmute back into EBs. This differentiation is asynchronous (Wolf et al., 2000, Hackstadt, 1999). Finally, the EBs are released either by host cell lyses or by exocytosis and a new infection cycle can start (Hybiske et al., 2007). The developmental cycle takes between 36-84 hours in dependency of the strain (Wolf et al., 2000, Hackstadt, 1999).

Additionally, *Chlamydia* can transmute into a persistent state triggered by external stimuli like nutrient depletion, interferon- $\gamma$  (IFN- $\gamma$ ) addition or antibiotic treatment (Beatty et al., 1994a, Beatty et al., 1993, Beatty et al., 1994b, Coles et al., 1993,

Harper et al., 2000, Raulston, 1997, Shemer et al., 1985). Persistence is defined as a culture-negative long term association between *Chlamydia* and the host, which may remain for years (Rottenberg et al., 2002). The big aberrant bodies show an atypical morphology. Their replication is either slowed down or stopped. Persistent *Chlamydia* are non-infectious but metabolic active (Rottenberg et al., 2002). The inclusion is smaller than in the active infection. After omission of the causing stimulus *Chlamydia* return to the normal replication (Beatty et al., 1994b).

### 1.5.1 *Chlamydia-associated diseases*

*Chlamydia* are among the most prevalent bacteria worldwide. They are responsible for millions of infections as well as an economic burden of billions of dollars year by year (Wyrick, 2000). The prevalence, tissue tropism and clinical consequence of *Chlamydia* infections are strongly strain dependent. The most prominent human pathogenic strains are *C. trachomatis* and *C. pneumoniae* (Wyrick, 2000).

The current gold standard in the diagnosis of *Chlamydia* infection is a combination of PCR (polymerase chain reaction), LCR (ligase chain reactions) and cell culturing. An active infection is treated with antibiotics like, macrolides (e.g. azithromycin) or tetracyclines (e.g. doxycycline). In a persistent infection the sensitivity against antibiotics is strongly decreased (Reveneau et al., 2005).

#### 1.5.1.1 *Chlamydia trachomatis*

*C. trachomatis* serovar A-C are the worldwide leading causes for infection caused blindness. More than 84 million people in 56 countries suffer from an active trachoma and more than 8 millions are visually impaired (WHO, 2012b). The highest prevalence occurs in very poor regions, where especially children under five years of age and their mothers are infected. The infection is transmitted from person to person by close contact e.g. through infectious eye discharge or contaminated personal belongings like towels. Additionally, the infection can be spread by insects (Schachter, 1999). A characteristic roughening of the inner surface of the eyelid is caused. If the so called granular conjunctivitis stays untreated and breaks out



recurrently a painful form of permanent blindness is the consequence (Schachter, 1999). The eyelid turns inward and makes the eyelashes scratching the cornea.

Serovar D-K are causative agents of sexual transmitted diseases. An infection leads to an inflammation of the urogenital tract. Unfortunately, most infections (70-75%) are asymptomatic for both men and women (Schachter, 1999, WHO, 2012a, WHO, 2001). Anyway, in most cases males only serve as carriers of the bacteria, spread the infection and do not suffer from long term consequences. In contrast females are at high risk for complications like pelvic inflammatory disease, ectopic pregnancy, infertility and chronic pelvic pain if the probably unnoticed infection becomes chronic (Schachter, 1999, WHO, 2012a, WHO, 2001). *C. trachomatis* infections are the most frequent reason for unintentional childlessness in the western hemisphere (WHO, 2012a, Schachter, 1999, Peeling et al., 1996). The prevalence is especially high amongst young women (24-27%) (WHO, 2001).

Further sexual transmitted serovars are L1-L3, which lead to a Lymphogranuloma venereum, an infection of local lymph nodes. Most cases are diagnosed in tropic and subtropic regions (Schachter, 1999).

#### 1.5.1.2 *Chlamydia pneumoniae*

The spread of *C. pneumoniae* is estimated to 50-70% of the population in western countries. The first infection usually occurs during the childhood and youth. In the age class of young adults the prevalence reaches 20% and increases thereafter further to around 70% (Schachter, 1999, Kuo et al., 1995). Re-infections are a common phenomenon and the infection is transmitted from human to human (Blasi et al., 1998).

The *C. pneumoniae* cause different respiratory diseases. Infections are responsible for approximately 5% of all bronchitis and sinusitis cases, as well as for 5-10% of the community acquired pneumoniae worldwide (Lim et al., 2001). Typical symptoms are unspecific, like during a cold, but anyway most infections are asymptomatic. *C. pneumoniae* recurring or persistent infections are linked to chronic pulmonary diseases, such as COPD and Asthma (Blasi et al., 1998, Branden et al., 2005, Hahn et al., 2012). In fact, a systematic spread of *Chlamydia* in the organism can occur

through infection of circulating monocytes, macrophages or lymphocytes (Quinn et al., 1999, Moazed et al., 1998, Gieffers et al., 2004), which may contribute to the development of Atherosclerosis, Alzheimer's disease or cardio vascular diseases (Blasi et al., 1998, Fazio et al., 2009, Shima et al., 2010).

### 1.5.2 *Previously described metabolic host-pathogen interactions between Chlamydia and the human host cell*

Analysis of obligate intracellular bacteria suffer from the absence of host free cultivation systems and lack of genetic manipulation opportunities. Investigations of the chlamydial metabolism need strategies to overcome these drawbacks. This is achieved by e.g. comparison of infected cells and non-infected ones, or inhibition of specific pathways either in the eukaryote or prokaryote (McClarty, 1999).

Despite the limitations several specific aspects of the metabolism of intracellular *Chlamydia* have been investigated and our knowledge of these fascinating bacteria has been increased during the last years. Previously, a number of excellent reviews have been given on the topic (Wyrick, 2000, Pavelka, 2007, Moulder, 1991, La et al., 2008, Cocchiaro et al., 2009, Blasi et al., 1998, McClarty, 1999). Sequencing of the chlamydial genome additionally delivered information about the putative metabolism (McClarty, 1999, Kalman et al., 1999, Stephens et al., 1998). Now, a short summary of our current knowledge about chlamydial metabolism and host-interactions should be given. Earlier studies have mainly focused on:

- (i) lipid modulation and -trafficking in infected cells
- (ii) influence of amino acid availability from the cell culturing media on bacterial development
- (iii) *Chlamydia* as an “energy parasite”
- (iv) the “peptidoglycan paradox” of the gram-negative *Chlamydia*

(i) Typical eukaryotic lipid species have been detected in purified *Chlamydia*, like several glycerophospholipids, sphingomyelins and cholesterol (Wylie et al., 1997, Hatch et al., 1998, Hackstadt et al., 1996, Carabeo et al., 2003, Su et al., 2004, Moore et al., 2008, Liu et al., 2010, Heuer et al., 2009). The eukaryotic nature of

these lipids suggests that they are host-derived. A vesicular transport from the human Golgi apparatus to the chlamydial inclusion is discussed (Heuer et al., 2009, Carabeo et al., 2003). Alternatively, a transport by multivesicular bodies or lipid droplets may also be involved in lipid delivery to the inclusion (Kumar et al., 2006, Beatty, 2008). Whereas sphingolipids and sterols are utilized by *Chlamydia* without any modification (Wylie et al., 1997), an incorporation of branched-chain fatty acids in sn-2 position has been described for glycerophospholipids. The necessity of sphingolipids for chlamydial growth, inclusion biogenesis and reactivation of a persistent infection has been revealed by Van Ooij et al. (van Ooij et al., 2000). Azenabor et al. have investigated the cholesterol depletion in macrophages related to the biosyntheses of glycerophospholipids after infection. The experiments indicated a shift in the ratio of sterol:phospholipid content in the host cell membrane from 1:2 to more than 1:4. This leads to an increased membrane fluidity, enhanced membrane fragility and higher adherence to epithelial cells. All these effects are linked to the progression of several disease (Azenabor et al., 2005). A further study has evidenced a diacylglycerol accumulation in the inclusion, which influences the host cell apoptosis mechanisms (Tse et al., 2005).

(ii) *Chlamydia* are capable of de-novo protein synthesis (Becker, 1978), thus experiments modulating the ingredients of the cell culture media have been performed analyzing the influence on the bacterial development. Allan et al. have used culturing media missing one amino acid to study the effect on chlamydial growth and transformation during the developmental cycle (EB→RB→EB). It has been described that a leakage of cysteine hinders the transformation of *Chlamydia* RBs to EBs. A reasonable explanation might be the requirement of cysteine for cysteine-rich proteins (Allan et al., 1985). Furthermore, an omission of leucine, glutamine, histidine, phenylalanine or valine reduces the inclusion size and interfere substantially with bacterial growth. In another study the authors have shown that leucine, phenylalanine und valine omission inhibits chlamydial multiplication, whereas, isoleucine, glutamine and tryptophan absence leads to a reduction of infection progeny without influencing the number of infected cells (Allan et al., 1983).

Abromaitis et al. have described an aromatic acid hydroxylase for the hydroxylation of phenylalanine, tyrosine and tryptophan (Abromaitis et al., 2009). They have speculated that the enzyme may have an important role in shaping the metabolism due to the high conversion in several *Chlamydia* strains. Furthermore, they have

described that minor changes in *Chlamydia* metabolism can strongly influence strain specific biology.

(iii) For nearly 40 years it has been believed that *Chlamydia* are energy parasites incapable of the biosynthesis of ATP (adenosine triphosphate) and high energy intermediates. This hypothesis has mainly based on the missing detection of enzymes in glycolysis, ATP generation and electron transport chain in *Chlamydia* (Moulder, 1991). In 1999 Iliffe-Lee and McClarty identified enzymes for carbohydrate catabolism (glycolysis and pentose phosphate pathway) and ATP generation in *C. trachomatis* (Iliffe-Lee et al., 2000, Iliffe-Lee et al., 1999). These findings have been supported by a shotgun proteomics approach (Skipp et al., 2005), which has revealed enzymes for glycolysis und pentose phosphate pathway in both RBs and EBs. Saka et al. have further investigated the proteome of *C. trachomatis* (Saka et al., 2011). Proteins of the central metabolism and of the glucose catabolism have been identified predominantly in EBs. RBs are geared towards nutrient utilization, increasing cellular mass and securing the resources for a transformation back into EBs. An investigation of the ATP related metabolism and glycolysis has been presented by Ojcius et al. (Ojcius et al., 1998). *C. psittaci* have been cultured for two days and investigated by NMR. An increased ATP level in the mid cultivation time has been described. In addition glutamate levels have been elevated and the glutamate synthesis correlated with the developmental cycle. Glucose consumption and enhanced lactate levels as well as a high expression of GLUT-1 (glucose transporter 1) have been found. However, even though we know now, that *Chlamydia* are in general capable of ATP synthesis, the major amount of ATP is delivered from the host in exchange for ADP (adenosine diphosphate) through nucleotide transporters. This transport has been initially described by Hatch et al. for *C. psittaci* and has been further verified by Trentmann et al. (Hatch et al., 1982, Trentmann et al., 2007). Whereas in a persistent infection the ATP production relies mainly on the host, in an acute infection the hosts' ATP is supplemented by the bacterias' own ATP synthesis (Gerard et al., 2002).

(iv) *Chlamydia* are sensitive to penicillin, equipped with the genes for peptidoglycan synthesis via aminotransferase pathway (McCoy et al., 2006) and important enzymes have been detected in a proteome analysis (Skipp et al., 2005), but it has never been achieved to detect chlamydial peptidoglycans. A very interesting review on this part of chlamydial metabolism has been given by Pavelka (Pavelka, 2007).

Moreover, a dependency of chlamydial growth on cofactors and vitamins has been examined. It has been described that *Chlamydia* fail to grow and replicate in thiamine lacking cell culturing media, but the deficiency of other B vitamins have not shown any comparable effect (Moulder, 1991). Lazarev et al. have identified decreased glutathione (GSH) levels after infection due to utilization of GSH for reduction of disulfide bonds during the initial stage of infection (Lazarev et al., 2010). Additionally, it has been described that host cells infected with *Chlamydia* produce proinflammatory chemokines, cytokines, growth factors and other cellular modulators (Stephens, 2003).

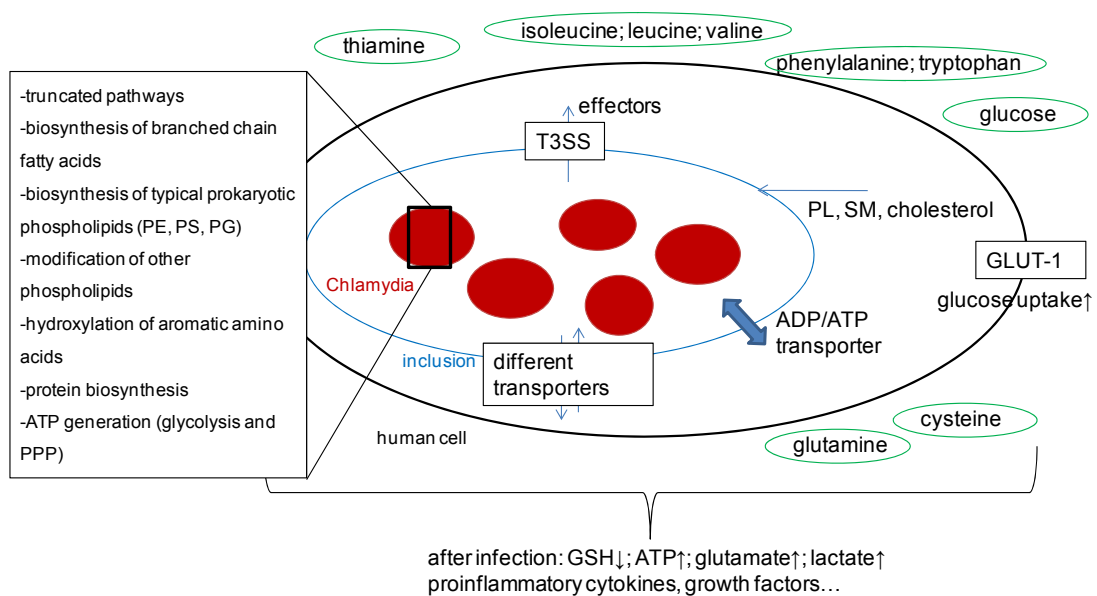


**Figure 15:** Summary and illustration of the described metabolic processes in infected human cells as well as important medium components (in green ellipses) (PPP pentose phosphate pathway, SM sphingolipids, PL glycerophospholipids, PE glycerophosphoethanolamines, PS glycerophosphoserines, PG glycerophosphoglycerols, T3SS type three secretion system)

### 1.5.3 Hypoxia and the impact of oxygen environment on *Chlamydia* infection

The oxygen content in different tissues of the human body varies between 0.5 and 14% (reviewed in Carreau et al., 2011). Under hypoxia the oxygen requirement in the tissue exceed the oxygen abundance (Bosco et al., 2008). A hypoxic environment can be found in several pathophysiological processes, like in inflammation, fast growing solid tumors, vascular blockage like in apopleptic stroke or heart attack. Hypoxia results in an activation of several adaption mechanisms, which

all aim at the maintenance of cellular functions and homeostasis. The most important one is the stabilization of the transcriptional factor HIF-1 (hypoxia-inducible factor). HIF-1 consists of two heterodimers, HIF-1 $\alpha$  and HIF-1 $\beta$ . In presence of oxygen HIF-1 $\alpha$  is iron-dependent degraded, whereas in the absence of oxygen this subunit is stabilized and binds to HIF-1 $\beta$  after translocation in the nucleus. As a result a multitude of hypoxia relevant cellular processes are activated to maintain homeostasis (Bruick *et al.*, 2001, Carreau *et al.*, 2011, Dietz *et al.*, 2011, Peyssonnaud *et al.*, 2005).

Recent studies evidence the stabilization of HIF-1 also in normoxic environment during an infection with several bacteria, viruses, fungi and parasites (reviewed in Dehne *et al.*, 2009, Dietz *et al.*, 2011). Underlying mechanisms seem to involve the reduction of intracellular oxygen content after bacterial infection, the competition for iron between the human cell and the pathogen, direct ligand-receptor or transcriptional interactions. A stabilization of HIF-1 in the early development of *Chlamydia* has been described under hypoxic and normoxic environment (Rupp *et al.*, 2007). In the later chlamydial developmental HIF-1 has been depleted probably to avoid host cell apoptosis. Additionally, an increased chlamydial inclusion size as well as accelerated replication has been documented under hypoxia (Juul *et al.*, 2007). Moreover, when HIF-1 had been blocked during the early stage of *Chlamydia* infection under normoxic conditions, a decreased number of infected cells have been found (Rupp *et al.*, 2007). Since HIF-1 leads to an increased expression of glucose transporter GLUT-1 and thus enhances glucose uptake, the chlamydial growth is enhanced (Rupp *et al.*, 2007).

Now, a brief overview of previous studies focusing on the effect of hypoxia on the cell metabolism is given. This is important to understand the results of the later presented non-targeted metabolomics approach:

Glucose can be metabolized into pyruvate via glycolysis in aerobic and anaerobic condition. Under normoxia pyruvate is transported into the mitochondria and is completely degraded into carbon dioxide and water within the TCA cycle (tricarboxylic acid cycle) and respiratory chain. In contrast under hypoxia, HIF-1 induces the expression of PDK1 (pyruvate dehydrogenase kinase 1), limiting the transformation of pyruvate into acetyl-CoA via inhibition of PDH (pyruvate dehydrogenase). In consequence, the TCA cycle activity and oxygen consumption is

reduced. The glycolysis remains the main source of ATP and declined ATP levels are evidenced in lower oxygen atmosphere since the glycolysis delivers much less ATP. Furthermore, an activation of LDHA (lactate dehydrogenase A) is stimulated via HIF-1, lactate is therefore increasingly produced (Semenza, 2007) and an intracellular acidosis is resulting.

An additional cellular process occurring under hypoxia is autophagy. Autophagy is a catabolic process involving the degradation of cellular components through the lysosomal machinery (Kroemer et al., 2010, Wilkinson et al., 2009). An enrichment of metabolites originating from protein- and lipid catabolism can be found, like e.g. kynurenine (tryptophan catabolite) and acyl-carnitine derivatives (fatty acid catabolites) (Frezza et al., 2011).

Moreover, an increased glutamine and leucine import has been revealed under hypoxic conditions (Soh et al., 2007). The cellular pools of aromatic amino acids, like phenylalanine and tyrosine, as well as alanine and valine are elevated, whereas cellular levels of leucine, methionine and glutamate have been found to be decreased. The concentration of histidine stays unaltered (Gleason et al., 2011, Perrin et al., 2002). A glucose independent glutamineolysis has been proposed by Le et al. (Le et al., 2012). In another study the concentrations of leucine, phenylalanine, tyrosine, lysine as well as hydroxybuturate, a downstream product of amino acid catabolism, has been increased (Weljie et al., 2010). Furthermore, a cellular glycogen accumulation under hypoxic conditions has been revealed by Pescador et al. (Pescador et al., 2010).

Studies investigating lipid modulations under hypoxia have shown an accumulation of dihydroceramide and a decrease in unsaturated very long fatty acids (Yin et al., 2009), as well as a modulation of eicosanoids (Shalinsky et al., 1989) and phospholipids (Stubbs et al., 2003, Griffiths et al., 2003, Glunde et al., 2008). A loss of essential sterols and unsaturated fatty acids has been found under hypoxia in yeast by Gleason et al. (Gleason et al., 2011).

The first global analysis of hypoxia induced processes has been performed by Swiderek et al. (Swiderek et al., 2008), who have shown an up-regulation of 53 genes and down regulation of 154 genes. Pathways that have been significantly changed are pyrimidine metabolism, purine metabolism, pentose phosphate pathway, fructose and mannose metabolism, glycolysis/gluconeogenesis, galactose

metabolism, inositol metabolism and one carbon pool by folate. A further profiling of the modulated metabolism under hypoxia has been given by Frezza et al. (Frezza et al., 2011).

Additionally, inflammatory processes are promoted under hypoxia and this might be important particularly in connection with *Chlamydia* infections (reviewed in Eltzschig, 2011).

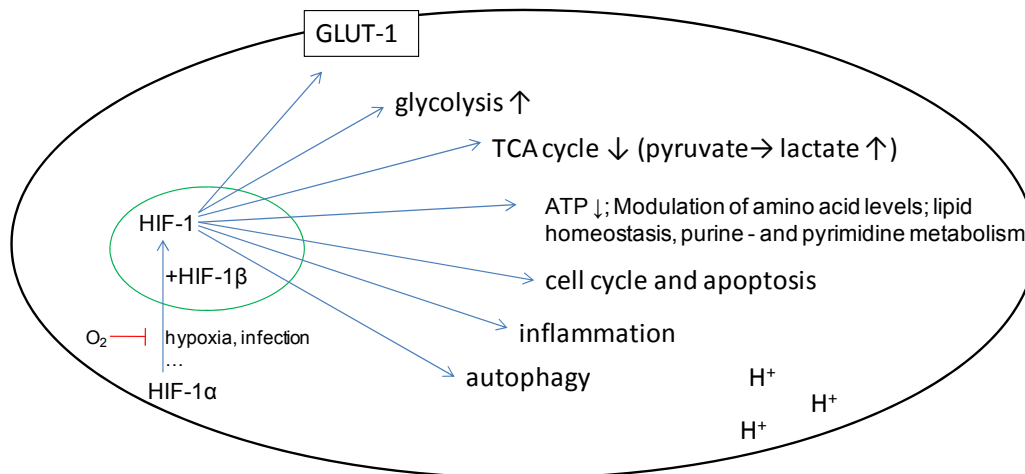


Figure 16: Summary and illustration of the described metabolic processes under hypoxia

#### 1.5.4 The role of IFN- $\gamma$ in the human immune response to *Chlamydia* infection

Intracellular pathogens pose a high challenge for the defense mechanisms of the immune system. After invasion and infection of epithelial cells proinflammatory interleukins and chemoattractants are released (Lu et al., 2000, Rasmussen et al., 1997), thus cells of the innate immune response are recruited to the areas of primary local infection. The immune cells recognize *Chlamydia* through so-called pathogen-associated molecular patterns (PAMPs) and phagocyte the pathogen (Darville, 2006). In consequence, effector molecules like IFN- $\gamma$  are released by the immune cells (Darville, 2006). Additionally, the adaptive immune system, in particular CD4<sup>+</sup> T cells, plays a key role in the host response (Rank, 2006). Stimulated CD4<sup>+</sup> T cells differentiate into Th1 and Th2 cells (Rank, 2006). The Th1 response is important for eradication of *Chlamydia*, since Th1 cells secrete IFN- $\gamma$ , which shows anti-chlamydial activity (Rank, 2006). IFN- $\gamma$  is a strong activator of IDO



(indoleamine 2,3-dioxygenase) leading in a depletion of tryptophan. The activation of IDO has been shown to inhibit the chlamydial growth (Summersgill et al., 1995, Thomas et al., 1993). Interestingly, the effect of IFN- $\gamma$  is concentration dependent, higher levels lead to an eradication of the pathogen, lower ones induce persistence (Beatty et al., 1993).

Recurring and persistent infections suggest an escape of *Chlamydia* from the defense mechanism. Instantly, *Chlamydia* can internalize, survive and replicate in a multitude of immune cells like monocytes, macrophages, dendritic cells lymphocytes and granulocytes (Gieffers et al., 2004, Moazed et al., 1998, Quinn et al., 1999). An infection of immune cells may cause a systemic spread of *Chlamydia* infection and contributes to the progression of chronic diseases (Blasi et al., 1998, Gieffers et al., 2004, Azenabor et al., 2005). Furthermore, *Chlamydia* are capable to inhibit the fusion of the inclusion with the host cells' lysosome, which would normally occur and mimic the host's lipids composition by incorporation of sphingolipids, glycerophosphocholines, glycerophosphoinositols or cholesterol into the inclusion (Carabeo et al., 2003, Hackstadt et al., 1996, Hatch et al., 1998, Wylie et al., 1997, Fields et al., 2002). Additionally, *Chlamydia* trigger already during its early internalization a series of events priming the host cell for a productive infection, e.g. rearrangement of the host cell cytoskeleton (Wyrick, 2000). The chlamydial type three secretion system (T3SS) functions hereby as a 'molecular syringe', providing the opportunity to inject virulence-related proteins into the cytoplasm of host cells (Hueck, 1998, Wyrick, 2000). Additionally, a secretion of the chlamydial protease CPAF (chlamydia protease-like activity factor) into the host cell reduces the expression of MHC class II complexes (major histocompatibility complex) by degradation of a human transcription factor (Zhong et al., 2001, Zhong et al., 1999). Another example is the ability to either provoke or inhibit the host cell apoptosis during different developmental phases (Byrne et al., 2004).

## 2 Molecular cartography in acute and persistent *C. pneumoniae* infections – a non-targeted metabolomic approach

### 2.1 Introduction

Metabolites play an important role in cell biology. They reflect genetic and environmental perturbations, and exhibit regulatory functions. In non-targeted studies the metabolism is investigated on a holistic level. Usually two, e.g. ill or healthy, or more phenotypes are compared with each other and statistically significant different metabolite patterns are determined. Investigations on the metabolism of the intracellular pathogen *Chlamydia*, have been in general rated as challenging, since host free cultivation and genetic transformation models are missing (McClarty, 1999). In consequence, our current knowledge about this interesting pathogen and its interactions with the human host cell is quite limited.

In particular persistent *Chlamydia* infections are a huge clinical problem. The underlying biology has never been investigated on a metabolome level. Therefore, a non-targeted metabolomics cell study has been initiated in collaboration with Inga Dietz and Prof. Dr. Jan Rupp and is presented. The study design includes different oxygen conditions as well as the addition of IFN- $\gamma$  to the cell cultures to stimulate both active and persistent infections (Figure 17). The investigation of the host-pathogen interactions in active and persistent *Chlamydia* infection promises an improved biological understanding, new diagnostic markers as well as therapeutic intervention options. Additionally, the study aims at the discovery of new details as starting points for future targeted follow-up studies.

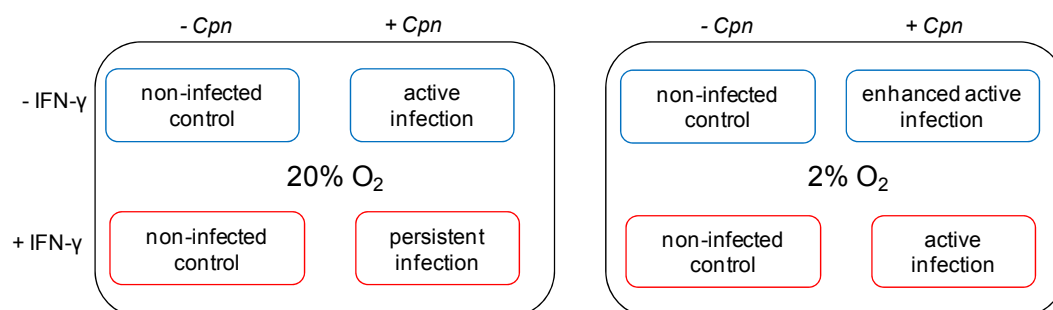


Figure 17: Illustration of experimental design: *C. pneumoniae* (*Cpn*) infection in different environmental conditions (oxygen content of 20% and 2%, and combination with IFN- $\gamma$  addition). The cultivation of infected cells in these different conditions leads to an active, a persistent or an enhanced active infection. Under hypoxia (2% O<sub>2</sub>) the effect of IFN- $\gamma$  is abolished and persistence does not occur.

A contribution of hypoxia to many pathophysiological processes and to the pathogenesis of several microorganisms is well evidenced (reviewed in Dehne *et al.*, 2009, Dietz *et al.*, 2011). *Chlamydia* stabilizes HIF-1, the major transcription factor to maintain cell homeostasis in low oxygen atmosphere, during the early developmental stage (Rupp *et al.*, 2007). Furthermore, an increased infection rate and faster developmental cycle of the pathogen under hypoxia have been reported (Juul *et al.*, 2007). IFN- $\gamma$  is a common agent to induce chlamydial persistence. Physiologically, IFN- $\gamma$  is the predominant cytokine provided by immune cells against *Chlamydia*, thus the addition of IFN- $\gamma$  in cell culture can be understood as simulation of one part of immune response to infection. Interestingly, the antichlamydial effect of IFN- $\gamma$  is inhibited under hypoxic conditions, resulting in a sustained active infection (Roth *et al.*, 2010, Dietz *et al.*, submitted) (Figure 18).

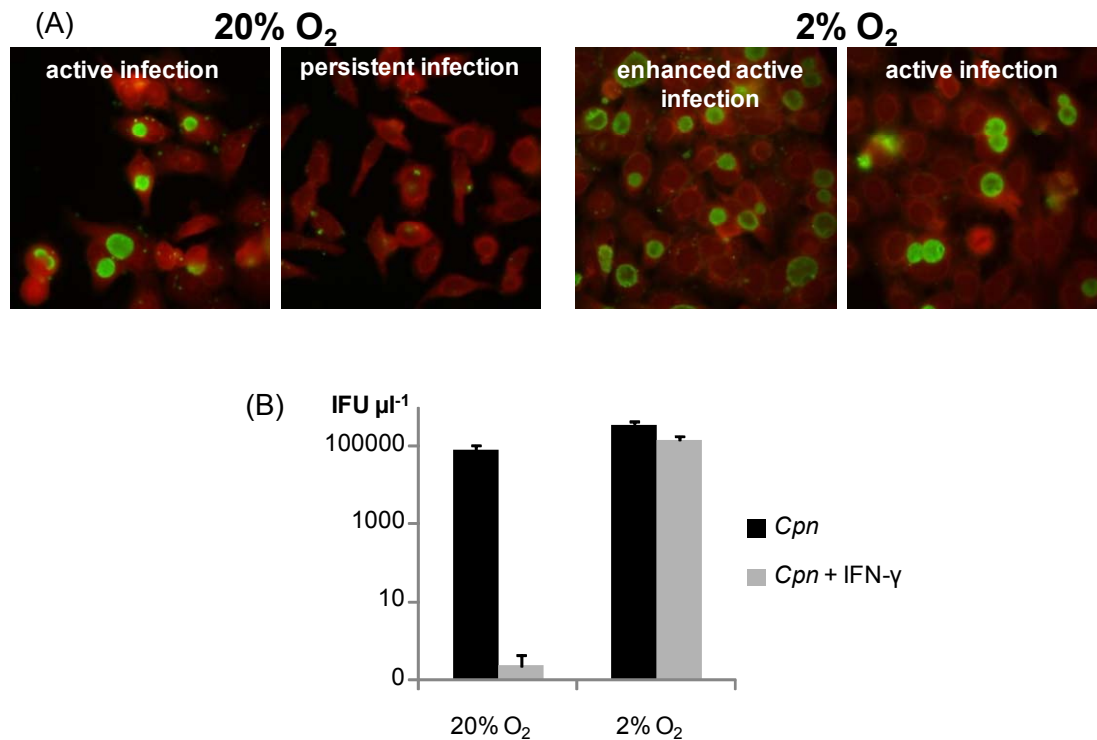


Figure 18: Effect of the investigated conditions on chlamydial development: (A) immunofluorescence staining 48h p.i. (FITC-labeled anti-*Chlamydia* LPS antibody) (Dietz *et al.* 2012, submitted); (B) infection forming units (IFU) after 72h p.i. (Dietz *et al.* 2012, submitted). The antichlamydial effect of IFN- $\gamma$  is abrogated in 2% oxygen atmosphere.

The metabolic alterations after *Chlamydia* infection is investigated analyzing human cells and the intracellular *Chlamydia*, together. Thus, it should be clarified that any

detected modification of the metabolism compared to non-infected cells can result either from bacterial or human cellular processes alone, or from their combined activity. The origin might be deeper investigated in follow-up studies.

Four main reasons led to the decision:

- (i) A clean-up of *Chlamydia* e.g. by density gradient centrifugation causes enormous mechanical stress for the bacteria and thus might induce changes in their metabolite profile. However, human contaminations are anyways unavoidable, since chlamydial reticulate bodies (RB) tend to have the same density like human mitochondria (McClarty, 1999).
- (ii) A distinction between bacterial and human metabolism is not necessarily required to discover putative biomarkers and drug target candidates.
- (iii) It is well known, that *Chlamydia* as intracellular bacteria lack many enzymes of the core metabolism and interact heavily with the host cell. The corresponding modulation of human host metabolism is not of less importance for a deeper understanding of biological processes.
- (iv) The inclusion membrane, which surrounds the pathogen, is lost during any clean-up of the bacterial cells.

From an analytical point of view the work is based on modern, state-of-the-art ultrahigh resolution mass spectrometry and ultrahigh performance liquid chromatography hyphenated to mass spectrometry. The obtained data is integrated and analyzed with multi- and univariate statistics. Furthermore, a Kendrick-analogous network analysis as novel visualization and interpretation tool is integrated.

## 2.2 Objectives

The initially aim of the study is the development of an analytical concept integrating several state-of-the-art techniques of metabolomics and apply this concept to investigate the metabolite variations in active and persistent *C. pneumoniae* infections. This includes the characterization of infection relevant metabolite alterations in non-infected cells under different treatments. The strategy and objectives, which need to be successively achieved is illustrated in Figure 19:

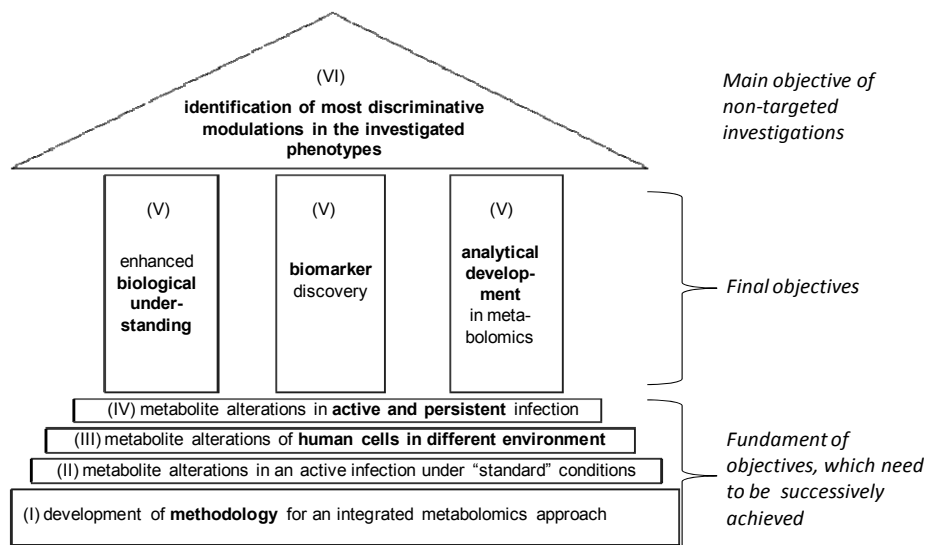


Figure 19: Illustration of objectives, which need to be successively achieved

## 2.3 Materials and method development

### 2.3.1 Materials

Methanol, acetonitrile and water have been purchased in LC-MS quality (trade name: CROMASOLVE<sup>®</sup>) from Fluka<sup>®</sup> Analytical (Sigma-Aldrich-Aldrich, St. Louis, USA). Standard compounds for UPLC<sup>®</sup>-ToF-MS methods are listed in the appendix (Supplementary table 1). An ESI tuning mix for MS calibration has been bought from Agilent (Santa Clara, USA).

*C. pneumoniae* (CWL 029) has been propagated in conventionally used HEp-2 cells (ATCC). The first cell culturing medium (medium A) has contained Eagle's minimum essential medium (RPMI 1640 PAA Laboratories, Cölbe, Germany), 5% fetal calf serum (FCS) (PAA Laboratories), 0.1mg/ml L-glutamine (PAA Laboratories) and 1xNEAA (Non-Essential Amino Acid, PAA Laboratories). The second cell culturing medium (medium B) has been composed of Eagle's minimum essential medium (RPMI 1640 PAA Laboratories), 0.1mg/ml L-glutamine (PAA Laboratories) and 1xNEAA (PAA Laboratories). Additionally, 0.1µg/ml cycloheximide (Sigma-Aldrich-Aldrich, St. Lois, USA) has been added to support the infection through the inhibition of eukaryotic protein biosynthesis. All cell cultivations and infections have been

performed by Inga Dietz (Group of Prof. Dr. Jan Rupp, Institute for Medical Microbiology and Hygiene, University of Lübeck, Lübeck, Germany).

### 2.3.2 Methods and method development

#### 2.3.2.1 General considerations

A multi-parallel approach has been built up for the investigation of *Chlamydia* infection caused metabolite alterations. The combination of different instrumentation improves the general scope of detectable metabolites. Putative drawbacks can be minimized, while the advantages of the single methods are conserved (Table 2) and thus the analytical concept is improved. Moreover, results obtained with one analysis can directly be validated with the data from the other instrument.

main advantage ICR/FT-MS	main advantage UPLC <sup>®</sup> -ToF-MS
- ultrahigh mass resolution and thus distinction of several thousand ions	- separation and differentiation of isomers
- ultrahigh mass accuracy	- retention time as an additional characteristic resulting from physico-chemical attributes of analytes
- very sensitive and fast analysis	- less ion suppression effects in comparison to direct injection experiments

Table 2: Comparison of main advantages of ICR/FT-MS and UPLC<sup>®</sup>-ToF-MS

The cell extracts have been analyzed by direct injection ICR/FT-MS in positive and negative electrospray mode, as well as with UPLC<sup>®</sup>-ToF-MS applying two orthogonal separation techniques, HILIC and RP, in positive electrospray. The two extracts of one sample have been pooled and either diluted or concentrated according to the need of the analytical method. The data analysis has been performed separately for the different instruments. Afterwards, the data for important discriminative metabolites from the different methods has been aligned and

compared with each other. The following section presents the applied methodology and required developments in more detail, divided into the main parts: sample preparation, analytical methods and data analysis (Figure 20).

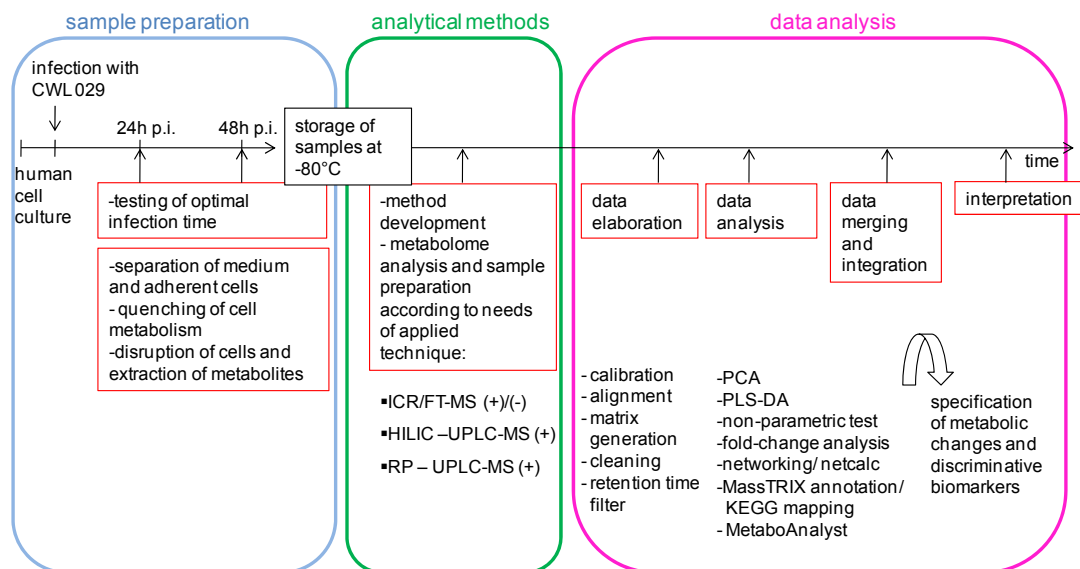


Figure 20: Overview of applied analytical concept and necessary steps during the study

### 2.3.2.2 Sample preparation procedures

#### 2.3.2.2.1 Cell cultivation, infection and metabolite extraction

All cell cultivations, infections and metabolite extractions have been done by Inga Dietz (Group of Prof. Dr. Jan Rupp, Institute for Medical Microbiology and Hygiene, University of Lübeck, Lübeck, Germany). Human cells have been cultivated in 175cm<sup>2</sup> cell culturing flasks at 37°C and 5% CO<sub>2</sub> for 3-4 days. The cell numbers have been counted and 2.5\*10<sup>5</sup> cells have been transferred into 6 well plates. The following experiments have either been done in an incubator without oxygen regulation (in the following referred to as normoxia) or in a hypoxic chamber with 2% oxygen (in the following referred to as hypoxia).

After 7 hours of cultivation the FCS containing medium A has been replaced by medium B without FCS. 10U/ml IFN-γ has been added to the medium for experiments investigating the IFN-γ effect. HEp-2 cells have been further cultivated and infected with *C. pneumoniae* CWL029 (5.6 IFUs/cell) by centrifugation (1h, 2000rpm, 30°C). Cycloheximide (0.2µg/ml) has been used to improve the infection.

24 hours post infection (*p.i.*) cells and media have been separated and the adherent cells have been quenched with 1ml ice-cold methanol (Teng *et al.*, 2009a). Thereafter, 1ml of ice-cold methanol-water mixture (50/50) has been added to the cells, which then have been scrapped from the plates and transferred into Eppendorf™ reaction cups. Mainly polar metabolites have been extracted in this methanol-water mixture within a cooled sonic bath for 30 minutes. Cell constituents have been separated by 5 minutes centrifugation (2000\*g, 4°C), followed by a second extraction for mid non-polar metabolites in 1ml methanol. This two step extraction procedure has been chosen to enhance the extraction efficiency and metabolite recovery. Both extracts have been separately stored at -80°C and pooled prior to analysis.

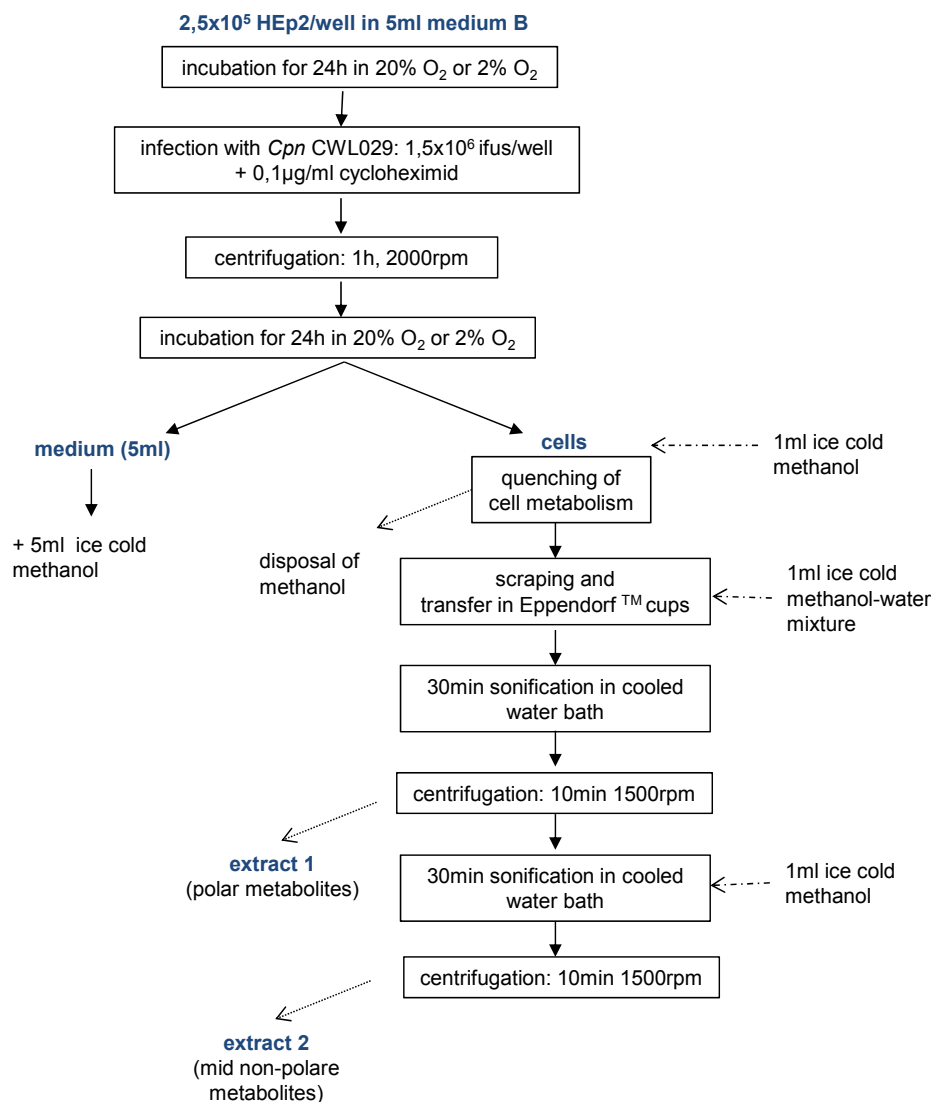


Figure 21: Developed workflow in cell culturing, quenching and metabolite extraction



For each cultivation condition ten biological replicates have been prepared, carried out on three different days. The number of cells and the infection rate has been monitored to ensure comparability of cell cultivation (Table 3). However, it needs to be mentioned that cells under hypoxia in general show an enhanced infection rate (Juul et al., 2007, Rupp et al., 2007).

condition	cell number ( $\times 10^6$ )			infection rate (% of big inclusions)		
	replicate 1-3 (day 1)	replicate 4-6 (day 2)	replicate 7-10 (day 3)	replicate 1-3 (day 1)	replicate 4-6 (day 2)	replicate 7-10 (day 3)
20% O <sub>2</sub> - IFN- $\gamma$	6.25	7.25	8	5	5	5
20% O <sub>2</sub> + IFN- $\gamma$	5	7.75	7.25	persistence	persistence	persistence
2% O <sub>2</sub> - IFN- $\gamma$	4.5	6.25	6.75	50	50	70
2% O <sub>2</sub> + IFN- $\gamma$	3.75	5	4.75	50	50	60

Table 3: Cell numbers and infection rates

#### 2.3.2.2.2 Determination of optimal infection time

The developmental cycle of *C. pneumoniae* takes approximately 72 hours. The metabolic active RBs appear mainly between 24 hours and 48 hours after infection. Within the first experiments, it has been investigated at which time the highest divergence in the cell metabolism compared to non-infected cells can be observed and should be in consequence chosen for the study. Positive direct injection ICR/FT-MS has been used. The detected molecular features as well as their annotations (1ppm error, MassTRIX (Suhre et al., 2008)) have been compared to each other in infected and non-infected cells. Samples infected for 24 hours have shown a higher variation in the detected signal intensities, resulting in an increased spreading of data points in the log ratio plot (Figure 22). The same trend has been observed when comparing the annotated metabolites (Figure 23); here samples

infected for 24 hours show approximately 70% conformance in the metabolite pattern in infected and non-infected samples and approximately 19% of the annotated metabolites are unique in infected cell extracts. In 48 hours infected cells about 80% of the metabolites are commonly detected in infected and non-infected samples and only 11% are exclusively present in infection. According to these observations, 24 hours of infection has been chosen for the non-targeted study.

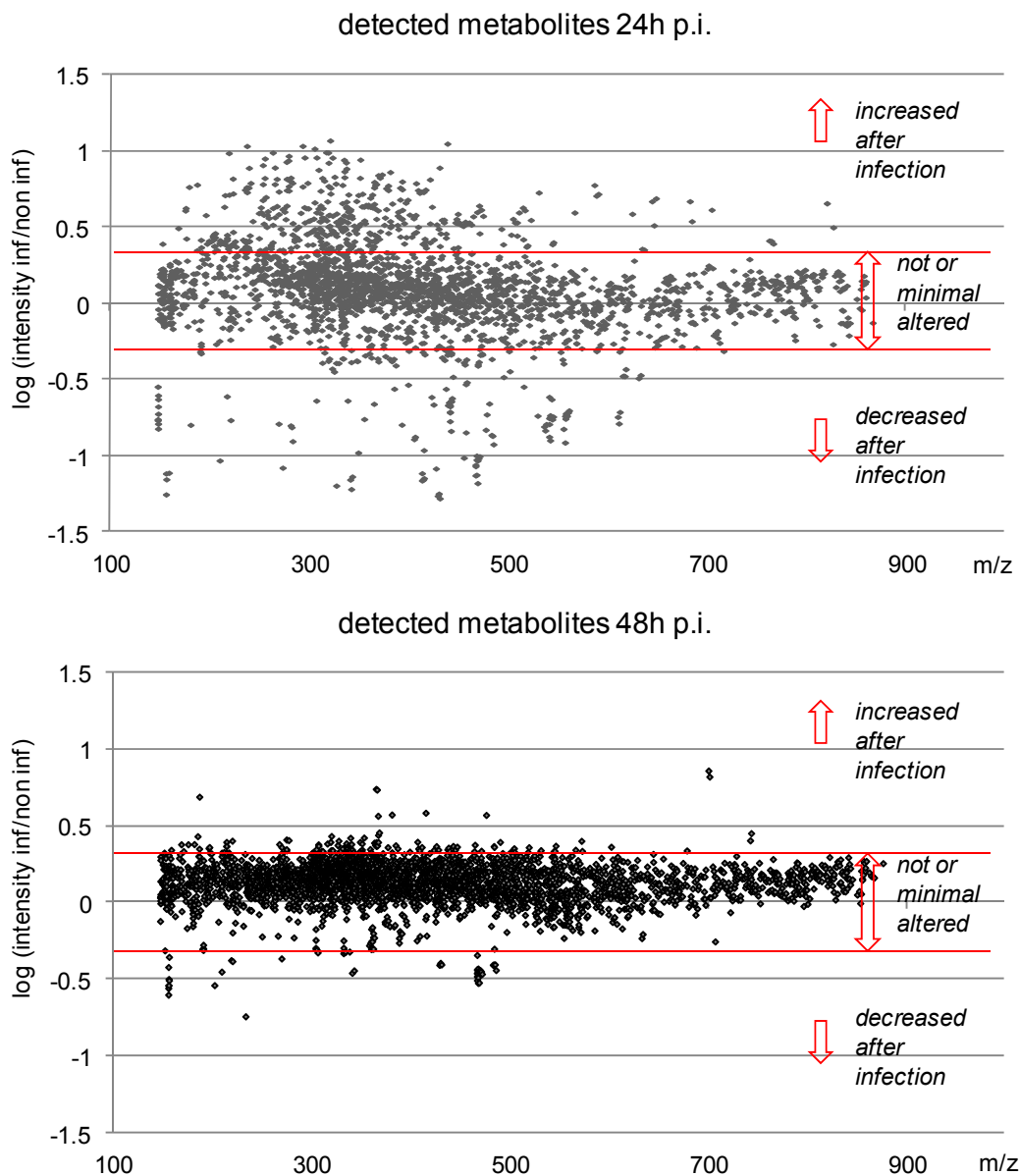


Figure 22: Logarithmic ratio of detected signal intensities for all commonly detected metabolites in infected and non-infected samples 24h p.i. and 48h p.i.

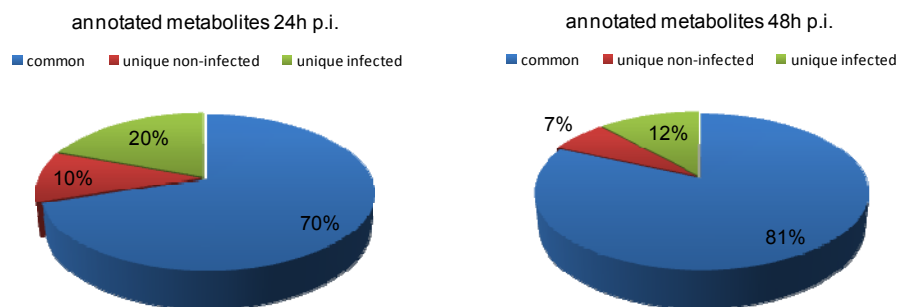


Figure 23: Comparison of annotated metabolites in infected and non-infected cells 24h p.i. and 48h p.i.

### 2.3.2.2.3 Investigation and selection of cell disruption procedure

Cell disruption is mandatory for the release of intracellular metabolites into the extraction solvent. Commonly used are mechanical forces or enzymatic reactions to destroy cell membranes and -walls (Villas-Boas et al., 2007). It needs to be ensured that no alterations of the metabolite profile occur during such procedures.

*Chlamydia* infected human cells contain three main barriers, the human cell membrane, the intracellular inclusion membrane and the bacterial gram negative cell wall, while the last named one is the strongest. To ensure a complete cleaving of the gram negative cell wall three mechanical disruption protocols, sonic bath (SB), shearing with sharp particles (P) and sonic finger (SF) have been investigated and compared. A two step experimental set-up has been used. The combination of the techniques in the second step should identify putative metabolite alterations and sources of contamination.

In the first step the cells have been disrupted by SB, P or SF. One third of each gained extract has been analyzed by direct injection (+)ICR/FT-MS. The remains have been divided, diluted and treated with another disruption method (SB or SF). Thereby, the sonification power has been either switched on or off. This has been done in order to be able to monitor metabolite alterations and contamination risks (Figure 24). All extracts from the second step have been also investigated by (+)ICR/FT-MS. The disruption experiments have been carried out with a model gram negative bacterium (*Pseudomonas aeruginosa*), since the cell wall characteristics are comparable to *Chlamydia*, but *Pseudomonas* are harmless for persons with

healthy immune status. Three technical replications have been included in the experimental design.

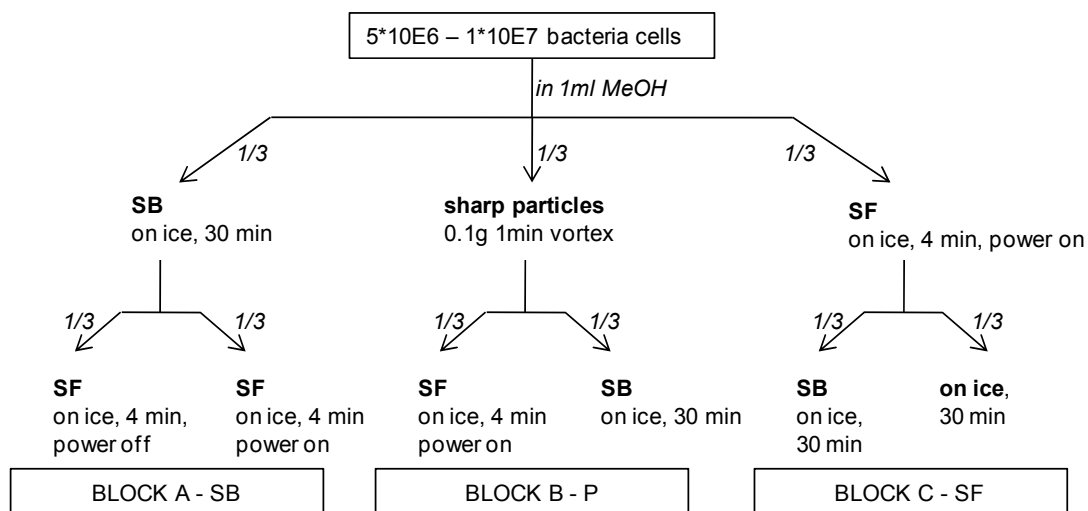


Figure 24: Experimental set-up to define the best suitable cell disruption method. SB, P and SF have been investigated. The obtained cell extracts have been divided into three equal parts, one has been directly analyzed, the other two have been used to identify metabolite alterations or contaminations. They have been subjected to an additional extraction.

	SB	P	SF
detected features	4605	3579	4657
annotated meta- bolites	607	454	631

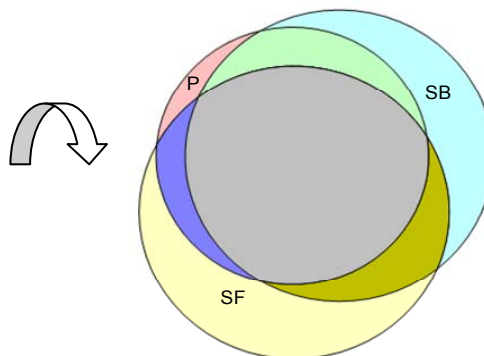


Table 4: Numbers of detected and annotated metabolites after the first step of disruption experiments

Figure 25: Comparison of detected m/z features after first step of disruption experiments

The numbers of detected molecular features after the first extraction are comparable in SB and SF, but in P extracts approximately 1000 features less have been detected (Table 4). The same trend can be observed for the annotated metabolites. The intersection of the detected features is visualized in the Venn diagram (Figure

25). Almost all features found in the particle extracts are also detected in the SF and SB extracts. SB and SF show additionally several unique features. The results suggest therefore an insufficient disruption of gram negative bacteria cell walls by shearing with sharp particles. SB and SF have been further monitored in the second step extraction experiments, one section of the obtained spectra is exemplarily illustrated in Figure 26 and the results are summarized in Table 5.

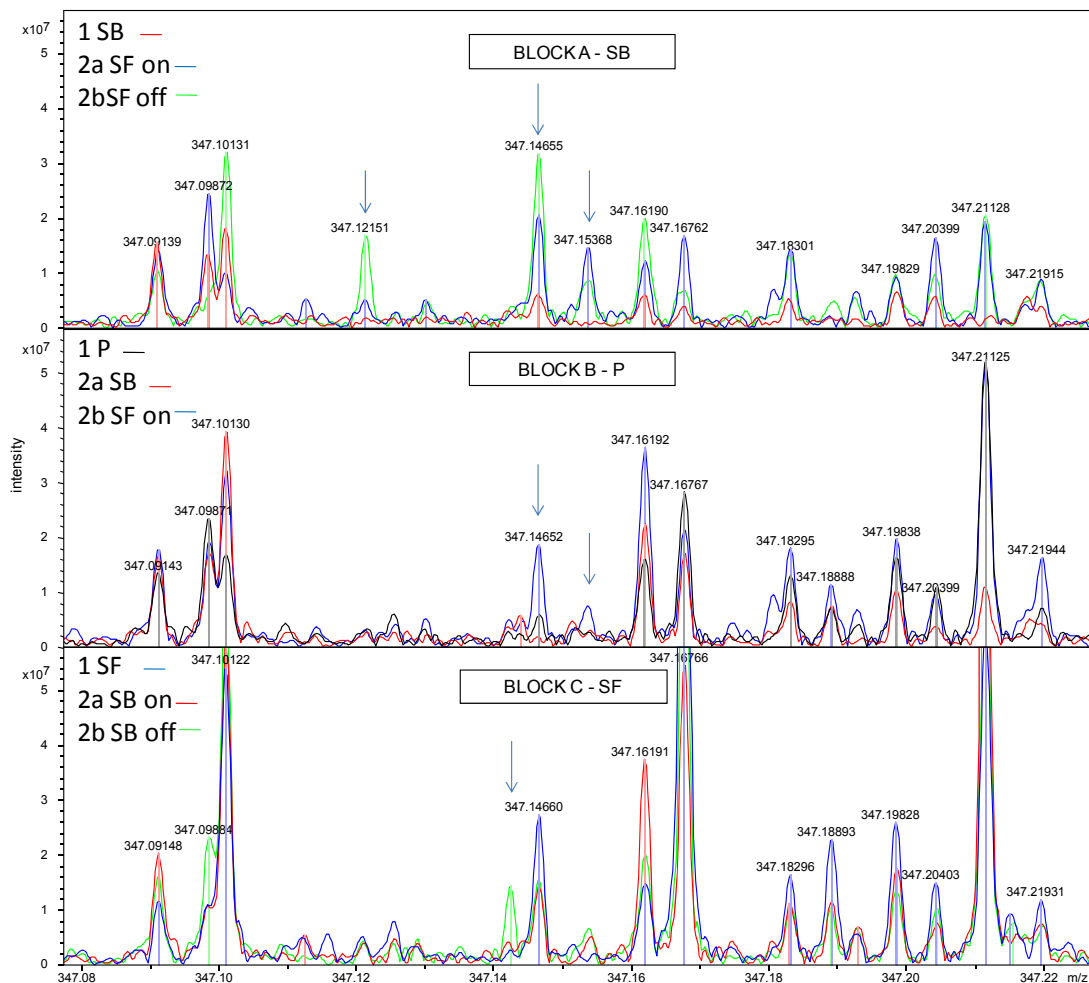


Figure 26: Section of (+)ICR/FT-MS mass spectra for disruption experiments in the mass range of 347.08 to 347.22 (blue arrows highlight peaks only occurring after SF treatment)

cell treatment	observation
BLOCK A - SB followed by SF on/off	several additional peaks appear after treatment of SB extracts with the SF (power on and off), interestingly the peak intensities of almost all peaks increased even though the dilution factor has been adapted
BLOCK B - particles followed by SB or SF treatment	the particle extract has been hardly altered after SB and SF treatment, only a few additional peaks have been observed after SF treatment
BLOCK C - SF followed by SB on/off	a high consistency between the initial extract and the extracts after additional treatment has been found

Table 5: Summary of observations after the second step of disruption experiments

In all experiments, that included SF, additional peaks have been detected. This suggests that the tip of sonic finger might be either a source of contaminations (even though it had been cleaned with care), or the metal surface of the tip might enhance several chemical reactions. All extracts from “Block C – SF” have been very comparable to each other, which indicates that no alteration of the samples has occurred during SB treatment. Following these results and considering the additional advantages of easy handling, labor costs and most importantly the very small risk of contaminations, SB has been chosen for the disruption of cells in this study.

### 2.3.2.3 Analytical methods

#### 2.3.2.3.1 ICR/FT-MS analysis

Ultrahigh resolution mass spectra have been acquired on a solariX™ ion cyclotron resonance Fourier transform mass spectrometer (Bruker Daltonics GmbH, Bremen, Germany) equipped with an Apollo II electrospray source (Bruker Daltonics GmbH, Bremen, Germany) and a 12 Tesla super conducting magnet (magnex scientific Inc., Yarnton, GB). Both extracts of one sample have been pooled and diluted in methanol (ESI(+)) 1to50 and ESI(-) 1to20. Afterwards, they have been injected with a flow rate of 2µl/min through a Gilson autosampler (sample changer 223, Gilson Inc., Middleton, USA). Additionally, the samples have been cooled (8°C) by this

autosampler unit during the analysis. The sample order has been randomized in blocks. One block consisted of the ten biological replicates of one cell culture conditions. After analyzing each block three spectra of pure methanol have been acquired to minimize the risk for cross-contamination and ion memory effects. In the same respect methanol has been further injected after acquisition of three biological replicates. Prior to analysis the instrument has been calibrated with a 1ppm arginine solution reaching a mass error below 100ppb. The instrument has been tuned in order to obtain highest sensitivity for metabolites in the  $m/z$  range of approximately 150 to 500Da in broad band detection mode and with a time domain transient of 2 MW (megaword) (Supplementary table 2). 300 and 380 scans have been acquired for one spectrum in positive and negative electrospray. The resolving power of the obtained spectra is of  $\sim 300000$  at  $m/z$  300 for both modes. The spectra have been elaborated in DataAnalysis 4.0 SP2 (Bruker Daltonics GmbH, Bremen, Germany).

One spectrum out of ten replicates has been internally calibrated according to endogenous abundant metabolites. The required mass calibration list has been elaborated after acquisition of a spiked sample. The obtained calibration has been conveyed to the other spectra. The mass lists have been generated with a signal-to-noise ratio (S/N) of four in ESI(+) or of two in ESI(-), exported and aligned within a 1ppm window (Matrix generator 0.4, in house written, M. Lucio).

#### 2.3.2.3.2 *RP separation*

Four chromatographic columns have been compared running a 20 minute water-acetonitrile gradient from 5% to 99% solvent B (solvent A: 100% water, 0.1% formic acid; solvent B 100% acetonitrile, 0.1% formic acid). Acetonitrile has been chosen because the elution of metabolites had been distributed over the complete run time in preliminary experiments. In contrast, when using methanol, metabolites had been mainly eluted in the last part of the run. According to the inner diameter of the column the flow rates have been adapted. This has been necessary to gain a comparable pressure profile for the different stationary phases. The column temperature has been set to 40°C.

In Table 6 the tested columns are ranked according to the number of molecular features detected in a test sample. A test sample has been preferred for method development and optimization, since the preparation of a quality control (QC) composed of an aliquot of each sample, would have led in multiple thawing freezing

cycles. The sample 1.6 (non-infected, 20% O<sub>2</sub>) has been randomly taken. It has been ten-fold concentrated (SpeedVac Concentrator, Savant SPD 121P, ThermoFisher Scientific, Waltham, USA) before analysis.

column	supplier	particle size [ $\mu\text{m}$ ]	dimension [mm]	flow rate [ml/min]	number of detected molecular features
ACQUITY UPLC <sup>®</sup> BEH C8	Waters	1.7	1.0*150	0.11	1416
ACQUITY UPLC <sup>®</sup> HSS T3	Waters	1.8	1.0*150	0.11	1346
ACQUITY UPLC <sup>®</sup> BEH C18	Waters	1.7	1.0*150	0.11	1142
Kinetex <sup>®</sup> C18	Phenomenex	1.7	2.1*150	0.3	840

*Table 6: Summary of RP column parameters and numbers of detected features*

The highest number of molecular features has been detected with an ACQUITY UPLC<sup>®</sup> BEH C8 column, which has thus been chosen for the non-targeted metabolite analysis of cell extracts.

After defining the stationary and mobile phase a set of additives (acetic acid, formic acid, ammonium formate and ammonium hydroxide) have been tested to evaluate the performance during chromatographic separation and support of electrospray ionization in positive and negative mode. A variety of standard compounds (Supplementary table 1) with different physicochemical properties have been analyzed. The detected intensities as well as the peak shapes have served as criteria to evaluate the chromatographic separation. Furthermore, the test sample (pellet 1.6) has been analyzed and the number of detected molecular features has been calculated as additional evaluation criterion. In contrast to the other additives, ammonium hydroxide has been used in a concentration of 0.02% (pH 9) to protect the chromatographic material and analytes from high pH values. This ensures a long



lifetime of the chromatographic column and avoids pH depended metabolite degradation.

additive	concentration [%]	number of detected molecular features	
		ESI(+)	ESI(-)
acetic acid	0.1	1167	494
formic acid	0.1	1422	403
ammonium formate	0.1	504	195
ammonium hydroxide	0.02	1665	119

*Table 7: Numbers of detected features for different additives in RP separation (molecular features, which have also been detected in the blank run have been subtracted)*

Ammonium hydroxide shows the best peak shapes and baseline separation for most standard compounds (Supplementary figure 1). Their elution is spread over the complete chromatographic run according to the physicochemical attributes of each standard compound. The analysis applying ammonium hydroxide delivers the highest numbers of molecular features (Table 7). Consequently, ammonium hydroxide has been chosen as best suitable additive. Since in positive mode a much higher sensitivity has been observed in all tested conditions, the following analysis have been done in positive electrospray mode.

Finally, the pre-concentration factor of the samples has been optimized. Detectable metabolites and the available sample volume have been considered. A five-fold concentration in connection with 10µl injection volume has been chosen (Table 8).

	pre-concentration factor			
	0	2-fold	5-fold	10-fold
molecular features	397	513	843	1088

*Table 8: Numbers of detected molecular features for different pre-concentrations (RP UPLC®-ToF-MS)*

According to the illustrated optimizations reversed phase UPLC<sup>®</sup>-ToF-MS analyses have been performed applying the following conditions:

Column: ACQUITY UPLC<sup>®</sup> BEH C8; 1.7 $\mu$ m; 1.0\*150mm  
Solvent A: water, 0.02% ammonium hydroxide  
Solvent B: acetonitrile, 0.02% ammonium hydroxide  
Gradient: 5% B to 99% B in 20min, followed by 3min equilibration (Figure 27 C)  
Flow rate: 0.11ml/min  
Sample volume: 10 $\mu$ l

One obtained BPC (base peak chromatogram) (A), density map (B), the applied gradient (C) and resulting pressure profile (D) are illustrated in Figure 27.

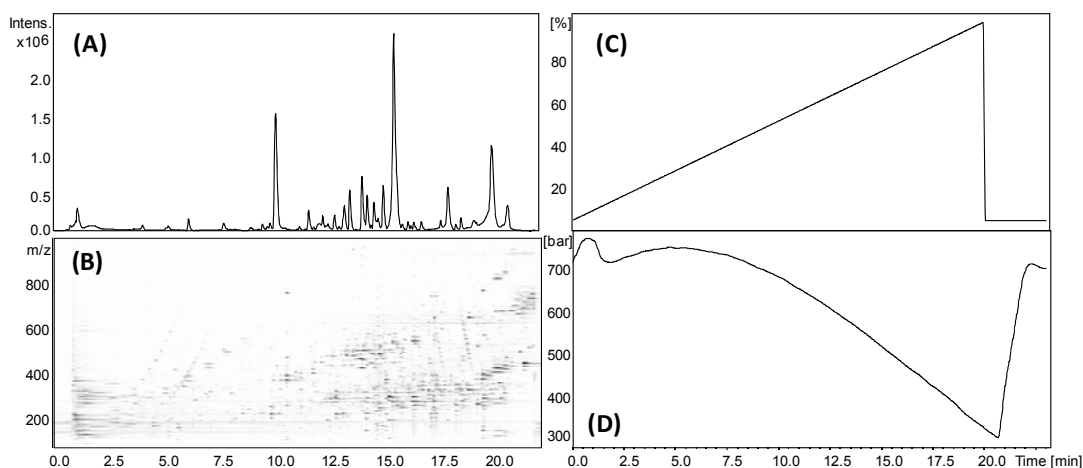


Figure 27: Illustration of : (A) BPC; (B) density map; (C) applied gradient; (D) obtained pressure profile in RP UPLC<sup>®</sup>-ToF-MS analysis

Both cell pellet extracts (water/methanol and pure methanol) have been pooled and five-fold concentrated prior to injection. Each sample has been measured in triplicate. The order of samples has been randomized blockwise according to the cultivation conditions. Furthermore, QC samples as well as a sample composed of standards have been integrated for column equilibration and monitoring of chromatographic quality. The acquired chromatograms have been calibrated reaching a mass error  $\leq 0.004$ Da (DataAnalysis 4.0 SP2, Bruker Daltonics GmbH,

Bremen, Germany). MZmine 2.6 (Pluskal et al., 2010) has been applied for alignment and peak extraction (see chapter 2.3.2.4.2).

### 2.3.2.3.3 HILIC separation

The chromatographic performance of an ACQUITY UPLC<sup>®</sup> BEH HILIC (Waters 1.7 $\mu$ m; 1.0\*150mm) and of a Vision HT<sup>™</sup> HILIC (Grace<sup>®</sup>, 1.5 $\mu$ m; 2.0\*150mm) has been compared by analyzing the mixture of different standard compounds. Additionally, the experiments have been carried out with a randomly taken sample 4.3 (infected, 20% O<sub>2</sub>). A 30 minute acetonitrile-water gradient from 0% to 50% solvent B (solvent A: 95% acetonitrile, 5% water; solvent B: 90% water, 10% acetonitrile) has been applied. The column temperature has been adapted to 25°C. The basis of a stable and well working HILIC separation is the interaction between the analytical column material and the mobile phase, which facilitate the formation of a very thin aqueous layer (Buszewski et al., 2011). Since the buffer system is very important in this respect, both parameters, stationary phase and buffer system, have been optimized together. The choice of chromatographic columns has based on previous tests. The implemented buffers (10mM ammonium formate and 10mM ammonium acetate) have been selected as they are most frequently described in literature (e.g. in Buszewski et al., 2011, Preinerstorfer et al., 2009). The criteria to evaluate the quality of the chromatographic system have been in accordance with the RP UPLC<sup>®</sup>-ToF-MS development, namely detection of standards, distribution of their elution over the chromatographic run, baseline separation, peak shape and number of molecular features in test sample.

	<b>ammonium formate</b>	<b>ammonium acetate</b>
Grace <sup>®</sup> Vision HT <sup>™</sup> HILIC	947	957
ACQUITY UPLC <sup>®</sup> BEH HILIC	1135	650

*Table 9: Numbers of detected features for evaluation of the column/buffer system in HILIC separation*

The Grace<sup>®</sup> Vision HT<sup>™</sup> HILIC column in combination with the ammonium formate buffer delivers the sharpest peaks and best baseline separation for the analyzed

standard compounds. The elution is spread over the first 17 minutes of the run. In contrast, when applying the ACQUITY UPLC<sup>®</sup> BEH HILIC under the same conditions elution of standards only occurs within the first 12 minutes. Thus, even though the number of detected features in the sample is lower when utilizing a Grace<sup>®</sup> Vision HT<sup>™</sup> HILIC compared to an ACQUITY UPLC<sup>®</sup> BEH HILIC (Table 9), the Grace<sup>®</sup> column has been chosen for further optimization.

In the following the chromatographic conditions have been kept constant and methanol-water system as mobile phase, as well as different buffer concentrations (5mM, 10mM and 15mM) have been tested (Table 10). The numbers of detected molecular features are comparable in all acetonitrile runs, but strongly decreased when using methanol. However, taking the peak shapes of standards and the distribution of their elution over the run into account (Figure 28), best results are delivered by the acetonitrile gradient in combination with 5mM ammonium formate.

	5mM acetonitrile	10mM acetonitrile	15mM acetonitrile	10mM methanol
molecular features	1092	947	1004	560

Table 10: Numbers of detected features for evaluation of optimal additive concentration and choice of organic solvent in HILIC separation

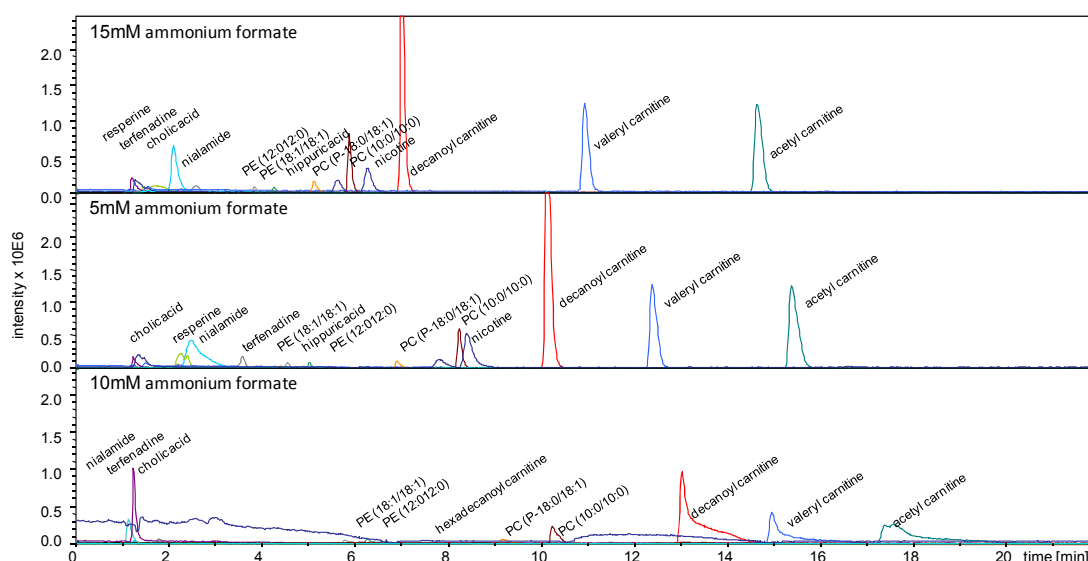


Figure 28: Retention time window of standard compounds for evaluation of additive concentration in HILIC separation

Afterwards, the gradient has been shortened and optimized leading to a final content of 30% solvent B (Figure 29C). Additionally, an isocratic step prior to the gradient elution has been inserted. Optimized run conditions and one resulting BPC, density map and pressure profile are furthermore illustrated in Figure 29. In summary HILIC<sup>®</sup>-UPLC<sup>®</sup>-TOF-MS analyses have been performed applying the following conditions:

Column:	Grace <sup>®</sup> Vision HT <sup>™</sup> HILIC; 1.5 $\mu$ m; 2.0*150mm
Solvent A:	95% acetonitrile, 5% water, 5mM ammonium formate
Solvent B:	90% water 10% acetonitrile, 5mM ammonium formate
Gradient:	2min 0% B, from 0% to 30% B in 10min, 2min 30% B, followed by 5min equilibration
Flowrate:	0.3ml/min
Sample volume:	10 $\mu$ l

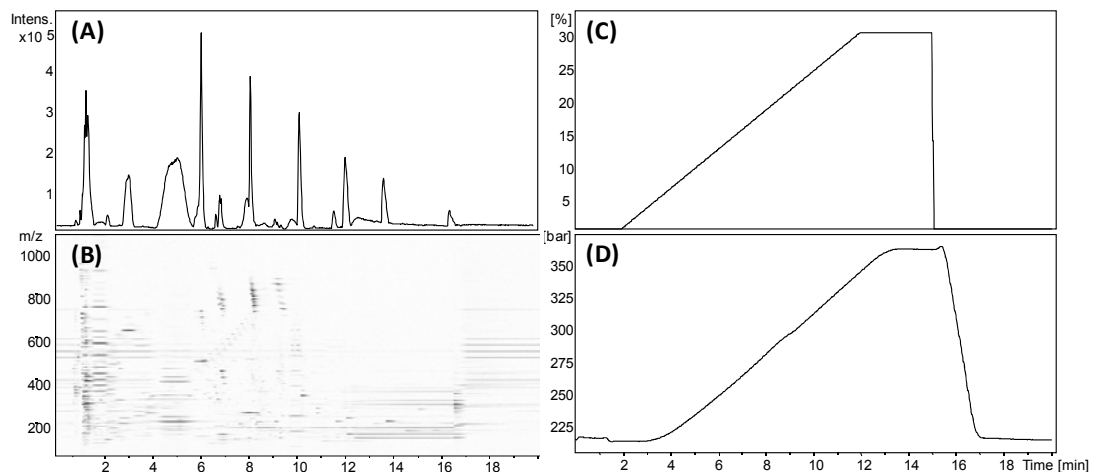


Figure 29: Illustration of (A) BPC; (B) density map; (C) applied gradient; (D) obtained pressure profile in HILIC UPLC<sup>®</sup>-TOF-MS analysis

Both extracts for one sample have been pooled, five-fold concentrated and three times injected. The randomization of the injection order has been done blockwise. Biological replicates are injected within one block. A sample consisting of standard compounds has been used to monitor drifts in retention time and mass accuracy. The acquired spectra have been calibrated to a maximal absolute mass error <0.003Da (DataAnalysis 4.0 SP2, Bruker Daltonics GmbH, Bremen, Germany) and exported to MZmine 2.6 (Pluskal et al., 2010) for data elaboration (see chapter 2.3.2.4.2)

#### 2.3.2.3.4 UPLC<sup>®</sup>-ToF-MS analyses

The UPLC<sup>®</sup>-ToF-MS measurements have been achieved on a ToF-MS (maXis<sup>™</sup>, Bruker, Bremen, Germany) featured with an Apollo II electrospray source (Bruker, Bremen, Germany). The ToF-MS has been coupled to an ACQUITY UPLC<sup>®</sup> (Waters, Manchester, UK). Prior to analyses the instrument has been calibrated with an ESI tuning mix in positive mode. Nevertheless, the acquired spectra have also been carefully calibrated, since mass shifts must be suspected for analysis over several days. The acquisitions have been carried out in profile spectra mode with 1Hz accumulation time. Instrument tuning has focused on detection and resolution of low molecular weight compounds in the mass range of 80-500Da. The main parameters are displayed in Supplementary table 3.

#### 2.3.2.4 Data analysis

RP UPLC<sup>®</sup>-(+)ToF-MS, HILIC UPLC<sup>®</sup>-(+)ToF-MS and (+)/(-)ICR/FT-MS data has been separately analyzed. The principle workflow for the data analysis is illustrated in Figure 30.

After data pre-treatment, like calibration, matrix generation, data cleaning and annotation, unsupervised multivariate statistics (PCA and HCA) have been applied for visualization and exploration of naturally occurring clusters. Afterwards, according to the biological questions, sub-groups of the sample set-up have been chosen and analyzed using different PLS-DA models. The discriminative markers obtained in the different models have been further tested with the non-parametric Wilcoxon-Mann-Whitney test and manually checked within the spectra and chromatograms. In addition to this “classical” data elaboration pipeline of metabolomics, network calculations as well as van Krevelen and Kendrick plots have been included. Networking, Van Krevelen and Kendrick plots have been used exclusively for ICR/FT-MS data, since only ICR/FT-MS provides the required mass resolution and accuracy.

The results delivered by the different applied instrumentations have been compared with each other. In this purpose the data of important metabolites, which have been identified as statistically significant altered after infection in the different analyses, have been merged.

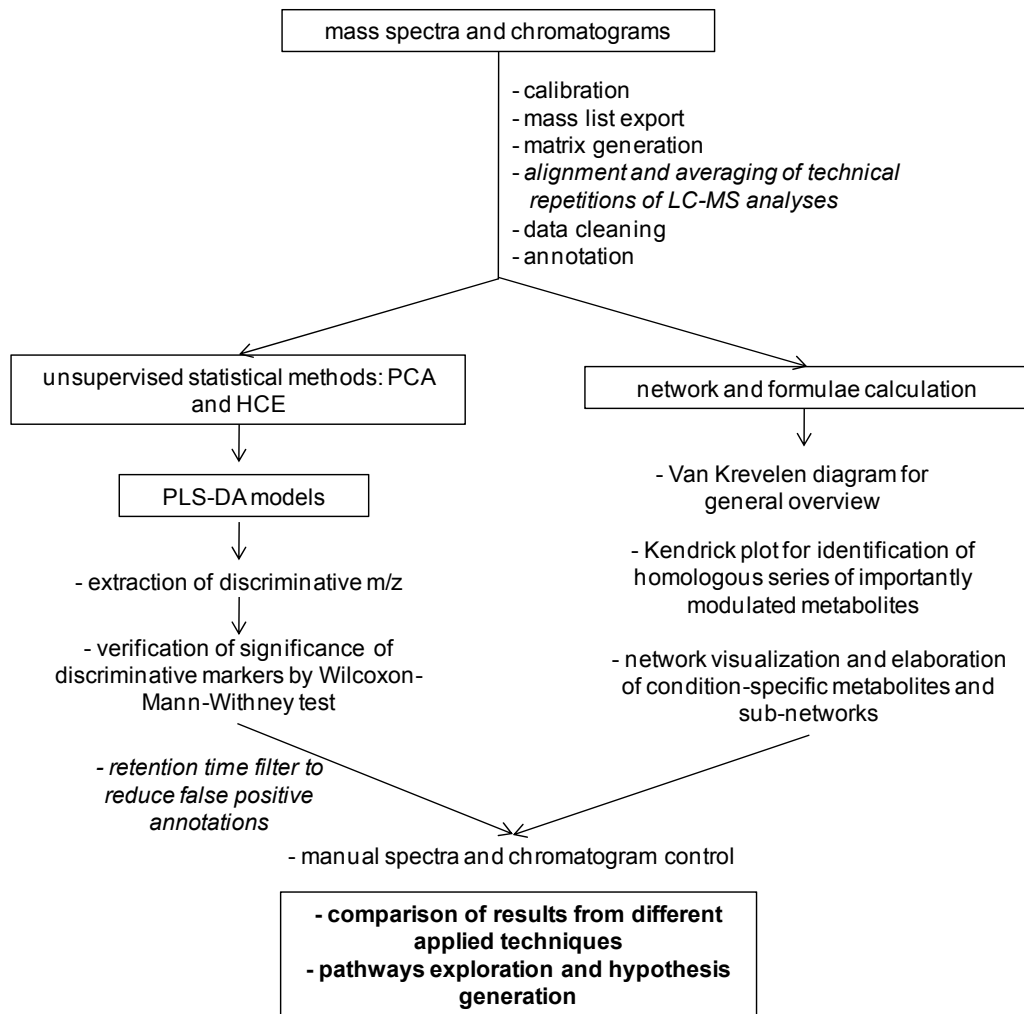


Figure 30: Overview of data analysis: Elaboration procedures illustrated on the left side have been separately done for RP UPLC<sup>®</sup>-ToF-MS, HILIC UPLC<sup>®</sup>-ToF-MS and (+)/(-)ICR/FT-MS data before the lists of important markers have been merged. UPLC<sup>®</sup>-ToF-MS data needed several extra working steps, which are shown in italic letters. The workflow shown at the right side has been exclusively performed for ICR/FT-MS data.

#### 2.3.2.4.1 Cleaning of ICR/FT-MS data

The extracted mass lists (S/N4 ESI(+)) and (S/N2 ESI(-)) from ICR/FT-MS spectra have been aligned applying a 1ppm window (Matrix generator 0.4, inhouse written, M. Lucio). Masses detected in the blank samples have been excluded from the data set if their detected intensity in the samples have not exceed ten times the detected intensity in the blank. Blanks are pure solvents, which have been equally treated like the samples from beginning of the cell cultivation and during the complete sample preparation and analyses. Furthermore, masses found in less than three out of ten biological repetitions have been excluded.

#### 2.3.2.4.2 *Treatment of UPLC<sup>®</sup>-ToF-MS data and MZmine elaboration*

UPLC<sup>®</sup>-ToF-MS data have been analyzed with MZmine 2.6. (Pluskal et al., 2010). A noise level of 100 (HILIC) or 200 (RP) has been set. Peaks needed to exceed the intensity amplitude of 150 (HILIC) or 200 (RP) for at least 5 seconds (5 scans) to be considered during chromatogram construction. A noise amplitude algorithm has been used for data deconvolution, followed by de-isotoping and duplicate filtering. Thereafter, the samples' chromatograms have been aligned by the join align algorithm with a m/z window of 0.005 and time span of 30 (HILIC) or 20 (RP) seconds. The described parameters had been optimized using the QC and LC-MS monitoring sample, which consisted of several standards. The aligned matrix has been exported in csv. format and imported to Excel 2007 (Microsoft<sup>®</sup>, Redmond, USA). Detected peak areas in three technical repetitions of one biological replicate have been averaged, if detected in at least two repetitions. This is necessary since technical replicates are not independent and thus might bias the statistical analyses. Afterwards, masses detected in the blank samples have been excluded if not meeting a ten-fold higher peak area in the samples. Peaks detected in less than three out of ten biological repetitions have been expelled from data analysis.

#### 2.3.2.4.3 *HCA*

Hierarchical cluster analysis has been performed using the open source software Hierarchical cluster explorer<sup>®</sup> (HCE) 3.0 (Human computer interaction lab, Maryland, USA). HCA is a non-supervised multivariate analysis to discover clusters (groups of samples) in the data set, which do exhibit comparable metabolite intensity profiles. The Pearson correlation coefficient has been used.

#### 2.3.2.4.4 *PCA*

PCA models have been used for data visualization and for discovery of naturally occurring patterns as well as for identification of putative outliers. The original data is hereby transferred into a few orthogonal variables called principal components, which still contain the main variation of the data set. Mean centering in combination with unit variance scaling has been applied for the data of this study. The multivariate modeling has been done in SIMCA-P<sup>®</sup> 9 (Umetrics, Umea, Sweden).



#### 2.3.2.4.5 *PLS-DA*

After exploration of naturally occurring patterns with unsupervised methods, the data has been further analyzed with PLS-DA in SIMCA-P<sup>®</sup> 9 (Umetrics, Umea, Sweden). Cross-validation and permutations test are essential to detect possible overfittings. The calculated  $Q^2$  (goodness of prediction) varies between 0 and 1, whereas 0 indicates no fit and 1 a perfect fit. In general values of  $Q^2 > 0.9$  are understood as excellent (Eriksson, 2006). A seven-fold cross-validation has been applied. Furthermore, a permutation test for validation of each model is necessary and has been done with 200 permutations. If the PLS-DA model has met all the required quality criteria the most discriminative m/z for the group separation have been extracted. M/z with a VIP-VALUE (variable importance in projection)  $>1$  has been considered relevant.

#### 2.3.2.4.6 *Wilcoxon-Mann-Whitney test*

The non-parametric Wilcoxon-Mann-Whitney test has been further used to vet, if the extracted observations (m/z) differ statistically significant from each other within two groups of samples. The calculated p-values give thereby the statistical confidence to reject the null hypothesis, which claims that the means are equal in the different samples. P-values  $<0.05$  have been considered sufficient. The advantage of such non-parametric test is that a normal distribution is not required. The test has been done with the open source software Multi experiment viewer (MeV) 4.6.2 (Saeed et al., 2006).

#### 2.3.2.4.7 *Correlation analysis*

The averaged signal intensities of ten biological replicates have been investigated to identify trends in metabolite abundance. Correlation analysis has been performed in Excel 2007 (Microsoft<sup>®</sup> Redmond, USA). The correlation coefficient indicates the strength and direction of association between the expression profiles of two metabolites. A correlation coefficient of 0 implies no correlation at all, -1 inverse and +1 complete correlation. Metabolites showing a correlation coefficient  $>+0.8$  have been considered as interrelated, the p-value of these correlations have been  $<0.017$ .

#### 2.3.2.4.8 *Annotation and pathway mapping*

Mass lists have been submitted to MassTRIX for annotation of detected m/z features (<http://metabolomics.helmholtz-muenchen.de/masstrix2/>) (Suhre *et al.*, 2008). A 1ppm error window has been used for ICR/FT-MS and 0.005Da for UPLC<sup>®</sup>-ToF-MS data. The submitted m/z values are on the fly corrected for proton or sodium attachment or abstraction of one proton according to the ionization mode, followed by data base search in HMDB (*Human Metabolome Database*), KEGG (*Kyoto Encyclopedia of Genes and Genomes*) and LIPID MAPS for corresponding metabolite masses. The annotated KEGG CIDS and HMDB IDs have been exported and plotted for further pathway analysis into the KEGG atlas ([http://www.genome.jp/kegg/tool/map\\_pathway2.html](http://www.genome.jp/kegg/tool/map_pathway2.html)) or uploaded to MetaboAnalyst 2.0 (Xia *et al.*, 2009) (<http://www.metaboanalyst.ca>).

#### 2.3.2.4.9 *MetaboAnalyst*

Besides the classical data analyzing methods for MS, LC-MS and NMR data (like univariate, multivariate and machine-learning methods as well as normalization and transformation) the web based tool MetaboAnalyst includes new developed approaches for interpretation of metabolomics data, namely “Metabolite set enrichment analysis” and “Metabolic pathway analysis” (Xia *et al.*, 2009). In particular these two functions help to identify biological meaningful sets of metabolites and pathways.

Lists of compounds (KEGG CID or HMDB ID) statistically significant increased or decreased in the different conditions have been uploaded to MetaboAnalyst and pathway analysis has been performed. The analysis is based on Kegg pathway topology, and the following tests are performed:

- (i) over-representation analysis (The systems tests, if the uploaded compounds are over-represented in a particular pathway. In this purpose a comparison of the data set to a list of random hits is performed.)
- (ii) pathway enrichment analysis for quantitative data according to the over-representation test
- (iii) topological analysis (The importance in terms of betweenness centrality and degree centrality) of metabolites in their pathway is evaluated.

The final result is a "metabolome view" (Figure 31), which contains all the matched pathways arranged by their p-values (calculated from (i) and (ii)) on the Y-axis, and pathway impact values (calculated from iii) on the X-axis (FAQ (2012) <http://www.metaboanalyst.ca>).

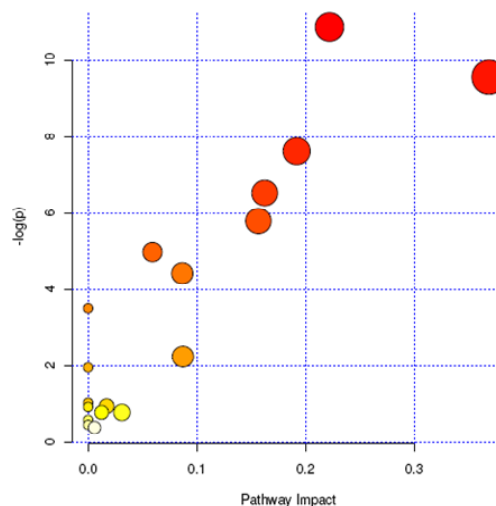


Figure 31: Exemplary illustration of resulting metabolome overview after pathway analysis with MetaboAnalyst. The colors are based on the p-value from pathway enrichment analysis. Bubbles' sizes correspond to the impact values from pathway topology analysis (source FAQ (2012) <http://www.metaboanalyst.ca>)

#### 2.3.2.4.10 Venn diagram

Venn diagrams are useful tools to visualize the intersections of different data. The Venn Diagram plotter version 1.4.3740.38143 (Kyle Littlefield, Matthew Monroe, USA) has been used in this work.

#### 2.3.2.4.11 Network visualization and elemental formula calculation

The inhouse written Matlab program netcalc (Tziotis et al., 2011) enables the calculation and illustration of ultrahigh resolution mass spectrometry data based on distinct mass differences. Within the network, vertices reflect the exact masses and the edges correspond to predefined mass differences according to common biochemical reactions. Additionally, elemental formula calculation is possible based on the high connectivity in such a network, as far as one formula is *a-priori* known. For the calculation a 0.1ppm error has been used for (+)ICR/FT-MS data and 0.2ppm for (-)ICR/FT-MS data. For the elemental composition carbon, hydrogen,

nitrogen, oxygen, sulfur as well as phosphorous have been considered. Visualization has been achieved in the open source Excel add in NodeXL 1.0.1.179 (Microsoft® Redmond, USA), using a Harel-Koren Fast Multiscale algorithm. Highly connected nodes are centered and less connected ones are assembled in the periphery.

During the non-targeted study of *Chlamydia* infection, at first all detected metabolites and thereafter metabolites only increased after infection have been investigated.

#### 2.3.2.4.12 *Filtering of UPLC®-ToF-MS annotations based on retention time-logD regression*

Due to the lower mass accuracy of ToF instruments compared to ICR/FT-MS and the consequently higher tolerated error during mass annotation (0.005Da), false positive annotations must be suspected. To enable the filtering of such false positive annotations a logD retention time correlation has been used. Retention times of standards (supplementary table 1) have been plotted against their logD value at pH 9 (RP) and pH 5 (HILIC). For reversed phase separation a linear correlation fitted the plot ( $r^2 > 0.9$ ), but for the HILIC separation no correlation could be observed. Consequently, only for RP UPLC®-ToF-MS runs a filtering of annotated metabolites has been performed. KEGG CIDs of detected metabolites have been submitted to chemical translation service (CTS) (Wohlgemuth et al., 2010) to get InChI- and smiles codes. Afterwards, the logD values for the annotated metabolites have been calculated with JChem for Excel 5.8.2.272 (ChemAxon, Budapest, Hungary). The calculated logDs have been plotted against the detected retention times. The metabolite annotation has been rated as false positive if its logD-retention time relation has not followed the regression of standards. A maximum tolerance of  $\pm 2$ logD units has been accepted (Figure 32).

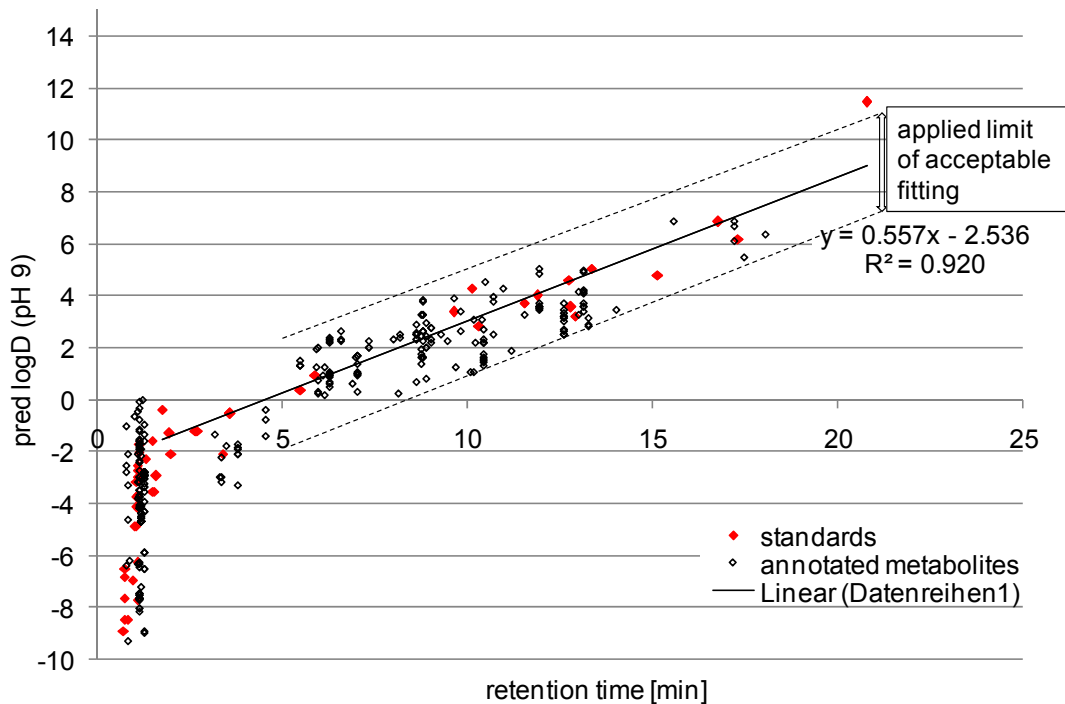


Figure 32: Plot of RP retention times of standard compounds against their predicted logD: Due to a linear correlation of retention times and logD values a filtering of putative metabolite annotations could be performed in order to minimize the risk of false positive annotations.

#### 2.3.2.4.13 Data alignment

After identification of discriminative markers in RP UPLC<sup>®</sup>-ToF-MS, HILIC UPLC<sup>®</sup>-ToF-MS and ICR/FT-MS data, the important masses have been merged. For this purpose the KEGG CIDs have been used for annotated metabolites. This keeps the advantage that KEGG CIDs are unique for each metabolite and independent from detected ion adducts. For “unknowns” the detected masses have been compared in Excel 2007 (Microsoft<sup>®</sup> Redmond, USA) applying a 0.005Da mass tolerance. During alignment it needs to be considered, that ions may be detected as different adduct ions in the different used methods. Instantly, glycerophospholipids tend to form sodium adducts in direct-injection (+)ICR/FT-MS but proton adducts in UPLC<sup>®</sup>-(+)ToF-MS analysis.

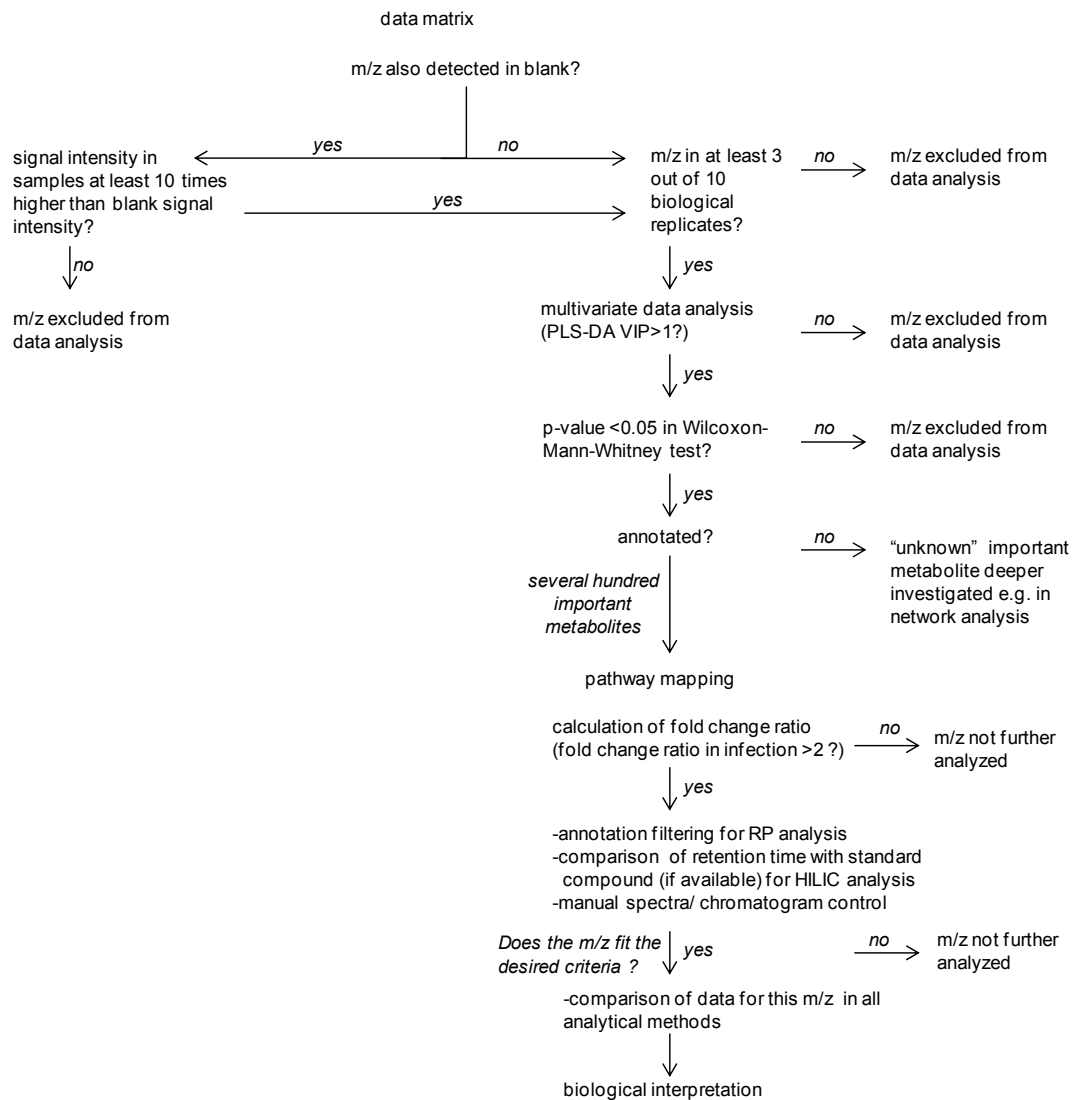


Figure 33: Summary and decision tree of data cleaning and -elaboration

## 2.4 Results and discussion

Due to the complex data set the results and discussion chapter is structured in three parts. At first, a principal data overview is given (chapter 2.4.1), thereafter important alterations in an active normoxic infection are documented and discussed (chapter 2.4.2). In the last part a deeper investigation of active and persistent infection is presented (chapter 2.4.3), this includes also the effects of different cultivation conditions to the non-infected cells (Figure 34).

### 2.4.1. Data overview

### 2.4.2. Metabolic permutations after an active, normoxic infection

- overview of pathway modulations
- main modulations of metabolites
  - amino acids metabolism
  - lipids metabolism
  - carbohydrates and nucleosides
  - summary
- key “unknown” compounds affected by infection

### 2.4.3. Metabolic permutations after an active and persistent infection

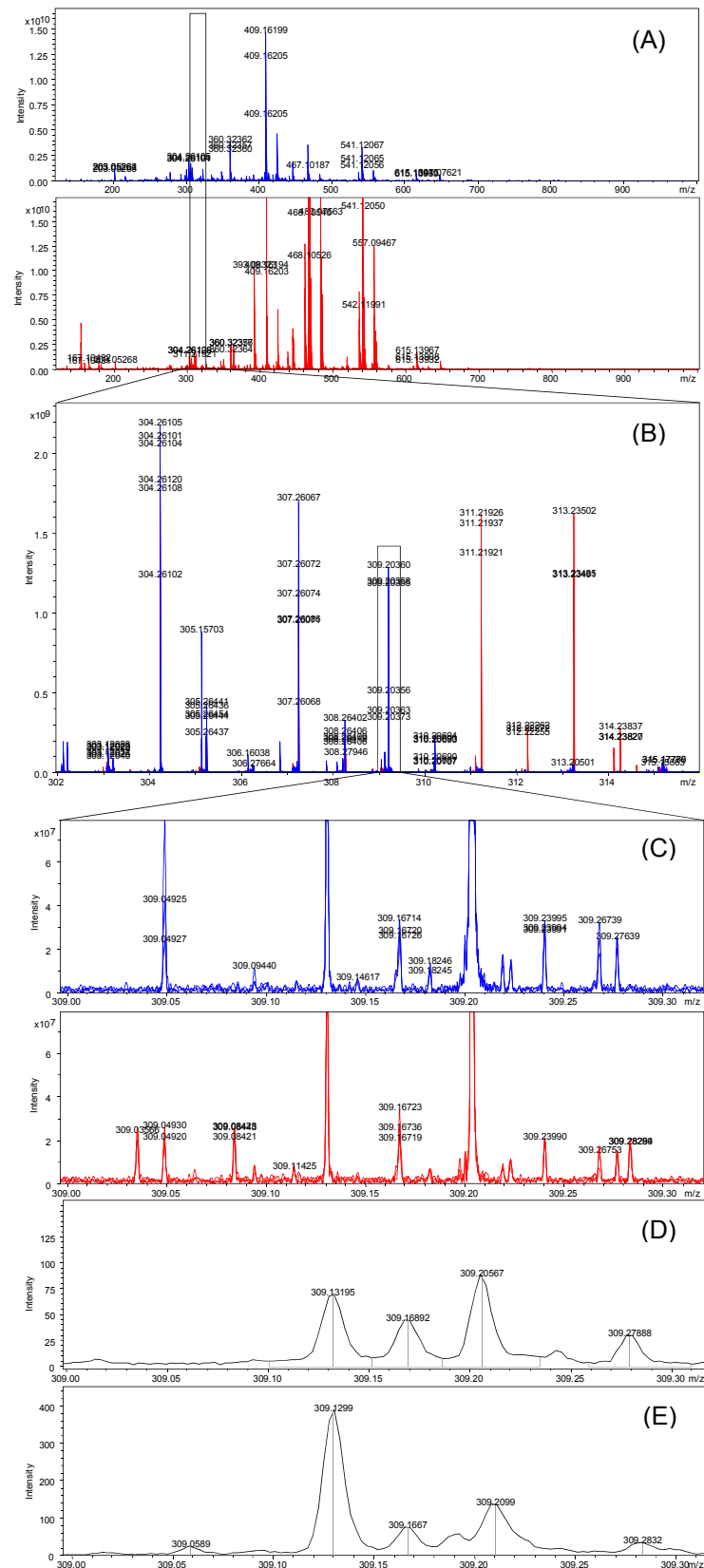
- investigation of non-infected cells
- *Chlamydia*-specific metabolic alterations in active and persistent infection

Figure 34: Structure of results and discussion section

## 2.4.1 Data overview

### 2.4.1.1 Reproducibility

The spectra and the chromatograms have been at first visually investigated for technical and biological reproducibility, as well as for putative contaminations. Three randomly chosen replicates from non-infected and infected samples cultivated in normoxia are exemplarily illustrated for positive ionization (Figure 35). Next to the good biological and analytical reproducibility the spectra show the abundance of different metabolite profiles in non-infected and infected samples and the enormous resolution power of ICR/FT-MS spectra (A-C) in comparison to ToF-MS measurements (D and E). Mass resolution and sensitivity of ToF-MS are not sufficient to detect and separate all the ICR/FT-MS  $m/z$  features, but the general mass profiles are comparable. Nevertheless, as mentioned previously, UPLC<sup>®</sup>-MS analyses are very helpful to verify putative markers and deliver further information based on the separation prior to ionization.



**Figure 35:** Illustration of spectra for three randomly chosen biological repetitions of non-infected (blue) and infected (red) samples cultivated under 20% oxygen atmosphere in (A) broad band (+)ICR/FT-MS spectra; (B) zoom in the mass range of 302 to 316 and (C) to the nominal mass 309. The nominal mass 309 is further illustrated in the summed up mass spectra of (D) HILIC UPLC®-ToF-MS and (E) RP UPLC®-ToF-MS analyses



The reproducibility of ICR/FT-MS measurements has been further evaluated by the detection frequencies of  $m/z$  features. For instance, 71% of all peaks are detected in at least 50% of the biological replicates of normoxic infected samples (Supplementary figure 2). The coefficient of variation (CV) of detected intensities for  $m/z$  detected in these biological replicates are very good. 90% of the peaks show an intensity variation of less than 44%. UPLC<sup>®</sup>-ToF-MS measurements have been monitored by injection of standard compounds over the complete analysis. The peak areas of standard compounds vary in both RP UPLC<sup>®</sup>-ToF-MS and HILIC UPLC<sup>®</sup>-ToF-MS analysis maximal about 32% (CV). The retention times drift in average 7.5 seconds (RP) or 9 seconds (HILIC) (Supplementary figure 3 and 4). In both separation modes the highest shift has been observed after addition of freshly prepared solvents. In this respect, it is especially important to ensure a proper randomization, which assures the distribution of all samples over the complete analysis. The detected mass errors vary about maximal 0.004Da in RP and 0.003Da in HILIC UPLC<sup>®</sup>-ToF-MS analysis (Supplementary figure 3 and 4). In summary, these data illustrates that a further analysis of the obtained data is reasonable since the biological and analytical reproducibility can be taken for granted. The developed UPLC<sup>®</sup>-ToF-MS platforms are stable.

#### *2.4.1.2 Mass detection, metabolite recovery and convergence between different instrumentations*

In this section a short overview of the detected metabolite recovery and comparison of the different applied analytical technologies is given. The molecular composition of all  $m/z$  features detected in (+)/(-)ICR/FT-MS has been calculated and illustrated in the Van Krevelen diagrams and KEGG pathways. The Van Krevelen diagram (Figure 36) illustrates the nature of detected metabolites as mainly hydrogen rich and oxygen poor. Additionally, spectra acquired in negative mode are rich in unsaturated (hydrogen deficient) molecules. The cell composition appears to be very complex in CHO and CHONS containing compounds. In particular regions of lipids are extremely occupied. Even though a convergence between ionization in positive and negative mode can be observed; only by the combined data the metabolome can be comprehensively approached.

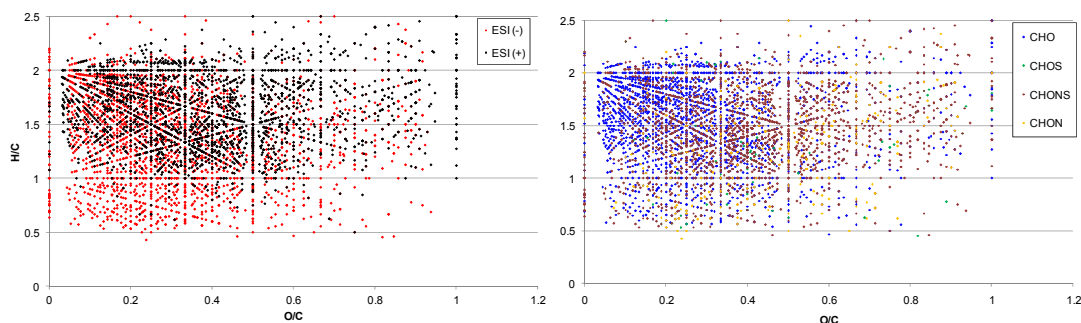


Figure 36: Van Krevelen diagram of (+)/(-)ICR/FT-MS detected masses

ICR/FT-MS detected masses have been additionally categorized according to the main pathways, in which they are involved in to monitor the general metabolite recovery (Figure 37A). Detected metabolites are distributed in all major pathways, from carbohydrates to cofactors and vitamins. Nevertheless, main classes are carbohydrates, lipids and amino acids. Classes of mostly detected lipids are sterols, fatty acyls and phospholipids.

The convergence between the different applied technologies in terms of metabolite recovery has been compared by means of KEGG CIDs. The Venn diagram and the glycolysis pathway show the intersections of metabolite annotations (Figure 37 B and C). 60% of all annotations have been detected in at least two analytical procedures. Unique annotations are up to 15% in RP UPLC<sup>®</sup>-ToF-MS, 13% in HILIC UPLC<sup>®</sup>-ToF-MS and 11% in (+)/(-)ICR/FT-MS. 55% of RP UPLC<sup>®</sup>-ToF-MS and HILIC UPLC<sup>®</sup>-ToF-MS annotated metabolites are common in both analyses. It should be clarified, that due to the different tolerated mass errors for the annotation (ICR/FT-MS 1ppm, UPLC<sup>®</sup>-ToF-MS 0.005Da), the numbers of UPLC<sup>®</sup>-ToF-MS detected metabolites might tend to be over-represented and a number of false positive annotations must be suspected. Thus, the RP UPLC<sup>®</sup>-ToF-MS data has been filtered prior to KEGG mapping. In the exemplarily illustrated glycolysis (Figure 37C) several metabolites have been directly verified by at least two applied methods. However, a much more comprehensive picture is delivered when the data from all methods is integrated.

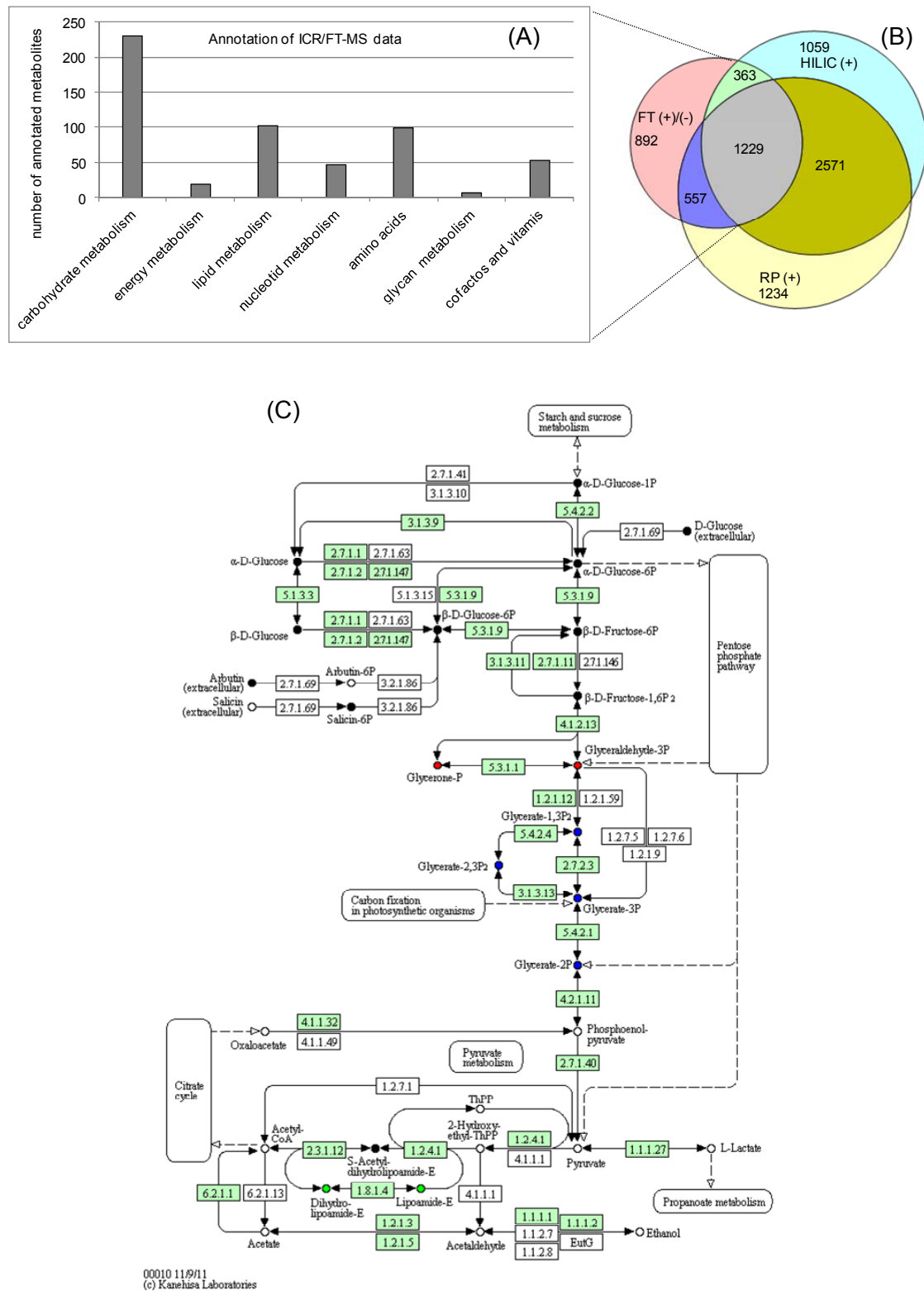


Figure 37: (A) Metabolite recovery of (+)/(-)ICR/FT-MS data; (B) Venn diagram showing the convergence between data of different applied instrumentations; (C) glycolysis illustrating the enhanced metabolite recovery in multi-parallel analysis (ICR/FT-MS-red, HILIC-green, RP-blue, black-verified in at least two methods).

### 2.4.2 Metabolic permutations after an active, normoxic infection

Since most experiments dealing with cell cultures are done under normoxia, this condition serves also in this work as starting point to investigate the metabolism of *Chlamydia* infected cells (Figure 38).

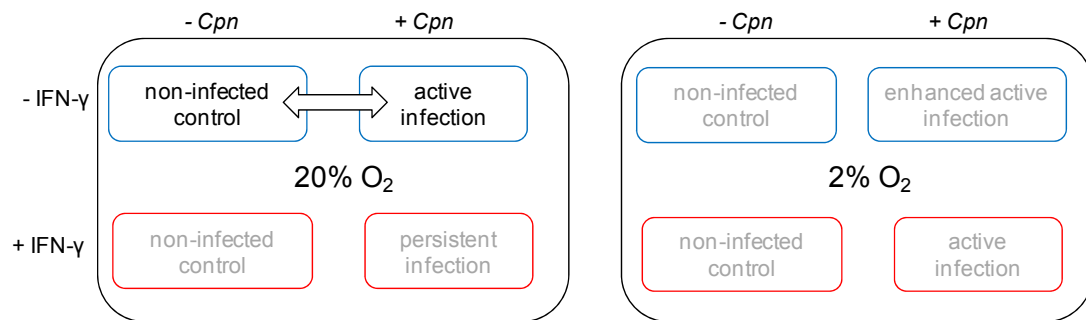


Figure 38: Illustration of the study design and data analysis: The active infection in normoxic atmosphere has been initially chosen to study metabolic alterations after *C. pneumoniae* (*Cpn*) infection.

Metabolite alterations after infection compared to the non-infected control samples have been elaborated with multivariate and univariate statistics. For multivariate analysis the data have been mean centered and unit variance scaled. It could be observed that in particular (+)ICR/FT-MS and RP UPLC<sup>®</sup>-ToF-MS delivered excellent PLS-DA models, in which infected and non-infected cells separate with statistical validity (Figure 39). No overfitting in the first component has been observed in both models during cross-validation with 200 permutations (Supplementary figure 5). The models calculated for (-)ICR/FT-MS and HILIC UPLC<sup>®</sup>-ToF-MS separate also non-infected and infected samples (Figure 39). However, it needs to be mentioned that a slide trend for overfitting has been seen for these models (Supplementary figure 5). Discriminative variables (*m/z*) of all models have been chosen according to their VIP-value and further validated with a non-parametric Wilcoxon-Mann-Whitney test. A *p*-value <0.05 has been considered statistically significant. Within the ICR/FT-MS analysis 1911 discriminative masses have been discovered, in RP UPLC<sup>®</sup>-ToF-MS 2601 and in HILIC UPLC<sup>®</sup>-ToF-MS 1104. The masses have been classified into annotated and „unknown“ metabolites, according to existence of data base entries. An overview of the numbers of statistically significant metabolites in each applied technique is given in the Table 11. In particular, the RP UPLC<sup>®</sup>-ToF-MS analysis of non-infected and infected cell extracts reveals a high number of significant discriminative metabolites. Due to the

high number of statistically significant variation in the metabolite pattern after infection, a fold change ratio of detected intensities in the two sample groups has been calculated and metabolites varying in at least 100% in their detected intensity in infected and non-infected samples are further illustrated in the table.

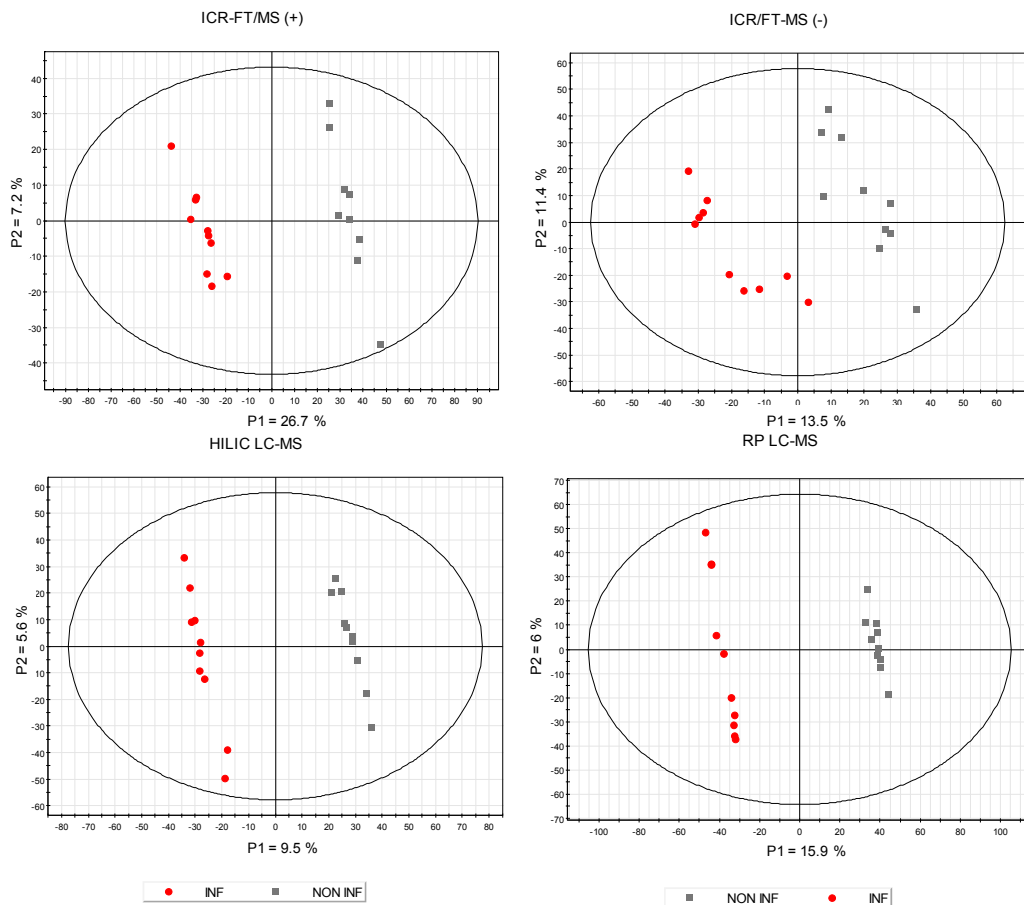


Figure 39: PLS-DA models separating infected and non-infected cells ( $R^2Y/Q^2$  (+)ICR/FT-MS 0.961/0.917, (-)ICR/FT-MS 0.774/0.47, HILIC UPLC<sup>®</sup>-ToF-MS 0.971/0.622 and RP UPLC<sup>®</sup>-ToF-MS 0.986/0.875)

	(+)(-) ICR/FT-MS	RP UPLC <sup>®</sup> - (+)ToF-MS	HILIC UPLC <sup>®</sup> - (+)ToF-MS
discriminative m/z	1911	2601	1104
annotated discriminative metabolites	186	1281	563
annotated discriminative metabolites fold change >100%	140	621	209

Table 11: Numbers of discriminative m/z detected with different techniques

The discriminative annotated metabolites have been thereafter mapped into the KEGG pathways and categorized into main metabolite classes in order to obtain a general overview of affected metabolite groups. The same trend in the data can be observed for all analytical methods (Figure 40). All in all, classes of metabolites with a high number of variations are carbohydrates, lipids and intermediates from the amino acid metabolism. However, it should be kept in mind that several metabolites are annotated for one detected mass. This might influence especially the metabolite classes of carbohydrates and lipids, since they are very rich in isomeric compounds. Nevertheless, altered lipid profiles after infection are reasonable, because cell wall and cellular membranes as well as the inclusion membrane of *Chlamydia* contain lipid species. The same accounts for carbohydrates since carbohydrates are major cellular energy sources and after infection the demand for energy might be increased as two instead of one organism need to survive in infected cells. The variations in the amino acid metabolism can result from amino acid *de novo* biosynthesis, protein biosynthesis and -degradation.

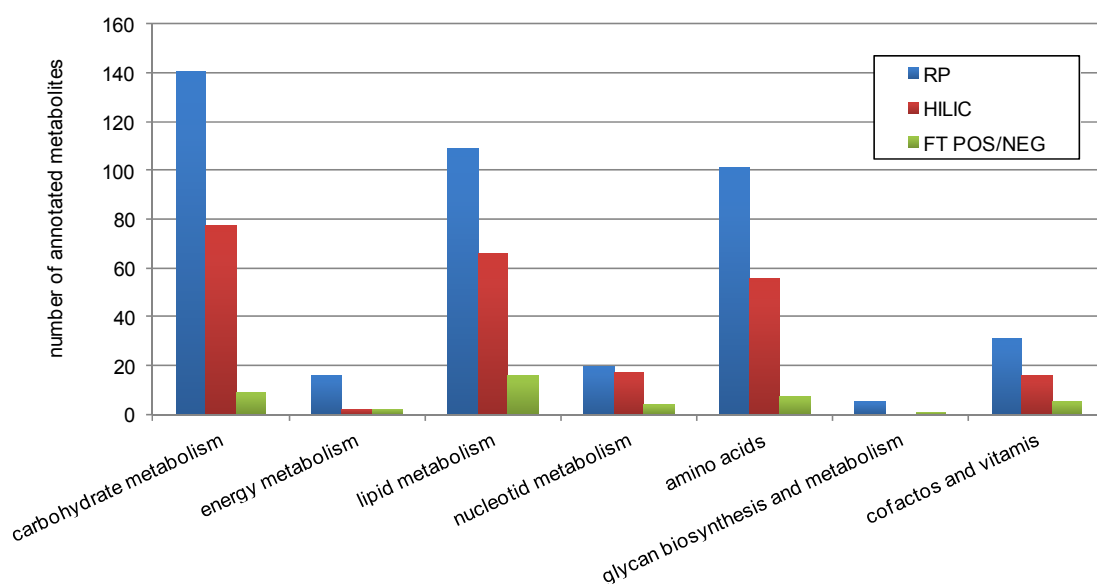


Figure 40: Distribution of statistically significant metabolites over the KEGG metabolite classes

Based on this general overview, single pathways containing discriminative masses have been examined (Figure 41). The metabolism of arachidonic acid, arginine and proline as well as amino sugars is mainly influenced after *Chlamydia* infection. 25% of all discriminative annotated metabolites found in HILIC UPLC<sup>®</sup>-ToF-MS are within these pathways, for RP UPLC<sup>®</sup>-ToF-MS and ICR/FT-MS it is 15% and 18%. Further

important modulated pathways are the steroid biosynthesis, glycerophospholipid- and sphingolipid metabolism, alpha-linolenic acid and fatty acid biosynthesis; several pathways from the carbohydrate metabolism (galactose-, starch/sucrose- and fructose/mannose metabolism), histidine and tryptophan metabolism. Besides these, the thiamine and ubiquinone as well as the purine and pyrimidine metabolisms contain a high number of important metabolites. For the first time this data gives an overview of metabolic modulations in a human cell after infection. Previous studies only focused mainly on single aspects, which have been summarized in the introduction (chapter 1.5.2). The observed modulations within this non-targeted study reflect these previous results very well and expand our knowledge.

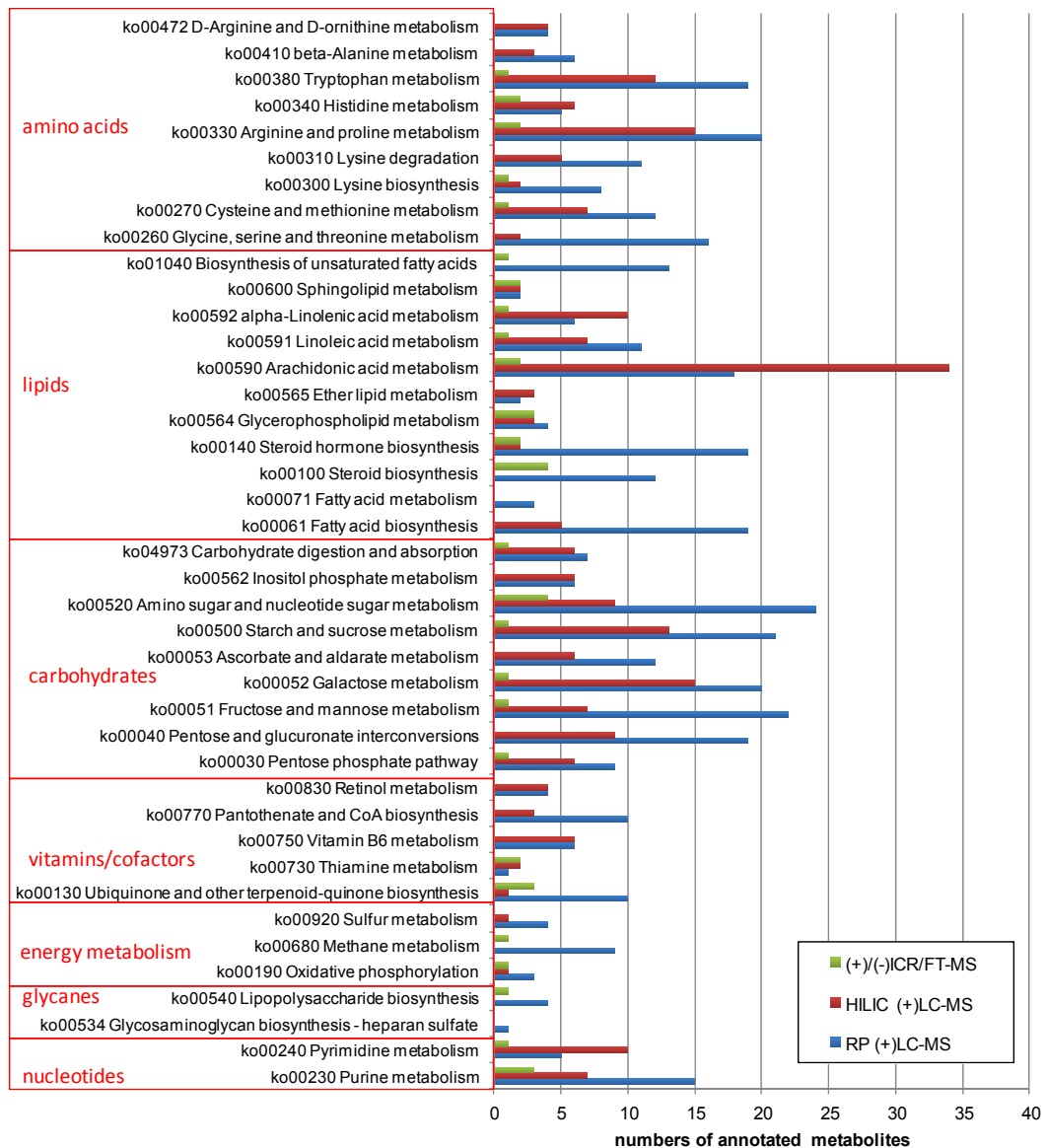
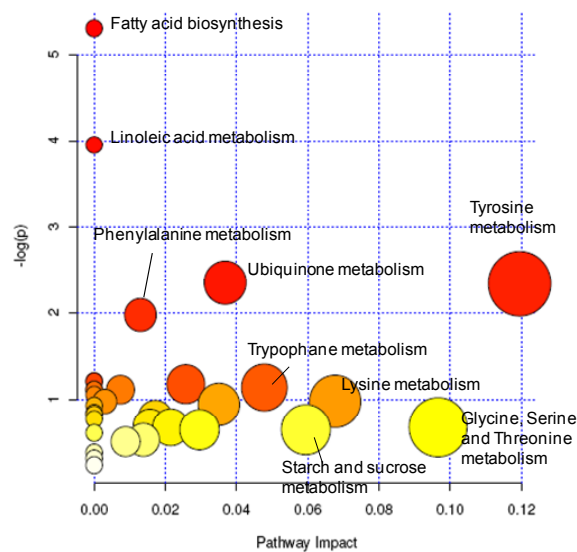


Figure 41: Distribution of statistically significant metabolites over the KEGG pathways

To accommodate the very high numbers of significantly affected metabolites, in the following data analysis only metabolites with a variation of at least 100% signal intensity in infected and non-infected cells have been further investigated. The metabolite annotations of RP UPLC<sup>®</sup>-ToF-MS data have been filtered to minimize false positive annotations. The data from ICR/FT-MS, RP UPLC<sup>®</sup>-ToF-MS and HILIC UPLC<sup>®</sup>-ToF-MS analyses have been merged and statistically significant annotated metabolites have been compared. At first the focus is on annotated metabolites, an extension to „unknown“ species will be given later (see chapter 2.4.2.5).

The KEGG CIDs of important regulated metabolites (Supplementary table 4) have been uploaded in the web-based metabolomics platform MetaboAnalyst (Xia et al., 2009) and a pathway analysis has been performed (Figure 42). This is useful to visualize the data and determine mainly modulated pathways based on pathway topology and over-representation tests (Xia et al., 2009).



*Figure 42: Pathway analysis of statistically significant discriminative metabolites with a signal intensity fold-change  $\geq 100\%$  in infected and non-infected cells. The size of the bubbles demonstrates the number and position of important metabolites within the pathway. (aligned data from ICR/FT-MS and UPLC<sup>®</sup>-ToF-MS analyses, after filtering)*

The pathway analysis revealed that metabolites varying in at least 100% of their detected intensity are mainly contributors in the amino acid and lipid metabolism. Furthermore, disaccharides and nucleoside diphosphates (NDP) have been importantly altered after infection.



### 2.4.2.1 Important modifications in amino acid metabolism

*Chlamydia* encode a few genes for biosynthesis of some amino acids itself, although mostly with truncated pathways (McClarty, 1999). But the bacterium still depends strongly on nutrients delivered from the host cell cytosol, accordingly a substantial number of transporters are also encoded in its genome (McClarty, 1999). It is in consequence not surprising that reduced levels of several amino acids have been found in infected cells, like e.g. threonine, tyrosine and leucine/isoleucine (Figure 43). Probably, most of these amino acids are utilized as building blocks during protein biosynthesis; furthermore leucine, isoleucine or valine might be consumed as precursors for branched-chain fatty acids.

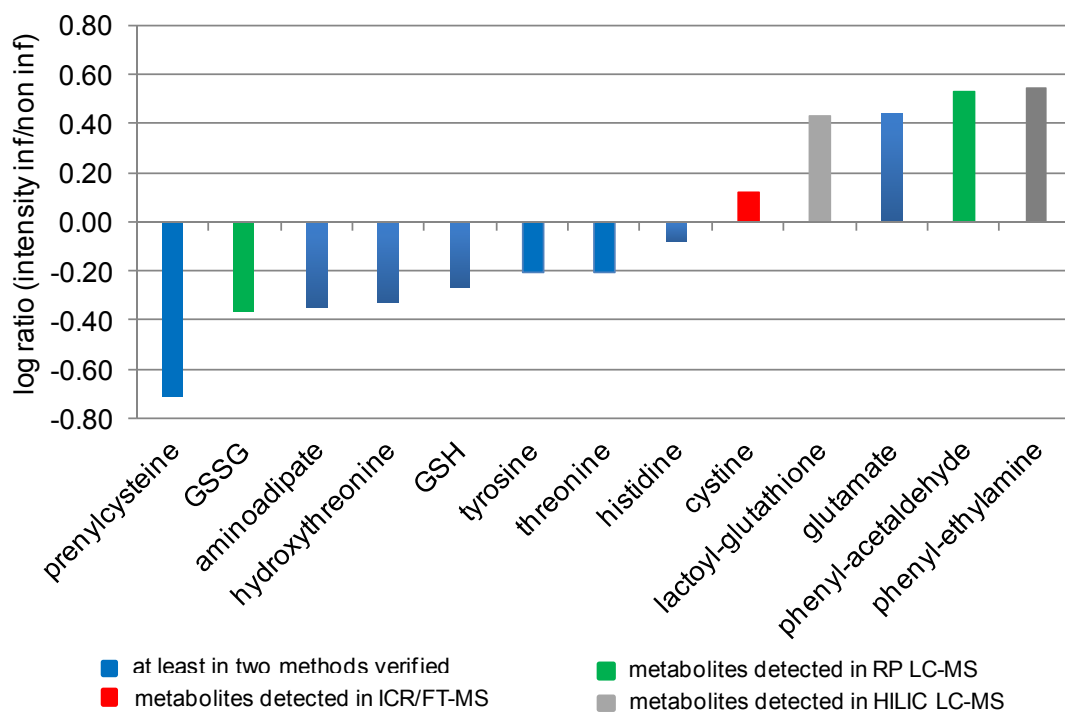


Figure 43: Mainly affected amino acids and -derivates (the origin of the data is shown in the color code, levels of C<sub>6</sub>H<sub>13</sub>NO<sub>2</sub> (leucine/isoleucine/valine) and several additional metabolites drop below limit of detection in infected samples)

In contrast to the above mentioned amino acids, glutamate has been detected with increased signal intensity after infection (Figure 43). This is consistent with the earlier work of Ojcius et al., who have found an increased level of glutamate occurring midway during the developmental cycle of *Chlamydia psittaci* (Ojcius et al., 1998). Glutamate is of outstanding importance for the connection between nitrogen and carbon metabolism. An increased glutamate level indicates furthermore

an elevated glutamineolysis, which is evidenced for hypoxia (Le *et al.*, 2012) and might be in case of *Chlamydia* infection an effect of the activation of HIF-1 during chlamydial development (Rupp *et al.*, 2007). Furthermore, cystine, the oxidized dimeric form of cysteine (cys-S-S-cys) has been detected increased by 30% after infection. Cysteine and cystine levels are highly connected: while cystine is the dominant form in the extracellular space, cysteine occurs mainly inside cells (Conrad *et al.*, 2011). Even though cysteine may be biosynthesized from methionine in some cell lines, most cells import either of the forms from extracellular space to manage the intracellular cysteine demand (Conrad *et al.*, 2011). Several chlamydial proteins are very rich in cysteine, they are strongly interconnected by disulfide bonds. A dependency of the chlamydial development from cysteine has been identified earlier (Allan *et al.*, 1985). The transformation of *Chlamydia* morphological forms EB and RB is inhibited, when cysteine is absent in the cell culturing medium (Allan *et al.*, 1985). The cysteine/cystine system is moreover important for maintaining the cellular physiological redox conditions (Conrad *et al.*, 2011). Furthermore, both are important precursors for glutathione (GSH), which is also a major compound in the cellular redox system. GSH has a key role at the initial stage of the infection (Lazarev *et al.*, 2010). Consistent with the literature, decreased GSH levels after infection have been seen in the data. In addition, reduced levels of oxidized glutathione (GSSG) (Figure 43) have been identified. Moreover, we found an increase in lactoyl-glutathione, which is a known modulator of the microtubule assembly (HMDB, 2012b) and consequently also of the cytoskeleton and intracellular transport processes. In summary, next to alterations in the amino acid pool the results clearly suggest a modification of the cellular redox system after infection.

Moreover, metabolites like phenyl-acetaldehyde, phenyl-ethylamine, hydroxyl-phenyllactate, hydroxyl-indoleacetaldehyde as well as hydroxylthreonine indicate an effect of *Chlamydia* infection on the metabolism of aromatic amino acids. The catabolism of the essential amino acid phenylalanine to phenyl-ethylamine and phenyl-acetaldehyde and further to phenylacetic acid (PAA) is encoded in the human genome. A further catabolism of PAA to phenylacetyl-CoA and later acetyl-CoA and succinyl-CoA and consequently the introduction into the TCA cycle has been shown for gram negative bacteria like *Pseudomonas putida* and *Escherichia coli* (Arias *et al.*, 2008, Navarro-Llorens *et al.*, 2005, Olivera *et al.*, 1998, Panoutsopoulos *et al.*, 2004, Arias-Barrau *et al.*, 2004) (Figure 44). Based on these

results the investigations of aromatic amino acids metabolism might be very interesting for targeted follow-up studies.

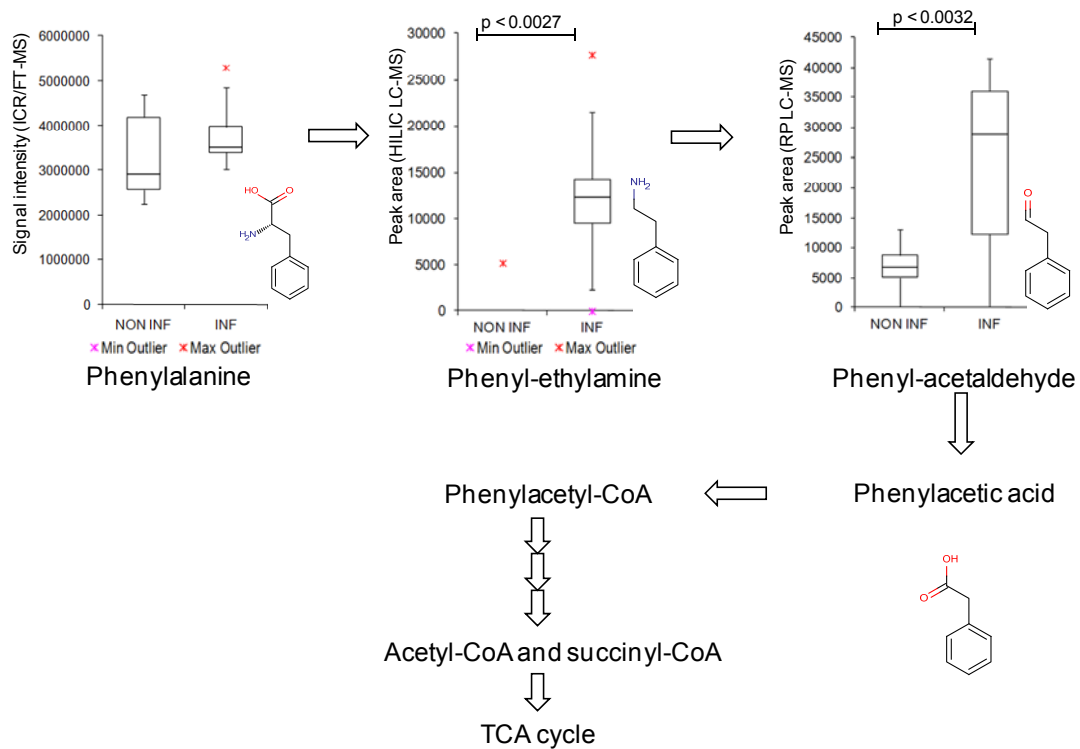


Figure 44: Detected metabolite abundance in *Chlamydia* infection in the proposed phenylalanine catabolism and connection to the TCA cycle in gram-negative bacteria

#### 2.4.2.2 Important modifications in the lipid metabolism

A depletion of the host cell's lipid homeostasis is further indicated by our data, particularly an activated metabolism of arachidonic acid and linoleic acid. The arachidonic acid metabolism is a key pathway in inflammatory processes, thus the detection of increased levels of eicosanoids suggests an inflammation in the host cell (Figure 45). The differentiation between the isomeric prostaglandins, however, needs further targeted optimization of UPLC<sup>®</sup> separation, for that reason only the elemental composition of the putative derivatives are illustrated.

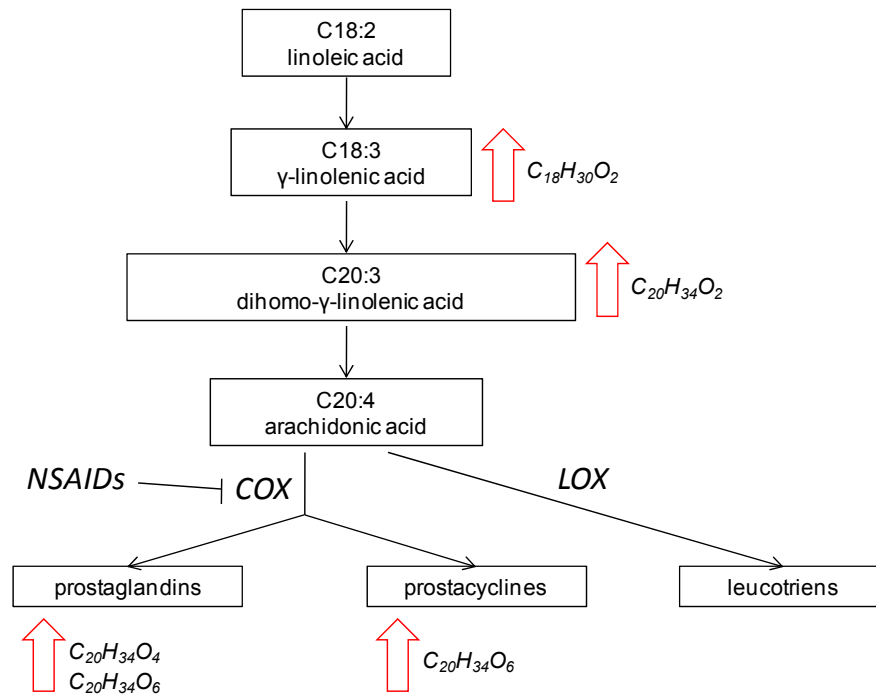
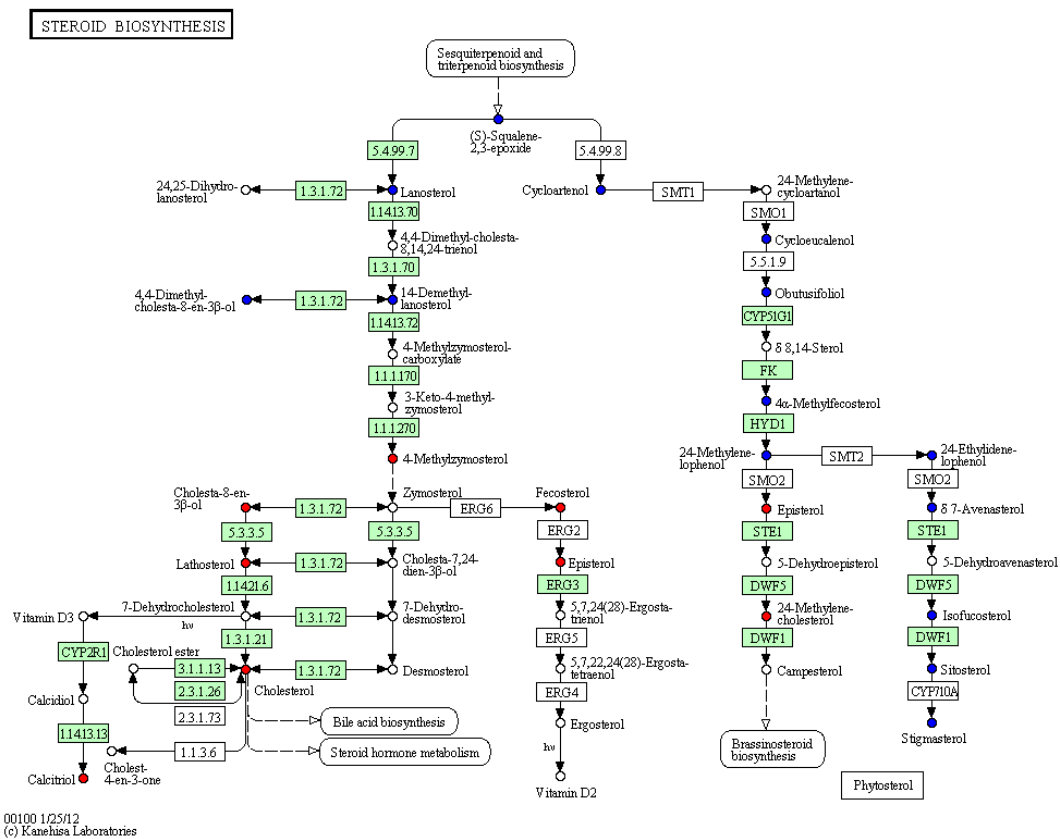


Figure 45: Eicosanoid metabolism affected by infection: Increased levels of putative metabolites are indicated by red errors and their elemental compositions (COX cyclooxygenase, LOX lipoxygenase, NSAIDs non-steroidal anti-inflammatory drugs)

Even though an inflammation is a physiological reaction against a potential harmful stimulus and it is very important for the eradication of such a stimulus, a deregulated inflammation is connected to many pathophysiological processes and diseases. A promotion of proinflammatory chemokines, cytokines and growth factors has been previously discussed after *Chlamydia* infection on a protein level (Stephens, 2003). In addition, Hyvarinen et al. have found increased levels of C<sub>20</sub>H<sub>34</sub>O<sub>2</sub> in the hepatic fatty acid content of chronic chlamydial infected mice, but observed a reduction of its precursor C<sub>18</sub>H<sub>30</sub>O<sub>2</sub> (Hyvarinen et al., 2009). An induction of COX-2 by *C. pneumoniae* in immune cells has been additionally reported as a potential risk factor for the development and the progression of chronic vascular diseases (Rupp et al., 2004). The presented results further name and confirm inflammatory processes within the host cell, which might also be targets for therapeutic intervention, since the blocking of the arachidonic acid cascade can be achieved by NSAIDs.

A further detected modulation in the lipid balance points towards the cholesterol biosynthesis (Figure 46). Cholesterol, a typical eukaryotic lipid, has been identified in the pathogen by previous work (chapter 1.5.2). Since *Chlamydia* do not encode for the enzymatic biosynthesis, cholesterol must be of human origin (Carabeo et al.,

2003). Cholesterol is synthesized in the human endoplasmic reticulum (ER) and transported with the Golgi apparatus to the chlamydial inclusion. There the Golgi apparatus is fragmented into ministacks and such ministracks surround the inclusion (Heuer et al., 2009). Cholesterol is due to its rigid planar structure an essential compound to maintain membrane fluidity. A decreased cholesterol level after *Chlamydia* infection is known and affects the membrane fluidity, as well as cellular functions including surface receptor binding, chemotaxis, signal transduction and susceptibility to microbial invasion (Azenabor et al., 2005, Tappia et al., 1997).



**Figure 46: Cholesterol biosynthesis (red dots illustrate statistically significant decreased metabolites, which met the strict criteria of at least two fold decrease in infected cells, blue dots show further statistically significant metabolites decreased after infection, but to a lower extent. (data inferred from ICR/FT-MS and RP UPLC<sup>®</sup>-ToF-MS analyses)**

The data also shows a modulation of sphinganine levels (dihydro-sphingosine) (Figure 47). Sphinganine is a blocker of post-lysosomal cholesterol transport (HMDB, 2012c). It has been described that sphingoid base backbones, like sphingosine and sphinganine are highly bioactive compounds for the regulation of second messengers important for cell proliferation, apoptosis, and differentiation

(Hannun et al., 2001, Shayman, 2000) as well as for membrane traffic (Friant et al., 2001, Friant et al., 2000, Zanolari et al., 2000). In the scope of this work sphinganine has been annotated by its exact mass, furthermore the predicted and detected retention times in RP UPLC<sup>®</sup>-ToF-MS have been in good accordance to each other, nevertheless a targeted study needs to confirm the finding.

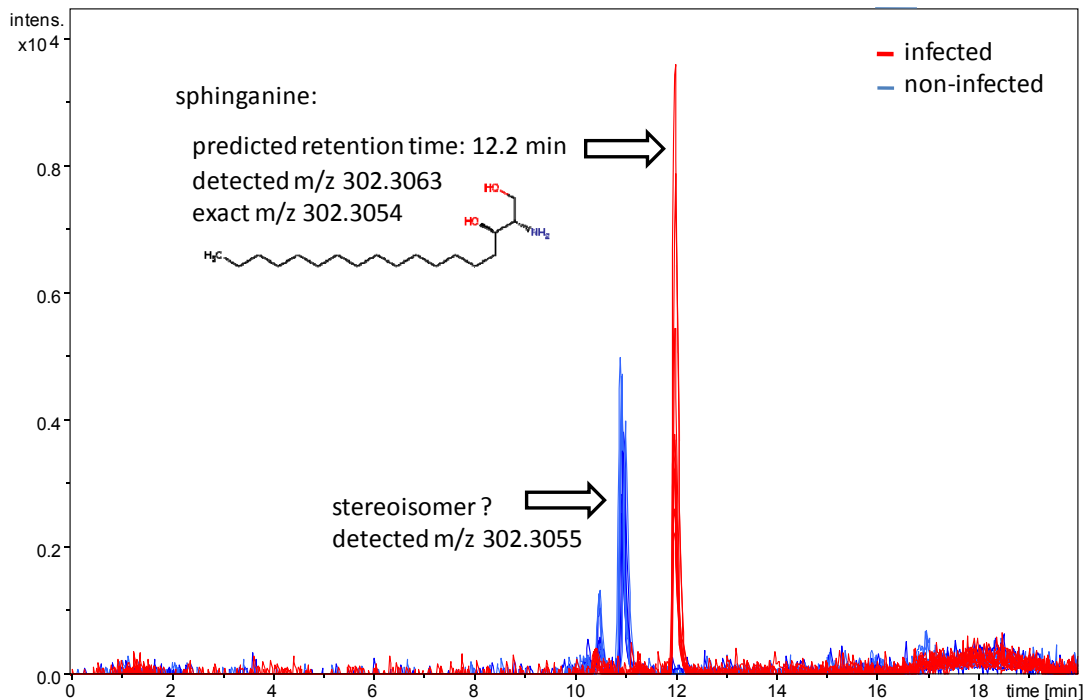


Figure 47: RP UPLC<sup>®</sup>-ToF-MS EIC of putative sphinganine [ $m/z$  302.305 $\pm$ 0.02] for one technical of each biological repetition

#### 2.4.2.3 Important modifications in the carbohydrate metabolism and nucleosides

A putative storage of carbon sources for the later development of *Chlamydia* or the extracellular state is indicated by an increase of the detected intensities of disaccharides about 600% after infection. Decreased levels of glucose phosphate and glucose might be explained by the activation of carbohydrate catabolism after infection (Ojcius et al., 1998).

Furthermore, drops in all NDPs are identified, either statistically significant or as a trend. NDPs and their energy richer analogs NTPs (nucleoside triphosphates) are usually in equilibrium (NDP/NTP~constant). Thus, decreased levels of NDPs indicate elevated levels of NTP, which is consistent with former studies (Ojcius et al., 1998). The detected intensities of NTPs themselves have been very low and very close to the limit of detection. In consequence, they are not interpreted.

Nucleotides are required for DNA and RNA synthesis and especially adenosine nucleotides are universal energy transducers.

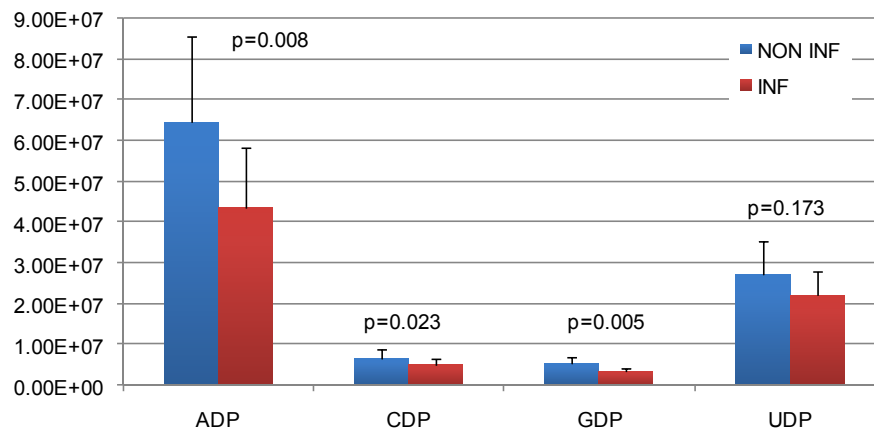


Figure 48: ICR/FT-MS NDP signal intensities (average  $\pm$  STD) in infected and non-infected cells (ADP and UDP decrease is UPLC<sup>®</sup>-ToF-MS confirmed)

#### 2.4.2.4 Summary of important permutations in the central metabolism

Discriminative metabolites are spread all over the complete known metabolic pathways. However, mainly modulated metabolite classes in infection are lipids, carbohydrates and amino acids. Due to the high amount of discriminative markers, a focusing on mainly altered compounds has been necessary. This could be achieved by strengthening the elaboration criteria. The data delivered complete new insights in infection specific alterations of amino acid, redox and lipid homeostasis and pinpointed several metabolites as key metabolites. The data is in very good consistency with previously described metabolic alterations after *Chlamydia* infection.

The above presented and discussed results regarding the amino acid, redox, carbohydrate and lipid metabolism are summarized in the Figure 49.

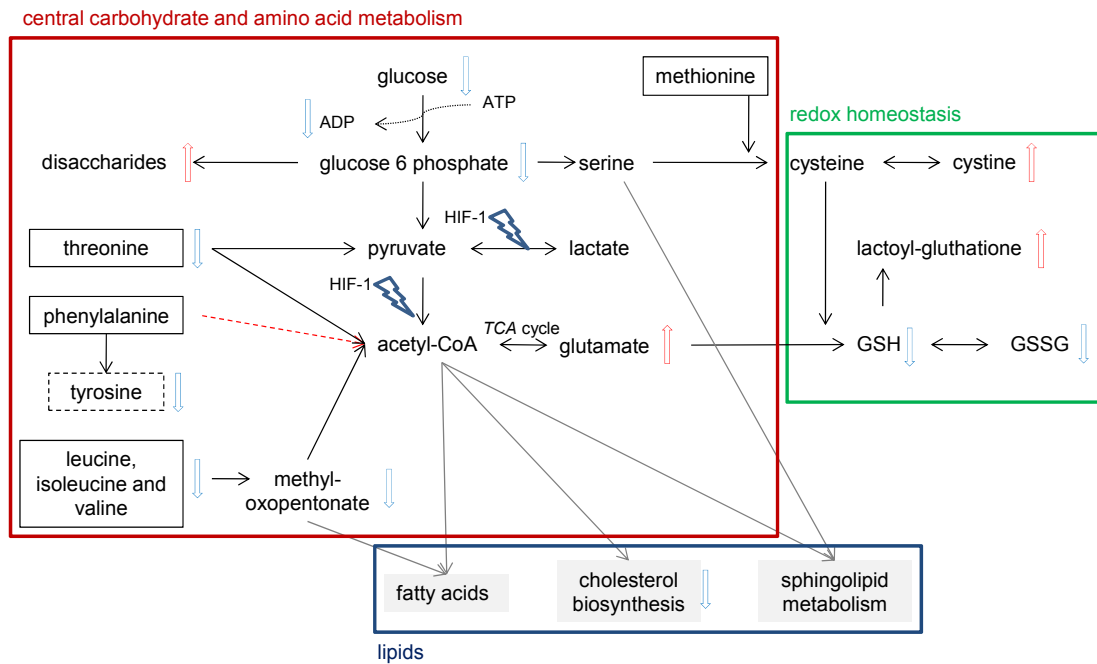


Figure 49: Summary of main metabolites affected by *C. pneumoniae* infection. The illustrated metabolites have been determined by strict elaboration criteria (VIP-value >1, p-value <0.05, two-fold ratio in infected and non-infected cells). Essential amino acids are framed in boxes.

#### 2.4.2.5 Key „unknown“ metabolites affected by infection

The above described results only reflect one part of the detected alterations in the metabolome of human cells after infection. Due to the high amount of statistically significant modified metabolites strict criteria have been used to focus on main effects of *Chlamydia* infection. However, annotated metabolites represent only approximately 10 to 20% of the data set. A huge number of discriminated compounds are “unknown” metabolites (Figure 50) and in particular these “unknowns” seem to be promising diagnostic biomarkers. In the following part a deeper analysis of those metabolites is presented. The results base on data, which has been detected with ICR/FT-MS.



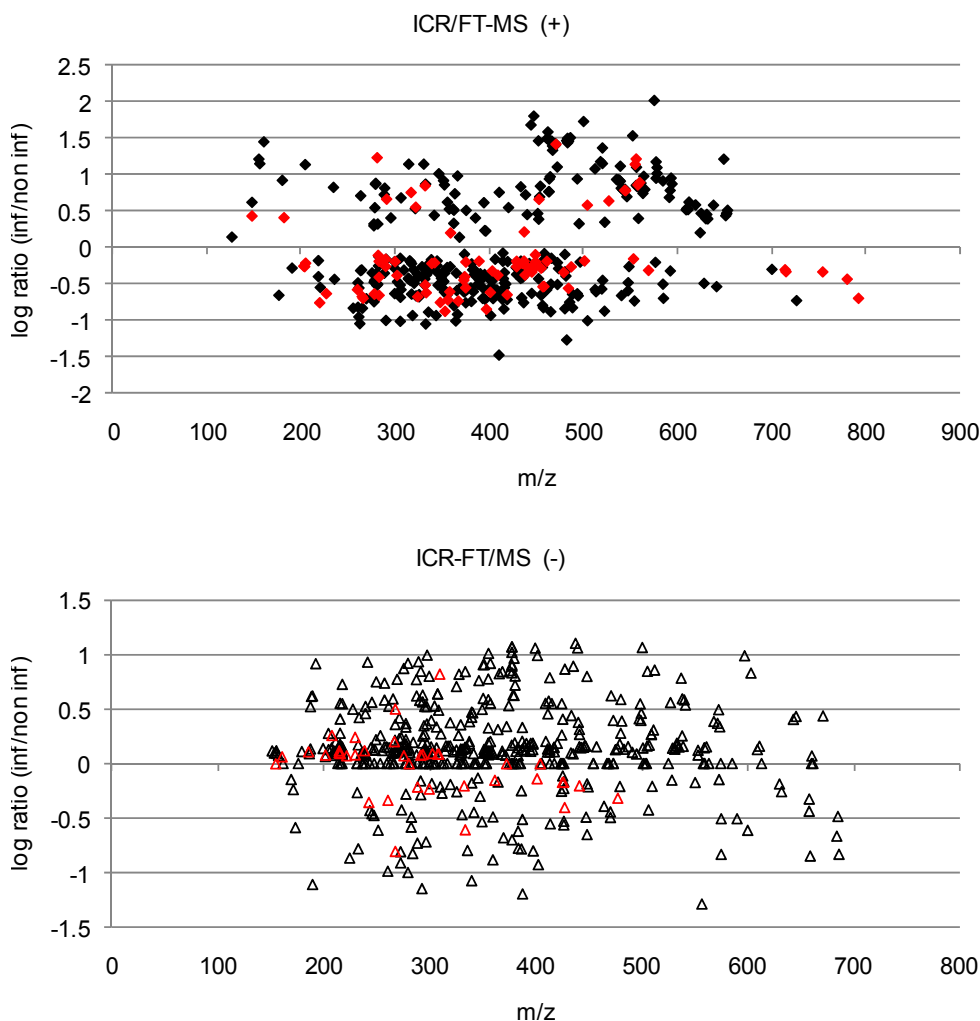


Figure 50: Logarithmic ratio of detected intensities of statistically significant affected metabolites ( $p$ -value  $<0.05$ , VIP-VALUE  $>1$ , annotated metabolites are colored in red and "unknowns" in black)

The elemental compositions of detected  $m/z$  have been calculated within a 0.1ppm error window by applying netcalc for ICR/FT-MS data (Tziotis et al. 2011). The ultrahigh mass accuracy and resolution of ICR/FT-MS enables such calculations. A list of common biotransformation and thus mass differences has been elaborated for the calculation of the network. The purpose of such network is on the one hand visualization of the connectivity of a data set, on the other hand it enables an association between the annotated and „unknown“ metabolism. For visualization  $m/z$  features showing a high connectivity are centered, whereas  $m/z$  with four or less connections are put in the lower periphery. The network for  $m/z$  detected in positive electrospray mode is illustrated in Figure 51. Masses annotated by MassTRIX (Suhre et al., 2008) are colored red, while „unknown“ metabolites are indicated by

black coloration. Discriminative compounds with a VIP-VALUE  $>1$  and p-value  $<0.05$  are represented by bigger bubbles.

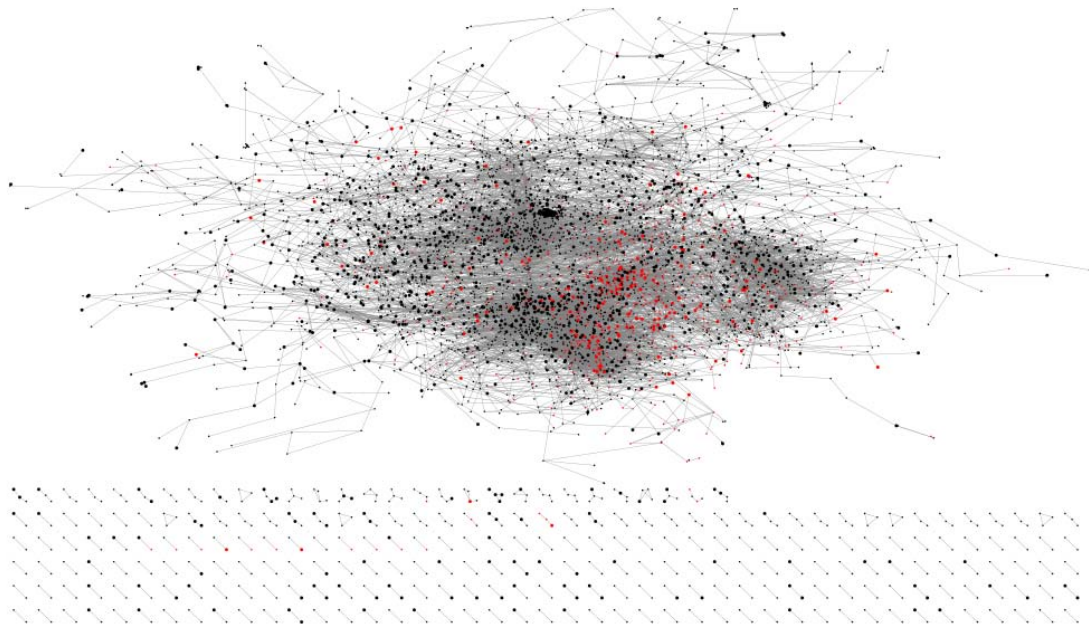


Figure 51: Kendrick-analogous mass difference network based on (+)ICR/FT-MS data (annotated metabolites are shown in red, „unknown“ compounds are illustrated in black, discriminated metabolites are indicated by bigger bubbles)

A dense network indicates a high connectivity of the detected masses within the data set. Several regions, where discriminative masses are concentrated, can be identified in the presented network, thus it can be suspected that those masses are closely related to each other. Furthermore, a local concentration of annotated important metabolites exists.

In the next step all pairs of connected masses, which do not include any discriminative m/z, have been excluded from the data set. This has been done in order to reduce the complexity of the network and simplify the data elaboration and interpretation. The resulting network still shows a high degree of connectivity (not shown). The above described local concentrations of discriminative masses have been conserved during the simplification. Therefore, it seems that the *Chlamydia*-affected part of the metabolism is quite connected in a biochemical manner. If the metabolic changes after infection appear in separated parts of the metabolome, a disconnected network would result. For a further data reduction only masses, which had been increased after infection, have been included (Figure 52). The resulting network reveals a very high connectivity for a set of markers. Above all, such

markers might be involved in many biochemical modulations, which do only appear in infected cells. Masses significantly increased after infection have been additionally illustrated in a Kendrick plot to spot homologous series of markers (Figure 53).

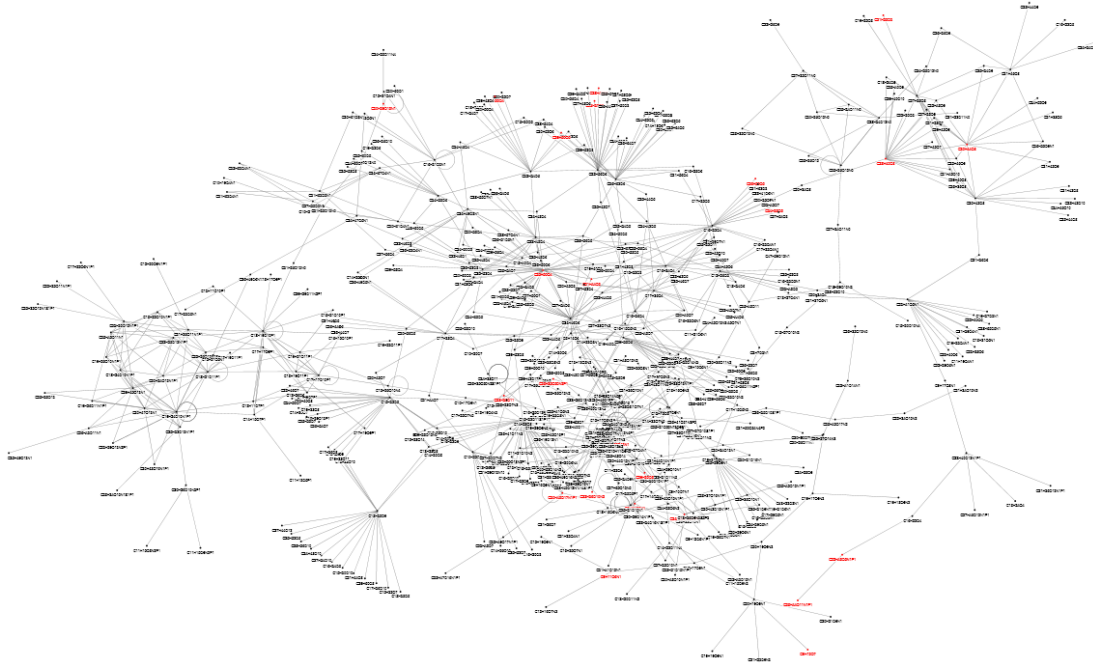


Figure 52: Kendrick-analogous mass difference network only including statistically significant increased metabolites (annotated metabolites are shown in red, „unknown“ compounds are illustrated in black)

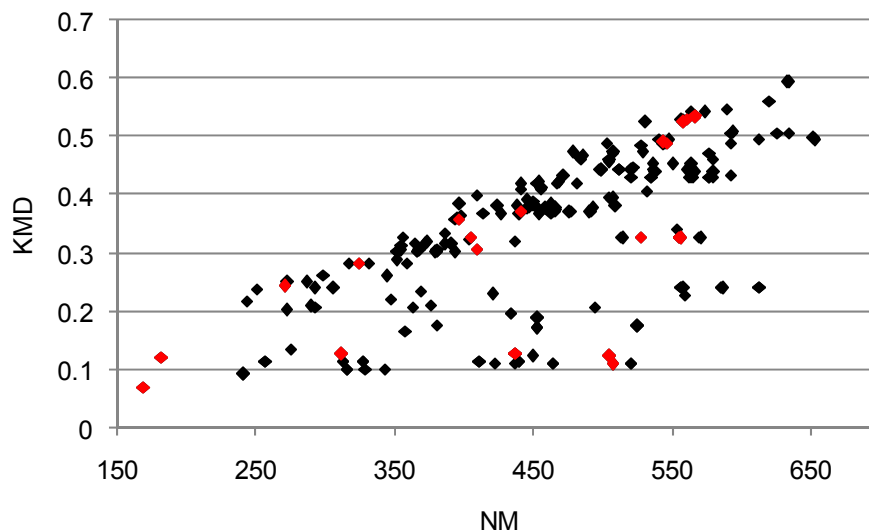


Figure 53: Kendrick plot of statistically significant increased compounds after infection: Several homologous series can be observed, which contain known (red) and „unknown“ (black) compounds

Taking both illustrations together, human cells infected with *C. pneumoniae* are characterized by putative structural related families of markers. Furthermore, both diagrams nicely illustrate the connection between annotated and „unknown“ metabolites, which offers the possibility to further characterize „unknowns“.

Interestingly, some of the discriminative masses have shown a very high connectivity (>10) (Figure 54) and might therefore play a key role in biochemical processes mediated by *Chlamydia*. For instance, the  $m/z$  437.3600, which has been annotated as monoacylglycerol  $[M+Na]^+$  with the elemental composition  $C_{25}H_{50}O_4$ , show 38 connections. These important key metabolites have been searched afterwards in the UPLC<sup>®</sup>-ToF-MS data and are highlighted with bold letters, if verified (applied error 0.005Da) (Table 12).

Within the presented workflow it has been possible to focus on mainly affected key „unknown“ metabolites, which might be very promising diagnostic markers. The isolation and structure elucidation of these important markers is a very interesting analytical task for my future research.

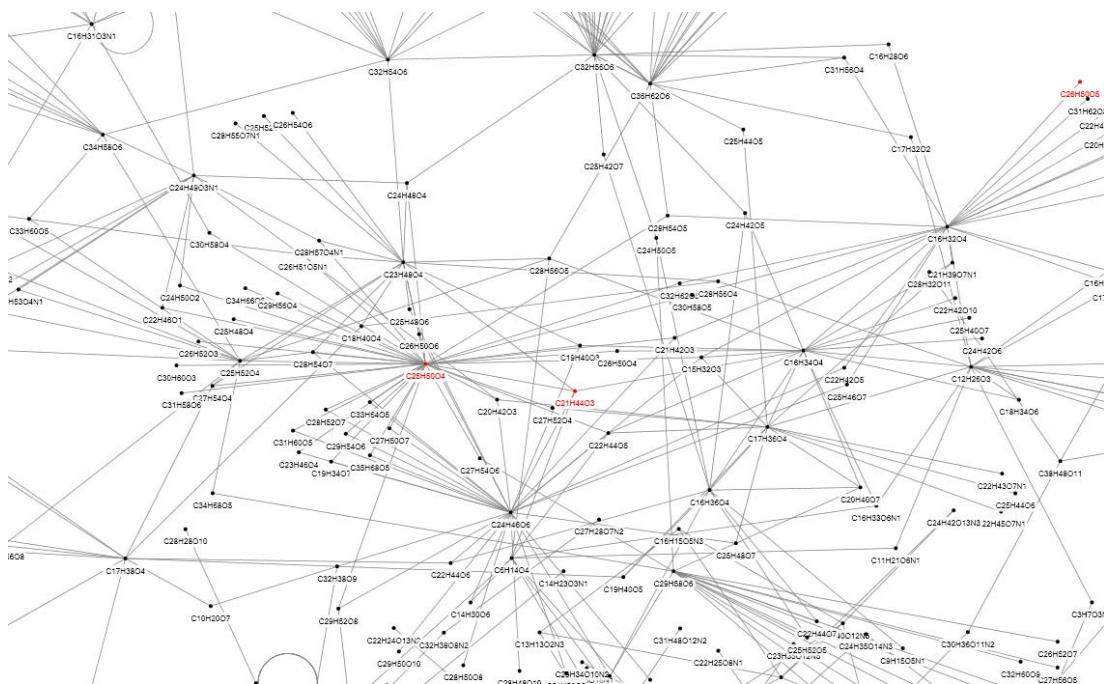


Figure 54: Zoom in the center Kendrick-analogous mass difference network only including statistically significant increased metabolites (annotated metabolites are shown in red, „unknown“ compounds are illustrated in black)

detected m/z	elemental composition	log ratio (inf/non inf)	connectivity
437.360043	C <sub>25</sub> H <sub>50</sub> O <sub>4</sub>	0.22	38
453.318618	C <sub>24</sub> H <sub>46</sub> O <sub>6</sub>	0.39	30
347.167571	C <sub>14</sub> H <sub>28</sub> O <sub>8</sub>	1.01	29
559.396854	C <sub>32</sub> H <sub>56</sub> O <sub>6</sub>	0.40	25
311.219228	C <sub>16</sub> H <sub>32</sub> O <sub>4</sub>	INF	22
<b>363.198851</b>	<b>C<sub>15</sub>H<sub>32</sub>O<sub>8</sub></b>	<b>0.51</b>	<b>21</b>
459.13551	C <sub>18</sub> H <sub>19</sub> O <sub>10</sub> P <sub>1</sub>	INF	19
<b>313.234881</b>	<b>C<sub>16</sub>H<sub>34</sub>O<sub>4</sub></b>	<b>INF</b>	<b>18</b>
411.34436	C <sub>23</sub> H <sub>48</sub> O <sub>4</sub>	0.76	18
<b>421.240754</b>	<b>C<sub>18</sub>H<sub>38</sub>O<sub>9</sub></b>	<b>0.55</b>	<b>18</b>
462.146476	C <sub>19</sub> H <sub>24</sub> O <sub>10</sub> N <sub>1</sub> P <sub>1</sub>	1.50	18
613.443726	C <sub>36</sub> H <sub>62</sub> O <sub>6</sub>	INF	18
<b>241.177362</b>	<b>C<sub>12</sub>H<sub>26</sub>O<sub>3</sub></b>	<b>INF</b>	<b>17</b>
525.412588	C <sub>29</sub> H <sub>58</sub> O <sub>6</sub>	INF	17
<b>527.261405</b>	<b>C<sub>28</sub>H<sub>40</sub>O<sub>8</sub></b>	<b>0.65</b>	<b>17</b>
<b>327.25053</b>	<b>C<sub>17</sub>H<sub>36</sub>O<sub>4</sub></b>	<b>INF</b>	<b>15</b>
513.245768	C <sub>27</sub> H <sub>38</sub> O <sub>8</sub>	1.08	15
529.117476	C <sub>18</sub> H <sub>21</sub> O <sub>11</sub> P <sub>1</sub>	INF	15
<b>434.287605</b>	<b>C<sub>23</sub>H<sub>41</sub>O<sub>5</sub>N<sub>1</sub></b>	<b>0.83</b>	<b>14</b>
439.375607	C <sub>25</sub> H <sub>52</sub> O <sub>4</sub>	0.72	14
557.381116	C <sub>32</sub> H <sub>54</sub> O <sub>6</sub>	1.10	14
553.27705	C <sub>30</sub> H <sub>42</sub> O <sub>8</sub>	1.54	13
555.292702	C <sub>30</sub> H <sub>44</sub> O <sub>8</sub>	1.15	13
<b>293.120584</b>	<b>C<sub>10</sub>H<sub>22</sub>O<sub>8</sub></b>	<b>INF</b>	<b>12</b>
<b>315.250549</b>	<b>C<sub>16</sub>H<sub>36</sub>O<sub>4</sub></b>	<b>INF</b>	<b>12</b>
329.266106	C <sub>17</sub> H <sub>38</sub> O <sub>4</sub>	INF	12
550.162497	C <sub>29</sub> H <sub>45</sub> O <sub>13</sub> N <sub>1</sub>	INF	12
<b>422.360314</b>	<b>C<sub>24</sub>H<sub>49</sub>O<sub>3</sub>N<sub>1</sub></b>	<b>INF</b>	<b>11</b>
426.108864	C <sub>25</sub> H <sub>31</sub> O <sub>10</sub> N <sub>1</sub>	INF	11
504.438534	C <sub>30</sub> H <sub>59</sub> NO <sub>3</sub>	0.59	11
564.178177	C <sub>30</sub> H <sub>47</sub> O <sub>13</sub> N <sub>1</sub>	INF	11
<b>257.172206</b>	<b>C<sub>6</sub>H<sub>14</sub>O<sub>4</sub></b>	<b>INF</b>	<b>10</b>
376.209453	C <sub>19</sub> H <sub>31</sub> O <sub>5</sub> N <sub>1</sub>	0.51	10
<b>445.119923</b>	<b>C<sub>17</sub>H<sub>17</sub>O<sub>10</sub>P<sub>1</sub></b>	<b>1.69</b>	<b>10</b>
506.172561	C <sub>28</sub> H <sub>45</sub> O <sub>11</sub> N <sub>1</sub>	INF	10
532.188228	C <sub>21</sub> H <sub>26</sub> O <sub>11</sub> N <sub>1</sub> P <sub>1</sub>	INF	10
562.198812	C <sub>22</sub> H <sub>28</sub> O <sub>12</sub> N <sub>1</sub> P <sub>1</sub>	INF	10
576.21446	C <sub>23</sub> H <sub>30</sub> O <sub>12</sub> N <sub>1</sub> P <sub>1</sub>	2.02	10

Table 12: Statistically significant increased metabolites with a very high connectivity (>10) in the network analysis (UPLC<sup>®</sup>-Tof-MS verified masses are given in bold letters)

### 2.4.3 Metabolic permutations after an active and persistent infection

The extracted ICR/FT-MS mass lists for all samples have been aligned (Matrix generator 0.4, inhouse written, M. Lucio) with 1ppm error. Masses detected in at least 3 biological replicates have been included in the multivariate analysis and annotated by MassTRIX (Suhre *et al.*, 2008). An overview of natural occurring patterns is given in the PCA models (Figure 55). For reasons of visualization the data set has been divided in normoxic and hypoxic cultivated samples.

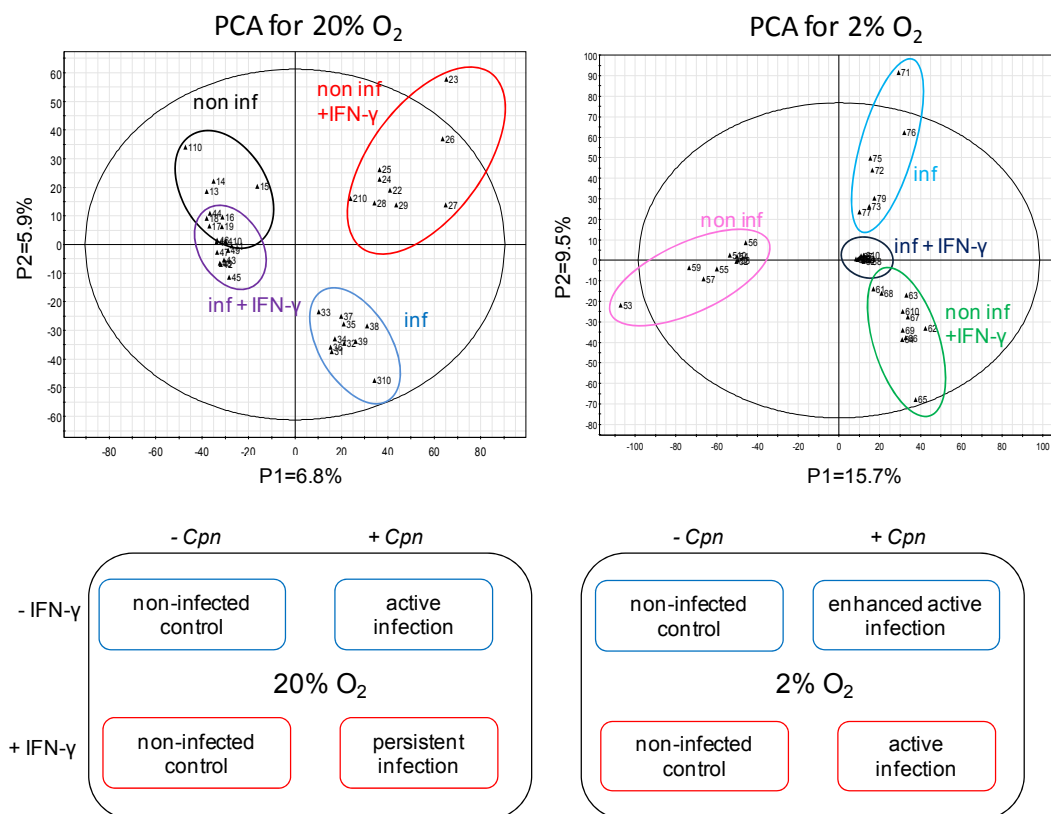


Figure 55: PCA for cells cultivated and infected under 20% or 2% oxygen atmosphere (+)ICR/FT-MS data)

Obviously, all cultivation conditions cause a shifting in the metabolite pattern, thus a nice separation can be observed. Under normoxic conditions both, the non-infected cells cultivated with an addition of IFN- $\gamma$  and the infected cells, separate from the non-infected controls (Figure 55 20% O<sub>2</sub>). But cells with a persistent infection do not separate within the first two principal components from non-infected controls. This degree in commonality of persistent infected samples and non-infected controls without IFN- $\gamma$  rather than with those with IFN- $\gamma$  is quite surprising, but might indicate

an interaction of *Chlamydia* and IFN- $\gamma$  signaling pathways at earlier cellular regulation levels (compare Figure 4).

Under hypoxia (Figure 55 2% O<sub>2</sub>) all samples show a clear separation. The IFN- $\gamma$  treated, infected samples are closely located to the infected samples without IFN- $\gamma$ , indicating a partly common metabolite pattern in both infections.

A further fact to be observed is the good reproducibility of the samples, for each group all ten biological repetitions cluster nicely together, the only exceptions are pellet 1.2 (non infected 20% O<sub>2</sub>, second replicate), 5.1 (non-infected 2% O<sub>2</sub>, first replicate) and three replicates of pellet 7 (infected, 2% O<sub>2</sub>, fourth, eighth and tenth replicate). The spectra of these extracts have been manually checked and it has been observed that even though the general metabolite profile of these samples is comparable to the other samples, they are characterized by several contamination peaks. Thus, these samples have been excluded from the multivariate data analysis, but not from univariate testings performed afterwards. Moreover, in particular the addition of IFN- $\gamma$  has a strong influence to shift the metabolism in one direction, pointed out by the very tight location of all samples in the first two principal components.

In the now following part of the thesis metabolic variations in active and persistent infection are addressed. Furthermore, reasons leading to the development of an active infection in IFN- $\gamma$  treated cells under hypoxia are investigated. Main question to be answered are thus:

- (i) Can we identify metabolites that lead to the enhanced growth (without IFN- $\gamma$ ) and a sustained active infection (with IFN- $\gamma$ ) under hypoxia, but to the development of persistence under normoxic IFN- $\gamma$  treatment? “Environmental” influences like nutrient bargain in the non-infected cells in different cultivation conditions might be very important in this regard. (chapter 2.4.3.1)
- (ii) What happens during infection in the different cultivations and how adapts *Chlamydia* to the different conditions existing in non-infected cells? Can we discover differences in the persistent and non-persistent infection leading to new ideas for targeted studies? (chapter 2.4.3.2)
- (iii) Can we spot biomarker candidates for the clinical problematic persistent infection? (chapter 2.4.3.2)

Due to the amount of data and complexity of data analysis a different data integration strategy than in the just presented part (chapter 2.4.2 – Important variations in the metabolome in an active, normoxic infection) has been used. Whereas in chapter 2.4.2 all analytical techniques have been included in the data analysis from the beginning and have been equally ranked, in the now following chapters the results base on ICR/FT-MS data and have only be verified with UPLC®-ToF-MS analyses.

#### 2.4.3.1 *Better growth, higher infectivity and persistence of Chlamydia as an environmental effect – investigation of metabolic adaption in non-infected cells to different cultivation conditions*

To answer the first question the metabolite equipment in non-infected cells and the shifting in the metabolic pattern caused by the cultivation conditions may play a key role, especially since *Chlamydia* strongly depends on nutrient input from the host cell cytosol. Thus, the non-infected samples have been analyzed deeper at first.

The non-infected samples have been investigated by PCA. Separation of all cultivation conditions could be achieved in the first three principal components (Supplementary figure 6), but cells cultivated under normoxia and cells cultivated under hypoxia with an addition of IFN- $\gamma$  do not separate within the first two principal components indicating a higher similarity of these cells (Figure 56A und B). One explanation might be opposite directed effects of hypoxia and IFN- $\gamma$ , which cancel each other when both conditions are combined.

Based on this hypothesis the data set has been analyzed in regard to identify metabolites anti-correlated under hypoxia and under normoxic IFN- $\gamma$  treatment. PLS-DA models (normoxic vs. hypoxic cells; and normoxic vs. normoxic IFN- $\gamma$  cells) have been built and the statistical significance of discriminative metabolites has been vetted with a Wilcoxon-Mann-Whitney test. A p-value <0.05 has been considered sufficient. No overfitting has been observed during cross-validation with 200 permutations (Supplementary figure 6). 486 annotated metabolites have been discriminative in both PLS-DA models. Their averaged (n=10) signal intensities are illustrated in the heat map (Figure 56 C). Cells cultivated under hypoxia and cultivated under normoxia with IFN- $\gamma$  addition, both contain a certain number of unique or increased concentrated metabolites (framed with white ellipses).



Clusters of metabolites inversely regulated under hypoxia and under normoxic IFN- $\gamma$  treatment, but showing the same abundance behaviors in the other two cultivation conditions have been extracted. In the heat map these metabolites are framed with white boxes. They might be essentially required nutrients/compounds for the development of an active or persistence infection, and responsible for an enhanced growth and infection rate under hypoxia.

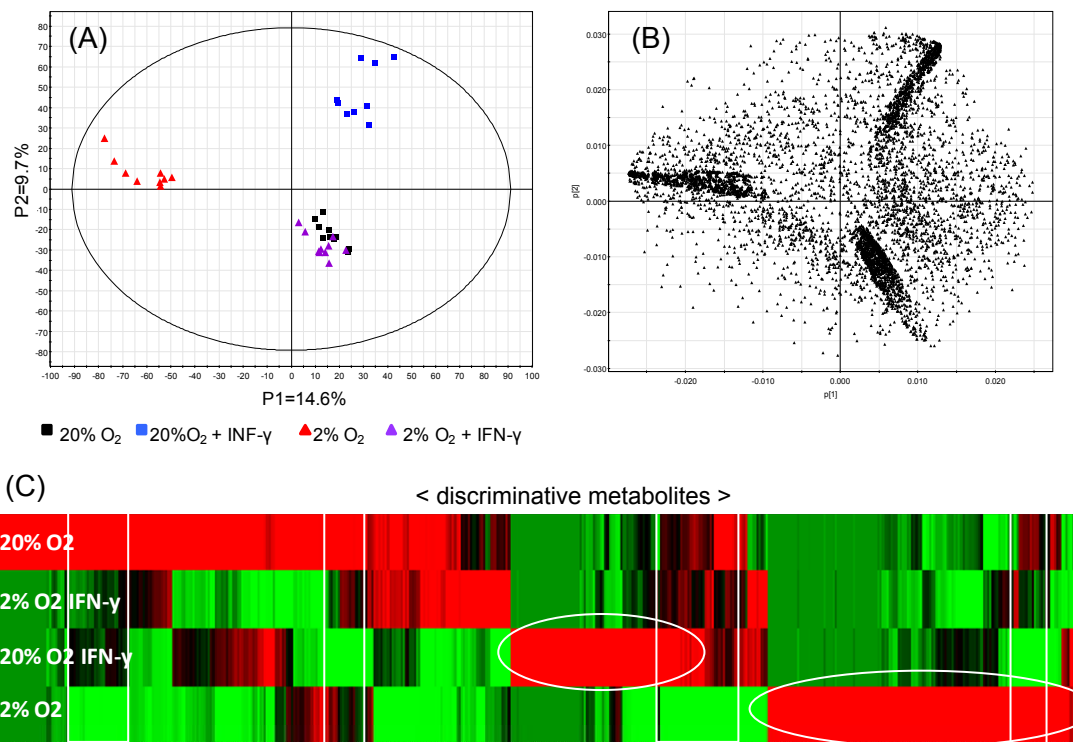


Figure 56: Investigation of non-infected cells: (A) PCA score plot; (B) PCA loading plot; (C) heat map of statistically significant ( $p$ -value  $< 0.05$ ) altered metabolites (clusters of opposite regulated metabolites are framed on white boxes, white ellipses mark either unique or increased metabolites in normoxia + IFN- $\gamma$  or hypoxia)

For confirmation of these important metabolites the UPLC<sup>®</sup>-ToF-MS data sets have been searched and a filtering to minimize false positive annotations has been performed (see chapter 2.3.2.4.12). 21 metabolites show a clear modulation in opposite direction under hypoxia and under IFN- $\gamma$  treatment, but no alteration in samples treated with both conditions (hypoxia + IFN- $\gamma$ ). Now at first, metabolites increased under hypoxia and decreased in normoxic IFN- $\gamma$  addition are presented, before compounds elevated in IFN- $\gamma$  treated samples are discussed.

Nutrient depletion as stimulus for persistence of *Chlamydia* is a well described phenomenon (Coles et al., 1993, Harper et al., 2000). Therefore, metabolites with

higher detected intensities under hypoxia and reduced levels in normoxic IFN- $\gamma$  treated samples might be very important and essentially required for chlamydial growth. Tryptophan, acetyl-aspartate as well as glycerophosphoethanolamine and -choline derivatives have shown such an abundance behavior (Figure 57A).

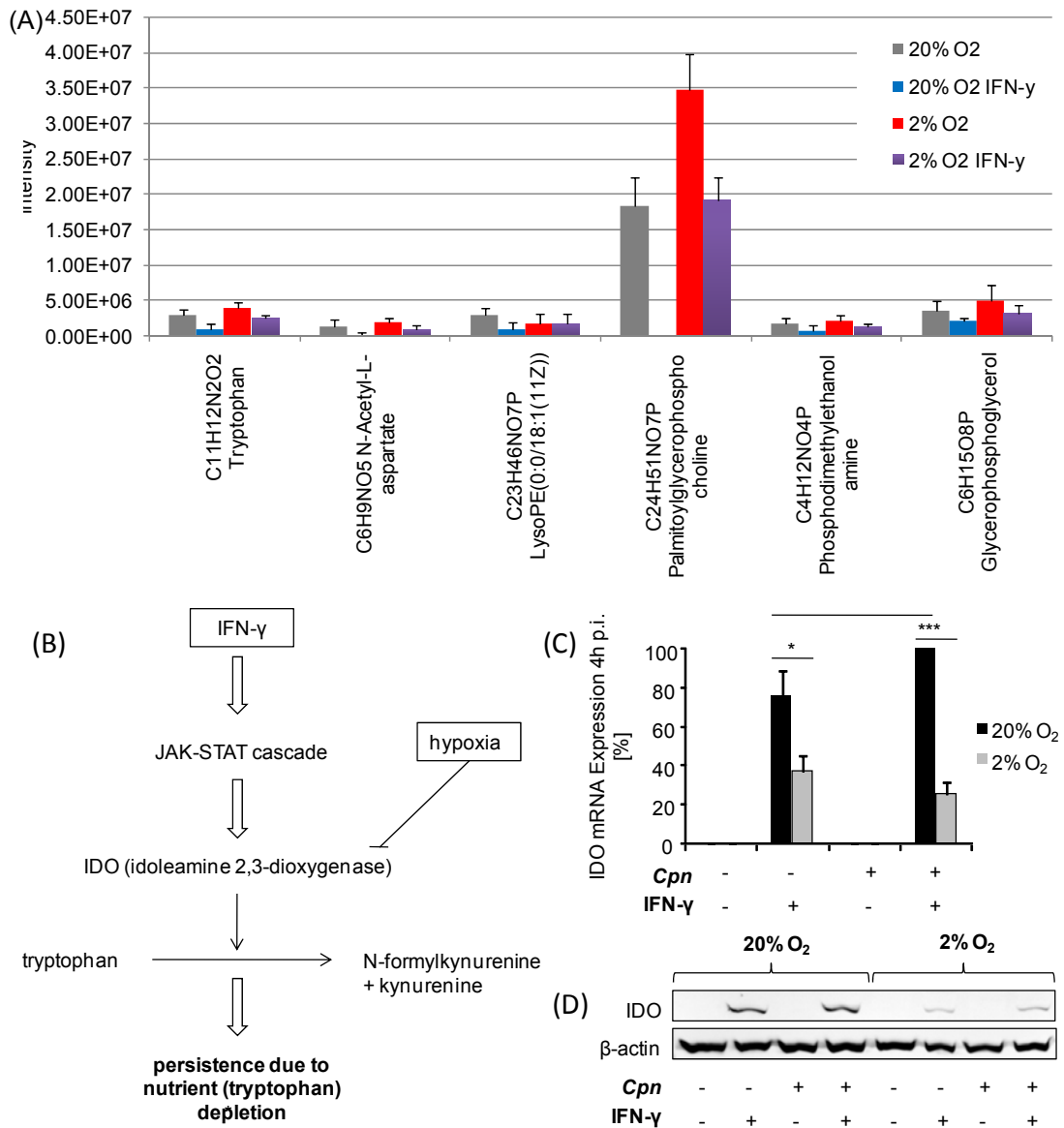


Figure 57: (A) Elemental composition with one annotation of metabolites increased in cells cultivated under hypoxia, and decreased in IFN- $\gamma$  treated normoxic cells, (B) IFN- $\gamma$  mediated signaling pathway, leading to chlamydial persistence; (C) IDO mRNA expression levels 4h p.i. (Dietz et al. 2012, submitted) (D) western blot of IDO protein expression 4h p.i. (Dietz et al. 2012, submitted)

A drop of tryptophan levels after IFN- $\gamma$  treatment could be expected since IFN- $\gamma$  stimulates IDO and leads consequently in a degradation of tryptophan (Pantoja et al., 2001, Beatty et al., 1994a) (Figure 57B). Additionally, we observed increased

levels ( $p=0.012$ ) of tryptophan in hypoxic cultivated samples, which has been also verified by IDO expression levels revealed by targeted investigations of our partners Inga Dietz and Prof. Dr. Jan Rupp (University of Lübeck) (Figure 57C/D). In samples cultivated in the combined condition (hypoxia + addition of IFN- $\gamma$ ) the tryptophan level has been comparable to normoxic controls.

The same trend as for tryptophan has been observed for  $C_6H_9NO_5$ , annotated as acetyl-aspartate or formyl-glutamate. Both are intermediates in the alanine, aspartate, glutamine or histidine metabolism. Acetyl-aspartate is additionally discussed as precursor in lipid- and myelin biosynthesis, as well as in the synthesis of the important neuronal dipeptide N-acetyl-aspartyl-glutamate or as intermediate in the glutamineolysis (HMDB, 2012a). An increased glutamineolysis during hypoxia has been recently evidenced (Le *et al.*, 2012).

An impact of IFN- $\gamma$  and oxygen environment to the cellular glycerophospholipid pool, as observed in our data set, might be also a strong factor for chlamydial persistence, especially since glycerophospholipids are able to trigger divers cellular signaling pathways, and a connection between *Chlamydia* infection and glycerophospholipid modulation is well evidenced (Wylie *et al.*, 1997, Su *et al.*, 2004, Kumar *et al.*, 2006, Hatch *et al.*, 1998, Azenabor *et al.*, 2005) (see also chapter 3).

On the other hand, several metabolites show an increased abundance in IFN- $\gamma$  treated samples cultivated under normoxia (Figure 58), while their signal intensities are reduced under hypoxia. This might indicate that those compounds can influence cellular processes leading to a persistent infection. Within this very interesting group of metabolites lipids like VLCFAs (very long chain fatty acids), wax monoesters, monoacylglycerols and diacylglycerols are annotated.

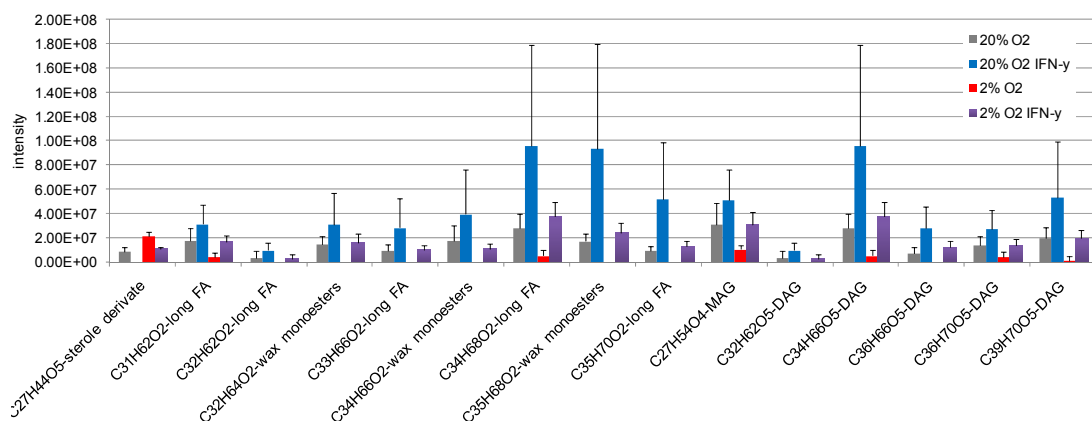


Figure 58: Elemental composition with one annotation of metabolites increased in IFN- $\gamma$  treated normoxic cells and decreased in cells cultivated under hypoxia (averaged intensities + standard deviation ( $n=10$ ), (FA fatty acyl, DAG diacylglycerol, MAG monoacylglycerol)

The elemental compositions of some of these lipids suggest odd carbon chains, which are classically understood to be only abundant in plants and some microorganisms. Recent investigations of mammalian lipid species with modern techniques have also suggested an abundance of such odd-chains in human cells and tissues (Ivanova et al., 2010). Nevertheless, the identification by targeted approaches and MS<sup>n</sup> as well as NMR is absolutely inevitable. From a biochemical point of view in particular diacylglycerols as second messenger are very attractive findings. Diacylglycerols are products of enzymatic hydrolysis of glycerophospholipids by phospholipase C (PLA C). They activate protein kinase C, which is a key regulator of cellular signaling. A study of the ionization and fragmentation behavior of diacylglycerols has been performed to enable a deeper investigation in future. It is presented in the annex.

In summary, several metabolites inversely regulated in the different non-infected samples have been detected. Those might be part of regulatory processes leading in a persistent, a sustained infection or even in an enhanced infection in the different environments. Interestingly, in particular IFN- $\gamma$  and hypoxia effects seem to cancel each other for several metabolites. The identification of the underlying regulatory processes might be very attractive research fields.

#### *2.4.3.2 Chlamydia-specific metabolite alterations in active and persistent infection*

Infected samples and their non-infected controls have been analyzed by multivariate statistics to evaluate the existence of metabolic alterations for the different infections. For each cultivation condition a PLS-DA model has been built and validated by 200 permutations (Supplementary figure 7). All models are valid. Discriminative markers (VIP-VALUE >1) have been exported and vetted by the Wilcoxon-Mann-Whitney test. The numbers of statistically significant metabolites in the different infection models are illustrated in Table 13. It has been of special interest, if the persistent infection exhibit a different pattern of statistically significant modulated metabolites compared to an active infection. The number of statistically significant altered metabolites in an active and persistent infection is comparable. Surprisingly, the proportion of annotated metabolites increased in infected samples is very high in the persistent infection (89%). Cells, cultivated and infected under hypoxia tend to have higher numbers in both annotated and “unknown” discriminative metabolites compared to normoxic samples.

	- IFN- $\gamma$		+ IFN- $\gamma$	
	20% O <sub>2</sub>	2% O <sub>2</sub>	20% O <sub>2</sub>	2% O <sub>2</sub>
	active infection	enhanced active infection	persistent infection	active infection
altered metabolites	1911	1852	2486	3022
annotated metabolites	240	252	329	451
annotated metabolites decreased after infection	164	82	160	322
annotated metabolites increased after infection	76	170	169	129

*Table 13: Numbers of statistically significant altered metabolites in infected cells under different cultivation conditions compared to the according non-infected controls*

To be able to concentrate on infection-specific effects occurring in the different cultivation conditions, first the infected cells have been compared (Figure 59 (i)), followed by the non-infected samples (Figure 59 (ii)), and afterwards both lists of important modulations have been compared with each other (Figure 59 (iii)). Figure 59 and Figure 60 illustrate and explain this principle of data analysis further.

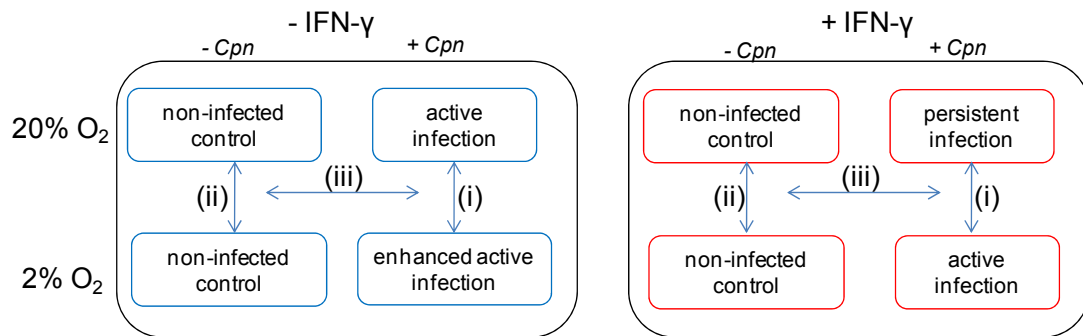


Figure 59: Overview of sample set and structure of data analysis; (i) comparison of infected samples (ii) same procedure for non-infected samples and (iii) subsequently comparison of results from infected and non-infected samples

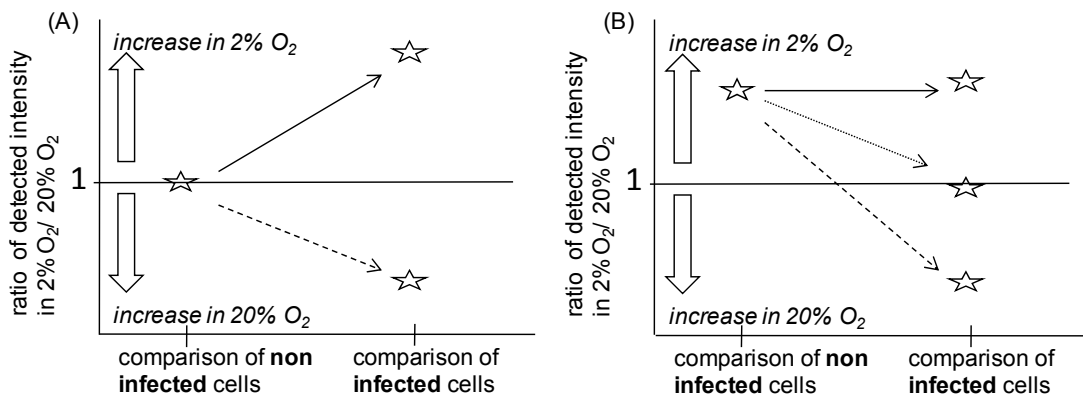


Figure 60: Principle of data analysis: The non-infected and infected samples cultivated under normoxia and hypoxia are separately analyzed, afterwards the resulting list of statistically significant alterations have been compared. Three observations can be made. (A) Metabolite's intensity does not significantly differ under normoxia and hypoxia in non-infected cells, but in infected cells, either an increased intensity under hypoxia (continuous line) or under normoxia (truncated line) has been observed. (B) A statistical significant difference in metabolite's intensity in non-infected cells exists and it is also detected (continuous line), absent (dotted line) or even inverted (truncated line) in infected samples. In the first mentioned case, the effect is caused by the environment and is not infection-specific.

The infection relevant alterations of the metabolome have been mapped into the KEGG pathways (Table 14). Statistically significant differences in the mass intensities in non-infected cells, which do not appear after infection, have been included (like explained in Figure 60B). Such modulations indicate an intervention of *Chlamydia* in the adaption mechanisms of non-infected cells to the cultivation condition or similar effects in *Chlamydia* infections. Statistically significant metabolome alterations, which only exist in infected cells are written in brackets.

	- IFN- $\gamma$		+ IFN- $\gamma$	
	20% O <sub>2</sub>	2% O <sub>2</sub>	20% O <sub>2</sub>	2% O <sub>2</sub>
	active infection	enhanced active infection	persistent infection	non-persistent, active infection
carbohydrate metabolism	89 (8)	47 (3)	93 (80)	25 (-)
energy metabolism	7 (5)	1 (-)	2 (2)	-
lipid metabolism	39 (6)	32 (30)	47 (47)	11 (-)
nucleotide metabolism	12 (8)	4 (1)	10 (6)	1 (-)
amino acids	11 (11)	12 (7)	2 (2)	4 (3)
glycan biosynthesis and metabolism	2 (2)	-	5 (5)	-
cofactors and vitamins	12 (8)	13 (5)	8 (7)	8 (-)

Table 14: Pathway contributions of metabolites differently regulated in infected cells cultivated under different conditions (modulations, which only appear in infected cells, but not in non-infected ones are given in brackets)

As pointed out in chapter 2.4.2 isomeric compounds cannot be distinguished within this analysis; and thus in particular the metabolite classes of carbohydrates and lipids might be over-represented. Nevertheless, the analysis gives important insights in the infection-specific metabolite alterations. In this manner it can be seen, that a quite huge number of metabolites has been detected with decreased levels when the non-infected cells had been cultivated under hypoxia compared to normoxia. But no alteration has been observed for infected samples. This can be explained by the expression of HIF-1 during the early developmental cycle of *C. pneumoniae* under normoxic and hypoxic conditions (Rupp et al., 2007) and has been observed mainly for carbohydrates and lipids, nucleotides and coactors.

Samples cultivated with IFN- $\gamma$  have a very high number of compounds statistically significantly increased in the persistent infection compared to the active one,

whereas only three metabolites, belonging to the amino acid metabolism, are increased in the active infection with IFN- $\gamma$  under hypoxia.

These important metabolites have been afterwards verified in the RP UPLC<sup>®</sup>-ToF-MS data set and loaded to MetaboAnalyst for pathway analysis (Xia et al., 2009).

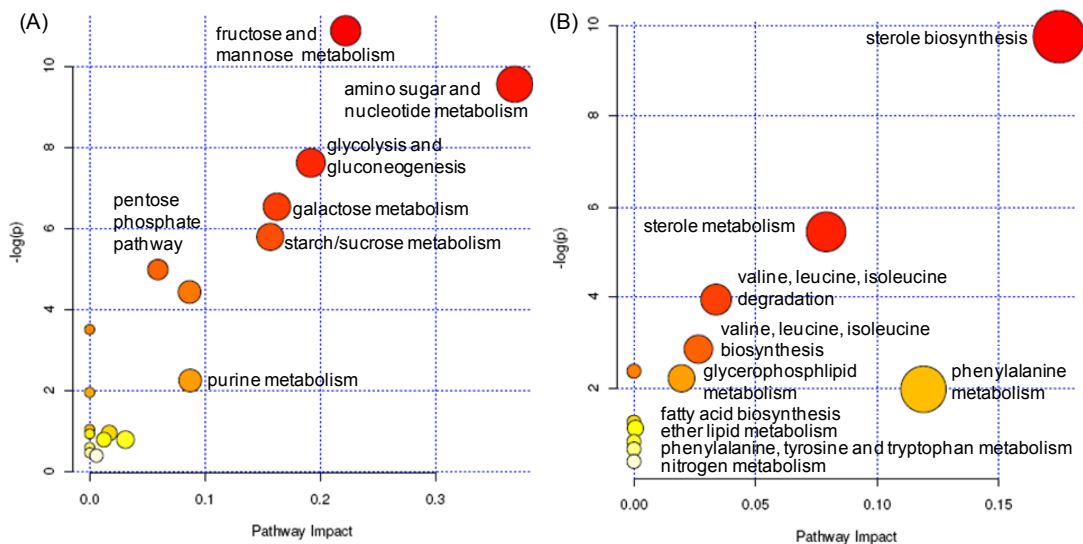


*Figure 61: Pathway analysis of metabolites statistically significantly altered in infected cells cultivated **without IFN- $\gamma$**  under different oxygen atmosphere: (A) metabolites, which show a clear variation in non-infected cells but not in infected cells, (B) statistically significant alterations only present in infected samples*

The comparison of cells cultivated under the different oxygen atmosphere **without IFN- $\gamma$**  (Figure 61) revealed the absence of the statistically significant carbohydrate variations in infected cells, which have been present in non-infected cells (Figure 61A). For instance, annotated glucose and glucose phosphate differ statistically significant in non-infected cells cultivated under hypoxia and normoxia, but not in infected cells. This can be explained by the early stimulation of HIF-1 during the infection, as already mentioned. Alterations in the metabolite pattern, which do only appear in infected cells cultivated under normoxia and hypoxia (Figure 61B) address mainly the sterole-, phospholipid- and amino acid metabolism (phenylalanine, tyrosine and leucine). Samples cultivated **with IFN- $\gamma$**  have been accordingly analyzed. Important compounds clustered into four groups: (i) increased in active and persistent infection, (ii) decreased in active infection, (iii) increased in active infection and (iv) inversely regulated in persistent and active infection (Table 15). Since these compounds are the most important and lead to ideas for targeted investigations, a correlation analysis has been additionally performed to discover metabolites following the same trend, but have not fulfilled the strict criteria of



statistical data elaboration. Correlating metabolites are also given in the Table 15. In Figure 62 the intensity behavior of one compound of each group (i-iv) is illustrated over the complete sample set.

	intensity compared to non-infected controls	example used for illustration	further metabolites
i	increased in active and persistent infection	tryptophan	acetyl-aspartate/formyl-glutamate, galactosylsphingosine, glycerophosphoglycerol, phosphodimethylethanolamine, amino-methyl-phosphomethylpyrimidine, carboxyethyl-arginine
ii	decreased in active infection	glutathione	ADP, AMP, cAMP, GDP, GMP, glutamate, cystine, glucose-phosphate, acetyl-glucosamine 6-phosphate, DGs, PC/PEs (lyso) ...
iii	increased in active infection	tyrosine	phenylalanine, acetyl-arginine, acetyl-leucine, acetyl-tyrosine, acetyl-muramate, acetyl-neuraminic acid, acetyl-glucosaminic acid, acetyl-glucosamine, Succinyl-glutamate, glycosyl-asparagate, neuraminic acid ...
iv	inverse in persistent and active infection	glucose	sterols, e.g. cholesterol, leucine, PC/PEs

Table 15: Groups of metabolites altered in infected cells **with IFN- $\gamma$**  under different oxygen atmosphere

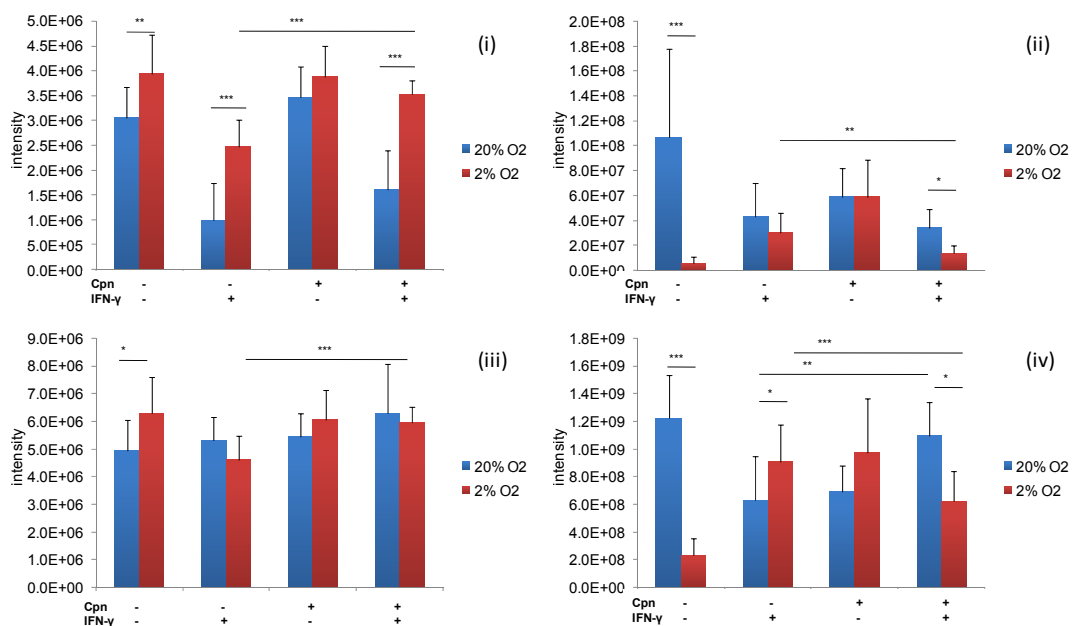


Figure 62: ICR/FT-MS signal intensities of metabolites statistically significant altered in infected cells cultivated **with IFN- $\gamma$**  under different oxygen atmosphere for the complete sample set: (i) tryptophan, (ii) tyrosine, (iii) glutathione (iv) glucose (n=10, average + STD, \*  $p < 0.05$ , \*\*  $p < 0.02$ , \*\*\*  $p < 0.001$ )

Tryptophan, a metabolite from the first group, has been degraded in IFN- $\gamma$  treated samples, which can be explained by the IDO expression (see chapter 2.4.3). The degradation of tryptophan has been minimized under hypoxia and abrogated in *Chlamydia*-infected samples under hypoxia. The targeted analysis of IDO expression (Inga Dietz and Prof. Dr. Jan Rupp, University of Lübeck, chapter 2.4.3) has confirmed these observations very well. Further metabolites correlating with the intensity profile are amino acid intermediates (e.g. acetyl-aspartate, see also chapter 2.4.3) and phospholipids precursors. In particular, the metabolites in this group might be markers for *Chlamydia* infection, an active and persistent one. Because of that, the correlation analysis has been extended to the completed data set (including „unknown“ metabolites) and 105 further compounds with a correlation coefficient  $>+0.8$  have been determined. The deeper investigation of these, including the identification of most abundant species might be very interesting in terms of diagnostic markers.

In addition, several metabolites have been discovered, which have either an increased or decreased intensity in the active, but not persistent infection. Interestingly the first mentioned ones are mostly amino acids (tyrosine, phenylalanine) and amino acid intermediates, like acetylated amino acids or succinyl-glutamate, as well as intermediates of amino sugar/glycan biosynthesis like acetyl-muramate, acetyl-neuraminate, acetyl-glucosaminat, acetyl-glucoseamine and neuraminic acid. Metabolites with reduced intensity levels in the active infection belong predominantly to glycerophosphoethanolamines and -cholines. Also several diacylglycerol species, purine nucleotides and the already as infection relevant described compounds glutathione and cystine have been found (chapter 2.4.2).

A last group of metabolites inversely regulated in active and persistent infection has been observed. In this group e.g. glucose or several sterols like cholesterol are to mention. A drop in glucose levels in active infection seems to be very reasonable since it is the main carbon source and an activated metabolic activity of *Chlamydia* surely increases the energy requirements.

## 2.5 Summary

The investigations of *C. pneumoniae* infections have included different cultivation conditions in which an active, a persistent and an enhanced active infection occur.

The developed multi-parallel methodology has based on ultrahigh resolution mass spectrometry and UPLC<sup>®</sup>-ToF-MS. The data analysis of the complex data set has been performed stepwise.

After the illustration of the general metabolite recovery, the reproducibility of the methods and the advantage of multi-parallel approaches, the metabolic alterations in the active infection under normoxic environment have been deeply investigated. Discriminative metabolites have been seen to be spread all over the complete known metabolic pathways. However, mainly modulated classes of metabolites in infection are lipids, carbohydrates and amino acids. Due to the high amount of discriminative markers, a focusing on mostly altered compounds has been necessary. This could be achieved by strengthening the elaboration criteria. The data delivered complete new insights in infection specific alterations of amino acid, redox and lipid homeostasis and pinpointed several metabolites (annotated and “unknowns”) as key metabolites. Several compounds are mainly abundant after infection and show a very high degree of connectivity in the network analysis. The data is in very good consistency with previously, sporadically described metabolic alterations after *C. pneumoniae* infection.

Thereafter, the data analysis has been expanded to the complete sample set. Important metabolites, which are inversely regulated in the different cultivation conditions and which are thus important for an enhanced active or persistent infection, have been identified. Metabolites, that have been depleted in IFN- $\gamma$  treated non-infected cells but increased under hypoxia might be very important nutrients essentially required for chlamydial infection. They are consequently of high interest for future targeted investigations. Such metabolites are e.g. tryptophan and glycerophospholipid derivates. In addition, several metabolites have been determined, which are only increased under normoxic IFN- $\gamma$  treatment, in a milieu where a persistent infection appears. Here long chain fatty acids and glycerolipids are to be mentioned. These observations indicate a putative inhibition of important pathways or cellular processes required for an active infection under normoxic IFN- $\gamma$  treatment.

In the last part of the presented work, the environmental influences have been filtered out, so that only bacterial adaption processes could be analyzed. Importantly modulated during the active infection in different oxygen atmosphere are metabolites of sterol-, glycerophospholipid- and amino acid metabolism. Moreover, at different stages of the data analysis it has been seen, that the infected cells

cultivated under hypoxia are geared towards to their non-infected controls, which indicates common underlying mechanisms like HIF-1 activation. Under IFN- $\gamma$  treatment some very important metabolites, which are comparably regulated in active and persistent infection, as well as putative „unknown“ biomarker candidates for both types of infection, have been determined. Furthermore, a clearly different metabolic activity of persistent and active infection has been observed. This is not of less interest since it can provide further biological knowledge about adaption processes triggered by *Chlamydia*.

Next to this biological information this chapter of my thesis illustrates the value of different data elaboration strategies. If only two conditions shall be analyzed an integrative data elaboration based on several analytical techniques is recommended. The combination of different techniques provides the advantage to be able to focus on main modulations detected with different techniques. The integration of logD calculation and retention time prediction, which enables filtering of metabolite annotations, has been seen to be very useful to avoid false positive annotations in UPLC<sup>®</sup>-ToF-MS. The visualization of metabolomic data in Van Krevelen diagrams, Kendrick plots and networks are very suitable to gain an overview of the data set, to identify homologous series of important marker compounds and to focus on key metabolites. When using such data elaboration tools the advantage of ultra-accurate mass spectrometry has been extremely important and thus such analysis may base mainly on ICR/FT-MS measurements followed by verification of the results with other techniques. Also for analysis of multi-condition experiments the outstanding characteristics of ICR/FT-MS have been very valuable and an according workflow is therefore recommended for future metabolomic investigations.

## 2.6 Perspectives

The identification of the biological function of the determined important metabolites in follow-up targeted studies is a future task. Such studies might also include investigations of the abundance behavior of these metabolites during the complete chlamydial developmental cycle and the localization of such markers inside the infected cells. Here, either a differentiation between the *Chlamydia*, the inclusion and the human host cells by clean-up strategies like density centrifugation or separation techniques like capillary electrophoreses has to be mentioned. However,

such clean-up burdens the discussed drawbacks like possible metabolite alterations. Thus, an application of high resolving imaging technologies like NanoSIMS might be of advantage.

The structure elucidation of several important, but currently „unknown“ markers is very promising in diagnostic and therapeutic respect. During the analysis several key markers have been determined as most important, as they are strongly increased in their signal intensity after infection and they are highly connected in the metabolic network. Several marker compounds are furthermore part of complete homologous series of importantly modulated metabolites. Since (+)ICR/FT-MS data has appeared more suitable for the differentiation of infected and non-infected samples during the statistical analysis than (-)ICR/FT-MS, the network analysis has included only positive electrospray data. As the general workflow has been now developed and illustrated, the networking may be extended to negative electrospray data, as well.

In respect of structure elucidation also stereochemical aspects might be an interesting topic.

Moreover, since the multi-parallel approach turned out to be of very high value, it is reasonable to extend the integrative concept also to other techniques, e.g. NMR. NMR provides several advantages compared to MS techniques, such as the possibility of quantification and identification of putative markers. The main drawback is nevertheless, the lower sensitivity compared to modern MS technologies. This lower sensitivity has hindered the direct application of NMR during this work. Within the NMR experiments, which have been realized by Dr. Silke Heinzmann and Dr. Norbert Hertkorn (Research unit Analytical BioGeoChemistry, Helmholtz Zentrum München, Munich, Germany), only a few signals have been detected, thus further optimization and higher cell numbers need to be achieved for future analysis. NMR experiments might be further implemented to study the metabolic flux of discriminative metabolites. An experimental design including stable isotope labeled nutrients and metabolites might be built up.

The analysis of the cell culturing medium (metabolic “footprint” of *Chlamydia* infection) promises complementary information to the obtained data of infected cell pellets. Such analysis of cell culturing requires a special sample clean-up for deproteination and desalting. The investigation of cell supernatants, which have been also collected during this project, have to be further focused. Moreover follow-

up studies of elaborated markers in patient samples would be an important step towards the implementation of novel diagnostic concepts.

### 3 *Effects of C. trachomatis infection on the lipid homeostasis*

#### 3.1 *Introduction*

Lipids are hydrophobic compounds essentially required for three main biological functions. They serve as

- (i) storage molecules,
- (ii) structural components of cellular membranes,
- (iii) cofactors and signaling molecules (Watson, 2006, van Meer, 2005).

The scientific interest on lipids increases very fast, since lipids are more and more recognized as modifiers of cell homeostasis in health and disease. In this regard an alteration in the lipidome has been described e.g. in conjunction with many acute and chronic diseases (reviewed in Hu et al., 2009, Shevchenko et al., 2010, Watson, 2006, Wenk, 2005). Several interesting reviews have focused on the analytical needs, purpose and progress in lipidomic research (Gross et al., 2011, Hu et al., 2009, Roberts et al., 2008, Shevchenko et al., 2010, Wenk, 2005, Wenk, 2006). An emerging topic is additionally lipidomics of infections with intracellular pathogens, mainly because lipids are key compounds during pathogen invasion, persistence and bacterial replication as well as in the human immune response (Walburger et al., 2004, Wenk, 2006).

Naturally abundant lipids are classified in eight distinct categories: fatty acids, glycerolipids, glycerophospholipids, sphingolipids, sterol lipids, prenol lipids, saccharolipids and polyketides (Fahy et al., 2005). Within the class of glycerophospholipids we distinguish between glycerophosphocholines, glycerophosphoethanolamines, glycerophosphoserines, glycerophosphoglycerols and glycerophosphoinositols (van Meer, 2005).

All glycerophospholipids consist of one or two hydrophobic hydrocarbon chains and a hydrophilic phosphorylated polar head group. They are thus amphiphilic compounds (Fagone et al., 2009) (Figure 63). The carbon chain in sn-1 position can be linked to the glycerol backbone by an ester or ether bond (Brites et al., 2004). In case of ester binding the lipid is referred to as diacyl-species, while ether lipids are named plasmanyl- or plasmenyl-glycerophospholipids in dependency to the presents of an adjacent vinyl-group. If a vinyl-group exists, the lipid is termed plasmalogen (plasmenyl-ether). Etherlipids are usually either glycerophosphoethanolamines or glycerophosphocholines. Plasmalogens are

known to be present in mammalian cells, as well as in anaerobic bacteria, but have never been identified in aerobic bacteria, like *Chlamydia* (Goldfine 2010).

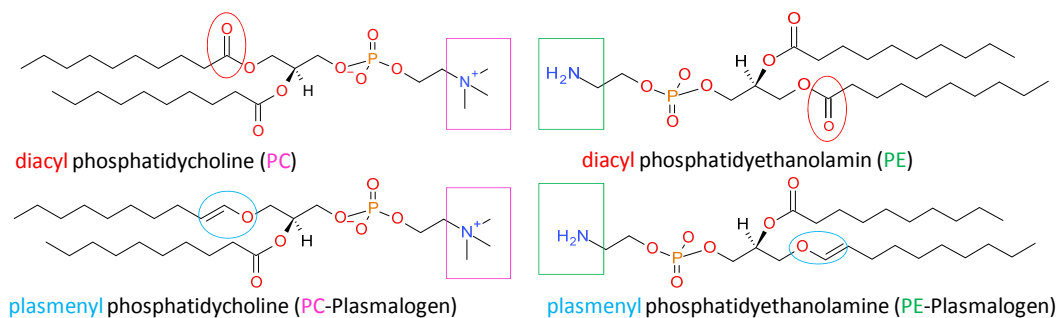


**Figure 63: Structure of glycerophosphocholines and -ethanolamines (diacyl- and plasmenyl-compounds):** Glycerophospholipids consist of hydrophobic hydrocarbon chains and a hydrophilic head group (e.g. ethanolamine: framed in green box or choline: framed in magenta box). The linkage of sn-1 hydrocarbon chain to the glycerol backbone can be e.g. an ester (red) or vinyl-ether (blue) bond.

Plasmalogens serve as reservoirs for polyunsaturated fatty acids (PUFAs), as natural antioxidants and they are important as structural components of cellular membranes. One fifth of all lipids in the human body are plasmalogens (Nagan et al., 2001). Moreover, they are involved in intracellular signaling and influence membrane dynamics, like fusion and ion transports (Albi et al., 2004, Farooqui et al., 2001, Farooqui et al., 2001, Nagan et al., 2001). Since etherlipids are more lipophilic due to the missing carbonyl oxygen in sn-1 position, membranes of high etherlipid content undergo faster membrane fusion (Brites et al., 2004). Furthermore, such membranes are less fluid than etherlipid deficient membranes. However, the complete biological function of both etherlipid classes is still not fully resolved, but the recent scientific interest in this special lipid class grows steadily as modulated cellular levels are important in various diseases, such as Zellweger's syndrome, Alzheimer's disease and cancer (reviewed in Brites et al., 2004, Nagan et al., 2001).

Recently, it has been observed that *Chlamydia* hijack a complete organelle, which is required for etherlipid biosynthesis, the peroxisomes (Dr. Agathe Subtil et. al, Unit of Biology of Cell Interactions, Institute Pasteur, Paris, France). Thus, we believe that *Chlamydia* might use peroxisomal activity to synthesize specific etherlipids, or to modify some host lipids. Additionally, as presented in the last chapter (Chapter 2 Molecular cartography in acute and persistent *C. pneumoniae* infections – a non-targeted metabolomic approach), an altered cellular lipid composition in infection has been observed. Therefore, a targeted approach focusing on both etherlipids and



mainly affected lipid class, namely glycerophospholipids, has been built up. In the previous chapter diacylglycerols have been also identified as important modulated metabolites during chlamydial infection (chapter 2.4.2 and 2.4.3). Glycerophospholipids and glycerolipids are tightly connected, thus any perturbation in one of these lipids is prone to induce a wider modulation. Due to this and the fact that such neutral lipids are known for their low ionization efficiency, a deep investigation of the possibilities of ionization and identification of diacylglycerols by MS<sup>2</sup> has been realized, which aimed at the facilitation of rapid targeted approaches for *Chlamydia*-relevant diacylglycerols and is presented later (annex).

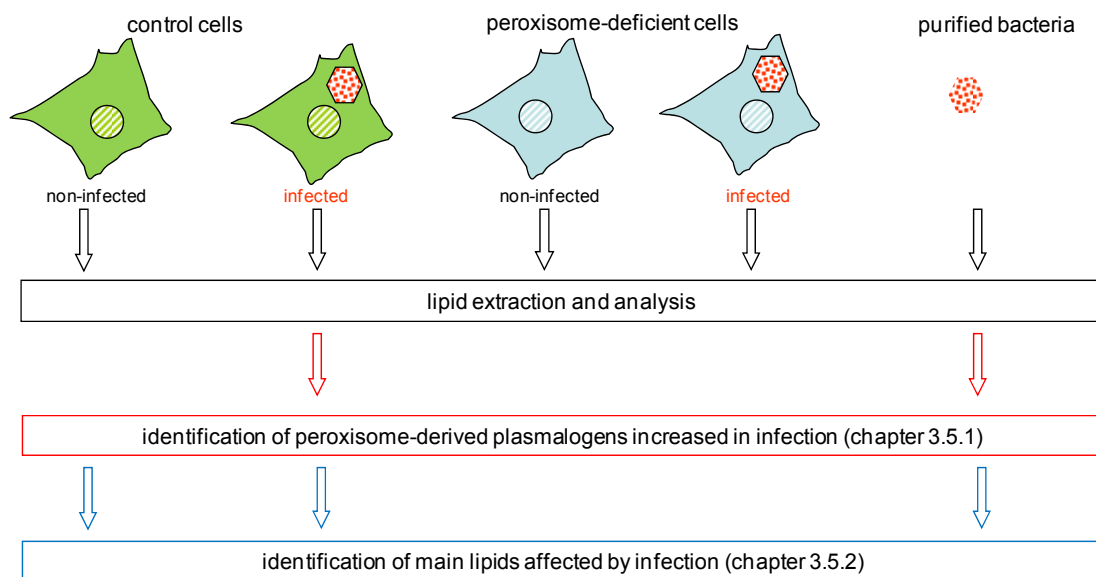


Figure 64: Illustration of sample set-up and objectives

The investigation of etherlipids and general lipid modulations after infection includes peroxisome-deficient cells (pex19), which are fibroblasts with approximately 90% decreased abundance of peroxisomes, control fibroblasts and purified bacteria (Figure 64). Due to their genomic mutation pex19 cells are perfect controls to prove a peroxisomal origin of lipids. Furthermore, the isolated chlamydial EBs have been used to localize important lipid species inside *Chlamydia*.

### 3.2 Objectives

This study aims at two objectives, first the identification of *Chlamydia*-specific plasmalogens, which evidence a contribution of peroxisomes during the infection,

and second, a deep investigation of lipid modulations after infection. The later one includes the identification of mainly affected lipid classes and structure elucidation of marker lipids for *C. trachomatis* infections.

### 3.3 Nomenclature of lipids

The lipid nomenclature in this work bases on LIPID MAPS (<http://www.lipidmaps.org/>). The class of glycerophospholipids is indicated by two capital letters, e.g. PC for glycerophosphocholines or PE for glycerophosphoethanolamines. The fatty acid substituents are either given by the number of carbon atoms in both fatty acid substituents together or by the illustration of fatty acids separately, followed by the number of present double bonds. For example PC 33:0 indicates a glycerophosphocholines with two saturated fatty acid chains having 33 carbon atoms together. If the fatty acid composition is analyzed in more detail, the lipid will be illustrated as e.g. PC (15:0/16:0). The later nomenclature gives additionally the stereochemistry, since the fatty acid in sn-1 position is written firstly, the one in sn-2 position thereafter. Additionally, plasmanyl-compounds are specified by an "O", whereas plasmenylys are indicated by a "P", for instance PE (O-14:0/14:0) or PE (P-14:0/14:0). The double bond of the vinyl-ether binding is commonly only indicated by the "P" and is not mentioned in the fatty acid again.

## 3.4 *Materials and method development*

### 3.4.1 *Materials*

A mixture of different glycerophospholipids standards has been used for the method development, validation and quality control before and after analysis. Two diacylglycerophosphoethanolamine standards (PE (18:1/18:1); PE (12:0/12:0)) and two diacylglycerophosphocholine standards (PC (18:0/18:1), PC (10:0/10:0)) have been purchased from Sigma-Aldrich Aldrich (St. Louis, USA). One plasmalogen standard (PC (P-18:0/18:1)) has been ordered from Avanti Polar Lipids, Inc. (Alabama, USA). Methanol, acetonitrile and water have been used in LC-MS grade quality (CROMASOLVE<sup>®</sup>, Fluka<sup>®</sup> Analytical, Sigma-Aldrich-Aldrich, St. Louis, USA). LC-MS grade n-propanol has been delivered from BioSolve (Valkenswaard, Netherlands), as well as ammonium formate, ammonium acetate and formic acid. Furthermore, an Agilent (Santa Clara, USA) ESI tuning mix has been used for calibration of the ToF instrument, and an arginine (Sigma-Aldrich Aldrich, St. Louis, USA) solution for ICR/FT-MS calibration. Control fibroblast and pex19 deficient fibroblasts have been obtained from Dr. R. Wanders (University of Amsterdam, Netherlands). Pex19 deficient fibroblasts are isolated from a patient deficient for the *pex19* gene and the control fibroblasts are isolated from a healthy donor.

### 3.4.2 *Methods and method development*

#### 3.4.2.1 *General consideration*

During this study two lipidomic strategies (UPLC<sup>®</sup>-ToF-MS analysis and direct injection MS, which is commonly named shotgun lipidomics) have been pursued according to the analytical needs of the different objectives (Table 16).

	<b>objective 1: targeted determination of plasmalogens increased after infection</b>	<b>objective 2: comprehensive investigation of (glycerophospho-) lipid alterations after infection</b>
expectation	a few low abundant plasmalogen species	up to 1000 important modulated glycerophospholipids
workflow	2D UPLC <sup>®</sup> -ToF-MS ↓ determination of important candidates ↓ verification via ICR/FT-MS and MS <sup>2</sup>	ICR/FT-MS ↓ overview of lipid alteration ↓ verification and isomer differentiation via 2D UPLC <sup>®</sup> -ToF-MS ↓ identification with ICR/FT-MS <sup>2</sup>
reasons for workflow	expected low abundance of plasmalogens and thus suspicion of ion suppression by higher abundant lipids  possibility of filter integration (mutant cells, hydrolysis) minimizes the risk for false positive discoveries and avoids misleading annotations, thus a lower mass accuracy can be expected during the first analysis	ultrahigh resolution and accuracy offers the best condition to enable the elaboration of the expected high amount of data and distinction between closely located signals, the low mass error minimizes false positive annotations

Table 16: Overview and comparison of applied workflows

#### 3.4.2.2 Protocols for cell cultivation, -disruption and lipid extraction

All cell cultivations, -disruptions and lipid extractions have been done by Dr. Agathe Subtil (Unit of Biology of Cell Interactions, Institute Pasteur, Paris, France). Control and pex19 fibroblasts have been grown in DMEM (Dulbecco's Modified Eagle Medium) supplemented with 10% FCS. Around  $1 \times 10^6$  cells have been used for each point. Both cell lines have been infected with *Chlamydia trachomatis* LGV L2 strain 434 (ATCC) for 24 or 48 hours or left non-infected. The numbers of infectious EBs

have been comparable in control and pex19 samples, which indicates that peroxisomes are dispensable for *Chlamydia* progeny. However, the inclusion size in pex19 cells has been reduced by 30 to 50% compared to controls (data from Dr. Agathe Subtil). The cells have been detached with 0.5mM EDTA in phosphate buffered saline (PBS), washed in PBS and re-suspended in 1ml methanol. Samples have been sonificated for 15 seconds, centrifuged at 16.000g (15min, 4°C) and the supernatant has been collected. A second methanol extraction has been performed following the same procedure. Both extracts have been pooled prior to analysis.

To perform analysis on purified bacteria, HeLa cells have been infected for 48 hours and the bacteria have been purified on density gradient following the state-of-the-art protocol (Scidmore, 2005) and re-suspended in 0.6ml methanol. The lipid extraction has been conducted as described above.

Three biological repetitions have been prepared for the fibroblast sample set and two for the purified bacteria. It should be mentioned, that the biological repetitions have been prepared independently during the last three years, and not in one batch. The cell extracts have been stored in -80°C until analysis. All analyses have been performed within two weeks after sample preparation.

Cell disruption methods and extraction solvents have been tested with spinal cord tissue (prepared by Dr. Agathe Subtil, Unit of Biology of Cell Interactions, Institute Pasteur, Paris, France), as it is especially rich in plasmalogens. A disruption by potter homogenizer versus sonification with a sonic finger has been evaluated. The extracts have been analyzed with (+)ICR/FT-MS. The recovered glycerophospholipid content has been found to be comparable in both extraction experiments. Therefore, the disruption has been chosen according to handling and labor costs. Cell disruption by sonification has been preferred.

Lipids are hydrophobic molecules, which are soluble in organic solvents such as methanol, acetone, benzene and chloroform, but only partly in water (Fahy et al., 2005). Hence, usually an extraction procedure using methanol/chloroform mixtures is used (extraction according to Folch or to Bligh and Dyer). Since in particular in ICR/FT-MS measurements a frequent formation of chloride adducts, which hinder identification via fragmentation, can be observed, the glycerophospholipid recovery in pure methanol and pure dichloromethane has been tested. Pure methanol has been preferred for glycerophospholipid extraction in this study. The main reasons are: (i) the plasmalogen profiles in the methanol extracts have been in accordance

with literature (Murphy et al., 1993a) and (ii) a high content of chloride adducts has been observed in dichloromethane extracts, which sustained also after evaporation of the organic solvent and resolution of the residue in methanol/acetonitrile.

#### 3.4.2.3 Overview of UPLC<sup>®</sup>-ToF-MS based targeted analyses of plasmalogens

For the first objective of this work, the identification of infection specific plasmalogens, the crude lipid extracts have been analyzed combining a HILIC and RP UPLC<sup>®</sup> separation (Figure 65 step 1). 2D UPLC<sup>®</sup> analysis delivers complementary data on both columns and reduce the co-elution of the complex glycerophospholipid content of the samples. The developed HILIC separation bases on the interaction of glycerophospholipids' polar head groups with a thin aqueous layer on the surface of the column (Figure 7). Glycerophosphoethanolamines have therefore been effectively separated from glycerophosphocholines. For both lipid classes the fractions have been collected and re-injected for RP separation, which is bases on the glycerophospholipids' carbon chains (Figure 7). In addition, the samples have been subjected to an acidic hydrolysis by 2M HCl before RP analysis. Under the acidic condition the vinyl-ether bond of plasmalogens are hydrolyzed, whereas other phospholipid species stay intact (Murphy et al., 1993b). This property has been used to identify plasmalogens and to differentiate them from their plasmanyli-isomers.

The collected chromatographic fractions of lipids of interest have been analyzed with a 12 Tesla ICR/FT-MS (Figure 65 step 3) to determine the exact mass of important plasmalogens and elucidate their exact structure. Mass spectra in positive and negative ionization mode have been acquired, since both modes deliver complementary data. The identification of low abundant plasmalogens after fraction collection, which correspond to a clean-up, has been preferred over the possibility of MS<sup>2</sup> or MS<sup>e</sup> experiments during UPLC<sup>®</sup>-ToF-MS runs, because a loss in sensitivity is unavoidable when applying parallel MS and MS<sup>2</sup> in ToF-MS. The isolation window in the maXis<sup>®</sup> quadrupole is furthermore not sufficient to select single lipid species and the mixed fragments spectra may lead to wrong structure assignments.

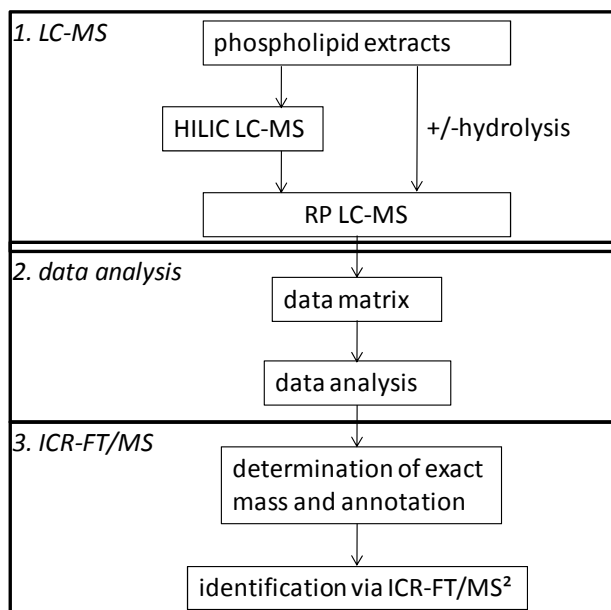


Figure 65: Workflow to determine *Chlamydia*-derived plasmalogens: 1. 2D UPLC<sup>®</sup>-ToF-MS analysis including hydrolysis of vinyl-ether bindings, 2. data analysis, 3. ICR-FT/MS and MS<sup>2</sup> for confirmation, determination of exact masses and identification

#### 3.4.2.4 Overview of ICR/FT-MS based shotgun lipidomics

The workflow for the second objective, the identification of mainly affected lipid alterations, has been based on ICR/FT-MS measurements. The crude methanol lipid extracts have been directly injected into the ICR/FT-MS (shotgun lipidomics) after dilution. Key glycerophospholipid species have been afterwards verified by the above explained 2D UPLC<sup>®</sup>-ToF-MS approach. Identification of such important species has been achieved with ICR/FT-MS<sup>2</sup> (SORI) experiments in positive and negative ionization mode. Structure elucidation has been therefor also achieved directly out of the lipid extracts (Figure 66).

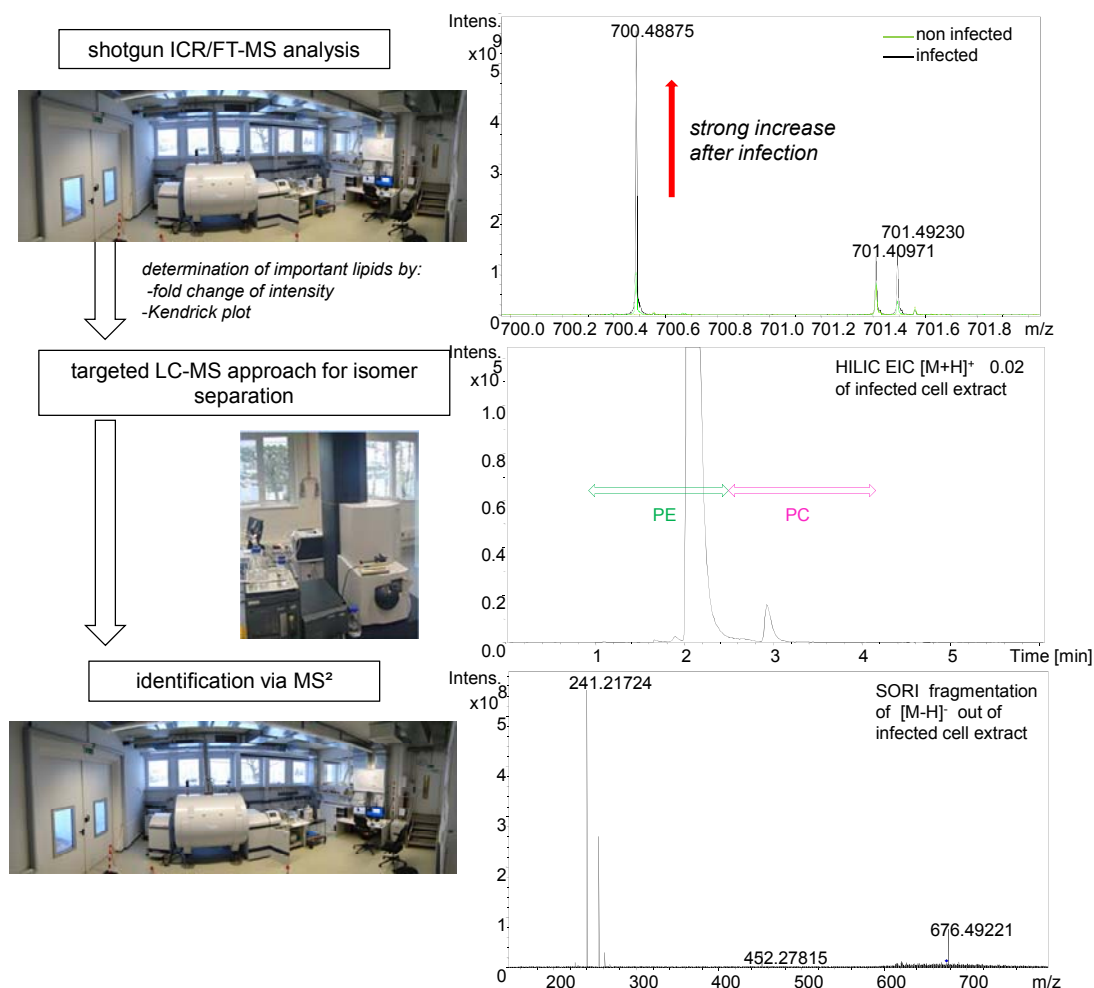


Figure 66: Workflow of combined shotgun ICR/FT-MS and UPLC<sup>®</sup>-ToF-MS approach to determine lipidome alteration after infection. Exemplary one important modulated m/z (700.488) is illustrated. ICR/FT-MS analysis have revealed a strong increase in intensity after infection. 2D UPLC<sup>®</sup>-ToF-MS analysis (HILIC illustrated) have identified several differently behaving isomers, and SORI ICR/FT-MS<sup>2</sup> have been used for structure elucidation of fatty acid residues.

### 3.4.2.5 Development of 2D UPLC<sup>®</sup>-TOF-MS

Since low concentrations of *Chlamydia*-derived plasmalogens have been expected, the UPLC<sup>®</sup>-ToF-MS methods have been developed to reach the highest sensitivity, peak capacity and mass resolution. A mixture of glycerophospholipid standards has been used in this respect. ToF mass spectra have been acquired in positive electrospray mode to be able to detect both glycerophosphocholines and glycerophosphoethanolamines within one run. Glycerophosphocholines as zwitterionic species are mainly detectable in positive electrospray, while glycerophosphoethanolamines are very well ionizable in both electrospray modes.



Parameters of the ToF instrument have been tuned for best mass resolution and accuracy in the mass range of approximately 500-900Da (Supplementary table 3).

For HILIC separation, five analytical columns have been compared in terms of sensitivity and chromatographic performance (Table 17). The Grace® VisionHT™ HILIC has been the only column separating glycerophosphocholines and glycerophosphoethanolamines efficiently. For the column elaboration a 6 minute isocratic run with 6% solvent B has been used (solvent A 10% water, 90% acetonitrile, 10mM ammonium acetate; solvent B 5% acetonitrile, 95% water, 10mM ammonium acetate). The flow rate has been set to 0.3ml/min. The column temperature has been adapted to 25°C.

column	diameters	retention time [min]				
		PE 18:1/18:1	PE 12:0/12:0	PC 18:0/18:1	PC 10:0/10:0	PC p18:0/18:1
ACQUITY UPLC® BEH Amid	2.1*150mm; 1.7µm	1.8	1.2/1.8	1.8	1.2/1.8	1.8
ACQUITY UPLC® BEH Amino	2.1*150mm; 1.7µm	2.3	2.3	2.3	3.0	2.3
ACQUITY UPLC® BEH HILIC	1.0*150mm; 1.7µm	0.6	0.6	0.9	1.1	0.9
ACQUITY UPLC® BEH HILIC	2.1*150mm; 1.7µm	-	2.2	3.2	3.8	3.2
Grace® Vision HT™ HILIC	2.0*150mm; 1.5µm	2.0	2.2	4.1	5.1	3.9

Table 17: Evaluation of HILIC columns for glycerophospholipid separation

For column evaluation 10mM ammonium acetate has been chosen as additive. Afterwards, the additives formic acid and ammonium formate have been additionally tested. Ammonium formate delivers best results in terms of peak shapes and peak intensity of all standards (Figure 67). The concentration has been further optimized

to 5mM. Furthermore a gradient optimization in terms of analysis time, peak shape and separation efficiency has been performed.

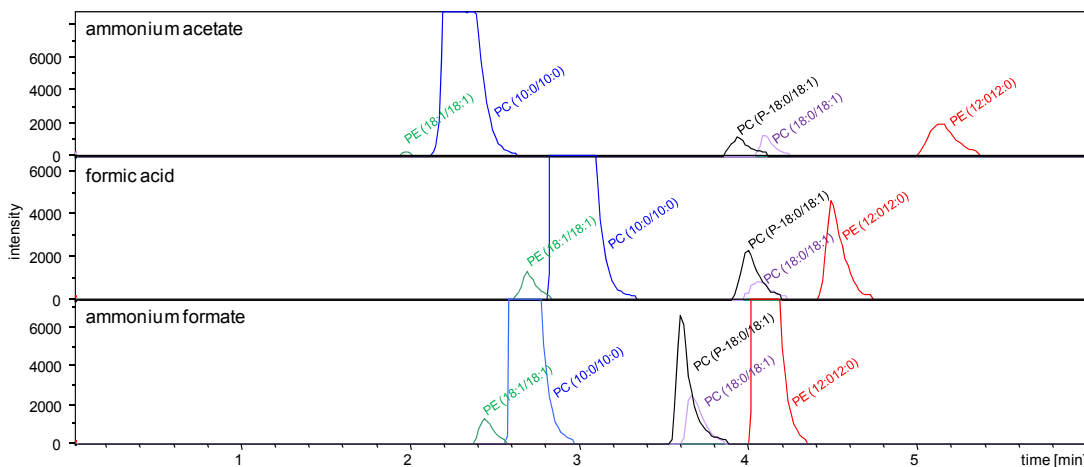


Figure 67: Evaluation of HILIC additives for glycerophospholipid separation

According to the presented method development the applied HILIC UPLC<sup>®</sup> separation conditions are:

Column:	Grace <sup>®</sup> VisionHT <sup>™</sup> HILIC; 1.5 $\mu$ m; 2.0*150mm
Solvent A:	10% water, 90% acetonitrile, 5mM ammonium formate
Solvent B:	5% acetonitrile, 95% water, 5mM ammonium formate
Gradient:	6% B to 40% B in 4min, followed by 4min equilibration
Flow rate:	0.3ml/min

For the second dimension separation of glycerophospholipids, four different RP columns have been compared (Figure 68). For these tests a 8 minute gradient from 50% to 99% solvent B has been chosen (solvent A 40% acetonitrile, 60% water, 10mM ammonium acetate; solvent B 10% acetonitrile, 90% n-propanol, 10mM ammonium acetate). The flow rate has been 0.3ml/min or 0.07ml/min according to the inner diameter of the column. The column temperature has been set to 45°C. Best results in terms of sensitivity are delivered by an ACQUITY UPLC<sup>®</sup> HSS T3 column (1.0\*150mm, 1.7 $\mu$ m) (Figure 68). The flow rate and gradient has been further optimized after column selection.

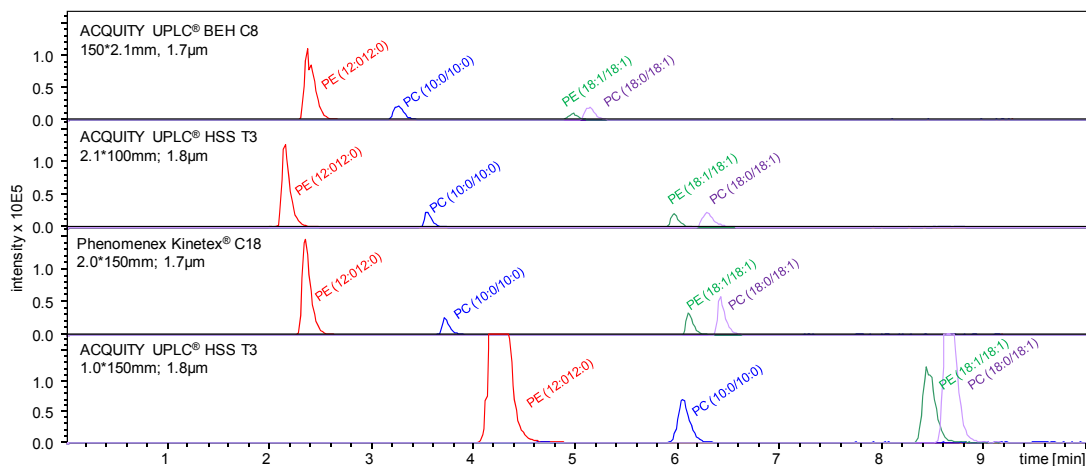


Figure 68: Evaluation of RP columns for glycerophospholipid separation

The RP UPLC® separation has been performed according to these optimizations:

Column:	ACQUITY UPLC® HSS T3 column (1.0*150mm, 1.7µm)
Solvent A:	40% acetonitrile, 60% water, 10mM ammonium acetate
Solvent B:	10% acetonitrile, 90% n-propanol, 10mM ammonium acetate
Gradient:	60% B to 90% B in 12min, followed by 1min plateau at 90% solvent B
Flow rate:	0.11ml/min

Furthermore, the injection volume and pre-concentration factor (2 and 4) of the samples have been evaluated. A full loop injection (10µl) has been chosen for both separation modes and the pre-concentration of factor two has shown the best compromise between sample availability and detected peak areas.

#### 3.4.2.6 Hydrolysis

An acidic hydrolysis (2M HCl) has been applied to distinguish between isomeric plasmanyl- and plasmenyl-species (Murphy et al., 1993b). Under the chosen condition (addition of 2M HCl, 30min reaction time, evaporization and afterwards solution in methanol) only the vinyl-ether linkage in plasmenyl-compounds (plasmalogens) are cleaved. Ether- and ester bindings of plasmanyl and diacyl-

glycerophospholipids stay intact (Figure 69). This is due to the formation of a reactive oxonium resonance structure in the electron-rich vinyl-ether bond.

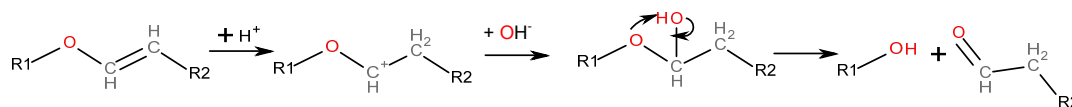


Figure 69: Mechanism of acidic hydrolysis of vinyl-ether bond in plasmenyl-compounds via hemiacetal formation

#### 3.4.2.7 ICR/FT-MS and MS<sup>2</sup> analyses

ICR/FT-MS spectra of crude lipid extracts have been acquired in positive mode. The instrument has been tuned to achieve best resolution and sensitivity in the  $m/z$  range of 500-900Da, the according parameters have been optimized for each sample set prior analysis as the samples have been successively prepared over the last three years. The first fibroblast sample set has thus been even analyzed with the Apex ICR/FT-MS system (Bruker Daltonics, Bremen, Germany), which have been afterwards updated to the solarix<sup>®</sup> ICR/FT-MS system (Bruker Daltonics, Bremen, Germany). The two extracts of one sample have been pooled and diluted in methanol. The samples have been injected with a flow rate of 2 $\mu$ l/min. Prior to injection a methanol blank spectrum has been acquired; furthermore methanol has been injected between different cell types to avoid cross-contaminations. The instrument has been calibrated with a 1ppm arginine solution reaching a mass error below 100ppb. A time domain transient of 2MW has been applied. The spectra have been calibrated according to endogenous abundant metabolites. For this purpose a mass calibration list has been elaborated after acquisition of a spiked sample. The mass lists have been extracted with a signal-to-noise ratio of four in DataAnalysis 4.0 SP2 (Bruker Daltonics, Bremen, Germany), aligned with an 1ppm error tolerance (Matrix generator 0.4, inhouse written, M. Lucio) and submitted to MassTRIX for annotation (1ppm error) (Suhre et al., 2008).

Furthermore, ICR/FT-MS provides the possibility to select very precisely single  $m/z$  units for their identification. For this purpose sustained off-resonance irradiation (SORI) fragmentation experiments have been performed. Prior to identification of glycerophospholipid species, the fragmentation patterns of standard glycerophospholipids have been studied. It has been observed that in positive mode the identification of the lipid class according to their head group can be easily

achieved, while the negative mode fragmentation facilitates conclusions about the fatty acid side chains. This is in accordance with literature (Hsu et al., 2009). The position of each fatty acid at the glycerol backbone can be inferred from the detected intensity of acyl-fragments, since loss in sn-2 is preferred (Hsu et al., 2009). Consequently, ICR/FT-MS<sup>2</sup> spectra have been obtained in both electrospray modes. The fragmentation experiments have been done either using the collected plasmalogen fractions (objective 1) or using the crude glycerophospholipid extracts (objective 2). Both have been injected with a flow rate of 2  $\mu$ l/min via a microliter pump. The putative plasmalogens have been isolated in the ICR cell with an isolation power of 20% and spectra of 80 scans have been acquired. Thereafter, the isolated ions have been fragmented by application of 1.5% SORI power. The parameter set-up for identification of further important glycerophospholipids may vary according to the analytical needs of each lipid.

#### 3.4.2.8 Lipid annotation

Mass lists from UPLC<sup>®</sup>-ToF-MS and ICR/FT-MS have been submitted to MasSTRIX (Suhre et al., 2008). For annotation based on the comparison of detected masses ( $[M+H]^+$  and  $[M+Na]^+$ ) with data base entries (LipidMAPS, KEGG, HMDB), a mass error tolerance of 0.005Da for UPLC<sup>®</sup>-ToF-MS analyses and 1ppm for ICR/FT-MS has been applied.

#### 3.4.2.9 Data analysis for identification of plasmalogens increased in infection

The data from the UPLC<sup>®</sup>-ToF-MS analyses has been extracted, aligned and merged with MZmine 2.6 (Pluskal et al., 2010) resulting in a data matrix containing the detected m/z, retention times and peak areas. The data of the following samples have been hereby included: fibroblasts non-infected, 24 hours p.i., 48 hours p.i., the corresponding pex19 samples and fibroblasts 48 hours p.i. after acidic treatment. In order to detect plasmalogens increased in infection, the data matrix has been searched for peaks fulfilling the characteristics of plasmalogens within the retention time window of minute 1 to minute 9:

- (i) quotient (peak area fibroblasts 24 hours p.i./peak area non-infected fibroblasts) >1 and quotient (peak area fibroblasts 48 hours p.i./peak area non-infected fibroblasts) >1

- (ii) absent in pex19 samples
- (iii) absent in hydrolyzed extracts of fibroblasts 48 hours p.i.
- (iv) annotation as plasmany- or plasmeryl-compound ( $C_xH_yNO_7P$ )

The extracted ion chromatographs of four  $m/z$ , which fulfilled the criteria, have been checked manually for correct automated data integration, sufficient peak shape, and complete hydrolysis in all samples after acidic incubation. One  $m/z$  has been excluded from further analysis because of very low peak intensity ( $\sim$ LoD) and residues in the hydrolyzed samples.

#### 3.4.2.10 Data analysis for identification of main lipids affected by infection

The annotated lipids derived from ICR/FT-MS spectra of the crude lipid extracts of three independent biological repetitions of the fibroblast sample set have been investigated in their signal intensity fold change after infection. The quotient of detected intensity in infected (24h or 48 h p.i.) and non infected sample has been calculated in this regard. Lipids have been included in the data analysis, if the fold change trend has been verified in all three biological repetitions (Figure 70). Afterwards these important lipids have been analyzed in two biological repetitions of purified bacteria to localize modulated lipid species within *C. trachomatis* EBs.

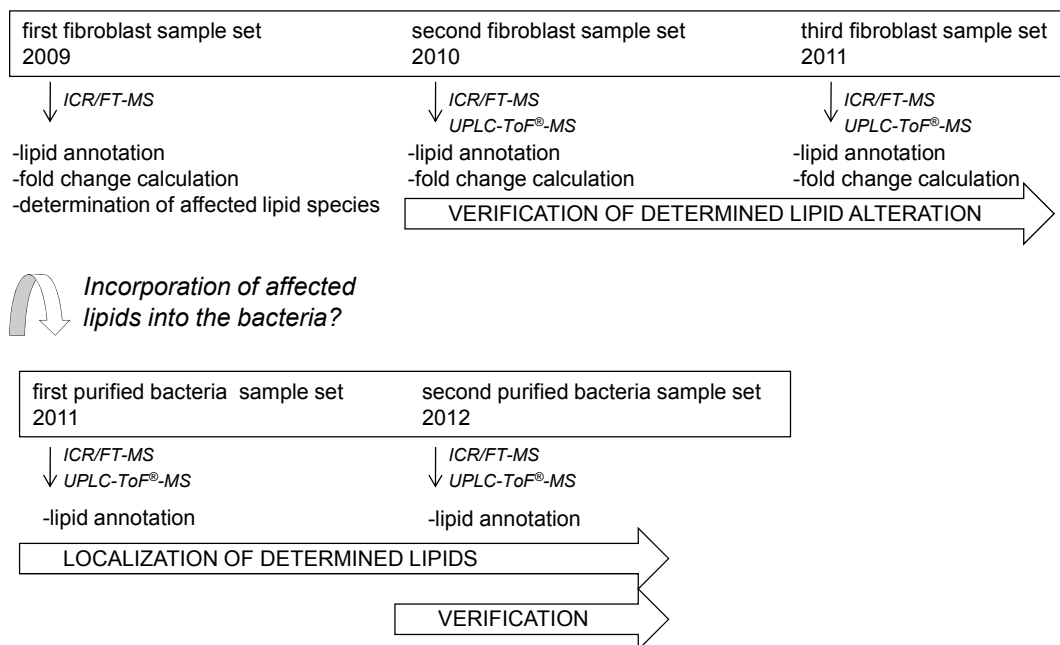


Figure 70: Overview of sample analysis to determine importantly affected lipids

### 3.4.3 Validation of methodology

#### 3.4.3.1 Validation with standard glycerophospholipids

A mixture of glycerophospholipid standards has been used to validate and monitor the methods (Figure 71). Effective separation of glycerophosphoethanolamines and -cholines during HILIC UPLC<sup>®</sup>-ToF-MS is achieved, followed by a separation of standards according to the fatty acid substituents in RP UPLC<sup>®</sup>-ToF-MS. Acidic incubation prior RP analysis results in the disappearance of plasmalogen standard compound, but not of diacyl-standard compounds.

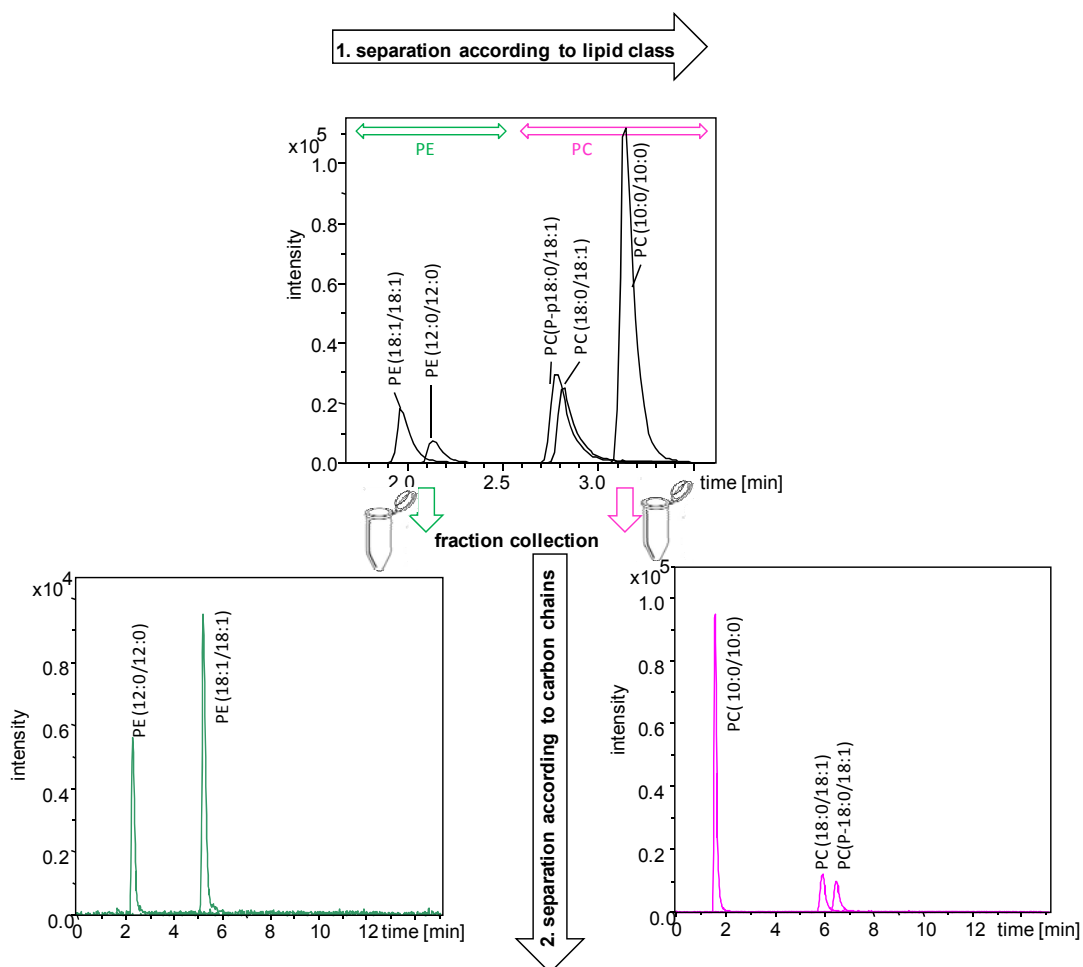


Figure 71: EIC ( $[M+H]^+ \pm 0.02$ ) of standard glycerophospholipids in the first (HILIC) and second dimension (after fraction collection (RP) (EIC ( $[M+H]^+ \pm 0.02$ ))

### 3.4.3.2 Detection of odd-chain fatty acid containing glycerophospholipids in infected samples

Through the developed methods several glycerophospholipids with fatty acids containing an odd number of carbons have been identified. Such species have been described in *Chlamydia*, and are predominantly absent from eukaryotic cells. These species have been only detected in infected samples, and they have been increased in their abundance with infection time (Figure 72). The detected peak areas have been comparable in control fibroblasts (CTL) and pex19 cells, which confirms that bacteria develop equally well in both cell lines.

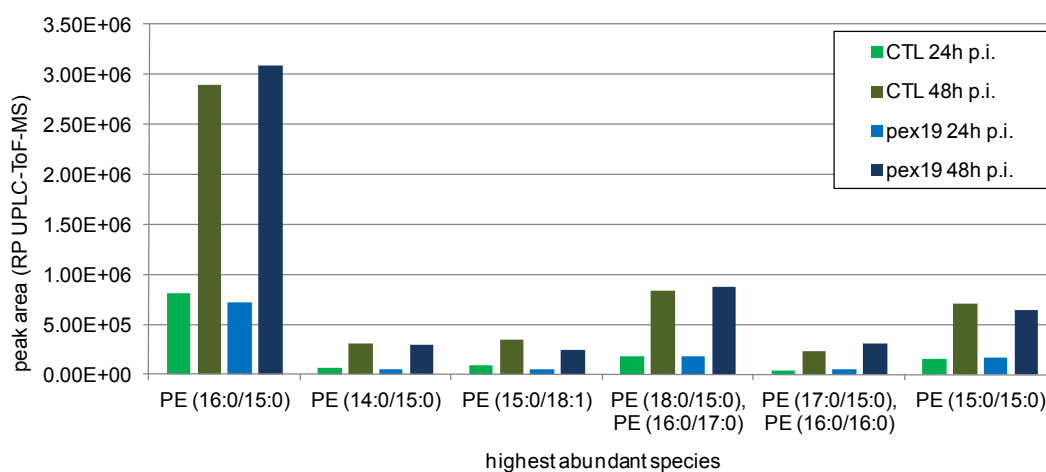


Figure 72: Odd-chain fatty acid containing glycerophospholipids (RP-UPLC<sup>®</sup>-ToF-MS peak areas, identified with ICR-FT/MS<sup>2</sup>)

### 3.4.3.3 Detection of eukaryotic plasmalogens

Additionally, several known eukaryotic plasmalogens have been identified. The corresponding peaks fulfill all characteristics of plasmalogens ((i) annotation with a mass error <1ppm in ICR-FT/MS analysis and (ii) complete degradation during acidic hydrolysis.) All such plasmalogens have higher peak areas in control fibroblast compared to pex19 samples or are completely absent in pex19 cells (Figure 73).



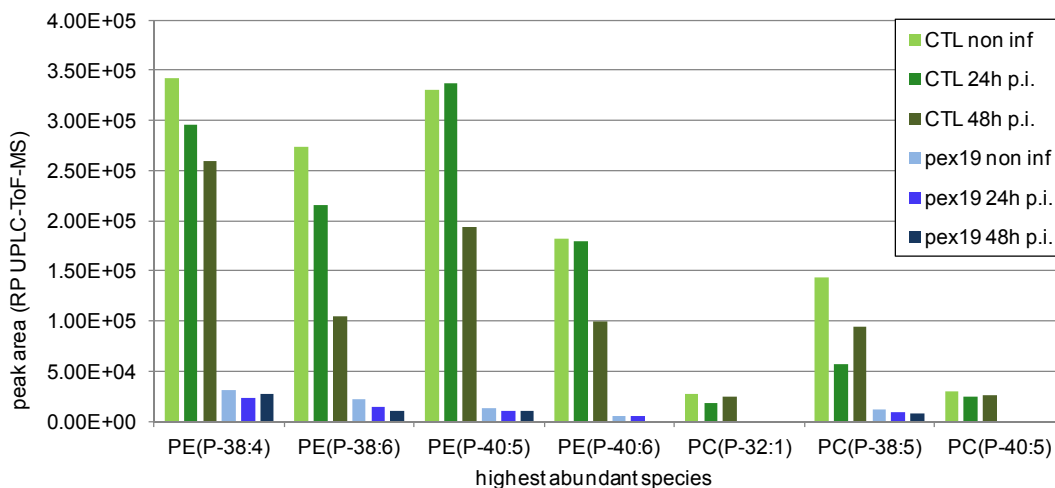


Figure 73: Plasmalogens in control and pex19 fibroblasts (RP UPLC<sup>®</sup>-ToF-MS peak areas)

### 3.5 Results and discussion

#### 3.5.1 Identification of plasmalogens increased in infection

The UPLC<sup>®</sup>-ToF-MS data analysis has been focused on peaks whose masses fitted with a  $C_xH_yNO_7P$  composition and which are completely hydrolyzed after acidic treatment, which is both expected for plasmalogens. Three out of these peaks have been more abundant in infected than in non-infected samples. The chromatographic fractions of these important plasmalogens have been collected and further analyzed with ICR/FT-MS. The corresponding plasmalogens have been identified as glycerophosphoethanolamines, with a total carbon number of 32, 33 and 34 in their chains (Figure 74).

The verification of the bacterial origin of these important plasmalogens and the identification inside *Chlamydia* has been achieved by analyses of purified EBs. The lipid extraction and all analytical procedures have been performed according to the previous analyses of fibroblast cell extracts. The detected extracted ion chromatograms are illustrated in Figure 75. Additionally, the data acquired after hydrolytic treatments is included. The chromatographic fractions of these plasmalogens have been collected and subsequently analyzed by SORI ICR/FT-MS<sup>2</sup> experiments for identification of the exact structure.

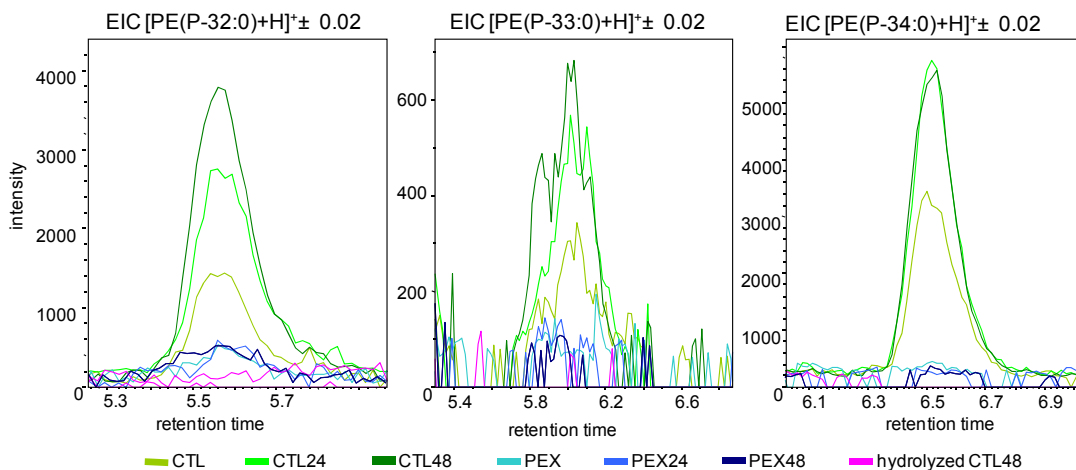


**Figure 74:** RP EIC( $M+H^+ \pm 0.02$ ) for *Chlamydia*-derived plasmalogens increased after infection. The important plasmalogens are only abundant in control fibroblast, absent in *pex19* cells and absent in control fibroblast after acidic hydrolysis

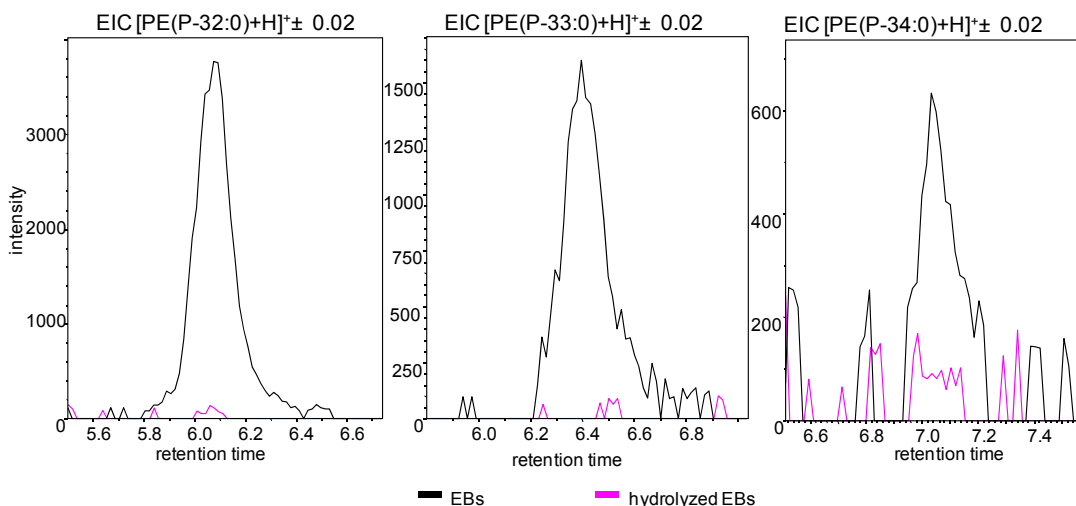


**Figure 75:** RP EIC( $M+H^+ \pm 0.02$ ) for *Chlamydia*-derived plasmalogens in isolated EBs: All three plasmalogens have been detected in the purified EBs, which lead to the conclusion that they are of bacterial origin and accumulate in *Chlamydia*.

In both kinds of samples, infected fibroblasts and purified chlamydial EBs, exactly the same fragmentation patterns have been observed in negative and positive electrospray mode. Negative electrospray fragmentation has allowed the identification of fatty acids, and to infer the composition of the plasmenyl-groups of putative plasmalogens. Several fatty acids have been detected as product ions from the putative plasmalogens PE(P-33:0) and PE(P-34:0), which shows the presence of several isomeric co-eluting parent ion structures (Kerwin et al., 1994) (Supplementary Figure 8). The intensities of these fatty acid products also allow conclusions about the abundance of the different isomeric plasmalogens (Table 18).

exact mass [M-H] <sup>-</sup>	formula	fatty acid fragment detected	plasmeyl- group inferred	abundance of fatty acid fragment
674.511917	PE(P-32:0)	C 16:0	C 16:0	2.64E+07
688.527567	PE(P-33:0)	C 17:0	C 16:0	4.64E+06
		C 15:0	C 18:0	2.13E+06
		C 16:0	C 17:0	9.53E+05
702.543217	PE(P-34:0)	C 16:0	C 18:0	1.41E+07
		C 18:0	C 16:0	2.46E+06

Table 18: Identified plasmalogens increased in infection

Fatty acids of 16 or 18 carbons, which correspond to the usual length of fatty acids in plasmalogens, have been observed, but interestingly also fatty acids of 15 and 17 carbons. Odd-chain fatty acids are typically prokaryotic. Therefore, we could evidence that the gram-negative *Chlamydia* contain not only host-derived plasmalogens, they also utilize peroxisomes for the biosynthesis of *Chlamydia*-specific species. This data evidences the existence of plasmalogens in aerobic bacteria, which has never been described before.

In positive electrospray mode a loss of the head group is the predominantly occurring process for glycerophosphocholines and glycerophosphoethanolamines. (Hsu *et al.*, 2009, Kerwin *et al.*, 1994, Pulfer *et al.*, 2003). Additionally neutral loss of both the alkenyl- and acyl-chain has been observed in case of the plasmalogen standard. However, since negative electrospray delivers directly the information about the carbonyl substituents, negative mode fragmentations are more frequently used in lipidomics investigations than positive fragmentation experiments. Nevertheless, positive mode fragmentation studies have also been performed for *Chlamydia*-derived plasmalogens, since prokaryotic lipids might exhibit different characteristics than human ones. The observed fragmentation pattern for all *Chlamydia*-derived plasmalogens do not completely correspond to the in literature

described mechanism for plasmalogens in positive electrospray mode (Kerwin et al., 1994). Consistently, for all plasmalogens, which have been synthesized after infection, additional fragments have been detected. These fragments correspond in all cases to a phosphoethylimin structure with the plasmenyl-carbon chain as substituent on the nitrogen (Figure 76).

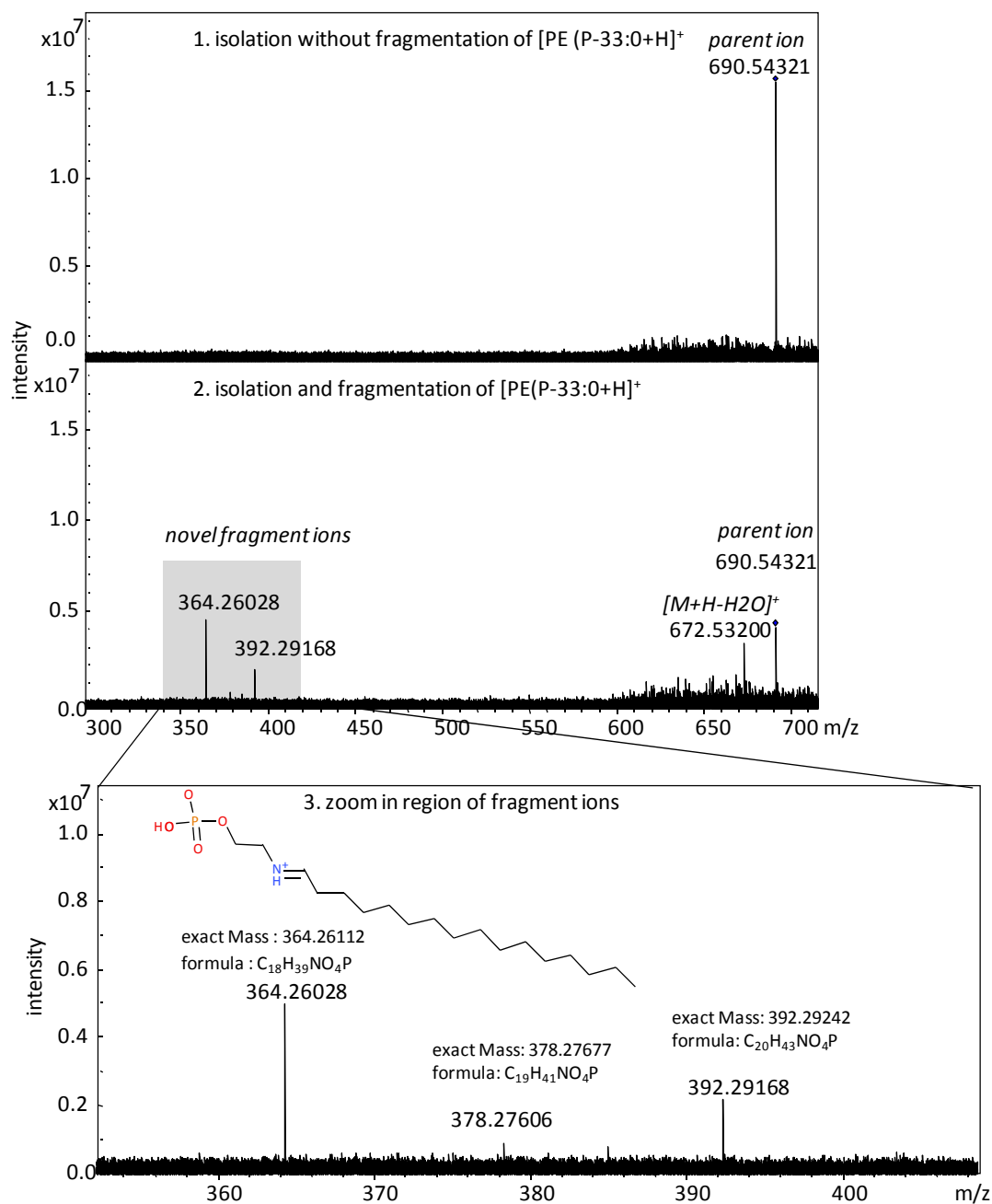


Figure 76: (+)ICR/FT-MS fragmentation pattern for  $[PE(P-33:0)]$ : 1. isolation of the parent ion  $[M+H]^+$ , 2. isolation and fragmentation, the region of product ion is colored grey, 3. zoom in region of product ions, three novel product ions have been detected, which do correspond to the inferred plasmenyl-chains from fragmentation in negative ESI mode

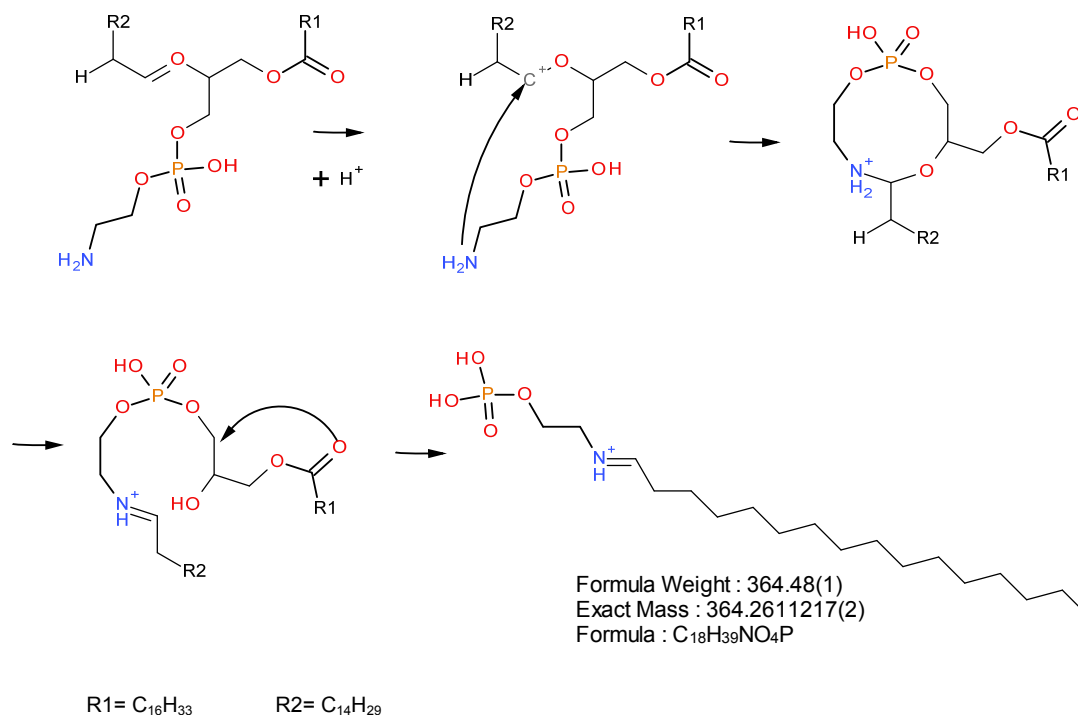


Figure 77: Proposed fragmentation mechanism for *Chlamydia*-derived plasmalogens

A putative fragmentation channel, which can deliver such fragments has been elaborated (Figure 77). The fact that the chain length of the fragments exactly correspond to the chain length of the plasmenyl-group, suggests an attack of the amino group on this chain. This is additionally reasonable because enol-ethers are activated and electron rich, as the adjacent oxygen can deliver electrons under the formation of a resonant oxonium structure. In consequence, a proton is attached to the  $\beta$ -carbon and the  $\alpha$ -carbon gets positively charged. A ring is formed by delivering of the free electron pair from the amino group to the  $\alpha$ -carbon and an imin structure is released. However, the novel fragment moieties and the elaborated fragmentation mechanism need further confirmation e.g. by fragmentation of standards compounds or quantum mechanical calculations (DFT). The interesting novel fragments have only been observed for *Chlamydia*-derived plasmalogens with consistency for all such species. The fact, that all other detected plasmalogens are decreased after infection (later illustrated in chapter 3.5.2.2, Figure 84) further supports the hypothesis that *Chlamydia*-derived lipids might be attributed by different structural characteristics. Considering the illustrated fragmentation mechanism, this structural specialty might be the positions of the plasmenyl-group at sn-2 instead of sn-1 position of glycerol backbone. It is planned to verify these very

interesting hints for a novel stereochemistry by experiments including a stereoselective enzymatic cleaving (PLA1 and PLA2), a stereoselective synthesizes of plasmalogen standards and DFT calculations for deeper theoretical determination of the putative fragmentation channel.

In summary, plasmalogens, containing odd- and even-chained fatty acids, have been identified in the lipid extracts of fibroblasts and isolated EBs, which prove the prokaryotic origin. They have been absent in pex19 cell extracts confirming the peroxisomal indispensability for their biosynthesis. Therefore, with this lipidomics approach it has been possible to identify one further spectacular specialty of *Chlamydia*: the production of bacteria-derived plasmalogens by the utilization of the host peroxisomes.

### 3.5.2 Identification of main lipids affected by infection

Shotgun ICR/FT-MS analysis followed by the annotation of the mass spectra revealed the putative lipid composition of the samples. Approximately 705 masses are annotated as lipids; annotations of natural occurring stable isotopes are hereby not considered. A differentiation between isomeric structures for one detected mass has not been possible at this stage, hence it must be suspected, that the lipid composition of the extracts is even more complex. The distribution of the annotated lipids over the different lipid classes is illustrated in Figure 78.

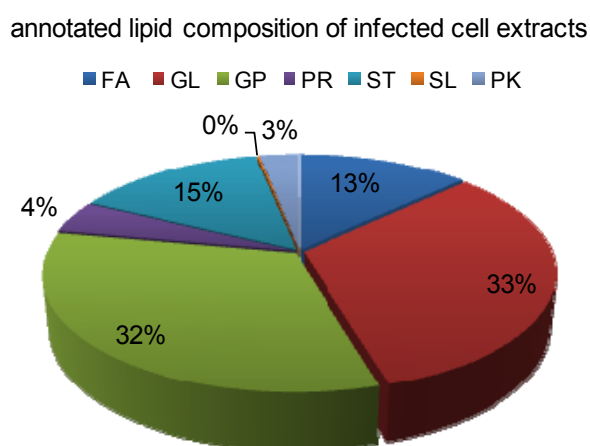


Figure 78: Lipid composition of cell extracts: Annotation of detected  $m/z$  and distribution over the lipid classes (PK polyketides, SL saccharolipids, PR prenol lipids, ST sterol lipids, GP glycerophospholipids, GL glycerolipids, FA fatty acyls). Annotations of different isomers for one detected  $m/z$  are not included.

According to the extraction regime the mainly detected lipid classes are of middle non-polar nature, like glycerophospholipids, glycerolipids or fatty acyls. The fold change of detected intensities has been calculated to reveal mainly affected lipid classes by infection and modulated lipids have been visualized with a Kendrick plot (Figure 79). The Kendrick plot is especially advantageous when dealing with lipids since different lipid classes are characterized by different sets of heteroatoms. Thus, different classes of lipids cover different areas in the diagram. The fold change of intensities after infection has been inserted as an additional dimension into the Kendrick plot and is expressed by the size of the bubbles.

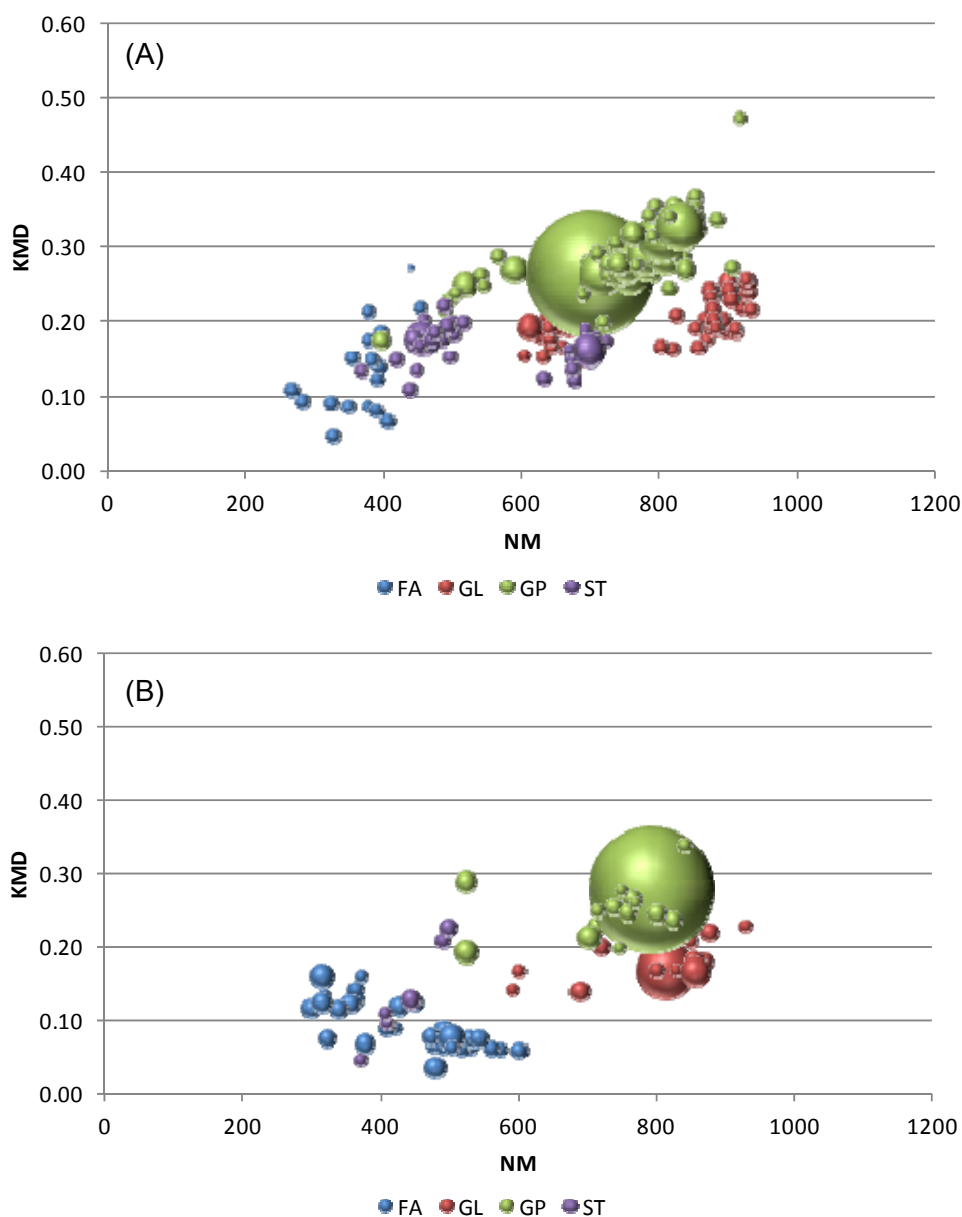


Figure 79: Kendrick plot of affected lipids (A) increased after infection and (B) decreased in infection (the diameter of the bubbles represent the fold change after infection (non-inf/inf), unique features are represented by a fold change of two)

Glycerophospholipids, glycerolipids and fatty acyls are predominating modulated after infection. 42% of all annotated glycerophospholipids have been detected with at least 50% higher signal intensities after infection, only 9% have been decreased in infected samples. The  $m/z$  700.488 has been outstandingly increased by about 180 times after infection. Its elemental composition ( $C_{36}H_{72}NO_8P$ ) suggests either a glycerophosphocholine or glycerophosphoethanolamine structure. Additional 90 masses, which are annotated as glycerophospholipids, show an important modulated intensity after infection. These are mostly putative glycerophosphocholine or -ethanolamine species, only one putative glycerolphosphoserine and four putative glycerophosphoglycerols have been detected with an altered intensity. Glycerolipids show the same trend, but to a lower extent. Next to several in infected cells exclusively abundant diacylglycerols and triacylglycerols, the putative DG (15:0/24:1) and DG (14:0/20:4) is highly increased after infection. In contrast, the intensities of 39% of all detected fatty acids have dropped after infection and 23% have been elevated. The opposite behavior of fatty acids and glycerol-/glycerophospholipids is reasonable since fatty acids are incorporated in these lipids, especially during cellular growth, when cellular membranes need to be synthesized to a higher extent (van Meer, 2005). Glycerophospholipids are the major membranes constituents in eukaryotic cells. In particular glycerophosphocholines make up more than 50% of the lipids found in eukaryotic membranes (Fagone et al., 2009, van Meer, 2005). Important functions of cellular membranes, to which glycerophospholipids contributed, are separation and protection from the environment, cell-cell interactions, compartmentalization, storage, protein synthesis and secretion and phagocytosis (Fagone et al., 2009). Glycerophosphocholines are also frequently found in bacteria closely interacting with their hosts, they are often required for pathogenicity and persistence of these microorganisms (Sohlenkamp et al., 2003).

The main lipids, which are affected by infection, have been deeper investigated by targeted UPLC<sup>®</sup>-ToF-MS analyses for verification and isomer separation/differentiation. Identification has been achieved with ICR/FT-MS<sup>2</sup>. The results will be presented in the following chapter categorized according to the identified structures into diacyl-glycerophospholipids and etherlipids.



### 3.5.2.1 Diacyl-glycerophosphocholines and -ethanolamines affected by infection

*Chlamydia* are incapable of de novo biosynthesis of typical eukaryotic glycerophosphocholines, but it has been previously shown, that the bacteria utilizes several lipids from the host to mimic the host cell's membrane composition (Hatch et al., 1998). Within this study the peak areas of all importantly modulated glycerophosphocholines are decreased after infection (Figure 80A) and indeed the detected glycerophosphocholine profile in isolated EBs follow the same trend as in non-infected host cells (Figure 80B).

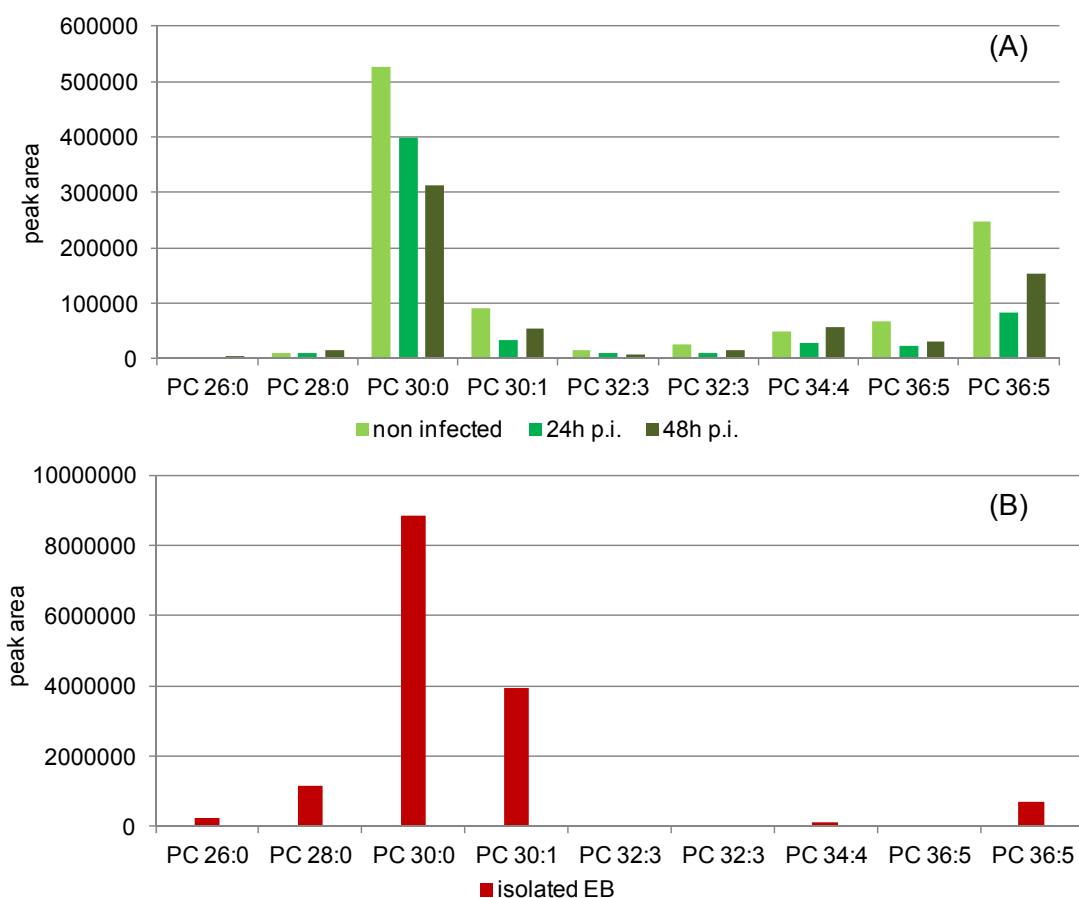
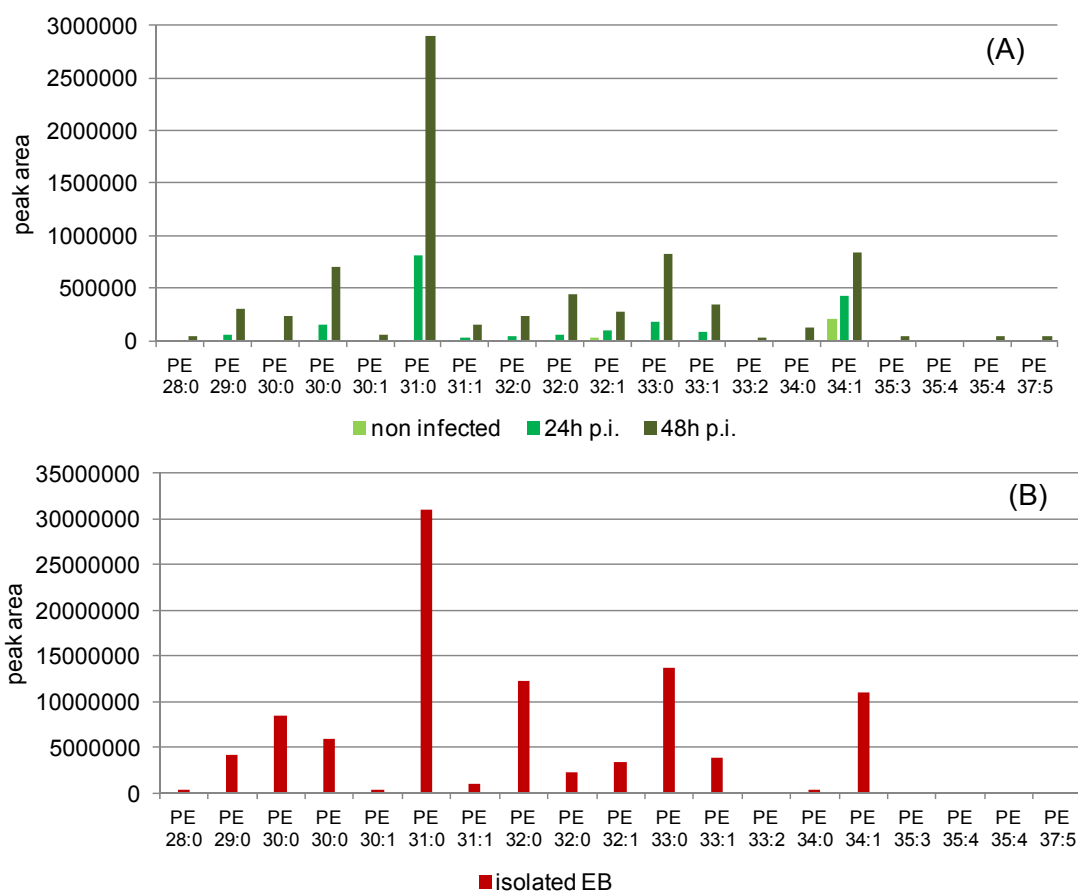


Figure 80: RP UPLC<sup>®</sup>-ToF-MS peak areas of glycerophosphocholines in (A) fibroblast and (B) isolated EBs (isomeric structures are illustrated separately): The profile of peak areas in isolated EBs follows the same trend as in non-infected fibroblasts. Additionally, an infection time dependent decrease of peak areas after infection can be observed.

Interestingly, the detected drop in the abundance of PC 26:0, PC 28:0, PC 30:1 PC 34:4, PC 36:5 (both isomers) is higher after 24 hours than after 48 hours of infection. This is in particular reasonable since the developmental cycle of *C. trachomatis* takes approximately 48 hours and the host's glycerophospholipid biosynthesis is independent from infection (Wylie et al., 1997). After 48 hours the transformation of

chlamydial RBs back to the metabolic inactive EBs is nearly finished and the requirements for host cell derived lipids decrease again. The data additionally suggests that besides the previously described incorporation of *Chlamydia*-modified glycerophosphocholines an incorporation of unaltered glycerophosphocholines into the chlamydial membranes occurs (Figure 80B). A modulation of glycerophosphocholines by *Chlamydia* in terms of exchange of sn-2 fatty acids against bacteria-made branched-chained ones has been reported (Hatch et al., 1998, Wylie et al., 1997). It can be assumed that the illustrated species do not contain branched-chain fatty acids since their retention times in RP UPLC<sup>®</sup>-ToF-MS analyses have matched perfectly in non-infected and infected fibroblasts, and as branched-chain fatty acids are more lipophilic than eukaryotic straight-chain ones a retention time shift could have been expected.



**Figure 81:** RP UPLC<sup>®</sup>-ToF-MS peak areas of glycerophosphoethanolamines in (A) fibroblast and (B) isolated EBs (isomers are separately illustrated). All altered diacyl-PE species have been increased in infection. Furthermore, several diacyl-PEs have been incorporated in the bacterial EBs.

In contrast to the detected glycerophosphocholines, all important modulated glycerophosphoethanolamine species show either a high increase of detected peak

areas or are exclusively abundant after infection (Figure 81A). *Chlamydia* synthesizes glycerophosphoethanolamines by decarboxylation of glycerophosphoserins, of which *Chlamydia* is capable for de-novo biosynthesis (Wylie et al., 1997). The detected glycerophosphoethanolamines show high peak areas in both infected cells and isolated EBs (Figure 81B). The most important markers have been further identified via ICR/FT-MS<sup>2</sup> in infected fibroblasts (Table 19).

PE species	elemental composition	exact mass	detected acyl-fragments (ESI (-))	inferred PE structures
PE 28:0	C <sub>33</sub> H <sub>66</sub> NO <sub>8</sub> P	635.452605	C14:0	PE (14:0/14:0)
PE 30:0	C <sub>35</sub> H <sub>70</sub> NO <sub>8</sub> P	663.483905	C15:0>C14:0>C16:0	PE (16:0/14:0), PE (15:0/15:0)
PE 31:0	C <sub>36</sub> H <sub>72</sub> NO <sub>8</sub> P	677.499555	C15:0>C16:0>C14:0> C17:0	PE (16:0/15:0), PE (17:0/14:0)
PE 31:1	C <sub>36</sub> H <sub>70</sub> NO <sub>8</sub> P	675.483905	C18:1>C16:1>C14:0 >C16:0>C15:0>C17:1	PE (15:0/16:1), PE (14:0/18:1), PE (17:1/15:0)
PE 32:0	C <sub>37</sub> H <sub>74</sub> NO <sub>8</sub> P	691.515205	C15:0>C16:0>C17:0	PE (17:0/15:0), PE (16:0/16:0)
PE 32:1	C <sub>37</sub> H <sub>72</sub> NO <sub>8</sub> P	689.499555	C18:1>16:1>C14:0> C16:0	PE (16:0/16:1), PE (14:0/18:1)
PE 33:0	C <sub>38</sub> H <sub>76</sub> NO <sub>8</sub> P	705.530855	C15:0>C18:0>C17:0> C16:0	PE (18:0/15:0), PE (16:0/17:0)
PE 33:1	C <sub>38</sub> H <sub>74</sub> NO <sub>8</sub> P	703.515205	C18:1>C15:0	PE (15:0/18:1)
PE 34:0	C <sub>39</sub> H <sub>78</sub> NO <sub>8</sub> P	719.546505	C15:0>C16:0	PE (18:0/16:0), PE (19:0/15:0)
PE 34:1	C <sub>39</sub> H <sub>76</sub> NO <sub>8</sub> P	717.530855	C18:1>C16:0>C16:1> C18:0	PE (16:0/18:1), PE (18:0/16:1)
PE 37:5	C <sub>42</sub> H <sub>74</sub> NO <sub>8</sub> P	751.515205	C20:4	PE (17:1/20:4)

Table 19: Identified glycerophosphoethanolamine markers of *Chlamydia* infection

Especially the PE 31:0 ( $C_{36}H_{72}NO_8P$ ) is predominantly present after infection. Its fatty acid composition is C15:0 and C16:0. In earlier studies C15:0 and C16:0 have been identified as highest abundant fatty acids in *Chlamydia* infection, which applies for both the free form and incorporated in glycerophospholipids (Bidawid et al., 1989, Gaugler et al., 1969, Wylie et al., 1997).

The abundance profile of modulated glycerophosphoethanolamines is very comparable in infected cells and isolated EBs, which suggests that almost all synthesized glycerophosphoethanolamines are incorporated in the bacteria.

### 3.5.2.2 Etherlipids affected by infection

In addition to the detected modulations in diacyl-glycerophospholipids, several etherlipid species are importantly affected by infection. Interestingly, the effect is quite different on the two etherlipid classes, plasmanyl- and plasmenyl-glycerophospholipids.

Most plasmanyl-glycerophosphocholines show an infection time dependent decrease, which is similar to the observed behavior of diacyl-glycerophosphocholines. The peak areas of PC (O-30:0), PC (O-32:0), PC (O-32:1) and PC (O-38:5) decrease after 24 hours p.i., but after 48 hours p.i. they are equally or even higher present compared to non-infected cells (Figure 82A). The abundance profile in isolated EBs is comparable to non-infected samples, only plasmanyl-glycerophosphocholines with a higher degree of unsaturation and longer chain length have not been detected in EBs (PC (O-36:4), PC (O-38:5), PC (O-40:4) and PC (O-40:6)) (Figure 82B). In particular these compounds might be storage compounds for PUFAs, like arachidonic acid (AA) and docosahexaenoic acid (DHA), which are important lipid mediators (Brites et al., 2004). PUFAs usually influence cellular signaling and inflammation processes after their enzymatic release from etherlipids (Brites et al., 2004, Farooqu et al., 2001).

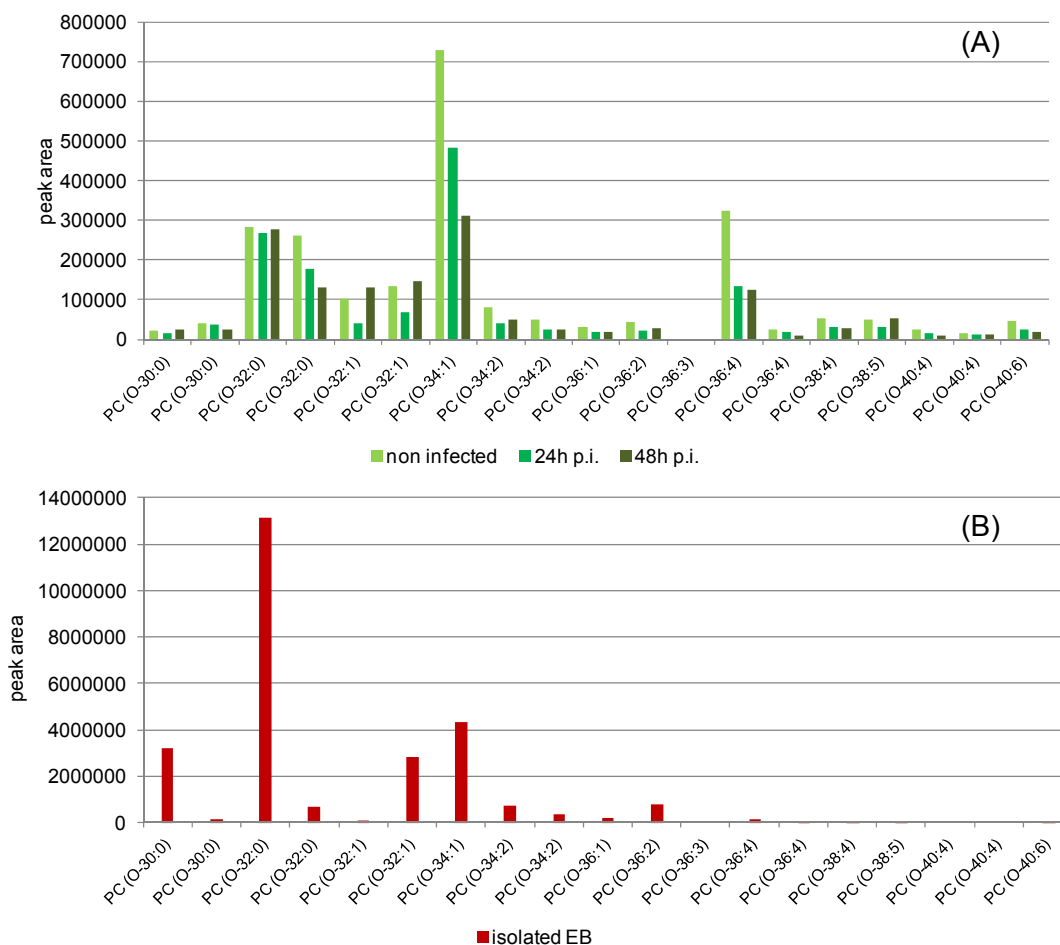


**Figure 82:** RP UPLC<sup>®</sup>-ToF-MS peak areas of plasmanyl-glycerophosphocholines in (A) fibroblasts and (B) isolated EBs (isomers are separately illustrated): An infection time depended decrease of peak areas after infection can be observed. Several plasmanyl-PCs are incorporated in the bacterial EBs.

In contrast to plasmanyl-glycerophosphocholines, all important modulated plasmanyl- glycerophosphoethanolamines are increased after infection (Figure 83A).

Some plasmanyl-glycerophosphoethanolamines are found to be unique in infected samples and isolated EBs (Figure 83B). Several highly unsaturated, long carbon fatty chain containing species are increased after infection. The fatty acid composition of these lipids has been investigated deeper. The identified fatty acid fragments and inferred glycerophospholipid structures are presented in Table 20. Both important lipid messengers, AA and DHA, are abundant in the modulated plasmanyl-glycerophosphoethanolamines.

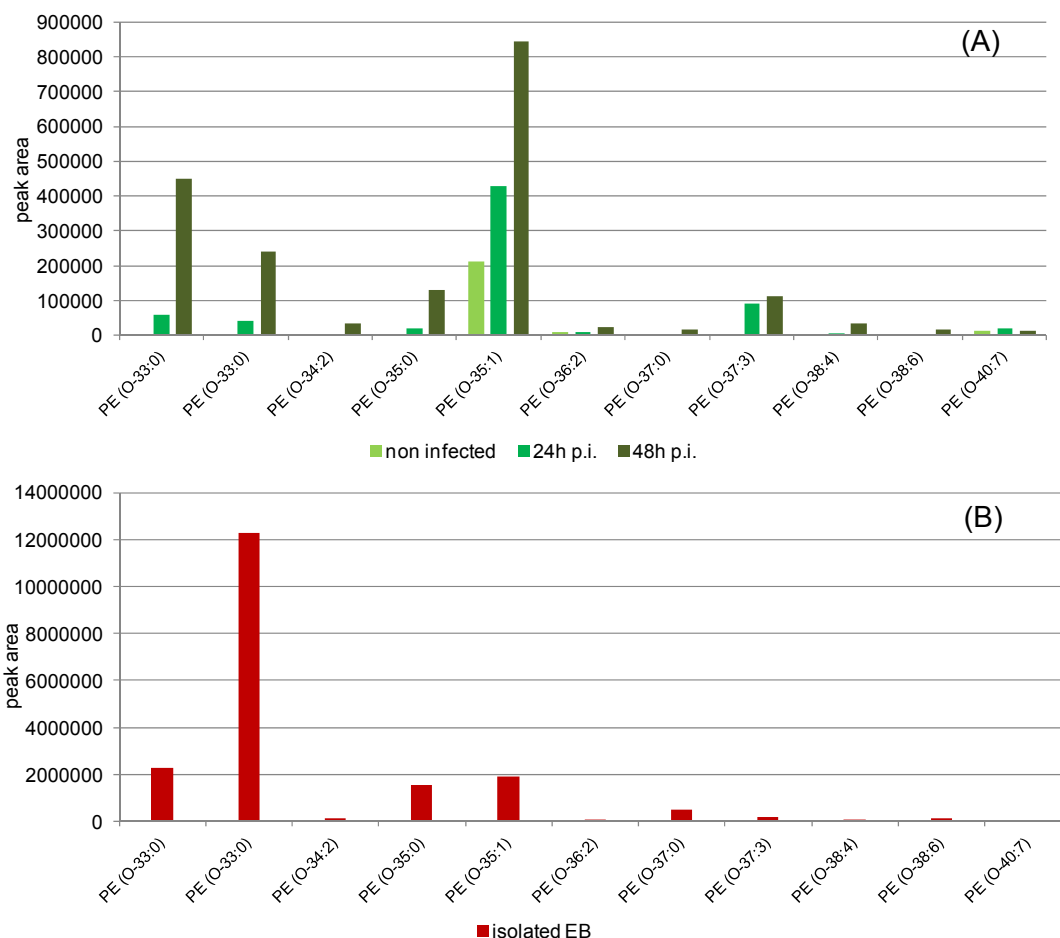


Figure 83: RP UPLC<sup>®</sup>-ToF-MS peak areas of plasmanyl-glycerophosphoethanolamines in (A) fibroblast and (B) isolated EBs

PE species	elemental composition	exact mass	detected acyl-fragments	inferred PE structures
PE (O-38:6)	C <sub>43</sub> H <sub>76</sub> NO <sub>7</sub> P	749.5359	C 22:6	PE (O-16/22:6)
PE (O-38:4)	C <sub>43</sub> H <sub>78</sub> NO <sub>7</sub> P	751.5515	C 20:4	PE (O-18:1/20:4)
PE (O-40:7)	C <sub>45</sub> H <sub>78</sub> NO <sub>7</sub> P	775.5515	C 22:6	PE (O-18:1/22:6)

Table 20: PUFA containing plasmanyl- glycerophosphoethanolamines

In the second etherlipid class, the plasmalogens, almost all compounds have decreased peak area after infection (Figure 84). The only exceptions are the already described glycerophosphoethanolamine plasmalogens (PE (P-16/16), PE (P-16/17),

PE (P-17/16), PE (P-18/15), PE (P-18/16) and PE (P-16/18) (chapter 3.5.1), which have been identified with the UPLC<sup>®</sup>-ToF-MS approach. They have not been detected in the shotgun investigation due to ion suppression effects. This fact illustrates the necessity of combined UPLC<sup>®</sup>-MS and shotgun approaches in lipidomics. The abundance of the important plasmalogens has also been investigated in the isolated EBs (Figure 85). An enrichment in several glycerophosphoethanolamine and -choline plasmalogens, with carbon numbers of 32:1, 34:0, 34:1, 36:1, 36:4 and C38:6 in their fatty acids, is observed.

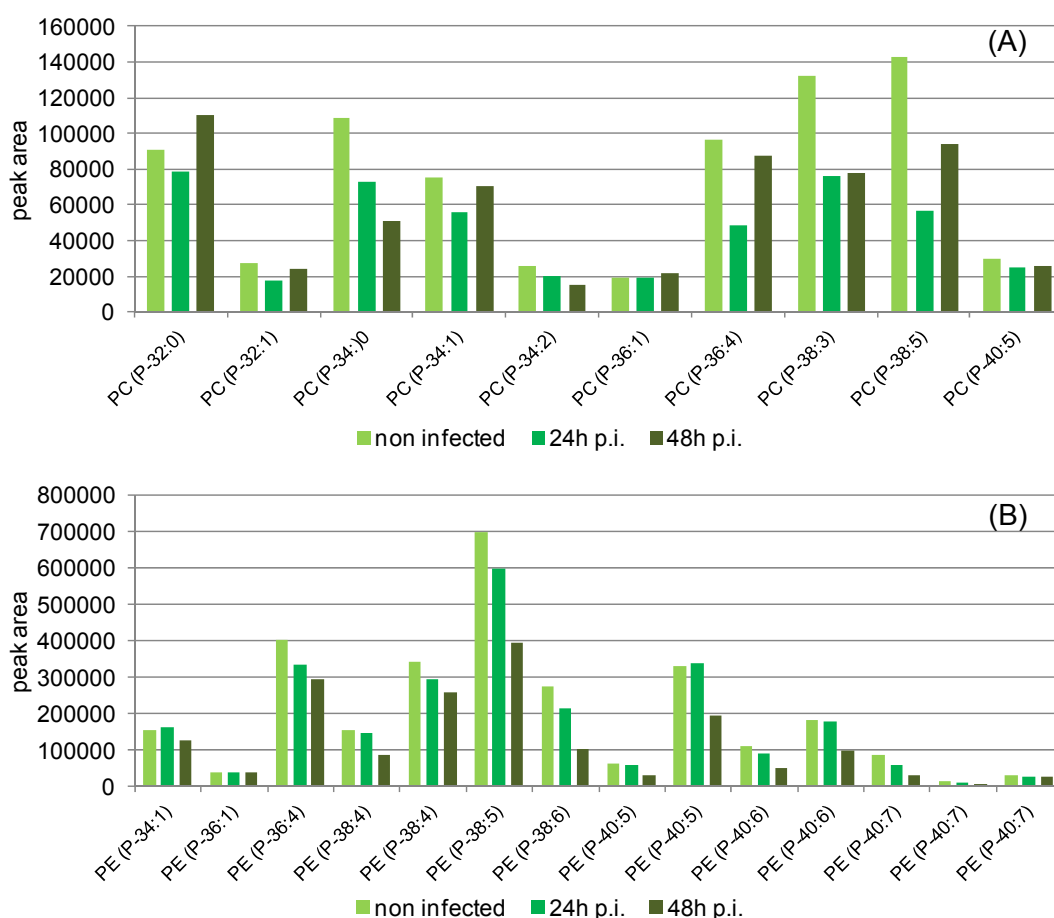


Figure 84: RP UPLC<sup>®</sup>-ToF-MS peak areas of (A) plasmeryl-glycerophosphocholines and (B) plasmeryl-glycerophosphoethanolamines in fibroblast detected with the shotgun approach (isomers are separately illustrated): All within the shotgun lipidomic approach detected and modulated plasmalogens have been decreased in infection.

The vinyl-ether linkage in plasmalogens is very sensitive to singlet oxygen and reactive oxygen species (ROS) (Brites et al., 2004, Nagan et al., 2001). Therefore, plasmalogens function as protective agents against oxidative stress. Considering the continuous formation of ROS during hypoxia (Carbonell et al., 2009), together with the induction of HIF-1 during *Chlamydiae*' early development, but not during the

later infection (Rupp et al., 2007) the observed drop in detected peak areas with a recovery afterwards is very reasonable (Figure 84).

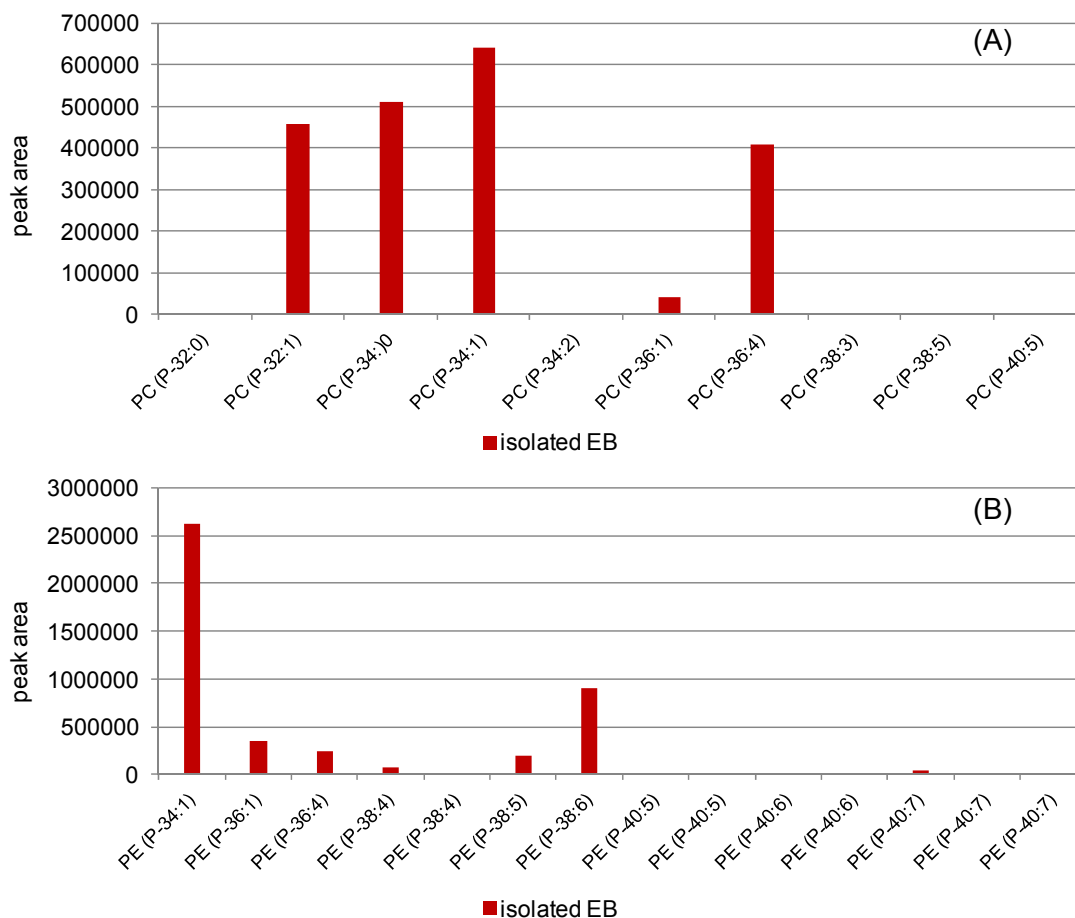


Figure 85: RP UPLC®-ToF-MS peak areas of (A) plasmeryl-glycerophosphocholine and (B) plasmeryl-glycerophosphoethanolamine in isolated EBs detected with shotgun approach

### 3.6 Summary

In the late 1990ies a modulation of the host cells' lipid composition after *Chlamydia* infection has been discovered. The main findings have been reviewed in chapter 1.5.2, but back then the focus has been on lipid classes. As we now have highly advanced analytical technologies we are able to investigate the lipid composition in more detail. For the first time a deep investigation of lipid modulations in *C. trachomatis* infection has been performed with modern techniques in this study. According to the objectives of the investigation two different lipidomic approaches have been built up, the first one has focused on probable very low abundant plasmalogens and the second one has been used to gain an overview of (glycerophospho-) lipid modulations after infection. Considering ion suppression



effects and the expected amount of data either an UPLC<sup>®</sup>-ToF-MS or shotgun ICR/FT-MS based platform has been preferred. The results obtained with the one instrument have always been verified with the other one.

The recent surprising discovery of hijacking peroxisomes by *Chlamydia* suggested a biosynthesis of etherlipids during infection. In the following lipidomics study six glycerophosphoethanolamine plasmalogens, which are synthesized in infected cells containing peroxisomes, but not in peroxisome-deficient cells, have been identified. Furthermore, these lipids have been found to be incorporated into the metabolical-inactive chlamydial EBs. This finding is very interesting, since never before plasmalogens have been identified in aerobic bacteria. Moreover, the deep investigation by ICR/FT-MS<sup>2</sup> shows a completely new fragmentation mechanism, which indicates a putative novel stereochemistry. The biological function of the discovered plasmalogens stays unclear since *Chlamydia* develop also in pex19 samples in the cell culture experiments, but with an decreased inclusion volume.

In the second part of this chapter, glycerol- and glycerophospholipids have been observed as predominantly affected lipid classes. Glycerophospholipids have thus been further investigated. Plasmalogens, revealed by the shotgun approach show a decreased concentration after infection. Plasmalogens are very susceptible to oxidative attack of radicals and ROS, which make them function as scavengers, protecting other cellular compounds against oxidative stress. The expression of HIF-1 during early *Chlamydia* infection explains the decreased levels of most plasmalogens. Nevertheless, up to now the physiological function of etherlipids is still largely unknown, but an alteration of the membrane content lead to a modulation of cellular signal transition and membrane dynamics. Furthermore, etherlipids are storage compounds for PUFAs, like DHA and AA, which have been also evidenced as affected by *Chlamydia* infection in this work. The abundance profiles of plasmalogen-lipids have differed from the ones of plasmalogens. In respect to plasmalogen-compounds an enrichment of glycerophosphoethanolamines and decrease of glycerophosphocholines has been observed, which is also the case for diacyl-glycerophospholipids. *Chlamydia* are capable of glycerophosphoethanolamines, but not of glycerophosphocholine biosynthesis. Several in infection highly or exclusively abundant glycerophosphoethanolamine species have been identified. Membranes composed of higher glycerophosphoethanolamines contents are more susceptible to an increased leakage of ions and allow increased membrane-membrane fusions (Glaser et al., 1994, Nagan et al., 2001). Membrane fusion is very important in several cellular

processes including endocytosis and secretion (Nagan et al., 2001). Considering the fact that the membrane composition strongly influences their function, the detected alterations in lipid composition might in general modulate important cellular mechanisms, such as nutrient and ion transport, inter- and intracellular signaling, fusion, receptor localization and -interactions. The incorporation of glycerophosphocholines into the chlamydial membranes leads to a mimicking of host cells lipid composition and thus might help *Chlamydia* to stealth during infection (Hatch *et al.*, 1998). Furthermore, it has been reported that glycerophosphocholines are important for pathogenity and persistence of other intercellular bacteria (Sohlenkamp et al., 2003). Finally, it can be claimed that a better understanding of modulation of membrane composition by intracellular pathogens within their host and how this affect the cellular mechanisms as well as the identified unique lipid entities may lead to new therapeutic opportunities (Wenk, 2006).

### 3.7 Perspectives

The obtained hints for a novel stereochemistry of identified *Chlamydia-derived* plasmalogens need further investigations in both biological and analytical respect. Due to the lack of available standards a stereoselective synthesis would be one opportunity to prove that the detected and novel fragmentation pattern is caused by a positioning of the alkylen-chain in sn-2 rather than sn-1 position. Additionally, DFT calculations might help to investigate the fragmentation pathways theoretically. Moreover, it is planned to apply an enzymatic cleavage of plasmalogens selectively in sn-1 and sn-2 position by PLA1 and PLA2 treatments.

The position of the double bond in the identified glycerophosphoethanolamines lipid markers has not been investigated. A previously described procedure is the stepwise fragmentation of the fatty acid carbon chains, but this procedure needs ion guides capable of enrichment and transition of very low masses. In addition ozonolysis can be used for selective cleavage of the double bonds. In collaboration with several colleagues, but in particular under the lead of Dr. Basem Kanawati (Research unit Analytical BioGeoChemistry, Helmholtz Zentrum München, Munich, Germany), we have started the development of an ionization source, which can be directly used as reactor for chemical modifications prior to MS detection. Instantly, ozone can be *in situ* generated by the use of UV irradiation. In future this work has to be finished and extended to other application fields. According to the investigated

group of analytes different reaction reagents might be introduced in the source to enable an enhanced detection, comparable to the concept of CIS-MS (*coordination-spray-MS* (Bayer *et al.*, 1999)).

Besides the detected alteration of glycerophospholipid alteration, important modulations of glycerolipids have been observed. Glycerolipids lack inherently ionizable groups in their molecular structure. They are thus usually detected with very low signal intensities, which complicates detailed studies of this very interesting lipid class. A detailed investigation of ionization and fragmentation processes of diacyl-glycerolipids has been performed in order to enable future analysis of *Chlamydia*-relevant species (annex). The application of the obtained results to investigate *Chlamydia*-host interactions is an additional future analytical task.

## 4 Summary and concluding remarks

The presented work illustrates the advantage of non-targeted metabolomics approaches to reveal non-intuitive insights into host-pathogen interactions. Infection associated biochemical modifications in the phenotype of *Chlamydia* infected human cells have been characterized on a holistic level, followed by a deep targeted investigation of important metabolite classes. This has been illustrated using the example of lipid modulations after infection in the second part of the thesis. Identification of *Chlamydia*-derived lipid species has been achieved. Metabolomics has thus been presented as powerful tool in both non-targeted screenings and targeted verification of a *priory* hypothesis.

Non-targeted approaches should base on multi-parallel analytical concepts, to enable the detection of as many as possible metabolites from infected cells. State-of-the-art direct injection ICR/FT-MS and UPLC<sup>®</sup>-ToF-MS techniques have been applied in this study. In particular by the implementation of ICR/FT-MS a wealth of knowledge unattainable with any other type of instrument has been obtained. UPLC<sup>®</sup>-ToF-MS has been seen to be very helpful in metabolite verification and identification by retention time comparison with standard compounds. However, such multi-parallel approach delivers a tremendous amount of data, which has to be integratively analyzed. A stepwise data analysis workflow has therefore been developed. The obtained results give for the first time an overview of metabolic interactions between *Chlamydia* and the human host cell. They are in very good accordance to the sporadically known metabolic effects of *Chlamydia* infection. The detected metabolite signal intensities could be furthermore verified instantly for tryptophan. The tryptophan signal intensities correlated very well with corresponding IDO expression levels, determined with molecular biological investigations.

A methodology required for targeted hypothesis verification has been illustrated in the second part of the thesis. The lipid alterations after infection have been deeply investigated with a special focus on etherlipid biosynthesis of *Chlamydia*. Two different lipidomics platforms have been built up, the first one, which focused on very low abundant species illustrated the necessity of isomer separation to minimize ion suppression effects. The second platform based on shotgun ICR/FT-MS and allowed the detection and determination of mainly present and affected lipids directly out of the sample extracts. In consequence, according to the objective of the work either a UPLC<sup>®</sup>-MS based or shotgun workflow needs to be chosen in lipidomics, if

a comprehensive analysis of the lipidome is aimed, a multi-parallel approach is inevitable.

## 5 Annex - Investigation of the ionization and fragmentation mechanism of diacylglycerols

### 5.1 Introduction

In this thesis several putative diacylglycerol (*DG*) species have been identified to play a regulatory role in persistent and active *Chlamydia* infection (chapter 2.4.3, summarized in Table 21), which leads us to a deep investigation of this particular lipid class.

annotated DG	ionization	modulation
C <sub>37</sub> H <sub>74</sub> O <sub>4</sub> -ether DG	[M+Na] <sup>+</sup>	decreased in active, but not in persistent <i>Chlamydia</i> infection (chapter 2.4.3.2)
C <sub>37</sub> H <sub>70</sub> O <sub>5</sub> -DG	[M+Na] <sup>+</sup>	
C <sub>39</sub> H <sub>74</sub> O <sub>5</sub> -DG	[M+Na] <sup>+</sup>	
C <sub>32</sub> H <sub>62</sub> O <sub>5</sub> -DG	[M+Na] <sup>+</sup>	increased after IFN- $\gamma$ addition in normoxia, but not in hypoxia (chapter 2.4.3.1)
C <sub>34</sub> H <sub>66</sub> O <sub>5</sub> -DG	[M+Na] <sup>+</sup>	
C <sub>36</sub> H <sub>66</sub> O <sub>5</sub> -DG	[M+Na] <sup>+</sup>	
C <sub>36</sub> H <sub>70</sub> O <sub>5</sub> -DG	[M+Na] <sup>+</sup>	
C <sub>39</sub> H <sub>70</sub> O <sub>5</sub> -DG	[M+Na] <sup>+</sup>	

Table 21: Diacylglycerol species important for *Chlamydia* infection

Diacylglycerols have a central role in the lipid metabolism, e.g. in biosynthesis and degradation of triacylglycerols and glycerophospholipids. Additionally, diacylglycerols are of high interest since they act as second messengers (Carrasco et al., 2007), especially through the activation of protein kinase C, and therefore take part in regulation of cell differentiation, proliferation, carcinogenesis, development, memory and other cell functions (Bishop et al., 1988, Dekker et al., 1994, Mochly-Rosen, 1995, Newton, 1995, Nishizuka et al., 1995). Different species of

diacylglycerols are hereby known to fulfill different cellular functions (reviewed in Carrasco et al., 2007, Goto et al., 2008). Along with the described involvement in *Chlamydia* infection, changes in the diacylglycerol content are evidenced in conjunction to other diseases (Erion et al., Kim et al., 2001, Saburi et al., 2003).

Diacylglycerols consist of a glycerol backbone and two covalently bond carboxylic acids (Figure 86). The carbonyl chains are linked to sn-1 and sn-2 position of the glycerol back bone, the hydroxyl group in sn-3 position is free. Because polar groups are absent in their structure, diacylglycerols are called neutral lipids.

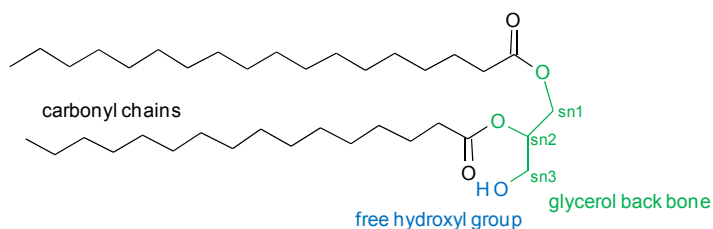


Figure 86: Structure of diacylglycerols

The deficiency of inherently ionizable groups hampers ESI ionization and thus MS detection and identification (Callender et al., 2007). Diacylglycerols have been detected as sodium adducts in this work (Table 21). The formation of several different adduct ions, like with alkali or ammonium cations, in positive ionization mode has been previously described (Gross et al., 2009, Murphy et al., 2007). However, sodium adducts usually do not deliver a fragmentation pattern. Negative ionization has only been described after derivatization (Li et al., 2007), but in particular negative ionization is beneficial for identification, since the fragmentation pattern directly reveals the fatty acid composition of the diacylglycerol structure.

In the following, the dimer formation of diacylglycerols in negative ion mode is described. The dimer of a standard has been isolated and fragmented. The underlying fragmentation pathways and intermolecular reactions have been intensively investigated based on observed fragments and verified by DFT calculations realized by Dr. Basem Kanawati (Research unit Analytical BioGeoChemistry, Helmholtz Zentrum München, Munich, Germany). The opportunity to ionize neutral lipids as dimers helps to enable deep investigations of important diacylglycerol markers, not only in *Chlamydia* infection. Additionally, the study improves our knowledge about gas phase reactions and evidences

intermolecular fragmentations, which have never been described before. The approach and the obtained results might be extended to other neutral lipid classes (monoacylglycerols, triacylglycerols).

## 5.2 *Materials and Methods*

### 5.2.1 *Materials*

1-Octadecanoyl-2-hexadecanoyl-glycerol (DG (18:0/16:0)) has been purchased from Avanti<sup>®</sup> Polar Lipids, Inc. (Alabaster, USA). The chloroform containing solution has been dried under vacuum (SpeedVac Concentrator, Savant SPD 121P, ThermoFisher Scientific, Waltham, USA) and resolved in methanol/n-propanol (1:1). Prior to injection into the ICR/FT-MS the standard solution has been diluted with methanol to 1,7mmol/l (50ppm). CROMASOLVE<sup>®</sup> methanol, has been bought from Fluka<sup>®</sup> Analytical (Sigma-Aldrich-Aldrich, St. Louis, USA) and n-propanol from BioSolve<sup>®</sup> (Valkenswaard, Netherlands).

### 5.2.2 *Methods*

All experiments have been performed on ICR/FT-MS (solariX<sup>™</sup>, Bruker, Bremen, Germany) equipped with a 12 Tesla superconducting magnet (magnex scientific Inc., Yarnton, GB). The instrument offers ultrahigh resolution and mass accuracy. The diacylglycerol standard solution has been injected in the Apollo2 electrospray ionization source via a microliter pump. The flow rate has been set to 120µl/h. Negative ionization mode has been chosen. The ions of interest have been selectively filtered in the quadrupole and accelerated with increasing potential differences (0-12eV) in the hexapole. Fragmentation has been achieved via collision of the accelerated ions with the abundant Argon atoms (CID). The spectra have been obtained with 2MW time domain in broad band detection mode. For each energy level 20 scans have been accumulated for one spectrum. The instrument has been calibrated by the usage of 2ppm arginine solution in methanol prior to analysis.



### 5.3 Results and discussion

An ionization of the neutral lipid diacylglycerol as dimer has been identified. The dimer consists of one neutral and one negatively charged diacylglycerol molecule  $[M+M-H]^-$  with the  $m/z$  1192 (Figure 87). We propose either a hydrogen bridging between the deprotonated and protonated hydroxyl functions or hydrophobic interactions between the carbonyl chains as driving forces for the dimer formation.

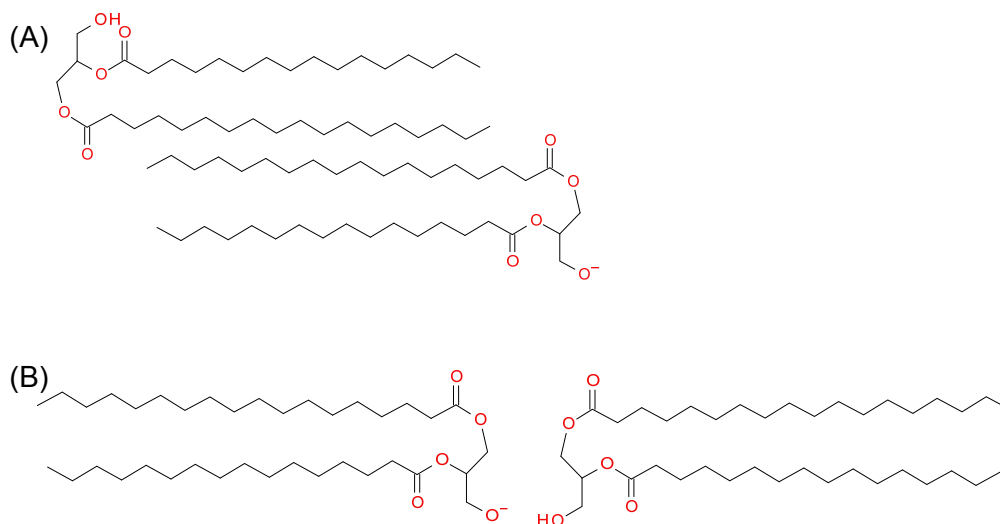


Figure 87: Conformation of diacylglycerol dimers in gas phase: (A) hydrophobic interaction (B) hydrogen bridging

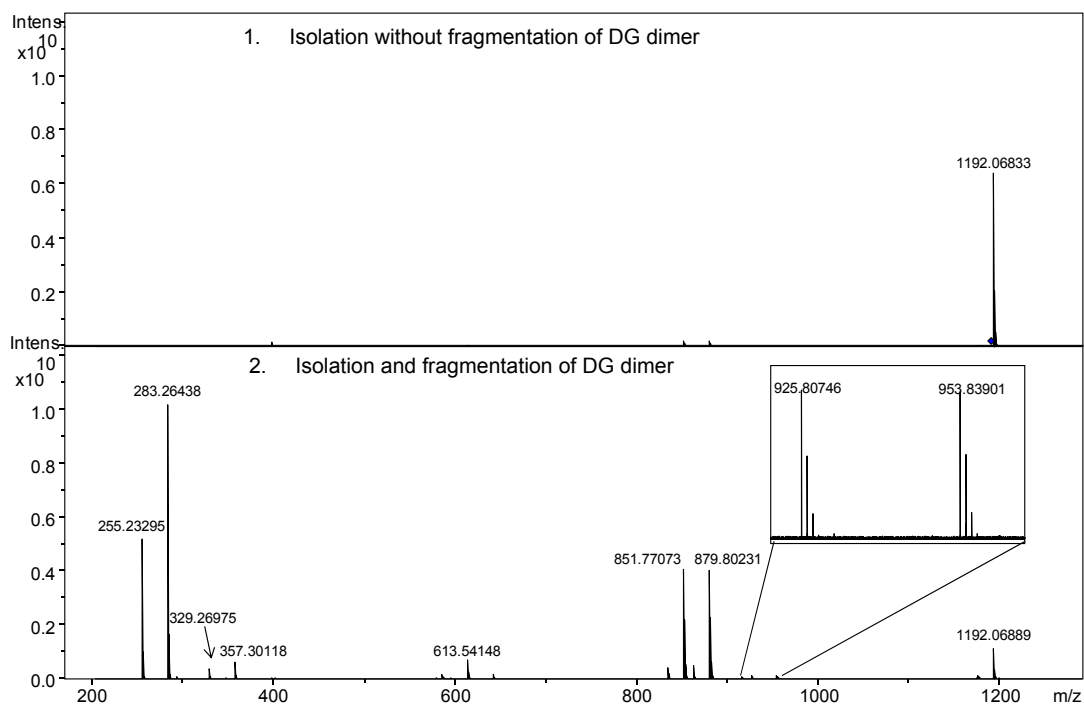


Figure 88: (-)ICR/FT-MS<sup>2</sup> fragmentation pattern of DG (18:0/16:0)-dimer: (1.) isolation of parent ion; (2.) fragmentation pattern after applying 8eV

The diacylglycerol dimer has been isolated and accelerated with different kinetic energy. Exemplarily two spectra applying 0 and 8eV are illustrated in Figure 88. The determined fragments with the corresponding elemental compositions are summarized in Table 22.

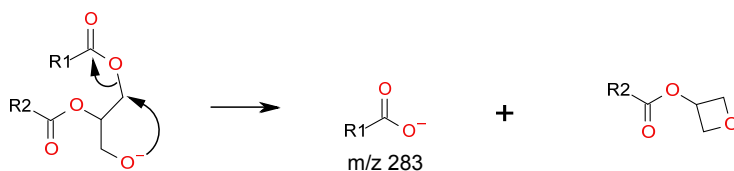
elemental composition	exactly calculated m/z	detected m/z	error [ppm]	error [mDa]
$C_{16}H_{31}O_2 + e^-$	255.2329535	255.23295	-0.001	-0.0035
$C_{18}H_{35}O_2 + e^-$	283.2642535	283.26425	-0.001	-0.0035
$C_{19}H_{37}O_4 + e^-$	329.2697335	329.26975	0.005	0.0165
$C_{21}H_{41}O_4 + e^-$	357.3010335	357.30106	0.007	0.0265
$C_{37}H_{70}O_4 + e^-$	613.540715	613.54135	0.103	0.635
$C_{53}H_{103}O_7 + e^-$	851.7709285	851.77102	0.011	0.0915
$C_{55}H_{107}O_7 + e^-$	879.8022285	879.80231	0.009	0.0815
$C_{56}H_{109}O_9 + e^-$	925.8077085	925.80777	0.007	0.0615
$C_{58}H_{113}O_9 + e^-$	953.8390085	953.83913	0.013	0.1215
$C_{74}H_{143}O_{10} + e^-$	1192.068674	1192.06845	-0.019	-0.2235

Table 22: Determined DG (18:0/16:0)-dimer fragment ions

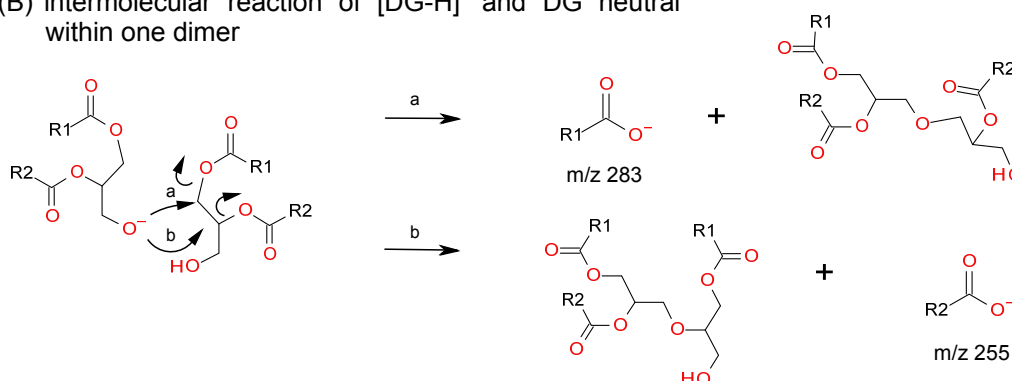
Elimination of the carboxylic acid in sn-1 position is the most favorable fragmentation process and is represented by a very high abundance of octadecane acid (m/z 283). In the underlying reaction the negatively charged oxygen attacks intramolecularly the carbon atom in sn-1 position of the glycerol backbone (Figure 89A). A stable oxetane ring structure is the neutral product next to octadecane acid (m/z 283)  $[R_1COO]^-$ . A nucleophilic attack of the deprotonated hydroxyl group on the carbon in sn-2 position is unlikely due to steric hindrance and resulting formation of

an unstable oxirane structure as neutral product. The detected fragment  $m/z$  255 is nonetheless belonging to hexadecane acid eliminated from sn-2 position. Hexadecane acid is the product of intermolecular reactions (Figure 89B/C).

(A) intramolecular reaction of  $[DG-H]^-$  within one dimer



(B) intermolecular reaction of  $[DG-H]^-$  and DG neutral within one dimer



(C) intermolecular reaction of  $[R1COO]^-$  and DG neutral

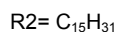
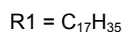
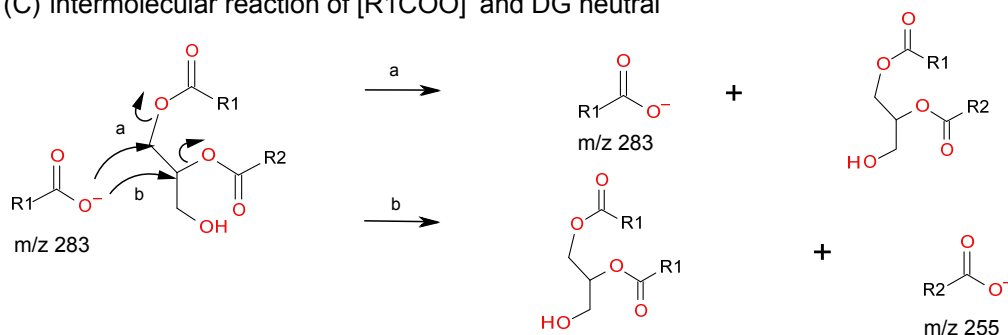


Figure 89: Proposed intra- and intermolecular fragmentation mechanisms for DG (18:0/16:0)-dimer

Two intermolecular fragmentation channels are proposed. In the first one the deprotonated hydroxyl group of one diacylglycerol attacks the other diacylglycerol either in sn-1 (a) or sn-2 (b) position within one dimer (Figure 89B). Octadecane- or hexadecane acid are equivalently abundant products. Another reaction opportunity for the intermolecular formation of  $m/z$  255 is given in Figure 89C. Octadecane acid  $[R1COO]^-$  as a product of the intramolecular reaction further reacts with one

diacylglycerol neutral. Since an alcohol is a much stronger base compared to carboxylic acids the first described fragmentation channel (Figure 89B) might be the favored one.

Further determined fragment ions are the  $m/z$  879 and  $m/z$  851. Both do correspond to an attachment of carboxylic acids fragments,  $[R1COO]^-$  and  $[R2COO]^-$  to one diacylglycerol neutral. This means, the negatively charged carboxylic acids interact with diacylglycerol neutrals originating from the ionized dimers in the gas phase. The  $m/z$  879 and 851 are detected with almost equal intensities, which indicates that this reaction occurs randomly. Furthermore, they are mostly abundant in CID spectra of smaller applied energy ( $\leq 8\text{eV}$ ). The interactions between the two molecules, the diacylglycerol neutral and charged carboxylic acid, might be a hydrogen bond or hydrophobic interaction as illustrated for the neutral lipid dimer (Figure 87).

Next to the elimination of carbonyl chains as carboxylic acids an elimination of ketenes has been determined (Figure 90). The fragments  $[M-H-(R1-C=C=O)]^-$  ( $m/z$  329) and  $[M-H-(R2-C=C=O)]^-$  ( $m/z$  357) both have one remaining carboxylic acid at the glycerol backbone. The elimination in *sn*-2 position is the preferred fragmentation compared to *sn*-1 position. The deprotonated hydroxyl function takes one hydrogen from the  $\alpha$ -carbon in *sn*-2 acyl-chain (Figure 90A). Consequently, a ketene is formed and eliminated as neutral. The negative charge moves intramolecularly from *sn*-3 to *sn*-2 position. The corresponding  $m/z$  357 shows a two times higher intensity compared to  $m/z$  329.  $m/z$  329 results from the elimination of the acyl-chain in *sn*-1 position. The underlying charge remote mechanism is explained in Figure 90B. In principal the elimination of ketenes is not the preferred mechanism compared to the elimination of carboxylic acids, thus we detected only very small intensities of the resulting fragments. Furthermore, it should be mentioned, that the fragment ions  $m/z$  357 and  $m/z$  329 also attach to one diacylglycerol neutral inside the gas phase, explaining the occurrence of  $m/z$  953  $[M+M-H-(R1-C=C=O)]^-$  and 925  $[M+M-H-(R2-C=C=O)]^-$ . As ultrahigh resolution and accuracy mass spectrometry has been implemented for our analyses, the mass error between predicted and detected products is less than 0.013ppm. Further verification of the predicted mechanisms has been achieved by comparison of theoretical and detected abundance of naturally occurring isotopes for the detected fragment ions.

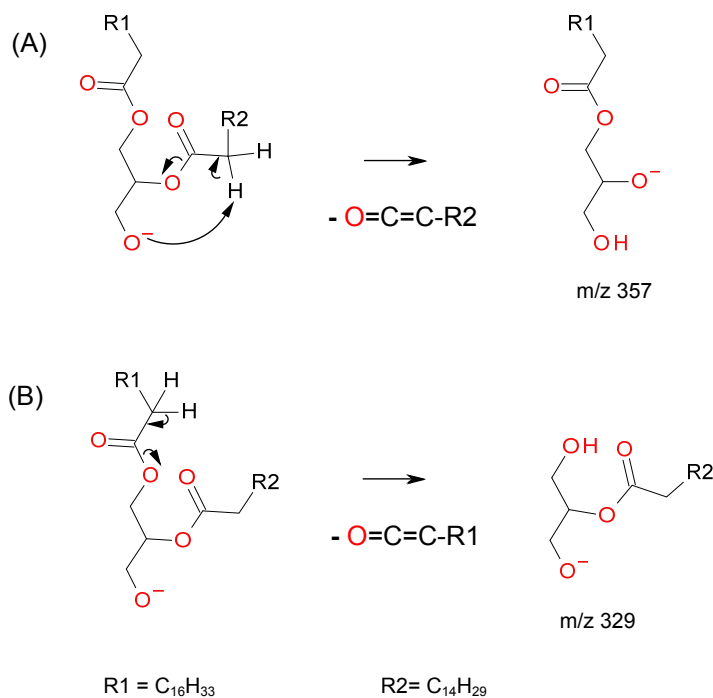


Figure 90: Proposed fragmentation mechanism of keten elimination

## 5.4 Summary

Based on the identification of important modulated diacylglycerol lipids in *Chlamydia* infection an investigation of possibilities for ionization and identification of such neutral lipids has been set up. We could discover a completely new ionization opportunity through the dimer formation as well as a novel fragmentation mechanism for diacylglycerol lipids. This will enable a deeper investigation of discriminative lipid species. Additionally, the obtained results may be transferred to other neutral lipid classes.

## 6 Supplementary data

Supplementary table 1: Standard compounds for method development (written with bold letters) and retention time verification/logD regression

name	supplier	purity
<b>sugars and -derivates</b>		
D(+)-glucose	Sigma-Aldrich	>99.5%
D(-)-ribose	Fluka	>99%
D(+)-galactose	Sigma-Aldrich	99%
D-sorbitol	Sigma-Aldrich	98%
D(+)-raffinose pentahydrate	Fluka	>99%
D(+)-melezitose monohydrate	Sigma-Aldrich	>99%
gentiobiose	Fluka	>99%
D(-)-jarabinose	Sigma-Aldrich	99%
L-rhamnose monohydrate	Sigma-Aldrich	99%
meso-erythritol	Sigma-Aldrich	>95%
<b>D(-)-fructose</b>	<b>Fluka</b>	<b>&gt;99%</b>
L(-)-fucose	Sigma-Aldrich	99%
glucose-6-phosphate	Boehringer Mannheim	99%
sodium pyruvate	Sigma-Aldrich	99%
citric acid	Sigma-Aldrich	99%
fumaric acid	Sigma-Aldrich	99%
sodium succinate dibasic hexahydrate	Sigma-Aldrich	99%
malic acid	Fluka	99%
glutaric acid	Alfa Aesar	99%
oxalic acid	Merck	p.A.
glutaconic acid	Fluka	>97%
mesaconic acid	Fluka	purum
pyrazine-2,3-dicarbonic acid	Merck	>98%
tartronic acid	Sigma-Aldrich	98%
meso-tartaric acid hydrate	Sigma-Aldrich	99%
benzoylformic acid	Fluka	>98%
D(+)-malic acid	Merck	99%
oxalacetic acid	Sigma-Aldrich	97%
sodium L-lactate	Sigma-Aldrich	99%
<b>fatty acids</b>		
caprylic acid	Fluka	99%
nonanoic acid	Sigma-Aldrich	96%
<b>capric acid</b>	<b>Fluka</b>	<b>99.5%</b>
undecanoic acid	Fluka	>97%
palmitic acid	Sigma-Aldrich	99%
stearic acid	Fluka	>99.5%
arachidic acid	Fluka	>99.5 %
heneicosanoic acid	Fluka	>98%
<b>amino acids</b>		
L-arginine	Sigma-Aldrich	> 98%
L-asparagine mono hydrate	Sigma-Aldrich	99%
<b>L(+)-glutamic acid</b>	<b>Merck</b>	<b>99%</b>
DL-histidine	Sigma-Aldrich	98%
DL-leucine	Sigma-Aldrich	99%
L-isoleucine	Sigma-Aldrich	99%
DL-methionine	Sigma-Aldrich	99%
DL-proline	Sigma-Aldrich	99%
DL-serine	Sigma-Aldrich	99%
DL-valine	Sigma-Aldrich	>99%
L-lysine hydrochloride	Sigma-Aldrich	99%
glycine	Merck	>98.5%
<b>D-phenylalanine</b>	<b>Sigma-Aldrich</b>	<b>99%</b>
DL-tryptophan	Ega	98%
D-alanine	Sigma-Aldrich	99%
L-tyrosine	Merck	99%
<b>nucleoside and nucleotides</b>		
adenosine	Sigma-Aldrich	>99%

cytidine	Sigma-Aldrich	>99%
guanosine	Sigma-Aldrich	>99%
uridine	Sigma-Aldrich	>99%
AMP	Sigma-Aldrich	>99.5%
ATP disodium salt hydrate	Sigma-Aldrich	99%
ADP	Sigma-Aldrich	95%
<b>steroids</b>		
<b>cholic-2,2,4,4-[d<sub>4</sub>] acid</b>	<b>Isotec</b>	<b>98%</b>
testosterone	Sigma-Aldrich	98%
cholesterol	Sigma-Aldrich	99%
<b>other lipids</b>		
methylstearate	Sigma-Aldrich	>96%
PGF 1a	Avanti lipids	
<b>PC (10:0/10:0)</b>	<b>Sigma-Aldrich</b>	<b>99%</b>
<b>PC (18:1/18:0)</b>	<b>Sigma-Aldrich</b>	<b>98%</b>
PE (16:0/0:0)	Avanti lipids	>99%
<b>PE (18:1/18:1)</b>	<b>Sigma-Aldrich</b>	<b>98%</b>
<b>PE (12:0/12:0)</b>	<b>Sigma-Aldrich</b>	<b>98%</b>
PC (P-18:1/18:0)	Avanti lipids	>99%
<b>vitamins, cofactors and others</b>		
<b>acetyl-L-carnitine.HCl</b>	<b>Sigma-Aldrich</b>	<b>&gt;99%</b>
carnitine HCl	Sigma-Aldrich	98%
biotin	Sigma-Aldrich	99%
<b>caffeine</b>	<b>Sigma-Aldrich</b>	<b>-</b>
<b>DL-decanoylcarnitine chloride</b>	<b>Sigma-Aldrich</b>	<b>-</b>
folic acid	Merck	>95%
<b>hexadecanoyl-L-carnitine HCl</b>	<b>Sigma-Aldrich</b>	<b>98%</b>
<b>hippuric acid</b>	<b>Sigma-Aldrich</b>	<b>98%</b>
sodium hippurate	Sigma-Aldrich	99%
<b>3-hydroxy 3-[d<sub>3</sub>]-methylglutaric acid</b>	<b>Dr. Herman J. ten Brink</b>	<b>-</b>
<b>nialamide</b>	<b>Sigma-Aldrich</b>	<b>95%</b>
nicotinamide	Sigma-Aldrich	99.5%
<b>(-)-nicotine</b>	<b>Sigma-Aldrich</b>	<b>&gt;99%</b>
<b>[3 Methyl-d<sub>2</sub>] phytanic acid</b>	<b>Dr. Herman J. ten Brink</b>	<b>-</b>
<b>reserpine</b>	<b>Fluka</b>	<b>99%</b>
spermidine	Sigma-Aldrich	99%
<b>sulfadimethoxine</b>	<b>Sigma-Aldrich</b>	<b>99.4%</b>
<b>terfenadine</b>	<b>Sigma-Aldrich</b>	<b>&gt;95%</b>
<b>[D<sub>3</sub>] trihydroxycoprostanic acid</b>	<b>Dr. Herman J. ten Brink</b>	<b>-</b>
uUracil	Sigma-Aldrich	>99%
<b>valeryl-L-carnitine HCl</b>	<b>Sigma-Aldrich</b>	<b>-</b>

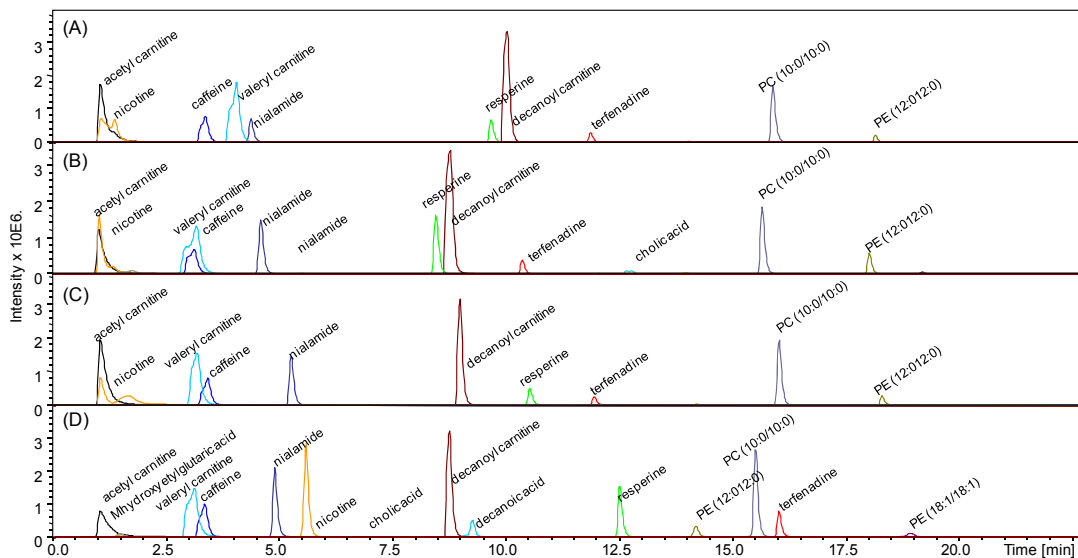
Supplementary table 2: Implemented ICR/FT-MS parameters

parameter	(+)ICR/FT-MS	(-)ICR/FT-MS
number of scans	300	380
transient time domain	2MW	2MW
source accumulation	0 sec	0 sec
ion accumulation time	0.2 sec	0.2 sec
time of flight	0.7 sec	0.6 sec
capillary	4.5 kV	4 kV
end plate offset	500 V	500 V
dry gas	2.4 l/min	4 l/min
dry gas temperature	200°C	200°C
nebulizer	1.1 l/min	1.0 l/min
side kick	-5 V	5
side kick off set	-5 V	10
sweep excitation	18 %	23.1 %
front plate	0.6 V	-0.4 V
back plate	0.9 V	-0.5 V
analyzer entrance	-9 V	4 V

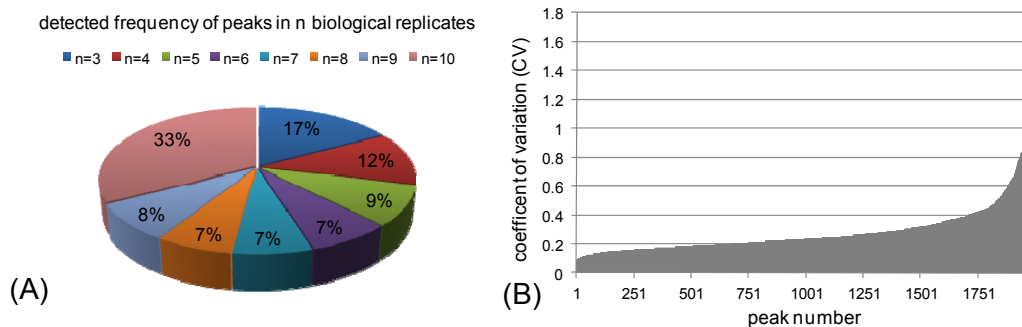
Supplementary table 3: Implemented ToF-MS parameters

parameter	non-targeted metabolomics	targeted lipidomics
spectra rate	1 Hz	1 Hz
capillary	4.5 kV	4.5 kV
end plate offset	500 V	500 V
dry gas	4 l/min	4 l/min
dry gas temperature	180°C	180°C
nebulizer	1.5 bar	1.5 bar
funnel RF	200 Vpp	377 Vpp
multipole RF	200 Vpp	333 Vpp
ion Energy	3 eV	3 eV
low mass	100 m/z	50 m/z
collision energy	8 eV	8 eV
collision RF	500 Vpp	3383.3 Vpp
transfer time	45 µsec	45 µsec
ion cooler RF	50 Vpp	100 Vpp
pre-pulse storage	10 µsec	20 µsec

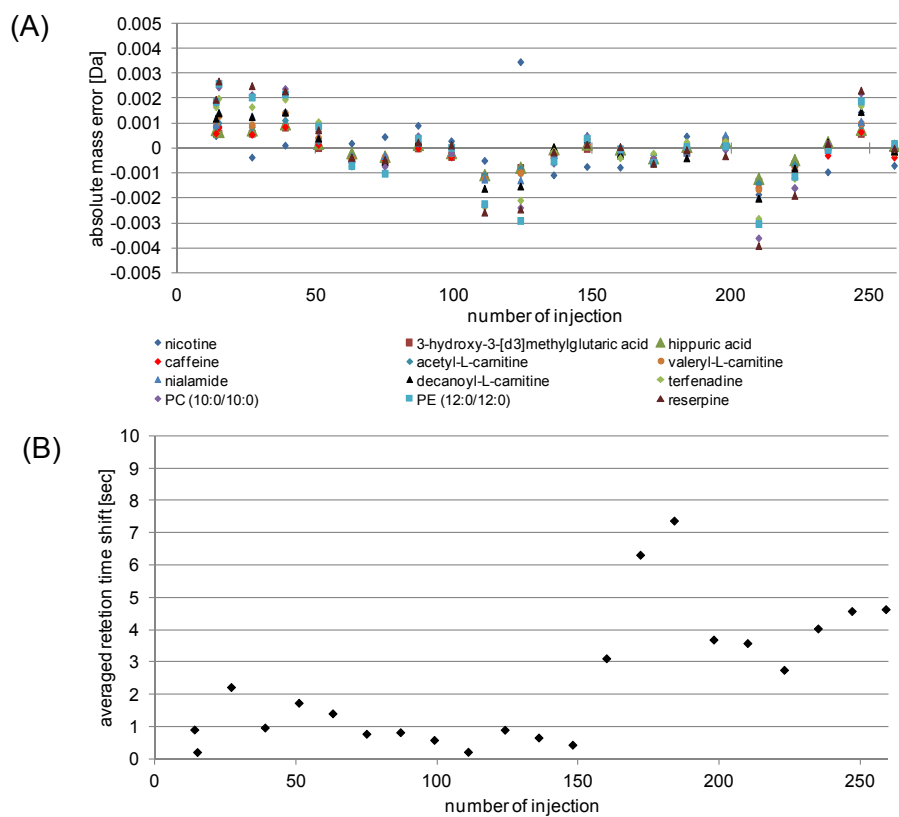




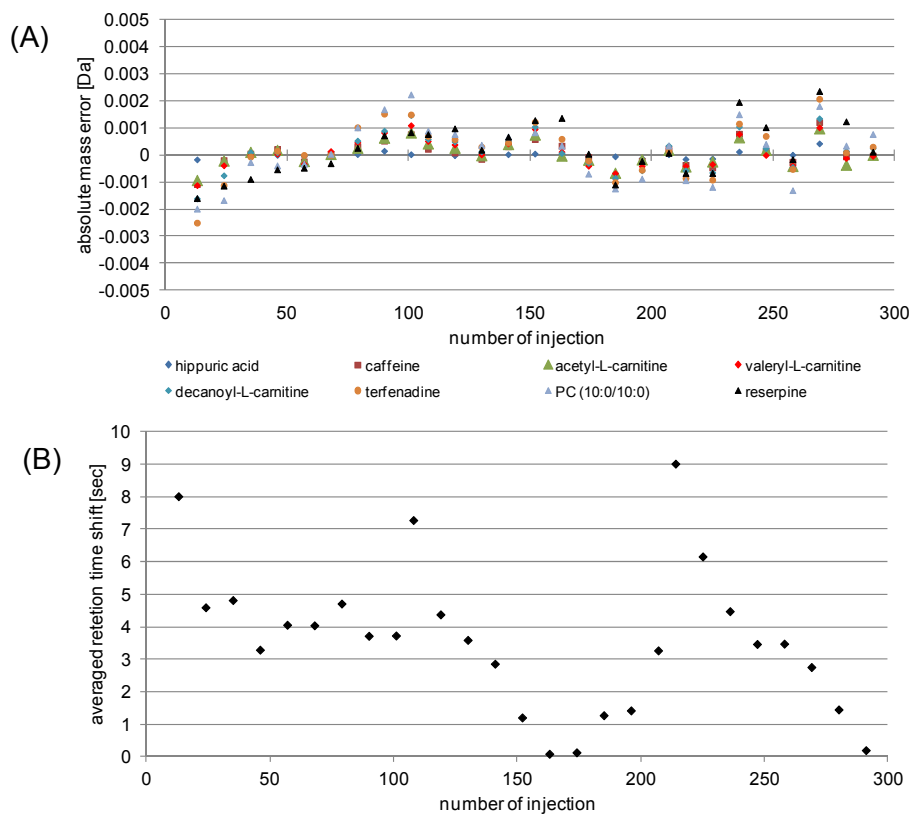
Supplementary figure 1: RP UPLC<sup>®</sup> separation of several standards during method development



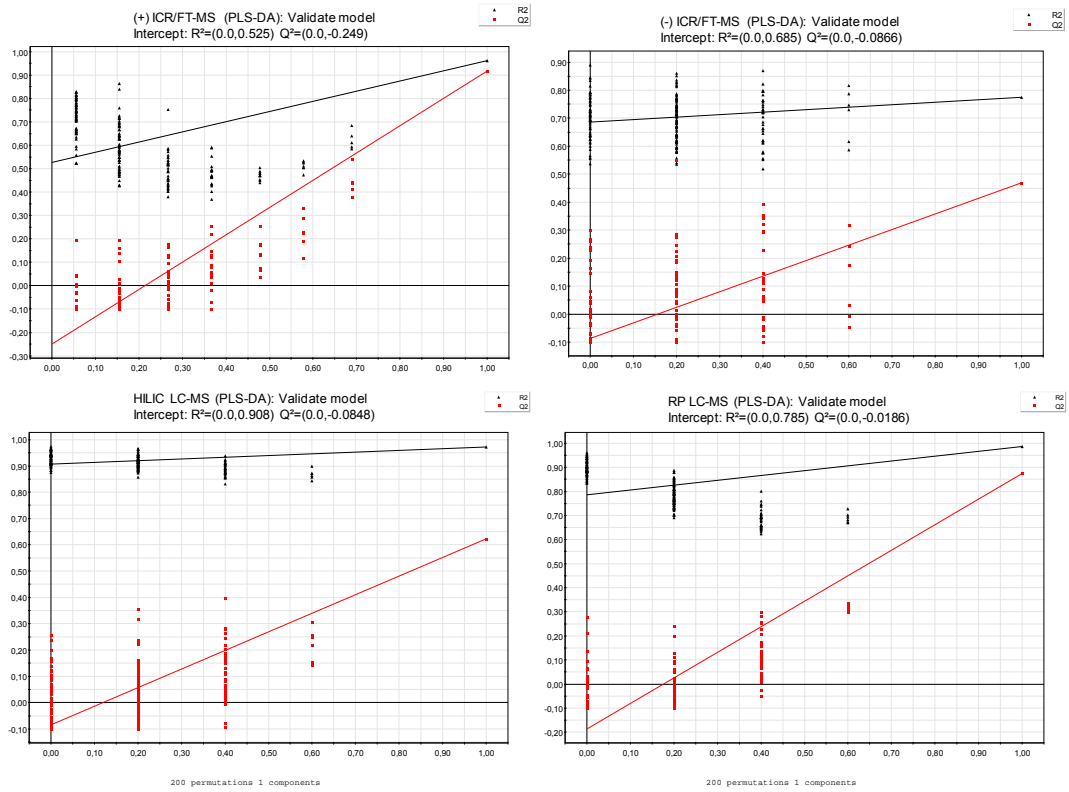
Supplementary figure 2: Evaluation of reproducibility for (+)/(-)ICR/FT-MS measurements: (A) Distribution of detected peaks over  $n$  biological replicates of infected, normoxic cells; (B) CV of intensities detected in all replicates of infected, normoxic cells.



Supplementary figure 3: (A) Obtained mass accuracy and (B) observed retention time shifts (in average) for injected standard compounds during RP UPLC<sup>®</sup>-ToF-MS analyses



Supplementary figure 4: (A) Obtained mass accuracy and (B) observed retention time shifts (in average) for injected standard compounds during HILIC UPLC<sup>®</sup>-ToF-MS analyses



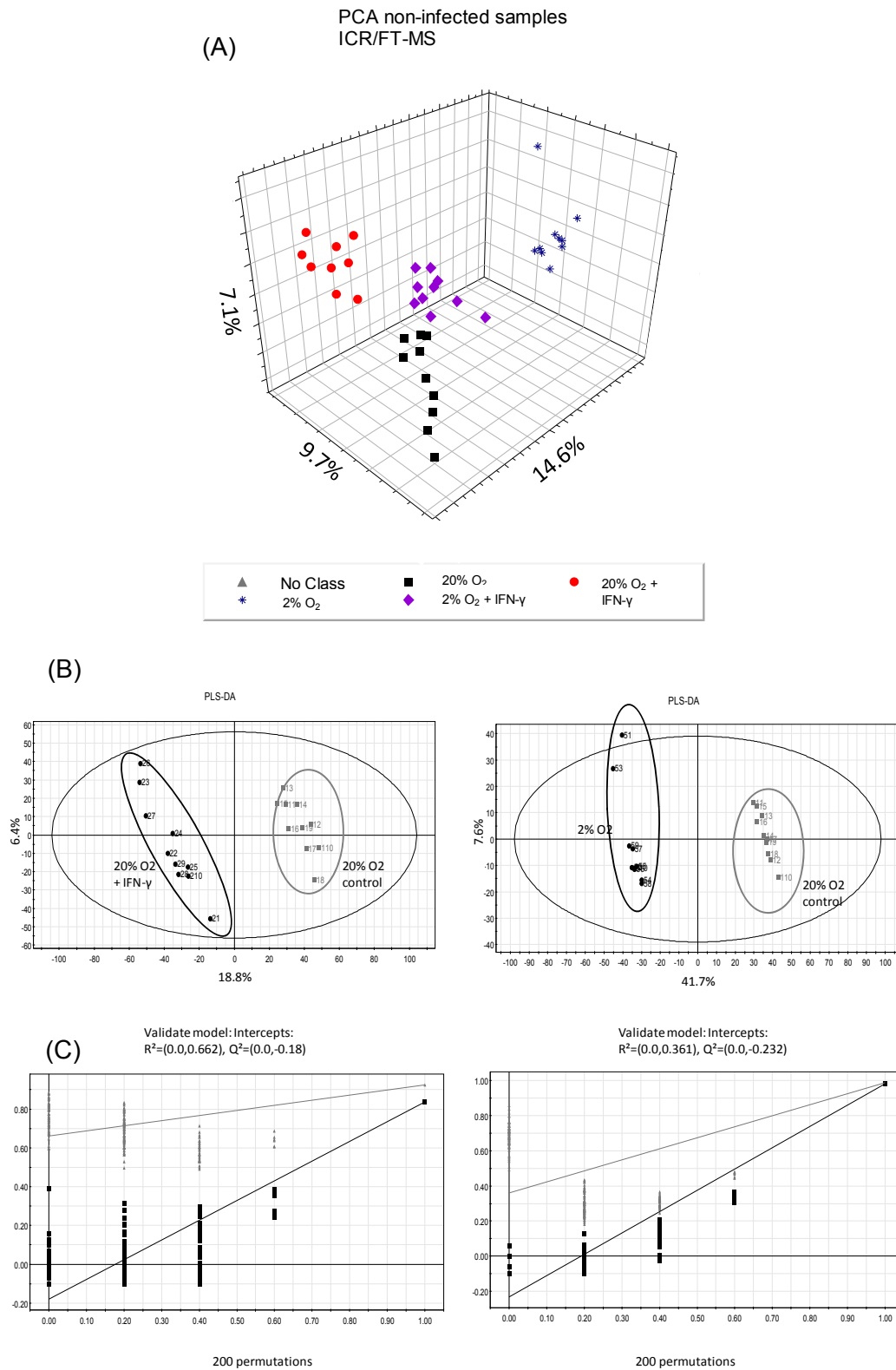
Supplementary figure 5: Cross-validation of PLS-DA models using 200 permutations

Supplementary table 4: Annotated metabolites with a fold change  $\geq 100\%$  in infected and non-infected samples

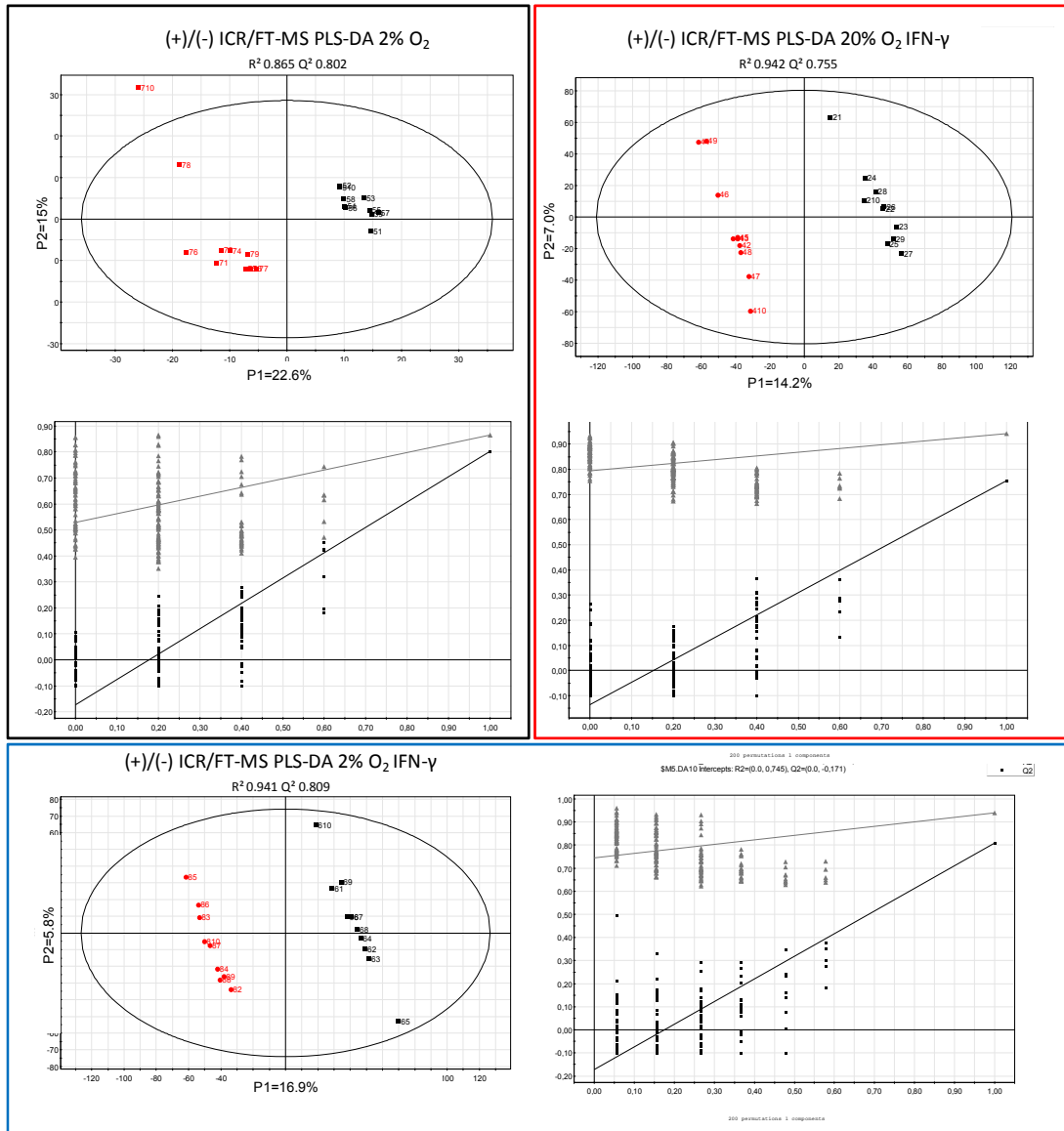
exact mass	elemental composition	detected with	log ratio(Inf/non inf)
344.329045268	C21H44O3	FT+HILIC+RP	-0.73318517
189.08234972	C8H15NO2S	RP	-0.70870482
298.105252916	C14H18O7	RP	-0.49962934
320.089602852	C16H16O7	RP	-0.49962934
253.081103832	C9H11N5O4	RP	-0.49427824
275.064116376	C10H13NO8	RP	-0.49427824
295.128054024	C12H17N5O4	RP	-0.39350959
612.151962464	C20H32N6O12S2	RP	-0.36631437
244.034804006	C6H13O8P	FT	-0.35490614
161.068807832	C6H11NO4	HILIC+RP	-0.35231862
422.448766476	C29H58O	FT	-0.33296243
135.053157768	C4H9NO4	HILIC+RP	-0.33187382
135.05449516	C5H5N5	HILIC+RP	-0.33187382
321.072586482	C10H16N3O7P	RP	-0.31383484
260.029718626	C6H13O9P	RP	-0.30490679
129.151749608	C8H19N	HILIC+RP	-0.23706612
181.073893212	C9H11NO3	FT+RP	-0.20466029
119.058243148	C4H9NO3	HILIC+RP	-0.20418869
427.02941494	C10H15N5O10P2	FT+RP	-0.17055421
267.095416504	C9H17NO8	FT+RP	-0.15632951
404.0021971	C9H14N2O12P2	FT+RP	-0.08136694
370.235514	C20H34O6	HILIC	0.17966814
172.109931	C9H16O3	HILIC	0.24462728
214.15688	C12H22O3	HILIC+RP	0.31701779
183.100776656	C8H13N3O2	RP	0.32102653
324.10564684	C12H20O10	HILIC+RP	0.32642185
182.094281	C10H14O3	RP	0.34584504
258.183109312	C14H26O4	RP	0.36230368
112.016043988	C5H4O3	HILIC+RP	0.36521133
222.093917448	C10H14N4S	HILIC	0.40899632
379.104935632	C13H21N3O8S	HILIC	0.43161409
379.248759946	C18H38NO5P	HILIC	0.44875904
120.057514876	C8H8O	RP	0.53140035
121.089149352	C8H11N	HILIC	0.54795267
218.167065324	C15H22O	HILIC+RP	0.5482632
180.15141526	C12H20O	RP	0.56092423
342.116211524	C12H22O11	RP	0.84202877
334.214392	C20H30O4	HILIC+RP	0.88770435
312.230042	C18H32O4	RP	0.88770435
138.104465068	C9H14O	RP	0.92514597
153.078978592	C8H11NO2	HILIC	INF

---

281.11240396	C11H15N5O4	HILIC	INF
143.058243148	C6H9NO3	HILIC	INF
105.032697096	C5H3N3	HILIC	INF
175.059305768	C5H9N3O4	HILIC	INF
174.115698448	C11H14N2	HILIC+RP	INF
175.063328528	C10H9NO2	HILIC+RP	INF
254.224571	C16H30O2	RP	INF
172.14632	C10H20O2	RP	INF
284.271521	C18H36O2	RP	INF
256.240221	C16H32O2	RP	INF
278.224571	C18H30O2	RP	INF
306.255873	C20H34O2	RP	INF
182.0579088	C9H10O4	RP	INF
329.235479232	C21H31NO2	RP	INF
310.120509056	C19H18O4	RP	INF
340.203844756	C22H28O3	RP	INF
398.354866092	C28H46O	FT	NON INF
130.06299418	C6H10O3	FT	NON INF
328.203844756	C21H28O3	FT	NON INF
450.480066604	C31H62O	FT	NON INF
156.053492116	C6H8N2O3	FT+HILIC	NON INF
401.038917004	C10H17N3O10P2	FT+HILIC	NON INF
304.090665472	C11H16N2O8	FT+RP	NON INF
131.094628656	C6H13NO2	FT+RP	NON INF
316.29774514	C19H40O3	FT+RP	NON INF
122.0579088	C4H10O4	FT+RP	NON INF
237.08485182	C8H15NO7	FT+RP	NON INF
153.055479874	C4H12NO3P	HILIC	NON INF
328.224952	C18H32O5	HILIC	NON INF
120.042258736	C4H8O4	HILIC	NON INF
131.069476528	C4H9N3O2	HILIC	NON INF
350.209302	C20H30O5	HILIC	NON INF
131.073499288	C9H9N	HILIC	NON INF
212.1412445	C12H20O3	HILIC+RP	NON INF
129.042593084	C5H7NO3	HILIC+RP	NON INF
166.06299418	C9H10O3	RP	NON INF
301.298079488	C18H39NO2	RP	NON INF
326.188194692	C21H26O3	RP	NON INF
300.245315644	C21H32O	RP	NON INF
273.26677936	C16H35NO2	RP	NON INF
207.110672644	C8H17NO5	RP	NON INF

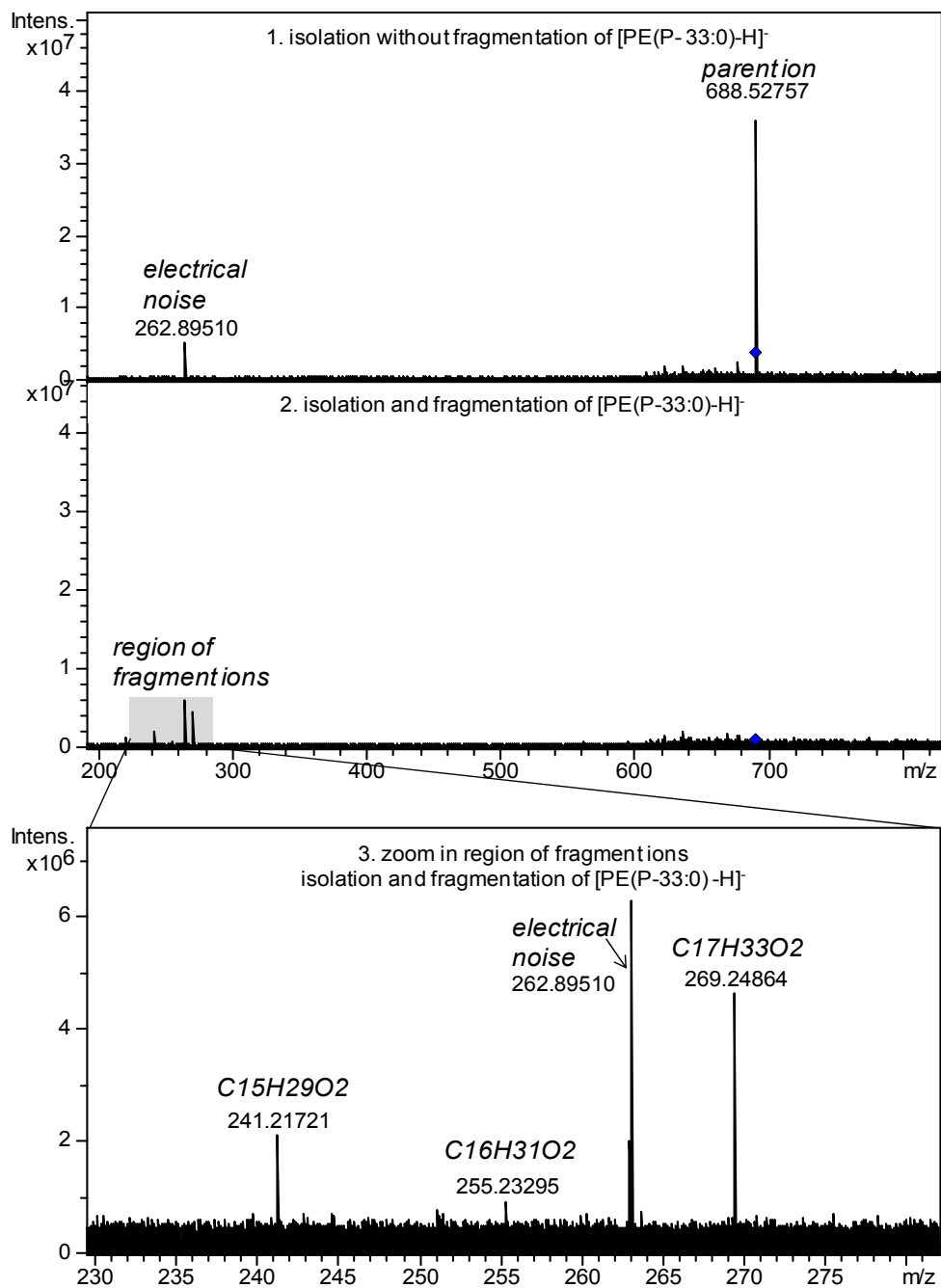


Supplementary figure 6: (A) PCA and (B) PLS-DA models of non-infected cells with (C) permutation test



Supplementary figure 7: PLS-DA models for the separation of infected (red) and non-infected (black) samples under different cultivation conditions (grey frame - 2% O<sub>2</sub>, red frame 20% O<sub>2</sub>, blue frame 2% O<sub>2</sub> + IFN-γ)





Supplementary figure 8: (-)ICR-FT/MS<sup>2</sup> fragmentation PE(P-33:0): 1. isolation of the parent ion [M-H]<sup>-</sup>, 2. isolation and fragmentation, the region of product ion is colored grey; 3. zoom in the region of product ions, three fatty acid product ions have been detected

## 7 Bibliography

- Abromaitis, S., Hefty, P.S. and Stephens, R.S. (2009). Chlamydia pneumoniae encodes a functional aromatic amino acid hydroxylase. *FEMS Immunol Med Microbiol* 55, 196-205.
- Albi, E. and Viola Magni, M.P. (2004). The role of intranuclear lipids. *Biol Cell* 96, 657-667.
- Allan, I., Hatch, T.P. and Pearce, J.H. (1985). Influence of cysteine deprivation on chlamydial differentiation from reproductive to infective life-cycle forms. *J Gen Microbiol* 131, 3171-3177.
- Allan, I. and Pearce, J.H. (1983). Differential amino acid utilization by Chlamydia psittaci (strain guinea pig inclusion conjunctivitis) and its regulatory effect on chlamydial growth. *J Gen Microbiol* 129, 1991-2000.
- Amann, R., Springer, N., Schonhuber, W., Ludwig, W., Schmid, E.N., Muller, K.D. and Michel, R. (1997). Obligate intracellular bacterial parasites of acanthamoebae related to Chlamydia spp. *Appl Environ Microbiol* 63, 115-121.
- Arias-Barrau, E., Olivera, E.R., Luengo, J.M., Fernandez, C., Galan, B., Garcia, J.L., *et al.* (2004). The homogentisate pathway: a central catabolic pathway involved in the degradation of L-phenylalanine, L-tyrosine, and 3-hydroxyphenylacetate in Pseudomonas putida. *J Bacteriol* 186, 5062-5077.
- Arias, S., Olivera, E.R., Arcos, M., Naharro, G. and Luengo, J.M. (2008). Genetic analyses and molecular characterization of the pathways involved in the conversion of 2-phenylethylamine and 2-phenylethanol into phenylacetic acid in Pseudomonas putida U. *Environ Microbiol* 10, 413-432.
- Azenabor, A.A., Job, G. and Adedokun, O.O. (2005). Chlamydia pneumoniae infected macrophages exhibit enhanced plasma membrane fluidity and show increased adherence to endothelial cells. *Mol Cell Biochem* 269, 69-84.
- Barie, P.S. (2012). Multidrug-resistant organisms and antibiotic management. *Surg Clin North Am* 92, 345-391, ix-x.
- Barrow, M.P., Burkitt, W.I. and Derrick, P.J. (2005). Principles of Fourier transform ion cyclotron resonance mass spectrometry and its application in structural biology. *Analyst* 130, 18-28.
- Bayer, E., Gfrörer, P. and Rentel, C. (1999). Coordination-Ionspray-MS (CIS-MS), a Universal Detection and Characterization Method for Direct Coupling with Separation Techniques. *Angewandte Chemie International Edition* 38, 992-995.
- Beatty, W.L. (2008). Late endocytic multivesicular bodies intersect the chlamydial inclusion in the absence of CD63. *Infect Immun* 76, 2872-2881.
- Beatty, W.L., Belanger, T.A., Desai, A.A., Morrison, R.P. and Byrne, G.I. (1994a). Tryptophan depletion as a mechanism of gamma interferon-mediated chlamydial persistence. *Infect Immun* 62, 3705-3711.
- Beatty, W.L., Byrne, G.I. and Morrison, R.P. (1993). Morphologic and antigenic characterization of interferon gamma-mediated persistent Chlamydia trachomatis infection in vitro. *Proc Natl Acad Sci U S A* 90, 3998-4002.
- Beatty, W.L., Morrison, R.P. and Byrne, G.I. (1994b). Persistent chlamydiae: from cell culture to a paradigm for chlamydial pathogenesis. *Microbiol Rev* 58, 686-699.

- Becker, Y. (1978). The chlamydia: molecular biology of procaryotic obligate parasites of eucaryocytes. *Microbiol Rev* 42, 274-306.
- Bhalla, R., Narasimhan, K. and Swarup, S. (2005). Metabolomics and its role in understanding cellular responses in plants. *Plant Cell Rep* 24, 562-571.
- Bidawid, S., Chou, S., Ng, C.W., Perry, E. and Kasatiya, S. (1989). Fatty acid profiles of Chlamydia using capillary gas chromatography. *Antonie Van Leeuwenhoek* 55, 123-131.
- Bishop, W.R. and Bell, R.M. (1988). Functions of diacylglycerol in glycerolipid metabolism, signal transduction and cellular transformation. *Oncogene Res* 2, 205-218.
- Blasi, F., Tarsia, P., Arosio, C., Fagetti, L. and Allegra, L. (1998). Epidemiology of Chlamydia pneumoniae. *Clin Microbiol Infect* 4 Suppl 4, S1-S6.
- Boccard, J., Veuthey, J.L. and Rudaz, S. (2010). Knowledge discovery in metabolomics: an overview of MS data handling. *J Sep Sci* 33, 290-304.
- Bosco, M.C., Puppo, M., Blengio, F., Fraone, T., Cappello, P., Giovarelli, M. and Varesio, L. (2008). Monocytes and dendritic cells in a hypoxic environment: Spotlights on chemotaxis and migration. *Immunobiology* 213, 733-749.
- Branden, E., Koyi, H., Gnarpe, J., Gnarpe, H.k. and Tornling, G.r. (2005). Chronic Chlamydia pneumoniae infection is a risk factor for the development of COPD. *Respiratory Medicine* 99, 20-26.
- Breitling, R., Vitkup, D. and Barrett, M.P. (2008). New surveyor tools for charting microbial metabolic maps. *Nat Rev Microbiol* 6, 156-161.
- Brereton, R.G. (2009). Chemometrics for Pattern Recognition. *Book*.
- Brites, P., Waterham, H.R. and Wanders, R.J. (2004). Functions and biosynthesis of plasmalogens in health and disease. *Biochim Biophys Acta* 1636, 219-231.
- Bruick, R.K. and McKnight, S.L. (2001). A conserved family of prolyl-4-hydroxylases that modify HIF. *Science* 294, 1337-1340.
- Buszewski, B. and Noga, S. (2011). Hydrophilic interaction liquid chromatography (HILIC)--a powerful separation technique. *Anal Bioanal Chem* 402, 231-247.
- Butte, A. (2002). The use and analysis of microarray data. *Nat Rev Drug Discov* 1, 951-960.
- Byrne, G.I. and Ojcius, D.M. (2004). Chlamydia and apoptosis: life and death decisions of an intracellular pathogen. *Nat Rev Microbiol* 2, 802-808.
- Callender, H.L., Forrester, J.S., Ivanova, P., Preininger, A., Milne, S. and Brown, H.A. (2007). Quantification of diacylglycerol species from cellular extracts by electrospray ionization mass spectrometry using a linear regression algorithm. *Anal Chem* 79, 263-272.
- Carabeo, R.A., Mead, D.J. and Hackstadt, T. (2003). Golgi-dependent transport of cholesterol to the Chlamydia trachomatis inclusion. *Proc Natl Acad Sci U S A* 100, 6771-6776.
- Carbonell, T. and Rama, R. (2009). Respiratory Hypoxia and Oxidative Stress in the Brain. Is the Endogenous Erythropoietin an Antioxidant?. *Current Chemical Biology* 3, 238-252(215).

- Carrasco, S. and Merida, I. (2007). Diacylglycerol, when simplicity becomes complex. *Trends Biochem Sci* 32, 27-36.
- Carreau, A., El Hafny-Rahbi, B., Matejuk, A., Grillon, C. and Kieda, C. (2011). Why is the partial oxygen pressure of human tissues a crucial parameter? Small molecules and hypoxia. *J Cell Mol Med* 15, 1239-1253.
- Castle, A.L., Fiehn, O., Kaddurah-Daouk, R. and Lindon, J.C. (2006). Metabolomics Standards Workshop and the development of international standards for reporting metabolomics experimental results. *Brief Bioinform* 7, 159-165.
- Chernushevich, I.V., Loboda, A.V. and Thomson, B.A. (2001). An introduction to quadrupole-time-of-flight mass spectrometry. *J Mass Spectrom* 36, 849-865.
- Cocchiari, J.L. and Valdivia, R.H. (2009). New insights into Chlamydia intracellular survival mechanisms. *Cell Microbiol* 11, 1571-1578.
- Coles, A.M., Reynolds, D.J., Harper, A., Devitt, A. and Pearce, J.H. (1993). Low-nutrient induction of abnormal chlamydial development: a novel component of chlamydial pathogenesis? *FEMS Microbiol Lett* 106, 193-200.
- Conrad, M. and Sato, H. (2011). The oxidative stress-inducible cystine/glutamate antiporter, system x (c) (-) : cystine supplier and beyond. *Amino Acids* 42, 231-246.
- Coustou, V., Biran, M., Breton, M., Guegan, F., Riviere, L., Plazolles, N., *et al.* (2008). Glucose-induced remodeling of intermediary and energy metabolism in procyclic Trypanosoma brucei. *J Biol Chem* 283, 16342-16354.
- Daltonics, B. (2008). maXis - User Manual.
- Darville, T. (2006) Innate Immunity. In *Chlamydia: Genomics and Pathogenesis*, P. Bavoil, P. Wyrick (eds.). Wyomondham, horizon bioscience, pp. 339-364.
- Dehne, N. and Brune, B. (2009). HIF-1 in the inflammatory microenvironment. *Exp Cell Res* 315, 1791-1797.
- Dekker, L.V. and Parker, P.J. (1994). Protein kinase C--a question of specificity. *Trends Biochem Sci* 19, 73-77.
- Dettmer, K., Aronov, P.A. and Hammock, B.D. (2007). Mass spectrometry-based metabolomics. *Mass Spectrom Rev* 26, 51-78.
- Dietz, I., Jerchel, S., Szaszak, M., Shima, K. and Rupp, J. (2011). When oxygen runs short: the microenvironment drives host-pathogen interactions. *Microbes Infect* 14, 311-316.
- Dixon, R.A. and Strack, D. (2003). Phytochemistry meets genome analysis, and beyond. *Phytochemistry* 62, 815-816.
- Dunn, W.B., Broadhurst, D., Begley, P., Zelena, E., Francis-McIntyre, S., Anderson, N., *et al.* Procedures for large-scale metabolic profiling of serum and plasma using gas chromatography and liquid chromatography coupled to mass spectrometry. *Nat Protoc* 6, 1060-1083.
- Eisenreich, W., Dandekar, T., Heesemann, J. and Goebel, W. Carbon metabolism of intracellular bacterial pathogens and possible links to virulence. *Nat Rev Microbiol* 8, 401-412.
- Eltzschig, H.K. (2011). Targeting Hypoxia-induced Inflammation. *Anesthesiology* 114, 239-242.

- Eriksson, L.J., E.;Kettaneh-Wold,N.;Trygg,J.;Wikström,C.;Wold,S. (2006). Multi- and Megavariate Data Analysis - Principles and Applications. *Book, 2nd Edition*.
- Erion, D.M. and Shulman, G.I. Diacylglycerol-mediated insulin resistance. *Nat Med* 16, 400-402.
- Everett, K.D., Bush, R.M. and Andersen, A.A. (1999). Emended description of the order Chlamydiales, proposal of Parachlamydiaceae fam. nov. and Simkaniaceae fam. nov., each containing one monotypic genus, revised taxonomy of the family Chlamydiaceae, including a new genus and five new species, and standards for the identification of organisms. *Int J Syst Bacteriol* 49 Pt 2, 415-440.
- Fagone, P. and Jackowski, S. (2009). Membrane phospholipid synthesis and endoplasmic reticulum function. *J Lipid Res* 50 Suppl, S311-316.
- Fahy, E., Subramaniam, S., Brown, H.A., Glass, C.K., Merrill, A.H., Jr., Murphy, R.C., *et al.* (2005). A comprehensive classification system for lipids. *J Lipid Res* 46, 839-861.
- Farooqu, A.A. and Horrocks, L.A. (2001). Plasmalogens, phospholipase A2, and docosahexaenoic acid turnover in brain tissue. *J Mol Neurosci* 16, 263-272; discussion 279-284.
- Farooqui, A.A. and Horrocks, L.A. (2001). Plasmalogens: workhorse lipids of membranes in normal and injured neurons and glia. *Neuroscientist* 7, 232-245.
- Fazio, G., Giovino, M., Gullotti, A., Bacarella, D., Novo, G. and Novo, S. (2009). Atherosclerosis, inflammation and Chlamydia pneumoniae. *World J Cardiol* 1, 31-40.
- Fernie, A.R., Aharoni, A., Willmitzer, L., Stitt, M., Tohge, T., Kopka, J., *et al.* Recommendations for reporting metabolite data. *Plant Cell* 23, 2477-2482.
- Fiehn, O. (2002). Metabolomics--the link between genotypes and phenotypes. *Plant Mol Biol* 48, 155-171.
- Fiehn, O., Kristal, B., van Ommen, B., Sumner, L.W., Sansone, S.A., Taylor, C., *et al.* (2006). Establishing reporting standards for metabolomic and metabonomic studies: a call for participation. *OMICS* 10, 158-163.
- Fields, K.A. and Hackstadt, T. (2002). The chlamydial inclusion: escape from the endocytic pathway. *Annu Rev Cell Dev Biol* 18, 221-245.
- Finlay, B.B. and Cossart, P. (1997). Exploitation of mammalian host cell functions by bacterial pathogens. *Science* 276, 718-725.
- Fischer, E. and Sauer, U. (2003). A novel metabolic cycle catalyzes glucose oxidation and anaplerosis in hungry Escherichia coli. *J Biol Chem* 278, 46446-46451.
- Forst, C.V. (2006). Host-pathogen systems biology. *Drug Discov Today* 11, 220-227.
- Frezza, C., Zheng, L., Tennant, D.A., Papkovsky, D.B., Hedley, B.A., Kalna, G., *et al.* (2011). Metabolic profiling of hypoxic cells revealed a catabolic signature required for cell survival. *PLoS ONE* 6, e24411.
- Friant, S., Lombardi, R., Schmelzle, T., Hall, M.N. and Riezman, H. (2001). Sphingoid base signaling via Pkh kinases is required for endocytosis in yeast. *EMBO J* 20, 6783-6792.
- Friant, S., Zanolari, B. and Riezman, H. (2000). Increased protein kinase or decreased PP2A activity bypasses sphingoid base requirement in endocytosis. *EMBO J* 19, 2834-2844.

- Fujita, Y. (2009). Carbon catabolite control of the metabolic network in *Bacillus subtilis*. *Biosci Biotechnol Biochem* 73, 245-259.
- Gaugler, R.W., Neptune, E.M., Adams, G.M., Sallee, T.L., Weiss, E. and Wilson, N.N. (1969). Lipid synthesis by isolated *Chlamydia psittaci*. *J Bacteriol* 100, 823-826.
- Gerard, H.C., Freise, J., Wang, Z., Roberts, G., Rudy, D., Krauss-Opatz, B., *et al.* (2002). *Chlamydia trachomatis* genes whose products are related to energy metabolism are expressed differentially in active vs. persistent infection. *Microbes Infect* 4, 13-22.
- Gieffers, J., van Zandbergen, G., Rupp, J., Sayk, F., Kruger, S., Ehlers, S., *et al.* (2004). Phagocytes transmit *Chlamydia pneumoniae* from the lungs to the vasculature. *Eur Respir J* 23, 506-510.
- Glaser, P.E. and Gross, R.W. (1994). Plasmenylethanolamine facilitates rapid membrane fusion: a stopped-flow kinetic investigation correlating the propensity of a major plasma membrane constituent to adopt an HII phase with its ability to promote membrane fusion. *Biochemistry* 33, 5805-5812.
- Gleason, J.E., Corrigan, D.J., Cox, J.E., Reddi, A.R., McGinnis, L.A. and Culotta, V.C. (2011). Analysis of hypoxia and hypoxia-like states through metabolite profiling. *PLoS ONE* 6, e24741.
- Glunde, K., Shah, T., Winnard, P.T., Jr., Raman, V., Takagi, T., Vesuna, F., *et al.* (2008). Hypoxia regulates choline kinase expression through hypoxia-inducible factor-1 alpha signaling in a human prostate cancer model. *Cancer Res* 68, 172-180.
- Goldfine, H. (2010). The appearance, disappearance and reappearance of plasmalogens in evolution. *Prog Lipid Res* 49, 493-498.
- Goodacre, R. (2007). Metabolomics of a superorganism. *J Nutr* 137, 259S-266S.
- Goto, K., Hozumi, Y., Nakano, T., Saino-Saito, S. and Martelli, A.M. (2008). Lipid messenger, diacylglycerol, and its regulator, diacylglycerol kinase, in cells, organs, and animals: history and perspective. *Tohoku J Exp Med* 214, 199-212.
- Griffiths, J.R. and Stubbs, M. (2003). Opportunities for studying cancer by metabolomics: preliminary observations on tumors deficient in hypoxia-inducible factor 1. *Adv Enzyme Regul* 43, 67-76.
- Gross, J.H. (2011). *Mass Spectrometry - A textbook*. 2nd Edition.
- Gross, R.W. and Han, X. (2009). Shotgun lipidomics of neutral lipids as an enabling technology for elucidation of lipid-related diseases. *Am J Physiol Endocrinol Metab* 297, E297-303.
- Gross, R.W. and Han, X. (2011). Lipidomics at the interface of structure and function in systems biology. *Chem Biol* 18, 284-291.
- Gruning, N.M., Lehrach, H. and Ralser, M. (2010). Regulatory crosstalk of the metabolic network. *Trends Biochem Sci* 35, 220-227.
- Guan, S. and Marshall, A.G. (1995). Ion traps for Fourier transform ion cyclotron resonance mass spectrometry: principles and design of geometric and electric configurations. *International Journal of Mass Spectrometry and Ion Processes* 146/147, 261-296.
- Guillarme, D., Nguyen, D.T., Rudaz, S. and Veuthey, J.L. (2008). Method transfer for fast liquid chromatography in pharmaceutical analysis: application to short columns packed with small particle. Part II: gradient experiments. *Eur J Pharm Biopharm* 68, 430-440.

- Guillarme, D., Ruta, J., Rudaz, S. and Veuthey, J.L. (2009). New trends in fast and high-resolution liquid chromatography: a critical comparison of existing approaches. *Anal Bioanal Chem* 397, 1069-1082.
- Hackstadt, T. (1999) Cell biology. In *Chlamydia: Intracellular Biology, Pathogenesis, and Immunity*, R. Stephens (ed.). Washington, D.C., ASM Press, pp. 101-138.
- Hackstadt, T., Rockey, D.D., Heinzen, R.A. and Scidmore, M.A. (1996). Chlamydia trachomatis interrupts an exocytic pathway to acquire endogenously synthesized sphingomyelin in transit from the Golgi apparatus to the plasma membrane. *EMBO J* 15, 964-977.
- Hahn, D.L., Schure, A., Patel, K., Childs, T., Drizik, E. and Webley, W. (2012). Chlamydia pneumoniae-Specific IgE Is Prevalent in Asthma and Is Associated with Disease Severity. *PLoS ONE* 7, e35945.
- Hannun, Y.A., Luberto, C. and Argraves, K.M. (2001). Enzymes of sphingolipid metabolism: from modular to integrative signaling. *Biochemistry* 40, 4893-4903.
- Harper, A., Pogson, C.I., Jones, M.L. and Pearce, J.H. (2000). Chlamydial development is adversely affected by minor changes in amino acid supply, blood plasma amino acid levels, and glucose deprivation. *Infect Immun* 68, 1457-1464.
- Hatch, G.M. and McClarty, G. (1998). Phospholipid composition of purified Chlamydia trachomatis mimics that of the eucaryotic host cell. *Infect Immun* 66, 3727-3735.
- Hatch, T.P., Al-Hossainy, E. and Silverman, J.A. (1982). Adenine nucleotide and lysine transport in Chlamydia psittaci. *J Bacteriol* 150, 662-670.
- Heeren, R.M., Kleinnijenhuis, A.J., McDonnell, L.A. and Mize, T.H. (2004). A mini-review of mass spectrometry using high-performance FTICR-MS methods. *Anal Bioanal Chem* 378, 1048-1058.
- Hendrickson, C.L. and Emmett, M.R. (1999). Electrospray ionization Fourier transform ion cyclotron resonance mass spectrometry. *Annu Rev Phys Chem* 50, 517-536.
- Hertkorn, N., Frommberger, M., Witt, M., Koch, B.P., Schmitt-Kopplin, P. and Perdue, E.M. (2008). Natural organic matter and the event horizon of mass spectrometry. *Anal Chem* 80, 8908-8919.
- Heuer, D., Rejman Lipinski, A., Machuy, N., Karlas, A., Wehrens, A., Siedler, F., *et al.* (2009). Chlamydia causes fragmentation of the Golgi compartment to ensure reproduction. *Nature* 457, 731-735.
- HMDB (2012a) Metabocard N-Acetyl-L-aspartic acid (HMDB00812). hmp.
- HMDB (2012b) Metabocard S-Lactoylglycyl-L-cysteine (HMDB01066). hmp.
- HMDB (2012c) Metabocard Sphinganine (HMDB00269). hmp.
- Hodinka, R.L., Davis, C.H., Choong, J. and Wyrick, P.B. (1988). Ultrastructural study of endocytosis of Chlamydia trachomatis by McCoy cells. *Infect Immun* 56, 1456-1463.
- Hsu, F.F. and Turk, J. (2009). Electrospray ionization with low-energy collisionally activated dissociation tandem mass spectrometry of glycerophospholipids: mechanisms of fragmentation and structural characterization. *J Chromatogr B Analyt Technol Biomed Life Sci* 877, 2673-2695.

- Hu, C., van der Heijden, R., Wang, M., van der Greef, J., Hankemeier, T. and Xu, G. (2009). Analytical strategies in lipidomics and applications in disease biomarker discovery. *J Chromatogr B Analyt Technol Biomed Life Sci*.
- Hueck, C.J. (1998). Type III protein secretion systems in bacterial pathogens of animals and plants. *Microbiol Mol Biol Rev* 62, 379-433.
- Hughey, C.A., Hendrickson, C.L., Rodgers, R.P., Marshall, A.G. and Qian, K. (2001). Kendrick mass defect spectrum: a compact visual analysis for ultrahigh-resolution broadband mass spectra. *Anal Chem* 73, 4676-4681.
- Hybiske, K. and Stephens, R.S. (2007). Mechanisms of host cell exit by the intracellular bacterium Chlamydia. *Proc Natl Acad Sci U S A* 104, 11430-11435.
- Hyvarinen, K., Tuomainen, A.M., Laitinen, S., Bykov, I.L., Tormakangas, L., Lindros, K., *et al.* (2009). Chlamydial and periodontal pathogens induce hepatic inflammation and fatty acid imbalance in apolipoprotein E-deficient mice. *Infect Immun* 77, 3442-3449.
- Ihmels, J., Levy, R. and Barkai, N. (2004). Principles of transcriptional control in the metabolic network of *Saccharomyces cerevisiae*. *Nat Biotechnol* 22, 86-92.
- Illife-Lee, E.R. and McClarty, G. (1999). Glucose metabolism in *Chlamydia trachomatis*: the 'energy parasite' hypothesis revisited. *Mol Microbiol* 33, 177-187.
- Illife-Lee, E.R. and McClarty, G. (2000). Regulation of carbon metabolism in *Chlamydia trachomatis*. *Mol Microbiol* 38, 20-30.
- Ivanova, P.T., Milne, S.B. and Brown, H.A. (2010). Identification of atypical ether-linked glycerophospholipid species in macrophages by mass spectrometry. *J Lipid Res* 51, 1581-1590.
- Juul, N., Jensen, H., Hvid, M., Christiansen, G. and Birkelund, S. (2007). Characterization of in vitro chlamydial cultures in low-oxygen atmospheres. *J Bacteriol* 189, 6723-6726.
- Kafsack, B.F. and Llinas, M. Eating at the table of another: metabolomics of host-parasite interactions. *Cell Host Microbe* 7, 90-99.
- Kalman, S., Mitchell, W., Marathe, R., Lammel, C., Fan, J., Hyman, R.W., *et al.* (1999). Comparative genomes of *Chlamydia pneumoniae* and *C. trachomatis*. *Nat Genet* 21, 385-389.
- Kebarle, P. and Verkerk, U.H. (2009). Electrospray: from ions in solution to ions in the gas phase, what we know now. *Mass Spectrom Rev* 28, 898-917.
- Kell, D.B. (2006). Theodor Bucher Lecture. Metabolomics, modelling and machine learning in systems biology - towards an understanding of the languages of cells. Delivered on 3 July 2005 at the 30th FEBS Congress and the 9th IUBMB conference in Budapest. *FEBS J* 273, 873-894.
- Kerwin, J.L., Tuininga, A.R. and Ericsson, L.H. (1994). Identification of molecular species of glycerophospholipids and sphingomyelin using electrospray mass spectrometry. *J Lipid Res* 35, 1102-1114.
- Kim, J.K., Fillmore, J.J., Chen, Y., Yu, C., Moore, I.K., Pypaert, M., *et al.* (2001). Tissue-specific overexpression of lipoprotein lipase causes tissue-specific insulin resistance. *Proc Natl Acad Sci U S A* 98, 7522-7527.
- Kim, S., Kramer, R.W. and Hatcher, P.G. (2003). Graphical method for analysis of ultrahigh-resolution broadband mass spectra of natural organic matter, the van Krevelen diagram. *Anal Chem* 75, 5336-5344.



- Kostiainen, R. and Kauppila, T.J. (2009). Effect of eluent on the ionization process in liquid chromatography-mass spectrometry. *J Chromatogr A* 1216, 685-699.
- Kroemer, G., Marino, G. and Levine, B. (2010). Autophagy and the integrated stress response. *Mol Cell* 40, 280-293.
- Kumar, Y., Cocchiaro, J. and Valdivia, R.H. (2006). The obligate intracellular pathogen *Chlamydia trachomatis* targets host lipid droplets. *Curr Biol* 16, 1646-1651.
- Kuo, C.C., Jackson, L.A., Campbell, L.A. and Grayston, J.T. (1995). *Chlamydia pneumoniae* (TWAR). *Clin Microbiol Rev* 8, 451-461.
- La, M.V., Raoult, D. and Renesto, P. (2008). Regulation of whole bacterial pathogen transcription within infected hosts. *FEMS Microbiol Rev* 32, 440-460.
- Lazarev, V.N., Borisenko, G.G., Shkarupeta, M.M., Demina, I.A., Serebryakova, M.V., Galyamina, M.A., *et al.* (2010). The role of intracellular glutathione in the progression of *Chlamydia trachomatis* infection. *Free Radic Biol Med* 49, 1947-1955.
- Le, A., Lane, A.N., Hamaker, M., Bose, S., Gouw, A., Barbi, J., *et al.* (2012). Glucose-independent glutamine metabolism via TCA cycling for proliferation and survival in B cells. *Cell Metab* 15, 110-121.
- Li, J.V., Wang, Y., Saric, J., Nicholson, J.K., Dirnhofer, S., Singer, B.H., *et al.* (2008). Global metabolic responses of NMRI mice to an experimental *Plasmodium berghei* infection. *J Proteome Res* 7, 3948-3956.
- Li, Y.L., Su, X., Stahl, P.D. and Gross, M.L. (2007). Quantification of diacylglycerol molecular species in biological samples by electrospray ionization mass spectrometry after one-step derivatization. *Anal Chem* 79, 1569-1574.
- Lim, W.S., Macfarlane, J.T., Boswell, T.C., Harrison, T.G., Rose, D., Leinonen, M. and Saikku, P. (2001). Study of community acquired pneumonia aetiology (SCAPA) in adults admitted to hospital: implications for management guidelines. *Thorax* 56, 296-301.
- Liu, W., He, P., Cheng, B., Mei, C.L., Wang, Y.F. and Wan, J.J. (2010). *Chlamydia pneumoniae* disturbs cholesterol homeostasis in human THP-1 macrophages via JNK-PPAR $\gamma$  dependent signal transduction pathways. *Microbes Infect* 12, 1226-1235.
- Loh, K.D., Gyaneshwar, P., Markenscoff Papadimitriou, E., Fong, R., Kim, K.S., Parales, R., *et al.* (2006). A previously undescribed pathway for pyrimidine catabolism. *Proc Natl Acad Sci U S A* 103, 5114-5119.
- Lu, H., Shen, C. and Brunham, R.C. (2000). *Chlamydia trachomatis* infection of epithelial cells induces the activation of caspase-1 and release of mature IL-18. *J Immunol* 165, 1463-1469.
- Lu, X., Zhao, X., Bai, C., Zhao, C., Lu, G. and Xu, G. (2008). LC-MS-based metabolomics analysis. *J Chromatogr B Analyt Technol Biomed Life Sci* 866, 64-76.
- Lucio, M. (2008). Datamining metabolomics: the convergence point of non-target approach and statistical investigation. *Dissertation Technische Universität München*.
- Marshall, A.G. (2000). Milestones in fourier transform ion cyclotron resonance mass spectrometry technique development. *International Journal of Mass Spectrometry* 200, 331-356.

- Marshall, A.G., Hendrickson, C.L. and Jackson, G.S. (1998). Fourier transform ion cyclotron resonance mass spectrometry: a primer. *Mass Spectrom Rev* 17, 1-35.
- Martin, F.P., Verdu, E.F., Wang, Y., Dumas, M.E., Yap, I.K., Cloarec, O., *et al.* (2006). Transgenomic metabolic interactions in a mouse disease model: interactions of *Trichinella spiralis* infection with dietary *Lactobacillus paracasei* supplementation. *J Proteome Res* 5, 2185-2193.
- Mashego, M.R., Rumbold, K., De Mey, M., Vandamme, E., Soetaert, W. and Heijnen, J.J. (2007). Microbial metabolomics: past, present and future methodologies. *Biotechnol Lett* 29, 1-16.
- McClarty, G. (1999) Chlamydial metabolism as inferred from the complete genome sequence. In *Intracellular Biology, Pathogenesis, and Immunity*, R. Stephens (ed.). Washington, D.C., ASM press, pp. 69-100.
- McCoy, A.J., Adams, N.E., Hudson, A.O., Gilvarg, C., Leustek, T. and Maurelli, A.T. (2006). L,L-diaminopimelate aminotransferase, a trans-kingdom enzyme shared by Chlamydia and plants for synthesis of diaminopimelate/lysine. *Proc Natl Acad Sci U S A* 103, 17909-17914.
- Moazed, T.C., Kuo, C.C., Grayston, J.T. and Campbell, L.A. (1998). Evidence of systemic dissemination of *Chlamydia pneumoniae* via macrophages in the mouse. *J Infect Dis* 177, 1322-1325.
- Mochly-Rosen, D. (1995). Localization of protein kinases by anchoring proteins: a theme in signal transduction. *Science* 268, 247-251.
- Monack, D.M., Mueller, A. and Falkow, S. (2004). Persistent bacterial infections: the interface of the pathogen and the host immune system. *Nat Rev Microbiol* 2, 747-765.
- Moore, E.R., Fischer, E.R., Mead, D.J. and Hackstadt, T. (2008). The chlamydial inclusion preferentially intercepts basolaterally directed sphingomyelin-containing exocytic vacuoles. *Traffic* 9, 2130-2140.
- Moulder, J.W. (1991). Interaction of chlamydiae and host cells in vitro. *Microbiol Rev* 55, 143-190.
- Murphy, E.J., Anderson, D.K. and Horrocks, L.A. (1993a). Phospholipid and phospholipid fatty acid composition of mixed murine spinal cord neuronal cultures. *J Neurosci Res* 34, 472-477.
- Murphy, E.J., Stephens, R., Jurkowitz-Alexander, M. and Horrocks, L.A. (1993b). Acidic hydrolysis of plasmalogens followed by high-performance liquid chromatography. *Lipids* 28, 565-568.
- Murphy, R.C., James, P.F., McAnoy, A.M., Krank, J., Duchoslav, E. and Barkley, R.M. (2007). Detection of the abundance of diacylglycerol and triacylglycerol molecular species in cells using neutral loss mass spectrometry. *Anal Biochem* 366, 59-70.
- Nagan, N. and Zoeller, R.A. (2001). Plasmalogens: biosynthesis and functions. *Prog Lipid Res* 40, 199-229.
- Navarro-Llorens, J.M., Patrauchan, M.A., Stewart, G.R., Davies, J.E., Eltis, L.D. and Mohn, W.W. (2005). Phenylacetate catabolism in *Rhodococcus* sp. strain RHA1: a central pathway for degradation of aromatic compounds. *J Bacteriol* 187, 4497-4504.
- Newton, A.C. (1995). Protein kinase C: structure, function, and regulation. *J Biol Chem* 270, 28495-28498.

- Nicholson, J.K., Lindon, J.C. and Holmes, E. (1999). 'Metabonomics': understanding the metabolic responses of living systems to pathophysiological stimuli via multivariate statistical analysis of biological NMR spectroscopic data. *Xenobiotica* 29, 1181-1189.
- Nishizuka, Y. and Nakamura, S. (1995). Lipid mediators and protein kinase C for intracellular signalling. *Clin Exp Pharmacol Physiol Suppl* 22, S202-203.
- Ohta, D., Kanaya, S. and Suzuki, H. (2010). Application of Fourier-transform ion cyclotron resonance mass spectrometry to metabolic profiling and metabolite identification. *Curr Opin Biotechnol* 21, 35-44.
- Ojcus, D.M., Degani, H., Mispelter, J. and Dautry-Varsat, A. (1998). Enhancement of ATP levels and glucose metabolism during an infection by Chlamydia. NMR studies of living cells. *J Biol Chem* 273, 7052-7058.
- Oliver, S.G., Winson, M.K., Kell, D.B. and Baganz, F. (1998). Systematic functional analysis of the yeast genome. *Trends Biotechnol* 16, 373-378.
- Olivera, E.R., Minambres, B., Garcia, B., Muniz, C., Moreno, M.A., Ferrandez, A., *et al.* (1998). Molecular characterization of the phenylacetic acid catabolic pathway in *Pseudomonas putida* U: the phenylacetyl-CoA catabolon. *Proc Natl Acad Sci U S A* 95, 6419-6424.
- Olszewski, K.L., Morrissey, J.M., Wilinski, D., Burns, J.M., Vaidya, A.B., Rabinowitz, J.D. and Llinas, M. (2009). Host-parasite interactions revealed by Plasmodium falciparum metabolomics. *Cell Host Microbe* 5, 191-199.
- Ossewaarde, J.M. and Meijer, A. (1999). Molecular evidence for the existence of additional members of the order Chlamydiales. *Microbiology* 145 ( Pt 2), 411-417.
- Ott, M.A. and Vriend, G. (2006). Correcting ligands, metabolites, and pathways. *BMC Bioinformatics* 7, 517.
- Panoutsopoulos, G.I., Kouretas, D., Gounaris, E.G. and Beedham, C. (2004). Enzymatic oxidation of 2-phenylethylamine to phenylacetic acid and 2-phenylethanol with special reference to the metabolism of its intermediate phenylacetaldehyde. *Basic Clin Pharmacol Toxicol* 95, 273-279.
- Pantoja, L.G., Miller, R.D., Ramirez, J.A., Molestina, R.E. and Summersgill, J.T. (2001). Characterization of Chlamydia pneumoniae persistence in HEp-2 cells treated with gamma interferon. *Infect Immun* 69, 7927-7932.
- Patil, K.R. and Nielsen, J. (2005). Uncovering transcriptional regulation of metabolism by using metabolic network topology. *Proc Natl Acad Sci U S A* 102, 2685-2689.
- Pavelka, M.S., Jr. (2007). Another brick in the wall. *Trends Microbiol* 15, 147-149.
- Peeling, R.W. and Brunham, R.C. (1996). Chlamydiae as pathogens: new species and new issues. *Emerg Infect Dis* 2, 307-319.
- Perrin, A., Roudier, E., Duborjal, H., Bachelet, C., Riva-Lavieille, C., Leverve, X. and Massarelli, R. (2002). Pyruvate reverses metabolic effects produced by hypoxia in glioma and hepatoma cell cultures. *Biochimie* 84, 1003-1011.
- Pescador, N., Villar, D., Cifuentes, D., Garcia-Rocha, M., Ortiz-Barahona, A., Vazquez, S., *et al.* (2010). Hypoxia promotes glycogen accumulation through hypoxia inducible factor (HIF)-mediated induction of glycogen synthase 1. *PLoS ONE* 5, e9644.

- Peyssonnaud, C., Datta, V., Cramer, T., Doedens, A., Theodorakis, E.A., Gallo, R.L., *et al.* (2005). HIF-1alpha expression regulates the bactericidal capacity of phagocytes. *J Clin Invest* 115, 1806-1815.
- Pluskal, T., Castillo, S., Villar-Briones, A. and Oresic, M. (2010). MZmine 2: modular framework for processing, visualizing, and analyzing mass spectrometry-based molecular profile data. *BMC Bioinformatics* 11, 395.
- Preinerstorfer, B., Schiesel, S., Lammerhofer, M. and Lindner, W. (2009). Metabolic profiling of intracellular metabolites in fermentation broths from beta-lactam antibiotics production by liquid chromatography-tandem mass spectrometry methods. *J Chromatogr A* 1217, 312-328.
- Pulfer, M. and Murphy, R.C. (2003). Electrospray mass spectrometry of phospholipids. *Mass Spectrom Rev* 22, 332-364.
- Quinn, T.C. and Gaydos, C.A. (1999). In vitro infection and pathogenesis of Chlamydia pneumoniae in endovascular cells. *Am Heart J* 138, S507-511.
- Rank, R.G. (2006) The Role of the CD4 TCell in the Host Response to Chlamydia. In *Chlamydia: Genomics and Pathogenesis*, P. Bavoil, P. Wyrick (eds.). Wyomondham, horizon bioscience, pp. 339-364.
- Rasmussen, S.J., Eckmann, L., Quayle, A.J., Shen, L., Zhang, Y.X., Anderson, D.J., *et al.* (1997). Secretion of proinflammatory cytokines by epithelial cells in response to Chlamydia infection suggests a central role for epithelial cells in chlamydial pathogenesis. *J Clin Invest* 99, 77-87.
- Raulston, J.E. (1997). Response of Chlamydia trachomatis serovar E to iron restriction in vitro and evidence for iron-regulated chlamydial proteins. *Infect Immun* 65, 4539-4547.
- Roberts, L.D., McCombie, G., Titman, C.M. and Griffin, J.L. (2008). A matter of fat: an introduction to lipidomic profiling methods. *J Chromatogr B Analyt Technol Biomed Life Sci* 871, 174-181.
- Robertson, D.G., Watkins, P.B. and Reilly, M.D. (2011). Metabolomics in toxicology: preclinical and clinical applications. *Toxicol Sci* 120 Suppl 1, S146-170.
- Roth, A., Konig, P., van Zandberger, G., Klinger, M., Hellwig-Burgel, T., Daubener, W., Bohlmann, M.K. Rupp, J. (2010) Hypoxia abrogates antichlamydial properties of IFN-gamma in human fallopian tube cells in vitro and ex vivo. *Proc Natl Acad Sci USA* 107, 19502-19507.
- Rottenberg, M.E., Gigliotti-Rothfuchs, A. and Wigzell, H. (2002). The role of IFN-gamma in the outcome of chlamydial infection. *Curr Opin Immunol* 14, 444-451.
- Rupp, J., Berger, M., Reiling, N., Gieffers, J., Lindschau, C., Haller, H., *et al.* (2004). Cox-2 inhibition abrogates Chlamydia pneumoniae-induced PGE2 and MMP-1 expression. *Biochem Biophys Res Commun* 320, 738-744.
- Rupp, J., Gieffers, J., Klinger, M., van Zandbergen, G., Wrase, R., Maass, M., *et al.* (2007). Chlamydia pneumoniae directly interferes with HIF-1alpha stabilization in human host cells. *Cell Microbiol* 9, 2181-2191.
- Saburi, Y., Okumura, K., Matsui, H., Hayashi, K., Kamiya, H., Takahashi, R., *et al.* (2003). Changes in distinct species of 1,2-diacylglycerol in cardiac hypertrophy due to energy metabolic disorder. *Cardiovasc Res* 57, 92-100.

- Saeed, A.I., Bhagabati, N.K., Braisted, J.C., Liang, W., Sharov, V., Howe, E.A., *et al.* (2006). TM4 microarray software suite. *Methods Enzymol* 411, 134-193.
- Saito, K. and Matsuda, F. (2009). Metabolomics for functional genomics, systems biology, and biotechnology. *Annu Rev Plant Biol* 61, 463-489.
- Saka, H.A., Thompson, J.W., Chen, Y.S., Kumar, Y., Dubois, L.G., Moseley, M.A. and Valdivia, R.H. (2011). Quantitative proteomics reveals metabolic and pathogenic properties of *Chlamydia trachomatis* developmental forms. *Mol Microbiol* 82, 1185-1203.
- Schachter (1999) Infection and Disease Epidemiology. In *Chlamydia: Intracellular Biology, Pathogenesis, and Immunity*, R. Stephens (ed.). Washington, D.C., ASM press.
- Schmitt-Kopplin, P., Gelencser, A., Dabek-Zlotorzynska, E., Kiss, G., Hertkorn, N., Harir, M., *et al.* (2010). Analysis of the unresolved organic fraction in atmospheric aerosols with ultrahigh-resolution mass spectrometry and nuclear magnetic resonance spectroscopy: organosulfates as photochemical smog constituents. *Anal Chem* 82, 8017-8026.
- Scidmore, M.A. (2005). Cultivation and Laboratory Maintenance of *Chlamydia trachomatis*. *Curr Protoc Microbiol* Chapter 11, Unit 11A 11.
- Semenza, G.L. (2007). Oxygen-dependent regulation of mitochondrial respiration by hypoxia-inducible factor 1. *Biochem J* 405, 1-9.
- Shalinsky, D.R., McNamara, D.B. and Agrawal, K.C. (1989). Modulation of prostaglandin biosynthesis in hypoxic murine mammary adenocarcinoma cells by misonidazole. *Cancer Res* 49, 3853-3856.
- Shayman, J.A. (2000). Sphingolipids. *Kidney Int* 58, 11-26.
- Shemer, Y. and Sarov, I. (1985). Inhibition of growth of *Chlamydia trachomatis* by human gamma interferon. *Infect Immun* 48, 592-596.
- Shevchenko, A. and Simons, K. (2010). Lipidomics: coming to grips with lipid diversity. *Nat Rev Mol Cell Biol* 11, 593-598.
- Shima, K., Kuhlenbaumer, G. and Rupp, J. (2010). *Chlamydia pneumoniae* infection and Alzheimer's disease: a connection to remember? *Med Microbiol Immunol* 199, 283-289.
- Skipp, P., Robinson, J., O'Connor, C.D. and Clarke, I.N. (2005). Shotgun proteomic analysis of *Chlamydia trachomatis*. *Proteomics* 5, 1558-1573.
- Soh, H., Wasa, M. and Fukuzawa, M. (2007). Hypoxia upregulates amino acid transport in a human neuroblastoma cell line. *J Pediatr Surg* 42, 608-612.
- Sohlenkamp, C., Lopez-Lara, I.M. and Geiger, O. (2003). Biosynthesis of phosphatidylcholine in bacteria. *Prog Lipid Res* 42, 115-162.
- Stephens, R.S. (2003). The cellular paradigm of chlamydial pathogenesis. *Trends Microbiol* 11, 44-51.
- Stephens, R.S., Kalman, S., Lammel, C., Fan, J., Marathe, R., Aravind, L., *et al.* (1998). Genome sequence of an obligate intracellular pathogen of humans: *Chlamydia trachomatis*. *Science* 282, 754-759.
- Stubbs, M., Bashford, C.L. and Griffiths, J.R. (2003). Understanding the tumor metabolic phenotype in the genomic era. *Curr Mol Med* 3, 49-59.

- Su, H., McClarty, G., Dong, F., Hatch, G.M., Pan, Z.K. and Zhong, G. (2004). Activation of Raf/MEK/ERK/cPLA2 signaling pathway is essential for chlamydial acquisition of host glycerophospholipids. *J Biol Chem* 279, 9409-9416.
- Suhre, K. and Schmitt-Kopplin, P. (2008). MassTRIX: mass translator into pathways. *Nucleic Acids Res* 36, W481-484.
- Summersgill, J.T., Sahney, N.N., Gaydos, C.A., Quinn, T.C. and Ramirez, J.A. (1995). Inhibition of Chlamydia pneumoniae growth in HEp-2 cells pretreated with gamma interferon and tumor necrosis factor alpha. *Infect Immun* 63, 2801-2803.
- Swiderek, H., Logan, A. and Al-Rubeai, M. (2008). Cellular and transcriptomic analysis of NS0 cell response during exposure to hypoxia. *J Biotechnol* 134, 103-111.
- Tappia, P.S., Ladha, S., Clark, D.C. and Grimble, R.F. (1997). The influence of membrane fluidity, TNF receptor binding, cAMP production and GTPase activity on macrophage cytokine production in rats fed a variety of fat diets. *Mol Cell Biochem* 166, 135-143.
- Teng, Q., Huang, W., Collette, T., Ekman, D. and Tan, C. (2009a). A direct cell quenching method for cell-culture based metabolomics. *Metabolomics* 5, 199-208.
- Teng, R., Junankar, P.R., Bubb, W.A., Rae, C., Mercier, P. and Kirk, K. (2009b). Metabolite profiling of the intraerythrocytic malaria parasite Plasmodium falciparum by (1)H NMR spectroscopy. *NMR Biomed* 22, 292-302.
- Thomas, S.M., Garrity, L.F., Brandt, C.R., Schobert, C.S., Feng, G.S., Taylor, M.W., *et al.* (1993). IFN-gamma-mediated antimicrobial response. Indoleamine 2,3-dioxygenase-deficient mutant host cells no longer inhibit intracellular Chlamydia spp. or Toxoplasma growth. *J Immunol* 150, 5529-5534.
- Trentmann, O., Horn, M., van Scheltinga, A.C., Neuhaus, H.E. and Haferkamp, I. (2007). Enlightening energy parasitism by analysis of an ATP/ADP transporter from chlamydiae. *PLoS Biol* 5, e231.
- Tse, S.M., Mason, D., Botelho, R.J., Chiu, B., Reyland, M., Hanada, K., *et al.* (2005). Accumulation of diacylglycerol in the Chlamydia inclusion vacuole: possible role in the inhibition of host cell apoptosis. *J Biol Chem* 280, 25210-25215.
- Tziotis, D., Hertkorn, N. and Schmitt-Kopplin, P. (2011). Kendrick-analogous network visualisation of ion cyclotron resonance Fourier transform mass spectra: improved options for the assignment of elemental compositions and the classification of organic molecular complexity. *Eur J Mass Spectrom (Chichester, Eng)* 17, 415-421.
- van Meer, G. (2005). Cellular lipidomics. *EMBO J* 24, 3159-3165.
- van Ooij, C., Kalman, L., van, I., Nishijima, M., Hanada, K., Mostov, K. and Engel, J.N. (2000). Host cell-derived sphingolipids are required for the intracellular growth of Chlamydia trachomatis. *Cell Microbiol* 2, 627-637.
- Villas-Boas, S.G., Hojer-Pedersen, J., Akesson, M., Smedsgaard, J. and Nielsen, J. (2005). Global metabolite analysis of yeast: evaluation of sample preparation methods. *Yeast* 22, 1155-1169.
- Villas-Boas, S.G., Roessner, U., Hansen, M., Smedsgaard, J. and Nielsen, J. (2007) sampling and sample preparation. In *Metabolome analysis - An introduction*. Hoboken, John Wiley & Sons, Inc.
- Walburger, A., Koul, A., Ferrari, G., Nguyen, L., Prescianotto-Baschong, C., Huygen, K., *et al.* (2004). Protein kinase G from pathogenic mycobacteria promotes survival within macrophages. *Science* 304, 1800-1804.

- Wang, Y., Holmes, E., Nicholson, J.K., Cloarec, O., Chollet, J., Tanner, M., *et al.* (2004). Metabonomic investigations in mice infected with *Schistosoma mansoni*: an approach for biomarker identification. *Proc Natl Acad Sci U S A* 101, 12676-12681.
- Watson, A.D. (2006). Thematic review series: systems biology approaches to metabolic and cardiovascular disorders. Lipidomics: a global approach to lipid analysis in biological systems. *J Lipid Res* 47, 2101-2111.
- Weljie, A.M. and Jirik, F.R. (2010). Hypoxia-induced metabolic shifts in cancer cells: moving beyond the Warburg effect. *Int J Biochem Cell Biol* 43, 981-989.
- Wenk, M.R. (2005). The emerging field of lipidomics. *Nat Rev Drug Discov* 4, 594-610.
- Wenk, M.R. (2006). Lipidomics of host-pathogen interactions. *FEBS Lett* 580, 5541-5551.
- WHO (2001) Global prevalence and incidence of selected curable sexually transmitted infections - overview and estimations. W.H. Organization (ed.). Geneva.
- WHO. (2008). The top 10 causes of death - Fact sheet N°310. [WWW document]. URL <http://www.who.int/mediacentre/factsheets/fs310/en/>
- WHO. (2012a). Sexually Transmitted Diseases-Chlamydia trachomatis. [WWW document]. URL [http://www.who.int/vaccine\\_research/diseases/soa\\_std/en/index1.html](http://www.who.int/vaccine_research/diseases/soa_std/en/index1.html)
- WHO. (2012b). Trachoma. [WWW document]. URL <http://www.who.int/blindness/causes/priority/en/index2.html>
- Wilkinson, S., O'Prey, J., Fricker, M. and Ryan, K.M. (2009). Hypoxia-selective macroautophagy and cell survival signaled by autocrine PDGFR activity. *Genes Dev* 23, 1283-1288.
- Wohlgemuth, G., Haldiya, P.K., Willighagen, E., Kind, T. and Fiehn, O. (2010). The Chemical Translation Service--a web-based tool to improve standardization of metabolomic reports. *Bioinformatics* 26, 2647-2648.
- Wold, S. (1978). Cross-validated estimation of the number of components in factor and principal components models. *Technometrics* 20, 397-405.
- Wolf, K., Fischer, E. and Hackstadt, T. (2000). Ultrastructural analysis of developmental events in *Chlamydia pneumoniae*-infected cells. *Infect Immun* 68, 2379-2385.
- Wylie, J.L., Hatch, G.M. and McClarty, G. (1997). Host cell phospholipids are trafficked to and then modified by *Chlamydia trachomatis*. *J Bacteriol* 179, 7233-7242.
- Wyrick, P.B. (2000). Intracellular survival by *Chlamydia*. *Cell Microbiol* 2, 275-282.
- Xia, J., Psychogios, N., Young, N. and Wishart, D.S. (2009). MetaboAnalyst: a web server for metabolomic data analysis and interpretation. *Nucleic Acids Res* 37, W652-660.
- Yin, J., Miyazaki, K., Shaner, R.L., Merrill, A.H., Jr. and Kannagi, R. (2009). Altered sphingolipid metabolism induced by tumor hypoxia - new vistas in glycolipid tumor markers. *FEBS Lett* 584, 1872-1878.
- Zanolari, B., Friant, S., Funato, K., Sutterlin, C., Stevenson, B.J. and Riezman, H. (2000). Sphingoid base synthesis requirement for endocytosis in *Saccharomyces cerevisiae*. *EMBO J* 19, 2824-2833.
- Zhong, G., Fan, P., Ji, H., Dong, F. and Huang, Y. (2001). Identification of a chlamydial protease-like activity factor responsible for the degradation of host transcription factors. *J Exp Med* 193, 935-942.

Zhong, G., Fan, T. and Liu, L. (1999). Chlamydia inhibits interferon gamma-inducible major histocompatibility complex class II expression by degradation of upstream stimulatory factor 1. *J Exp Med* 189, 1931-1938.



## List of scientific communication

### Publications

B. Kanawati, V. von Saint Paul, C. Herrmann, AR. Schöffner, P. Schmitt-Kopplin, Mass spectrometric stereoisomeric differentiation between  $\alpha$ - and  $\beta$ -ascorbic acid 2-O-glucosides. *Experimental and density functional theory study*, *Rapid Commun Mass Spectrom.* 2011; 25 (6): 806-14

C. Müller, I. Dietz, D. Tziotis, F. Moritz, J. Rupp and P. Schmitt-Kopplin. "Molecular cartography in acute *Chlamydia pneumoniae* infections-a non-targeted metabolomics approach." *Anal Bioanal Chem.* 2013, in press

G. Boncompain, C. Müller, V. Malardé, C. Delevoye, N. Cayet, A. Dufour, R. J. Wanders, A. Dautry-Varsat, Ph. Schmitt-Kopplin, P. Lazarow and A. Subtil, The intracellular bacteria *Chlamydia* hijack peroxisomes and utilize their enzymatic capacity to produce bacteria-specific plasmalogens, submitted

Metabolic Features of *Protochlamydia amoebophila* Elementary Bodies - a Link between Activity and Infectivity in *Chlamydiae*, C. Müller\*, B. Sixts\*, A. Siegl\*, M. Watzka, A. Wultsch, D. Tziotis, J. Montanaro, A. Richter, Ph. Schmitt-Kopplin, M. Horn, submitted, \*equally contributed

C. Müller, B. Kanawati, Ph. Schmitt-Kopplin, Intermolekulare gasphase reactions of neutral lipid dimers, *Rapid Commun Mass Spectrom.* Manuskript

### Posters and presentations

ERA-NET Pathomics project meeting, Dez. 2011, Vienna (Austria)

- *Chlamydia trachomatis* and its peroximal activity in lipid biosynthesis, oral presentation, C. Müller, A. Subtil, P. Lazarow, B. Kanawati, Ph. Schmitt-Kopplin
- Effects of *Chlamydia* infection on the human metabolism - a non-targeted study including hypoxia and IFN- $\gamma$  influences, oral presentation, C. Müller, I. Dietz, J. Rupp, Ph. Schmitt-Kopplin
- Metabolomic activity of elementary bodies of environmental *Chlamydia*, oral presentation, C. Müller, B. Sixts, A. Siegl, M. Horn, Ph. Schmitt-Kopplin

Metabomeeting, 2011, Helsinki (Finland), Mass spectrometry based investigation of the phospholipid content of cells infected with the obligate intracellular pathogen *Chlamydiae*, poster, C. Müller, A. Subtil, P. Lazarow, B. Kanawati, Ph. Schmitt-Kopplin

2<sup>nd</sup> PhD-Student and Postdoc Retreat ERA-NET Pathomics, 2011, Düsseldorf (Germany)

- "Metabolomics in action" - examples of fields of applications, oral presentation, C. Herrmann
- Effects of *C. pneumoniae* infection on the host metabolism – a ultrahigh resolution mass spectrometry based approach, oral presentation, C. Herrmann, I. Dietz, J. Rupp, Ph. Schmitt-Kopplin

9. Deutschen Chlamydienworkshop, 2011, Ascona (Switzerland), Effects of *C. pneumoniae* infection on the host metabolism – a ultrahigh resolution mass spectrometry based approach, oral presentation, C. Herrmann, I. Dietz, J. Rupp, Ph. Schmitt-Kopplin

ERA-NET Pathomics project meeting, 2010, Paris (France)

- Investigation of peroxisomal activity within *Chlamydiae* inclusions, oral presentation, C. Herrmann, A. Subtil, P. Lazarow, Ph., B. Kanawati, Schmitt-Kopplin
- Interaction of *C. pneumoniae* and the human host on metabolomic level, oral presentation, C. Herrmann, I. Dietz, J. Rupp, Ph. Schmitt-Kopplin
- Metabolomic activity of elementary bodies of environmental *Chlamydiae*, oral presentation, C. Herrmann, A. Siegl, M. Horn, Ph. Schmitt-Kopplin

9<sup>th</sup> European Fourier Transform Mass Spectrometry Workshop, 2010, Lausanne (Switzerland), Mass spectrometry based analysis of host pathogen interactions between *Chlamydiae* and human cells, poster, C. Herrmann, I. Dietz, A. Fekete, M. Lucio, B. Wägele, J. Rupp, K. Suhre, Ph. Schmitt-Kopplin

1<sup>st</sup> PhD-Student and Postdoc Retreat ERA-NET Pathomics, 2010, Marseille (France)

- Experimental study design and sample preparation in metabolomics, oral presentation, C. Herrmann
- Statistical data analysis of metabolomic datasets, oral presentation, C. Herrmann

Metabolomics & More, 2010, Freising (Germany), Mass spectrometry based analysis of host pathogen interactions between *Chlamydiae* and human cells, poster, C. Herrmann, I. Dietz, A. Fekete, M. Lucio, B. Wägele, J. Rupp, K. Suhre, Th. Rattei, Ph. Schmitt-Kopplin

ERA-NET Pathomics project meeting, 2010, Valencia (Spain), Non-targeted analysis of infections with *Chlamydia pneumoniae* by FT-ICR-MS, oral presentation, C. Herrmann, I. Dietz, A. Fekete, M. Lucio, B. Wägele, K. Suhre, J. Rupp, Ph. Schmitt-Kopplin

18<sup>th</sup> International Mass Spectrometry Conference, 2009, Bremen (Germany), Ion cyclotron resonance Fourier transform mass spectrometry (ICR FT/MS) in metabolomic screening studies, poster, C. Herrmann, A. Fekete, I. Dietz, J. Rupp, B. Wägele, K. Suhre, Ph. Schmitt-Kopplin

## Curriculum vitae

-

### Constanze Müller (birth name Herrmann)

#### Academic grade

Dipl. - Pharmacist (licensed)

licensure grade (Pharmazeutische Prüfung): 1.58

diploma thesis grade: very good

#### Education and professional experience

- Since 05/09      *PhD student within the BMBF ERA-NET Pathomics Project in the research unit Analytical BioGeoChemistry, Helmholtz Zentrum München*
- *development of non-targeted and targeted LC-MS and MS methods (UPLC, q-TOF, FT-ICR-MS) focusing on host-pathogen interactions between pathogen microorganisms (Chlamydia) and human host cells aiming at biomarker and drug target discovery*
  - *contributions to international project meetings and conferences (oral and poster presentations)*
  - *research internships in Lübeck (08/09) and in Paris (12/10 and 12/11)*
- 01/09 - 04/09      *scientific assistant, chair for pharmaceutical technology, Friedrich-Schiller-University Jena*
- *analysis of loading possibilities and delivering profiles of bacteria-made nanocellulose as potential drug delivery system*
  - *supervision of student trainings (manufacture, formulation and quality control for liquid dosage forms)*
- 12/ 08      *licensure as pharmacist*
- 05/08 - 10/08      *second obligatory pharmaceutical internship, Zentral-Apotheke Korntal*
- 11/07 - 04/08      *first obligatory pharmaceutical internship and diploma thesis, BASF SE Ludwigshafen, title of diploma thesis: „Investigation of micronized crosprovidone as dry binder in roller compaction” (supervisor: Prof. Dr. K. Mäder)*
- 02/07      *internship Bayer HealthCare AG, Animal Health in Monheim*
- 08/06 - 09/06      *student exchange (IAESTE), Universidade Federal de Minas Gerais (Belo Horizonte/ Brazil)*

10/03 - 12/08	studies of pharmacy, Martin-Luther-Universität Halle/Wittenberg
07/03	A-levels (main subjects: chemistry and physics)
09/94 - 07/03	grammar school, Friederiken-Gymnasium Bernburg

Awards:

- 02/11 from the Comitee of the 9. Deutschen Chlamydienworkshops (Ascona, Schweiz) for the oral presentation „Effects of *C. pneumoniae* infection on the host metabolism – a ultrahigh resolution mass spectrometry based approach
- 07/03 from the „Förderverein Friederiken-Gymnasium Bernburg“ for excellent A-levels
- 07/03 from the German society of physics for very good results in the A-levels in physics

## *Erklärung*

*Ich erkläre an Eides statt, dass ich die der Fakultät für Wissenschaftszentrum Weihenstephan für Ernährung, Landnutzung und Umwelt der Technischen Universität München zur Promotionsprüfung vorgelegte Arbeit mit dem Titel: *Metabolomics in host-pathogen interactions – An investigation of Chlamydia infected human cells* unter der Anleitung und Betreuung durch Priv.-Doz. Dr. Philippe Schmitt-Kopplin ohne sonstige Hilfe erstellt und bei der Abfassung nur die gemäß § 6 Abs. 5 angegebenen Hilfsmittel benutzt habe.*

*(x) Ich habe die Dissertation in keinem anderen Prüfungsverfahren als Prüfungsleistung vorgelegt.*

*(x) Ich habe den angestrebten Doktorgrad noch nicht erworben und bin nicht in einem früheren Promotionsverfahren für den angestrebten Doktorgrad endgültig gescheitert.*

*Die Promotionsordnung der Technischen Universität München ist mir bekannt.*

*München, den 10.07.2012*